INTERNATIONAL JOURNAL OF
IJCOE
COASTAL, OFFSHORE AND
ENVIRONMENTAL ENGINEERING

**The Role of Dry Ports in Regional Economic Development: A Case Study of Yazd Dry Port**
Seyed Khalil Kebriaee, Jafar Sayareh

**Factors Influencing the Enhancement of Marine Oil Spill Response Operations: Application of Interpretive Structural Modeling at Chabahar Port**
Jasem Raeisi, Jafar Sayareh

**Environmental Risk Modeling and Management of Dredging and Dredged-Material Disposal Operations with a Sustainable Coastal and Marine Environment Approach**
Asghar Rashnoodi, Hossein Karimi Khosrow

**Machine Learning–Based Prediction of Temperature and Precipitation Using Historical Meteorological Time Series Data**
Mojtaba Zoljoodi, Mohammad Souri Laki, Maryam Alipour

**Experimental and Numerical Investigation of the Effect of Stator and rotor distance on the Hydrodynamic Performance of a PumpJet Propulsion System**
Mohammad Hossein Qaedsharaf

**Investigating the Role of Water Depth on Tsunami Shoaling and Coastal Amplification: Insights from Idealized and Realistic Numerical Experiments**
Ehsan Rastgoftar

**Using Microsilica and Nano copper oxide to improve mechanical properties and permeability in concrete channels and pressurized water and sewage pipes**
Salman Movahedkhah , Heydar Dashti Naserabadi ,Morteza Jamshidi

**Sensitivity Analysis of Wave and Current in Numerical Modeling and Comparison with Field Measurements During Small Storms in Northern Ports of Iran**
Rasul Koohzad, Reza Dezvareh

Volume 11 | Issue 11 | JAN 2026

WWW.IJCOE.org info@ijcoe.org

www.ijcoe.org

International Journal of Coastal, Offshore and Environmental Engineering (IJCOE) Vol.11/Issue 4/ NOV 2026



International Journal of
Coastal, Offshore
& Environmental
Engineering
Since 2015
ISSN: 2538-1571 (online)

Volume 11 | Issue4 | NOV2026

IJCOE

Editor-in-Chief: Prof. H. Mostepe Nuemi

International Journal of Coastal, Offshore & Environmental Engineering
Since 2015
ISSN: 2980-8721 (online)

**In The Name of God**

## Message from the Editor-in-Chief

The IJCOE journal office was established in 2015,and its first issue was published in 2016. TheIJCOE covers a wide range of research in thefields of oceanography & ocean technology, aswell as marine industries & marine engineering.The editorial board of IJCOE consists of nearly130 of the greatest scientists and researchersfrom over 30 countries worldwide, and thejournal's review board comprises 1,000 membersfrom all five continents. The membership andapplication process for joining the editorial andreview boards of this journal is ongoing. IJCOE isa research-academic quarterly journal that haspublication and distribution permissions fromthe Press Organization and permission topublish scientific-research articles from theMinistry of Science, Research, and Technology(MSRT) with an "A" rating. It also holds a "Q1"rating from the ISC institute with an impactfactor (IF) of approximately 0.43 and isconsidered a "core journal" (prestigious andoutstanding journal). IJCOE is an open-accessjournal and allows the download and receipt ofaccepted articles in full text for free. It respectsand adheres to copyright and COPE regulations.The journal's office operates 24/7, providingservices to researchers. In addition to publishinga regular quarterly journal, IJCOE has 16 specialissues on specific topics in preparation. It alsoprovides conditions for publishing specializedbooks, references, and handbooks. Moreover, itis ready to cooperate with the secretariats ofreputable international conferences to publishtheir selected and outstanding articles. IJCOEevaluates, appraises, and publishes books,articles, and the scientific achievements andfindings of esteemed researchers and scientistsworldwide who are innovating and conductingin-depth research in the "important and strategicfield of the maritime technology & Oceanengineering." It welcomes any form of jointcooperation with universities, research institutes,and related research centers at the national,regional, and international levels, and extends ahand for collaboration.

## Classification of Editorial Board in IJCOE

- Editor-in-Chief
- Director-in-Chief
- Deputy Editor
- Executive Managers
- English Text Editor
- Technical Editor
- International Editorial Board
- National Editorial Board
- Editorial Board Associate
- Editorial Board Assistant
- Guest Editorial Board
- Advisory Board
- Administrative Coordinator
- Honorary Board Member
- Methodology Advisor

## Author Benefits

- Open Access
- Rapid Publication
- Thorough Peer-Review
- No Copyright Constraints
- Coverage by Leading Indexing Services
- Discounts On Article Processing Charges (APC)
- No Space Constraints, No restriction on the maximum length of the papers, number of figures or colors

INTERNATIONAL JOURNAL OF IJCOE COASTAL, OFFSHORE & ENVIRONMENTAL ENGINEERING

## Aims of IJCOE

Hydrodynamics

Marine equipment

Structural mechanics

Ocean environmental predictions

Stochastic calculations Experimental

Automatic Control of Marine Systems

## Scope of IJCOE

Marine Hazards

Ocean Acoustics

Naval Architecture

Ocean Engineering

Coastal Engineering

Marine Meteorology

Marine Earth Sciences

Underwater Technology

Marine Renewable Energy

Polar & Arctic Engineering

Marine Renewable Energy

Marine Geography & Geodesy

Marine Environmental Engineering

Automatic Control of Marine Systems

Hydro Physics & Physical Oceanography

## Type of papers

- Case Studies
- Book Reviews
- Review Article
- Letters to the Editor
- Methodology Papers
- Editorials and Commentaries
- Response or Rejoinder Papers
- Perspective or Opinion Papers
- Conceptual or Theoretical Papers
- Meta-Analysis and Systematic Reviews
- Short Communications or Brief Reports
- Research Articles (Original Research Papers)

## Scientific Research Journal

**Ministry of Science, Research And Technology (MSRT)**

Jurnal Ranking 2023: A

**Ministry Of Science, Research And Technology (ISC)**

Citation Impact 2022: 0.429

Quartile 2022 : Q1

Core Collection



IJCOE is a Member of




## Cantact Us

**Office 1 |** Research Institute of Meteorology and Atmospheric Science

**Address |** Tehran, Shahid Kharrazi Highway, Pajoohesh Blvd, Research Institute of Meteorology and Atmospheric Science, Sand and Dust Storm International Research Center (SDS-IRC), No. 13, 1st floor.

**Phone |** +982144787652

**Postal code |** 13611-14977

**website |** www.rimac.ac.ir

**Office 2 |** Iranian National Institute for Oceanography and Atmospheric Science

**Address |** Tehran, Dr. Fatemi Gharbi St., Shahid Etemadzade St., No. 3, third floor.

**Phone |** +982166944873

**Postal code |** 13389 – 14118

**website |** www.inio.ac.ir

**Email |** Info@ijcoe.org

**Website |** www.ijcoe.org

## Follow Us

www.ijcoe.org

INTERNATIONAL JOURNAL OF IJCOE COASTAL, OFFSHORE & ENVIRONMENTAL ENGINEERING

**Volume & Issue:**

**Volume 11, Issue 4, NOV 2026**

**Number of Articles: 8**

# Content


| | |
|---|---|
| The Role of Dry Ports in Regional Economic Development: A Case Study of Yazd Dry Port<br><br>Seyed Khalil Kebriaee, Jafar Sayareh | 1 |
| Factors Influencing the Enhancement of Marine Oil Spill Response Operations: Application of Interpretive Structural Modeling at Chabahar Port<br><br>Jasem Raeisi, Jafar Sayareh | 15 |
| Environmental Risk Modeling and Management of Dredging and Dredged-Material Disposal Operations with a Sustainable Coastal and Marine Environment Approach<br><br>Asghar Rashnoodi, Hossein Karimi Khosrow | 32 |
| Machine Learning–Based Prediction of Temperature and Precipitation Using Historical Meteorological Time Series Data<br><br>Mojtaba Zoljoodi ,Mohammad Souri Laki, Maryam Alipour | 41 |
| Experimental and Numerical Investigation of the Effect of Stator and rotor distance on the Hydrodynamic Performance of a PumpJet Propulsion System<br><br>Mohammad Hossein Qaedsharaf | 46 |
| Investigating the Role of Water Depth on Tsunami Shoaling and Coastal Amplification: Insights from Idealized and Realistic Numerical Experiments<br><br>Ehsan Rastgoftar | 65 |
| Using Microsilica and Nano copper oxide to improve mechanical properties and permeability in concrete channels and pressurized water and sewage pipes<br><br>Salman Movahedkhah , Heydar Dashti Naserabadi , Morteza Jamshidi | 74 |
| Sensitivity Analysis of Wave and Current in Numerical Modeling and Comparison with Field Measurements During Small Storms in Northern Ports of Iran<br><br>Rasul Koohzad, Reza Dezvareh | 91 |


INTERNATIONAL JOURNAL OF IJCOE COASTAL, OFFSHORE & ENVIRONMENTAL ENGINEERING

INTERNATIONAL JOURNAL OF
COASTAL, OFFSHORE & ENVIRONMENTAL ENGINEERING IJCOE Vol.11/No. 4/Autumn 2026 (1-14)

Available online at: www. Ijcoe.org

# The Role of Dry Ports in Regional Economic Development: A Case Study of Yazd Dry Port

**Seyed Khalil Kebriaee[1], Jafar Sayareh[2*]**

[1] *MSc. In Port and Shipping, Chabahar Maritime University, Chabahar, Iran;* khalilkebriaee@gmail.com
[2*] *Associate Prof., Maritime Transport Department, Chabahar Maritime University, Chabahar, Iran;* j.sayareh@gmail.com

**ARTICLE INFO**

*Article History:*
Received: 8 July
Accepted: 5 Oct
Available online ….

*Keywords:*
**Dry Ports;**
**Economic Development;**
**Intermodal Transport;**
**Inland Terminal;**
**Yazd Dry Port**

**ABSTRACT**

Dry ports function as strategic intermodal terminals connecting inland and maritime networks via road and rail, playing an increasingly vital role in facilitating international trade and regional economic development. Given Iran's strategic geographic position at the crossroads of major trade corridors, the development of dry ports presents a significant opportunity to enhance freight transport efficiency and stimulate regional economic growth. This study aims to evaluate the impact of the infrastructure indicators of Yazd Dry Port on regional economic development.

A mixed-methods approach was employed, combining a comprehensive literature review, expert panel evaluation, and a survey of 96 experts and specialists in maritime transport, logistics, and economic planning. Data were analyzed using descriptive and inferential statistical methods, including factor analysis (KMO = 0.77; Bartlett's test: $\chi^2 = 686.36$, $p < 0.001$), one-sample t-tests, and the Friedman test for ranking variables. The reliability of the questionnaire was confirmed with a Cronbach's alpha of 0.89.

The findings revealed that all 11 identified infrastructure indicators have a positive and significant impact on regional economic development ($p < 0.001$). The Friedman test results ranked security (mean rank = 7.04) as the most critical factor, followed by accessibility (mean rank = 6.59) and economic and financial factors (mean rank = 6.42), while transit capacity (mean rank = 5.24) ranked lowest.

This study contributes empirical evidence on the economic impacts of dry ports in the Iranian context, addressing a gap identified in previous international research. The findings provide actionable insights for policymakers, transport planners, and infrastructure developers, particularly regarding investment prioritization in security, accessibility, and economic infrastructure. The results also underscore the importance of a clear executive framework and public-private partnerships to overcome government support limitations and accelerate dry port implementation in Iran.

## 1. Introduction

The dynamic transformations in the global business environment over recent decades have led to a significant increase in exports and imports across various regions worldwide. According to the World Trade Organization [1], world merchandise trade volume declined by 1.2% in 2023, driven largely by high energy prices and inflation that weighed on demand for manufactured goods, particularly in Europe. In value terms, merchandise exports fell by 5% to US$24.01 trillion in 2023. However, a gradual recovery is underway, with WTO economists projecting merchandise trade volume growth of 2.6% in 2024 and 3.3% in 2025 (. The Asia-Pacific region, in particular, has demonstrated remarkable resilience, with the region's share of global nominal exports and imports rising slightly to 38.9% and 36.7% in 2024, reflecting stronger trade growth compared to the global average. The region's merchandise trade reached approximately US$18.5 trillion in 2024, representing growth of 5.1% and outpacing the WTO's global trade growth forecast of 2.6% [2]. This sustained expansion

of international trade—particularly in the Asia-Pacific region—has placed considerable pressure on existing transport infrastructures, especially on port facilities and their associated hinterland connections.

The expansion of manufacturing enterprises, the emergence of new industries, and the rising volume of supply and demand for maritime-related cargo have collectively necessitated the development of ports and the enhancement of cargo transit routes to these ports. This increasing demand has, in turn, resulted in higher cargo traffic volumes and a corresponding reduction in available terminal space. As container transport volumes continue to grow, the sea flow generates an almost proportional inland flow, making the links with the hinterland critical factors for seaport functionality. Consequently, there is an urgent need for port modernization and structural reforms to improve access to the hinterland. A dry port, defined as an intermodal terminal located in the hinterland and connected to one or more seaports via a high-capacity transport mode—such as scheduled rail services—can offer a comprehensive range of services typically provided at coastal ports, often with superior quality and enhanced operational efficiency [3]. Roso [3] argues that a well-applied dry port concept can help identify ways of shifting freight volumes from road to more energy-efficient traffic modes, relieve seaport cities of congestion, and facilitate improved logistics solutions for shippers in the port's hinterland. These services include cargo warehousing, empty container storage, container repairs, customs clearance, and cargo consolidation and support.

On the other hand, Iran's vast geographical expanse and the considerable distance between most major cities and coastal ports have created substantial challenges for exporters, importers, and transit cargo operations. Furthermore, the high cost of road transport has increased the final cost of domestic products, thereby diminishing the competitive advantage of Iranian producers relative to their foreign counterparts and adversely affecting the country's international trade performance. As coastal production costs in many countries rise, producers are moving inland to remain competitive, further emphasizing the need for efficient inland logistics solutions [4]. In addition to these economic challenges, severe traffic congestion in port cities and along the country's transport corridors—largely attributable to heavy truck movements—is a widely recognized problem [5]. Moreover, coastal cities and seaports, given their touristic nature, experience significant passenger traffic during certain periods of the year, which further exacerbates traffic congestion and, at times, leads to restrictions on truck movements and delays in cargo clearance from ports.

While certain operational issues—such as extended loading and unloading times and space shortages—may be addressed through targeted improvements, the more fundamental difficulties associated with truck congestion and urban traffic cannot be easily resolved through incremental measures alone [5]. Therefore, it appears that studying logistics systems such as dry ports could offer valuable insights for reducing congestion in ports and adjacent urban areas while simultaneously supporting broader regional development objectives. Roso and Lumsden [5] found that implementation of a dry port in a seaport's hinterland enables the seaport to increase its terminal capacity, while the modal shift from road to rail results in reduced congestion at seaport gates and improved inland access.

At present, various types of dry ports have been successfully established in numerous countries, where they play a pivotal role in improving and advancing transport conditions. Research has shown that dry ports are crucial to marine logistics, providing significant economic, environmental, and social benefits [6]. The strategic location of a dry port should satisfy at least three key criteria: (1) it should offer ease of access at a reasonable cost; (2) it should be situated in close proximity to production centers; and (3) it should be located within distribution clusters to facilitate efficient cargo handling and dispersion [4]. Notteboom and Rodrigue [4] note that the growing focus on inland/dry ports is indicative of transport development strategies gradually shifting inland to address capacity and efficiency issues in the light of global supply chains.

Recent studies on dry port implementation in Iran have begun to address these challenges. Hatami Nasab et al. [6] identified 17 key indexes for dry port implementation using a Delphi model, which were classified into eight groups, and validated a conceptual model using Partial Least Squares (PLS). Golghamat Raad and Rajendran [7], in a study tested on Iranian case data, suggested that high-capacity dry ports should be established in the cities of Sirjan and Tehran, while smaller dry ports should be built in Isfahan and Ahvaz, with connections to the national railway network for Chabahar and Anzali seaports. Similarly, research on the Zahedan dry port identified "reduction of road traffic" (mean = 3.65), "access to multimodal transport" (mean = 3.58), and "influx of private sector investment" (mean = 3.48) as paramount indicators, highlighting the critical need for infrastructure modernization [8]. However, challenges such as inadequate infrastructure, poor institutional coordination, and significant socio-economic inequalities limit the potential of these developments [7].

Accordingly, the development of dry ports may be considered an effective strategy for addressing these multifaceted challenges. The central research question that arises is: How can an efficient dry port be successfully established in Iran? In other words, what are the most critical factors influencing the successful implementation of a dry port in the Iranian context? This research, in addition to identifying these key

factors, aims to explore the interactive effects and causal interrelationships among them, thereby contributing to a more comprehensive understanding of the implementation pathway for dry port projects in Iran.

## 2. Methodology

This study employs a combination of descriptive and inferential statistical methods. Data collection was conducted through a structured questionnaire as part of a field-based research design, which also incorporated semi-structured interviews with subject matter experts. The questionnaire was developed following a comprehensive identification of dry port concepts and the key factors influencing regional economic development, which are briefly outlined in the subsequent sections. This mixed-methods approach, combining quantitative and qualitative data collection techniques, aligns with the framework proposed by Creswell and Creswell [9], who advocate for the integration of multiple data sources to enhance the robustness and depth of research findings.

### 2.1 Population and Sample

The target population of this study comprised university professors and academic specialists, maritime transport experts, logistics and multimodal transport professionals, and economic analysts from the Ministry of Roads and Urban Development, all of whom possess direct or indirect involvement with the Yazd Dry Port project. The minimum required sample size for identifying and ranking the factors affecting regional economic development and the establishment of Yazd Dry Port was determined to be 96 experts. This sample size calculation was guided by recommendations for multivariate analysis, which suggest a minimum ratio of 5 to 10 observations per variable [10]. In total, 105 questionnaires were distributed among the selected sample. Of these, 96 fully completed and valid questionnaires were deemed suitable for further statistical analysis and hypothesis testing.

### 2.2 Research Design and Analytical Framework

The overall analytical framework of this study incorporates both quantitative and qualitative dimensions. The quantitative dimension involves the application of specific statistical computations, while the qualitative dimension encompasses the interpretation, reasoning, and inference derived from the statistical results, ultimately enabling generalization to the broader population under investigation [9]. This integrated approach allows for a more comprehensive understanding of the complex interrelationships between dry port implementation and regional economic development.

The statistical procedures and methods employed in this study are outlined in Table 1.

**Table 1. Statistical procedures and methods employed in this study**

| Analytical Step | Statistical Method / Test | Purpose |
|---|---|---|
| 1 | Kolmogorov–Smirnov (K-S) test | To determine whether the data follow a normal (parametric) or non-normal (non-parametric) distribution |
| 2 | Normality assessment | To verify distributional assumptions prior to parametric testing |
| 3 | Validity and reliability analysis | To ensure the internal consistency and construct validity of the measurement instrument |
| 4 | One-sample t-test | To compare sample means against a hypothesized population mean |
| 5 | Friedman test | To rank the relative importance of identified variables |
| 6 | Spearman's rank correlation coefficient | To examine the strength and direction of monotonic relationships between variables |
| 7 | Kruskal–Wallis H test | To compare differences across multiple independent groups (non-parametric alternative to one-way ANOVA) |

The selection of these statistical techniques was informed by established methodological guidelines for social science research. Field [11] provides comprehensive guidance on the application of these tests within the SPSS environment, emphasizing the importance of testing underlying assumptions prior to parametric analysis. Similarly, Hair et al. [10] recommend the use of both parametric and non-parametric approaches to ensure the robustness of findings when distributional assumptions are uncertain.

### 2.3 Instrumentation and Data Analysis

All statistical analyses and graphical representations were performed using Microsoft Excel and SPSS version 19.0. The questionnaire instrument was designed based on an extensive review of the relevant literature and expert consultations. Prior to full-scale distribution, the questionnaire was pilot-tested to assess clarity, comprehensiveness, and appropriateness of the items, in accordance with the recommendations of Creswell and Creswell [9] for instrument development and validation.

### 2.4 Validity and Reliability

Content validity was established through expert review, wherein the questionnaire items were evaluated by a panel of academic and industry specialists to ensure that the constructs were adequately represented [10]. Reliability was assessed using Cronbach's alpha coefficient, with a threshold of $\alpha \geq 0.70$ considered acceptable for internal consistency [12]. Field [11] further notes that Cronbach's alpha values above 0.80 indicate good reliability, while values above 0.90

indicate excellent reliability. The specific reliability coefficients for each construct are reported in the Results section.

### 2.5 Ethical Considerations

All participants were informed of the research objectives and provided their voluntary consent prior to participation. Anonymity and confidentiality were guaranteed, and participants were assured that their responses would be used solely for academic research purposes. These procedures adhere to the ethical guidelines for research involving human subjects as outlined by Creswell and Creswell [9].

### 2.6 Limitations of the Methodology

While the chosen methodological framework provides valuable insights, several limitations should be acknowledged. First, the reliance on self-reported questionnaire data may introduce response [11]. Second, the cross-sectional design captures perceptions at a single point in time and does not account for temporal changes in the factors under investigation. Third, the generalizability of the findings may be limited to contexts similar to the Yazd Dry Port project. Future research could address these limitations through longitudinal designs and comparative case studies across multiple dry port locations.

### 2.7 Recommendations and Practical Implications

Following the analysis and interpretation of findings, a set of practical recommendations will be proposed. These recommendations are intended to serve as actionable insights for policymakers, transport planners, and infrastructure developers, as well as to provide a foundation for future research endeavors in the field of dry port logistics and regional economic development. The methodological approach employed in this study may also serve as a template for similar investigations in other developing countries seeking to implement dry port infrastructure.

## 3. Dry Port Typology and Characteristics

Based on their functional characteristics and spatial positioning, dry ports can be classified into three distinct categories: distant dry ports, midrange dry ports, and near dry ports. This typology reflects the varying geographical relationships between inland terminals and their associated seaports, as well as the differing operational and logistical roles they perform within the broader supply chain [13].

### 3.1 Distant Dry Ports

Distant dry ports represent the most common and historically established type of dry port, with a longer developmental trajectory compared to other categories. The primary rationale for utilizing this type of dry port is predominantly cost-driven: given the considerable distance from the seaport and the substantial volume of inbound cargo, rail transport emerges as a more economically viable and operationally efficient mode of transportation compared to road haulage [13]. Distant dry ports are typically located far inland, often in regions with high cargo generation or consumption, and serve as key nodes for consolidating and distributing freight over long distances [3].

A significant portion of the benefits associated with distant dry ports relates to the modal shift from road transport to rail networks, which consequently reduces congestion at seaport gateways and in their surrounding areas [3, 13]. The dry port concept is based on a seaport directly connected by rail to inland intermodal terminals, where shippers can leave and/or collect their goods in intermodal loading units as if directly at the seaport [3]. Each freight train can replace approximately 35 trucks in Europe and up to 100 trucks in the United States, thereby substantially mitigating the environmental externalities associated with road-based freight transport, including greenhouse gas emissions, air pollution, and road accidents [3, 14]. The primary rationale for collaboration between maritime seaports and distant dry ports is that through this integration, seaports can offer enhanced services at lower operational costs while simultaneously extending their coverage to a broader and more diversified hinterland [13].

Figure 1 illustrates the spatial relationship between a maritime seaport, its hinterland areas, and a distant dry port, demonstrating how the dry port functions as an extended gateway for cargo movement [13].

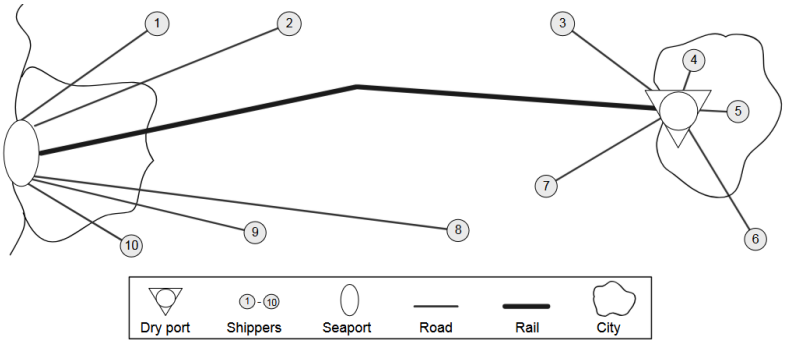



**Figure 1. Schematic representation of a seaport, its hinterland, and a distant dry port [13].**

### 3.2 Midrange Dry Ports

Considering the price-to-quality ratio of various transport systems, the competition between rail and road transport is largely contingent upon the geographical characteristics of the region and the spatial distribution of the population. Midrange dry ports are situated at a distance from the seaport where, as illustrated in Figure 2, road transport typically remains the predominant mode of access [13].

In this configuration, the midrange dry port functions as a consolidation center for rail services, serving as a strategic node where cargo from multiple origins is aggregated for efficient onward transportation. This arrangement demonstrates that specialized maritime transport management and equipment—such as X-ray scanning devices required for security screening and customs inspections—need only be present at a single terminal, rather than at every inland facility, thereby generating significant cost efficiencies. Consequently, the midrange dry port can effectively act as an intermediary, providing additional warehousing capacity for cargo that would otherwise be stored at congested seaport facilities [13].

Where warehouse space constraints exist at coastal ports, and provided that cost differentials are negligible, shippers whose locations are relatively equidistant from both the seaport and the dry port may be incentivized to route their cargo through the dry port rather than the congested seaport terminal. In other dimensions, the benefits of this type of dry port are broadly comparable to those associated with distant dry ports, including congestion reduction at seaport gateways, modal shift benefits, and extended hinterland coverage [13].

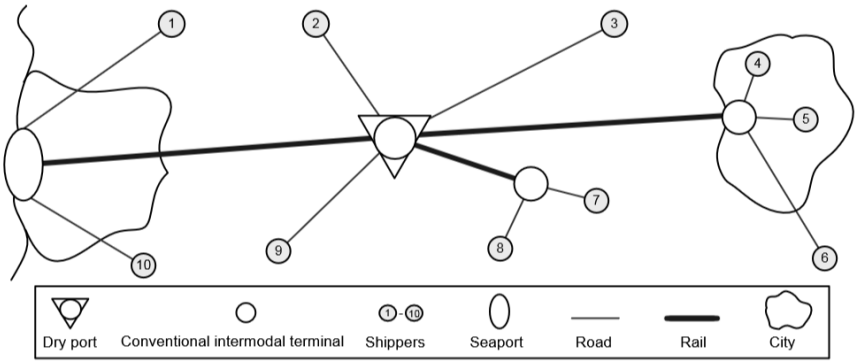



**Figure 2. Schematic representation of a midrange dry port and its relationship to the seaport and hinterland [13].**

### 3.3 Near Dry Ports

With the growth of container transport by sea, the primary challenges facing seaports are insufficient terminal space and inadequate access to inland transport networks. To effectively respond to the demands of shippers, seaports can establish near dry ports in their hinterland or in the suburban areas adjacent to the port city. By expanding container terminal capacity through the development of near dry ports, seaports can achieve increased operational efficiency and profitability while simultaneously accommodating the berthing of larger vessels [13].

Compared to other types of dry ports, near dry ports serve as a more effective intermediary for container handling and facilitate faster loading and unloading of container ships [15]. However, this function—particularly when aimed at preventing increased container dwell time—requires a reliable and well-integrated rail system to ensure seamless connectivity between the seaport and the near dry port [15].

Figure 3 illustrates a near dry port in relation to a seaport and a conventional intermodal terminal, demonstrating the spatial and operational relationships among these nodes [13].

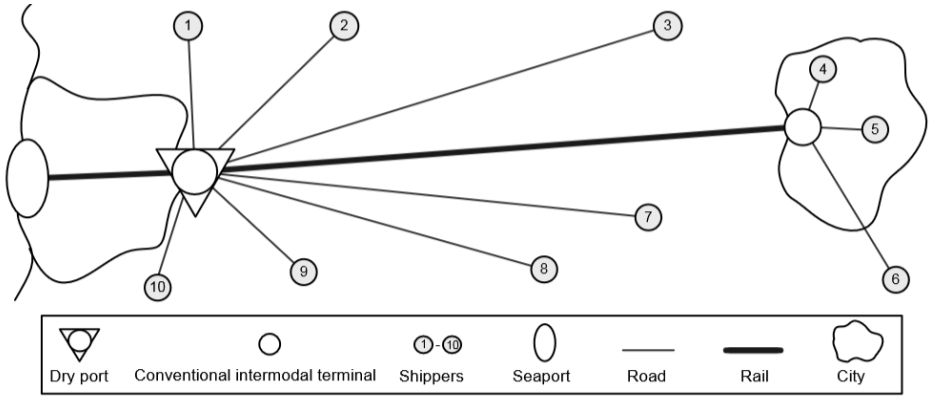



**Figure 3. Schematic representation of a near dry port, seaport, and conventional intermodal terminal [13].**

## 4. Literature Review

International research on dry ports has a considerably longer history compared to domestic studies. In Iran, despite numerous research efforts and policy decisions, executive actions remain limited. Therefore, this review examines the literature at both national and international levels.

### 4.1 National Studies

Dadvar et al. [16] investigated the importance of establishing dry ports for logistics development in Iran, concluding that the majority of services provided at seaports—including customs clearance, warehousing, container stripping and stuffing, and container repairs—can be effectively offered at dry ports. They further noted that dry ports serve as key cargo consolidation and distribution centers and play a significant role in intermodal and multimodal transport.

Sheikholeslami et al. [17] examined the impacts of dry ports on resolving seaport challenges, identifying insufficient warehousing space and inadequate access to cargo destinations as primary issues. They argued that dry ports offer solutions to these problems while providing additional benefits, including reduced road congestion, decreased fuel consumption, and lower land acquisition costs.

Saeidi et al. [18] explored the dry port concept with particular attention to Iran's needs. After reviewing the three dry port typologies—distant, midrange, and near—they concluded that dry ports can effectively reduce energy consumption, minimize environmental damage, alleviate seaport congestion, and improve logistical support for cargo vessels in hinterland areas.

Chahshouri et al. [19] conducted a feasibility study for establishing a dry port at Bushehr Port using SWOT analysis. They noted that globalization and increased competition have compelled ports to enhance efficiency through various strategies, including physical expansion and collaboration with international port operators. However, physical expansion is not always feasible, particularly in urban settings. Their findings indicated that Bushehr Port's current strategic position is characterized by weaknesses and opportunities (WO).

Hazeri et al. [20] analyzed the hardware, economic, and environmental factors influencing dry port establishment in Anzali Port. Using a Delphi method combined with DEMATEL and ANP techniques, they identified and prioritized key factors. Their results revealed that environmental factors ranked first, followed by economic factors and hardware infrastructure, with protection of fertile land emerging as the highest-priority individual factor.

### 4.2 International Studies

Beresford and Dubey [21] examined the environmental impacts of dry ports, concluding that efficient use of inland terminals and transport equipment can significantly reduce greenhouse gas emissions and pollutant discharge. Their research emphasized the modal shift from road to rail for inland transport between dry ports and seaports.

ESCAP [22] defined a dry port as an inland terminal for cargo consolidation and distribution, possessing characteristics similar to seaports, including customs services. Facilities available at dry ports include container handling equipment, intermodal transport infrastructure, presence of logistics service providers, and value-added services such as customs valuation, tax payment, warehousing, maintenance, banking, and ICT services.

Roso et al. [15] specified that beyond basic intermodal services, dry ports should provide cargo warehousing, empty container storage and repair, comprehensive customs services, and other related logistics functions.

Roso et al. [13] introduced the dry port concept and classified dry ports into three categories—distant, midrange, and near—concluding that the dry port concept facilitates modal shift from road to more energy-efficient and environmentally sustainable transport systems. Their research demonstrated that dry ports relieve seaport cities of congestion, reduce environmental impact, and provide advanced logistics capabilities in the hinterland.

The InterBaltic project [23] conceptualized dry ports as "extended gateways" for seaports, enabling control and regulation of cargo flows based on seaport conditions. This perspective emphasizes that dry ports are more closely related to organizational, service, and commercial needs within supply chains than to purely physical infrastructure.

ESCAP [24] concluded that dry port development can promote regional trade and serve as seaport equivalents for landlocked countries. Furthermore, dry ports directly contribute to intermodal transport development and sustainable transport systems through modal shift from road to rail.

Henttu and Hilmola [25] studied the financial and environmental effects of dry port structures in Finland. Using analytical models and linear integer programming, they estimated the benefits of implementing the dry port concept in Finland's transport network. Their findings demonstrated that relative transport costs can be significantly reduced by increasing the number of dry port distribution locations, with optimal benefits achieved at up to six locations. Gravity models confirmed that Finland benefits from dry port implementation.

Nguyen et al. [26] examined the spatial dynamics of dry ports in developing economies, concluding that these differ substantially from Western advanced economies due to geographic diversity, varying regional development speeds, and local practices. Their research indicated that dry ports in developing economies tend toward cluster formation rather than supply chain integration. The Indian government, for

example, expects dry ports to catalyze regional economic development, with their establishment predicated on the assumption that dry ports can become self-sustaining and generate spillover effects.

Witte et al. [27] addressed the relationship between dry ports and regional economic development, noting that the economic dimension of dry port development has received relatively little systematic attention at the local and regional levels. They called for further research on the regional economic development impacts of dry ports.

Liu et al. [28] investigated the relationship between dry ports and regional economies using a gravity model and predictive analysis of 1,040 observations across 104 cities along the Yangtze River Economic Belt from 2008 to 2017. Variables included economic indicators, logistics variables, foreign relations variables, and human capital variables. Their results demonstrated a positive correlation between dry ports and trade volume. GDP per capita, road area, railway infrastructure, and foreign relations variables showed positive correlations with trade volume, while human capital did not exhibit a significant effect. Government policy implications concerning dry ports and industrial clusters resulting from foreign investment were also highlighted.

### 4.3 Research Gap

The literature review reveals that although substantial international research has addressed various aspects of dry ports—including their classification, environmental benefits, and role in logistics—relatively limited attention has been paid to the regional economic development impacts of dry ports, particularly in the context of developing economies and landlocked regions [27]. Furthermore, while several Iranian studies have examined feasibility, site selection, and implementation factors, there remains a notable gap in quantitative empirical research specifically evaluating the economic impact of existing or proposed dry ports on their surrounding regions. The present study aims to address this gap by investigating the impact of Yazd Dry Port on regional economic development in Iran.

## 5. Key Infrastructure Indicators for Yazd Dry Port

Based on an extensive review of the existing literature—encompassing both national and international studies related to the research topic—and the results of an expert panel evaluation, a total of 11 key indicators were identified as influential factors in the establishment of Yazd Dry Port and its impact on regional economic development. These indicators are presented in Table 2 and serve as the analytical foundation for this study. Furthermore, these indicators were operationalized as the core items in the final research questionnaire, forming the basis for data collection and subsequent statistical analysis.

**Table 2. Key Infrastructure Indicators for Yazd Dry Port Establishment and Regional Economic Development**

| No. | Indicator | Number of Sub-Indicators | Sources |
|---|---|---|---|
| 1 | Infrastructure availability | 3 | [18, 25] |
| 2 | Transit capacity | 3 | [17, 25, 13] |
| 3 | Security | 2 | [18] |
| 4 | Environment | 2 | [16] |
| 5 | Traffic congestion | 4 | [15, 16] |
| 6 | Centrality / Geographic position | 5 | [17] |
| 7 | Economic and financial factors | 13 | [17, 16, 25] |
| 8 | Employment and entrepreneurship | 4 | [29, 18] |
| 9 | Future development potential | 9 | [30, 25] |
| 10 | Accessibility | 3 | [18, 31, 16] |
| 11 | Proximity to production centers | 3 | [16] |

*Note.* These indicators were derived from the literature review and validated through expert panel evaluation.

## 6. Data Analysis and Results

This section is dedicated to the analysis of data using descriptive and inferential statistical methods. Following the collection of research questionnaires and the organization of the obtained data, this section presents the analysis of the data. Initially, the findings derived from descriptive statistics (including background, age, educational level, and position) are reported. Subsequently, the descriptive findings related to the research variables are presented, followed by an assessment of the data distribution. In the inferential statistics section, SPSS software was utilized to examine and prioritize various factors within each dimension. For the hypothesis testing, the one-sample t-test was employed, and the Friedman test was used for ranking the factors. Additionally, confirmatory factor analysis was conducted. The significance level for all tests was set at $\alpha = 0.05$.

### 6.1 Questionnaire Distribution and Collection

In this study, a total of 105 questionnaires were distributed among university professors and academic specialists, maritime transport experts, logistics and multimodal transport professionals, and economic analysts from the Ministry of Roads and Urban

Development with involvement in the Yazd Dry Port project. Of these, 96 fully completed and valid questionnaires were deemed suitable for further statistical analysis and hypothesis testing.

### 6.2 Demographic Characteristics of Respondents

This section presents the demographic characteristics of the respondents, including age, educational level, and professional experience. As shown in Table 3, the majority of respondents (32.3%) were in the 41–50 years age bracket, followed by those under 30 years (25.0%), those aged 31–40 years (21.9%), and those over 50 years (20.8%). This suggests that the majority of participants have attained a sufficient level of intellectual maturity and professional expertise, making them well-qualified to provide informed responses on the subject matter.

Regarding educational attainment, the majority of respondents (47.9%) held a Bachelor's degree, followed by those with a Master's degree or higher (20.8%), a Higher National Diploma (HND) (18.8%), and a high school diploma (12.5%). This indicates that the respondents possess a relatively high level of formal education, enhancing the credibility and reliability of their responses.

With respect to professional experience, the majority of respondents (53.1%) had 5 to 10 years of professional experience, followed by those with 10 to 15 years (25.0%), those with more than 15 years (11.5%), and those with less than 5 years (10.4%). This indicates that the majority of participants possess sufficient practical experience in their respective fields, further strengthening the validity of their expert judgments.

**Table 3. Demographic Characteristics of Respondents**

| Characteristic | Category | Frequency (n) | Percentage (%) |
|---|---|---|---|
| Age | Less than 30 years | 24 | 25.0 |
| | 31–40 years | 21 | 21.9 |
| | 41–50 years | 31 | 32.3 |
| | More than 50 years | 20 | 20.8 |
| Educational Level | Diploma | 12 | 12.5 |
| | HND | 18 | 18.8 |
| | Bachelor | 46 | 47.9 |
| | Master | 20 | 20.8 |
| Professional Experience | Less than 5 years | 10 | 10.4 |
| | 5–10 years | 51 | 53.1 |
| | 10–15 years | 24 | 25.0 |
| | More than 15 years | 11 | 11.5 |
| **Total** | | **96** | **100.0** |

*Note.* N = 96 respondents.

### 6.3 Normality Assessment of Data

Following the design of the main research questionnaire, it was distributed among the target population and collected. The data were then analyzed as described below.

A prerequisite for conducting all parametric statistical tests is the normality of the statistical distribution of the variables. In general, parametric tests are predominantly based on the mean and standard deviation. If the population distribution is not normal, accurate inferences cannot be drawn from the results. Therefore, this section first examines the normality of the variables using the Kolmogorov–Smirnov (K-S) test.

Table 4 presents the Kolmogorov–Smirnov test results for the observed variables included in the research model. As shown in the table, the skewness and kurtosis values for all variables fall within the acceptable range of –2 to +2. Consequently, it is concluded that the data distribution is normal, satisfying the assumption for parametric statistical tests.

**Table 4. Kolmogorov–Smirnov Normality Test Results**

| Indicator | Skewness | Kurtosis |
|---|---|---|
| Infrastructure availability | –0.34 | –0.16 |
| Transit capacity | 0.00 | –0.03 |
| Security | –0.37 | –0.34 |
| Environment | –0.15 | –0.33 |
| Traffic congestion | –0.40 | –0.22 |
| Centrality / Geographic position | –0.40 | –0.27 |
| Economic and financial factors | –0.26 | 0.29 |
| Employment and entrepreneurship | –0.76 | –0.63 |
| Future development potential | –0.76 | –0.67 |
| Accessibility | –0.86 | –0.37 |
| Proximity to production centers | –0.53 | –1.00 |

*Note.* Skewness and kurtosis values within the range of –2 to +2 indicate a normal distribution ([10, 11].

### 6.4 Inferential Analysis of Findings

In the inferential statistics section, the following tests were employed to accept or reject the research hypothesis:

Research Hypothesis: The effective infrastructure indicators of Yazd Dry Port have a positive and significant impact on regional economic development.

#### 6.4.1 Factor Analysis of Questionnaire Data (Factor Loading Analysis)

Prior to testing the research hypothesis, the factor loadings of the items associated with each variable were examined to ensure the validity of the data for analysis. Factor analysis was employed to determine the factor loading of each component (questionnaire item).

**KMO Test:**

If the KMO value is less than 0.5, the data are not suitable for factor analysis. Values between 0.5 and 0.69 indicate moderate suitability, while values greater than 0.7 indicate that the correlations among the data are appropriate for factor analysis (Kaiser, 1974).

## Bartlett's Test:

Bartlett's test of sphericity examines the null hypothesis that the observed correlation matrix belongs to a population with independent variables. For a factor model to be meaningful and useful, the variables must be correlated. Therefore, prior to factor analysis, a correlation matrix among the variables must be constructed. The correlation matrix is a square matrix of correlation coefficients between variables.

Table 5 presents the results of the KMO and Bartlett's tests. The KMO value was 0.77, indicating that the data are suitable for reduction to underlying factors and that the correlations among the data are appropriate for factor analysis. The significance level of Bartlett's test was less than 0.05, indicating that the correlation matrix is not an identity matrix. This means that there are high correlations among the components within each variable, while no significant correlations exist between components of different variables.

**Table 5. KMO and Bartlett's Test Results**

| Test | | Value |
|---|---|---|
| **KMO Measure of Sampling Adequacy** | | 0.77 |
| **Bartlett's Test of Sphericity** | Approx. Chi-Square | 686.36 |
| | Degrees of Freedom (df) | 91 |
| | Significance (p-value) | 0.000 |

*Note.* KMO > 0.7 indicates data are suitable for factor analysis. Bartlett's test $p < 0.05$ indicates the correlation matrix is not an identity matrix.

To determine the extent to which the measurement indicators (observed variables) are acceptable for measuring the latent variables, the minimum acceptable factor loading is 0.3 [32]. As shown in Table 6, the factor loadings for all components exceed 0.3, with values ranging from 0.62 to 0.89. Therefore, none of the questionnaire items were excluded, and all 52 items play a significant and determinative role in this research.

**Table 6. Factor Loadings of Questionnaire Items**

| Indicator | Item No. | Factor Loading | Indicator | Item No. | Factor Loading |
|---|---|---|---|---|---|
| **Infrastructure availability** | 1 | 0.73 | **Employment and entrepreneurship** | 33 | 0.73 |
| | 2 | 0.75 | | 34 | 0.76 |
| | 3 | 0.76 | | 35 | 0.82 |
| **Transit capacity** | 4 | 0.71 | | 36 | 0.81 |
| | 5 | 0.74 | **Future development potential** | 37 | 0.77 |
| | 6 | 0.76 | | 38 | 0.71 |
| **Security** | 7 | 0.80 | | 39 | 0.74 |
| | 8 | 0.71 | | 40 | 0.65 |
| **Environment** | 9 | 0.76 | | 41 | 0.77 |
| | 10 | 0.69 | | 42 | 0.84 |
| **Traffic congestion** | 11 | 0.73 | | 43 | 0.75 |
| | 12 | 0.80 | | 44 | 0.76 |
| | 13 | 0.85 | | 45 | 0.75 |
| **Centrality** | 14 | 0.77 | **Accessibility** | 47 | 0.89 |
| | 15 | 0.64 | | 48 | 0.79 |
| | 16 | 0.82 | | 49 | 0.74 |
| | 17 | 0.72 | **Proximity to production centers** | 50 | 0.77 |
| | 18 | 0.80 | | 51 | 0.79 |
| | 19 | 0.80 | | 52 | 0.71 |
| **Economic and financial factors** | 20 | 0.71 | | | |
| | 21 | 0.78 | | | |
| | 22 | 0.73 | | | |
| | 23 | 0.78 | | | |
| | 24 | 0.87 | | | |
| | 25 | 0.83 | | | |
| | 26 | 0.80 | | | |
| | 27 | 0.83 | | | |
| | 28 | 0.69 | | | |
| | 29 | 0.73 | | | |
| | 30 | 0.79 | | | |
| | 31 | 0.74 | | | |
| | 32 | 0.62 | | | |

*Note.* All factor loadings exceed the minimum acceptable threshold of 0.3 [32], indicating that all items significantly contribute to their respective constructs.

### 6.4.2 Reliability Analysis of the Questionnaire

Reliability, or dependability, is one of the technical characteristics of a measurement instrument. This concept concerns the extent to which a measurement instrument yields consistent results under identical conditions. The reliability coefficient ranges from 0 to 1, and the closer this coefficient is to 1, the higher the reliability. In this study, Cronbach's alpha coefficient was employed to determine the reliability of the questionnaire. This method is used to calculate the internal consistency of the measurement instrument.

As shown in Table 7, the Cronbach's alpha values for all variables exceeded the acceptable threshold of 0.70, with the overall questionnaire achieving a Cronbach's alpha of 0.89. Therefore, it can be concluded that the questionnaire possesses good reliability, confirming that the data collected are suitable for testing the research hypothesis: *The effective infrastructure indicators of Yazd Dry Port have a positive and significant impact on regional economic development.*

**Table 7. Reliability Coefficients (Cronbach's Alpha) of Research Variables**

| Variable | Item Numbers | Cronbach's Alpha |
|---|---|---|
| Infrastructure availability | 1–3 | 0.76 |
| Transit capacity | 4–6 | 0.75 |
| Security | 7–8 | 0.73 |
| Environment | 9–10 | 0.82 |
| Traffic congestion | 11–14 | 0.83 |
| Centrality / Geographic position | 15–19 | 0.73 |
| Economic and financial factors | 20–32 | 0.76 |
| Employment and entrepreneurship | 33–36 | 0.72 |
| Future development potential | 37–46 | 0.73 |
| Accessibility | 47–49 | 0.75 |
| Proximity to production centers | 50–52 | 0.88 |
| **Total Questionnaire** | **1–52** | **0.89** |

*Note.* Cronbach's alpha values above 0.70 indicate acceptable internal consistency [12].

### 6.4.3 Hypothesis Testing

**Research Hypothesis:** The effective infrastructure indicators of Yazd Dry Port have a positive and significant impact on regional economic development.

To examine the effective infrastructure indicators of Yazd Dry Port on regional economic development—namely, infrastructure availability, transit capacity, security, environment, traffic congestion, centrality, economic and financial factors, employment and entrepreneurship, future development potential, accessibility, and proximity to production centers (shown in Table 8)—a one-sample t-test was employed. This test compares the mean of a variable against a specified value and determines whether the observed difference is statistically significant.

Since all questionnaire items were measured on a 5-point Likert scale, the hypothetical mean (test value) was set at 3 (the neutral/midpoint value). By comparing the obtained results, it is possible to determine whether there is a statistically significant difference between the mean of each variable and the midpoint value of 3.

The hypotheses for this test are:

**$H_0$:** There is no statistically significant difference between the variable mean and the midpoint value of 3.

**$H_1$:** There is a statistically significant difference between the variable mean and the midpoint value of 3.

**Table 8. Descriptive Statistics of Infrastructure Indicators for Regional Economic Development**

| Indicator | N | Mean | Standard Deviation | Standard Error Mean |
|---|---|---|---|---|
| Infrastructure availability | 96 | 3.33 | 0.99 | 0.10 |
| Transit capacity | 96 | 3.31 | 0.87 | 0.09 |
| Security | 96 | 3.75 | 0.74 | 0.08 |
| Environment | 96 | 3.39 | 0.81 | 0.08 |
| Traffic congestion | 96 | 3.47 | 0.74 | 0.08 |
| Centrality / Geographic position | 96 | 3.37 | 0.80 | 0.08 |
| Economic and financial factors | 96 | 3.60 | 0.55 | 0.06 |
| Employment and entrepreneurship | 96 | 3.43 | 1.41 | 0.14 |
| Future development potential | 96 | 3.42 | 1.20 | 0.12 |
| Accessibility | 96 | 3.56 | 1.27 | 0.13 |
| Proximity to production centers | 96 | 3.43 | 1.30 | 0.13 |

As shown in Table 9, the results of the one-sample t-test indicate that at the 99% confidence level, the significance level (p-value) for all variables is less than 0.05, and the t-statistic for all research variables exceeds the critical value of 1.96. Furthermore, there is a statistically significant positive difference between the mean of each infrastructure indicator and the midpoint value of 3. Therefore, it can be concluded that the infrastructure indicators of Yazd Dry Port have a positive and significant impact on regional economic development, and the research hypothesis is supported.

**Table 9. One-Sample t-Test Results Comparing Mean Infrastructure Indicators Affecting Economic Development**

| Test Value = 3 | | | | | | |
|---|---|---|---|---|---|---|
| | | | | | 95% Confidence | |
| **Indicator** | **t** | **df** | **Sig. (2-tailed)** | **Mean Difference** | **Lower** | **Upper** |
| Infrastructure availability | 3.28 | 95 | 0.00 | 0.33 | 0.13 | 0.53 |
| Transit capacity | 3.43 | 95 | 0.00 | 0.31 | 0.13 | 0.48 |
| Security | 9.98 | 95 | 0.00 | 0.75 | 0.60 | 0.90 |
| Environment | 4.67 | 95 | 0.00 | 0.39 | 0.22 | 0.55 |
| Traffic congestion | 6.27 | 95 | 0.00 | 0.47 | 0.32 | 0.62 |
| Centrality / Geographic position | 4.52 | 95 | 0.00 | 0.37 | 0.21 | 0.53 |
| Economic and financial factors | 10.60 | 95 | 0.00 | 0.60 | 0.48 | 0.71 |
| Employment and entrepreneurship | 2.98 | 95 | 0.00 | 0.43 | 0.14 | 0.72 |
| Future development potential | 3.40 | 95 | 0.00 | 0.42 | 0.17 | 0.66 |
| Accessibility | 4.27 | 95 | 0.00 | 0.56 | 0.30 | 0.81 |
| Proximity to production centers | 3.23 | 95 | 0.00 | 0.43 | 0.16 | 0.69 |

*Note.* df = degrees of freedom. A p-value < 0.05 indicates a statistically significant difference from the test value of 3. All variables show a positive mean difference, confirming a positive and significant impact on regional economic development.

### 6.4.4 Friedman Test Results for Ranking Infrastructure Indicators

The Friedman test was employed to prioritize and rank the infrastructure indicators of Yazd Dry Port affecting regional economic development based on their relative importance within the studied components. To examine the hypothesis that the rankings of the variables are equal, the following hypotheses were proposed:

**$H_0$:** The priorities of the variables are equal (there is no significant difference between the mean ranks of the variables).

**$H_1$:** At least two priorities are different (there is a significant difference between the mean ranks of the variables).

If the significance level (p-value) of the test statistic is less than the significance level ($\alpha = 0.05$), the null hypothesis is rejected, and the claim that the rankings of the variables are equal is not accepted. The ranking of the infrastructure indicators is presented in Table 10.

**Table 10. Mean Ranks of Infrastructure Indicators**

| Indicator | Mean Rank | Rank Priority |
|---|---|---|
| Infrastructure availability | 5.50 | 9 |
| Transit capacity | 5.24 | 11 |
| **Security** | **7.04** | **1** |
| Environment | 5.57 | 8 |
| Traffic congestion | 5.65 | 7 |
| Centrality / Geographic position | 5.40 | 10 |
| Economic and financial factors | 6.42 | 3 |
| Employment and entrepreneurship | 6.29 | 4 |
| Future development potential | 6.17 | 5 |
| Accessibility | 6.59 | 2 |
| Proximity to production centers | 6.13 | 6 |

As shown in Table 11, the significance level of the Friedman test statistic is 0.000, which is less than 0.05. This indicates a significant difference among the rankings. In other words, the alternative hypothesis ($H_1$)—that at least two priorities are different—is accepted, and the null hypothesis is rejected. It is noteworthy that the infrastructure indicators have varying impacts on the economic development of Yazd Dry Port, with security ranking as the most important factor among all components.

**Table 11. Friedman Test Results**

| Test Statistic | Value |
|---|---|
| Sample Size (N) | 96 |
| Chi-Square ($\chi^2$) | 28.79 |
| Degrees of Freedom (df) | 10 |
| Significance (p-value) | 0.000 |

*Note.* A p-value < 0.05 indicates a significant difference among the rankings.

## 7. Discussion

The primary objective of this study was to investigate the impact of the infrastructure indicators of Yazd Dry Port on regional economic development. The findings provide empirical evidence supporting the research hypothesis that the effective infrastructure indicators of Yazd Dry Port have a positive and significant impact on regional economic development.

### 7.1 Interpretation of Findings

The one-sample t-test results (Table 7) revealed that all 11 infrastructure indicators had mean scores significantly above the midpoint value of 3, with p-values < 0.001 for all variables. The highest mean scores were observed for security (M = 3.75, t = 9.98), economic and financial factors (M = 3.60, t = 10.60), and accessibility (M = 3.56, t = 4.27). These findings suggest that from the perspective of experts and specialists, these three factors are the most critical infrastructure components influencing the economic development of the Yazd Dry Port.

The Friedman test results (Table 8) further corroborated these findings, with security ranking first (mean rank = 7.04), followed by accessibility (mean rank = 6.59) and economic and financial factors (mean

rank = 6.42). Conversely, transit capacity (mean rank = 5.24) and centrality (mean rank = 5.40) ranked lowest, indicating that while these factors remain significant, they are perceived as relatively less critical compared to other indicators.

The predominance of security as the highest-ranked factor is noteworthy. This finding aligns with the research of Saeidi et al. [18], who emphasized the importance of security in dry port operations, particularly given the high-value nature of containerized cargo and the need for customs inspection and anti-smuggling measures [13]. Security concerns at dry ports extend beyond physical security to encompass cargo integrity, customs compliance, and the prevention of illicit activities, all of which are fundamental to attracting international trade and investment [26].

The high ranking of accessibility is consistent with the dry port literature. Roso et al. [13] identified accessibility as a key criterion for dry port location, emphasizing that dry ports must be easily and economically accessible to serve their function as extended gateways for seaports. The fact that accessibility ranked second in this study underscores its critical role in ensuring efficient cargo flow between the dry port, seaports, and hinterland areas.

The third-ranked factor, economic and financial factors, reflects the findings of Henttu and Hilmola [25] and Liu et al. [28], who demonstrated that dry ports can significantly reduce transport costs and stimulate economic growth through enhanced trade volumes and foreign direct investment. The substantial number of sub-indicators under this dimension (13 items) in Table 1 further indicates its multifaceted nature, encompassing investment incentives, tax policies, financial institutions, and operational cost efficiencies.

The relatively lower rankings of transit capacity and centrality suggest that while these factors are essential, they may already be adequately addressed in the Yazd context or are perceived as less critical compared to other pressing concerns. However, this does not diminish their importance; as noted by Sheikholeslami et al. [17], transit capacity and geographical centrality remain fundamental to the strategic positioning of dry ports within national and international transport corridors.

### 7.2 Comparison with Previous Studies

The findings of this study are broadly consistent with international research on dry port economic impacts. Liu et al. [28], in their study of 104 cities along the Yangtze River Economic Belt, found that dry ports had a positive correlation with trade volume, and that GDP per capita, road infrastructure, railway infrastructure, and foreign relations variables positively correlated with trade volume. Similarly, the present study confirms that economic and financial factors, accessibility, and infrastructure availability are significant determinants of dry port success.

Witte et al. [27] noted that the regional economic development dimension of dry ports has received relatively little systematic attention. The present study addresses this gap by providing empirical evidence from the Iranian context, demonstrating that infrastructure indicators significantly contribute to regional economic development.

Nguyen et al. [26] observed that dry ports in developing economies tend toward cluster formation rather than supply chain integration. This is particularly relevant to the Yazd Dry Port, given its strategic location at the intersection of six national railway lines and its proximity to the special economic zone in Yazd province. The clustering effect may amplify the economic benefits identified in this study, as the concentration of logistics activities can generate synergies and spillover effects [23].

### 7.3 Theoretical Implications

This study contributes to the theoretical literature on dry port economics in several ways. First, it provides empirical validation of the conceptual framework proposed by Roso et al. [13], demonstrating that the three dry port typologies (distant, midrange, and near) can be operationalized through measurable infrastructure indicators. Second, it extends the work of Liu et al. [28] by applying their economic model to a new geographical context—Iran—thereby enhancing the generalizability of their findings. Third, it responds to the call by Witte et al. [27] for more systematic attention to the regional economic dimension of dry port development.

### 7.4 Practical Implications

The findings of this study have several practical implications for policymakers, transport planners, and infrastructure developers:

1. **Investment Prioritization:** Given that security, accessibility, and economic factors ranked highest, policymakers should prioritize investments in security infrastructure (surveillance systems, customs facilities, and cargo tracking), accessibility improvements (road and rail connectivity), and financial incentives (tax breaks, foreign investment facilitation).
2. **Public-Private Partnerships:** The challenges of government support limitations identified in this study suggest that public-private partnerships may be an effective mechanism for financing and operating dry port infrastructure. Clear delineation of responsibilities between government agencies and private operators is essential.
3. **Integrated Planning:** The importance of accessibility and centrality underscores the need for integrated transport planning that connects dry ports to national railway networks, highways, and

seaports. The Yazd Dry Port's location at the intersection of six railway lines provides a unique opportunity for seamless intermodal connectivity.

4. **Environmental Sustainability:** While environmental factors ranked eighth in the Friedman test (mean rank = 5.57), the modal shift from road to rail inherent in the dry port concept can significantly reduce carbon emissions [14]. Policymakers should leverage the environmental benefits of dry ports to attract international funding and comply with global sustainability standards.

### 7.5 Limitations of the Study

While this study provides valuable insights, several limitations should be acknowledged:

1. **Regional Specificity:** The findings are based on a single case study of Yazd Dry Port. The generalizability of the results to other Iranian dry ports or developing country contexts may be limited.
2. **Cross-Sectional Design:** The study employed a cross-sectional survey design, capturing perceptions at a single point in time. Longitudinal studies would be valuable to assess changes in infrastructure indicators and their economic impacts over time.
3. **Subjective Data:** The data were collected through self-reported questionnaires, which may be subject to response bias. Future research could incorporate objective economic indicators (GDP growth, employment statistics, trade volumes) to complement perceptual data.
4. **Limited Geographic Scope:** The study focused on a single province. Comparative studies across multiple dry ports in Iran (e.g., Sarakhs, Zahedan, Anzali) would provide a more comprehensive understanding of dry port economic impacts.

## 8. Conclusion

This study investigated the impact of 11 infrastructure indicators on the economic development of Yazd Dry Port. The findings confirm that all identified indicators have a positive and significant impact on regional economic development, with security, accessibility, and economic and financial factors emerging as the most critical determinants.

The strategic location of Yazd at the intersection of six national railway lines and its proximity to the special economic zone position it as a potential logistics hub capable of serving both national and international trade corridors. However, realizing this potential requires overcoming significant challenges, including limited government support, unclear executive frameworks, and coordination gaps among stakeholders.

The establishment of dry ports in Iran represents a very important opportunity for economic diversification, job creation, and sustainable development. With a better understanding of the environment and available tools, the implementation process can be accelerated, and the benefits of such ports can be fully realized. As developing countries increasingly turn to dry ports to enhance trade connectivity and regional economic growth, the insights from this study provide valuable guidance for policymakers, transport planners, and infrastructure developers in Iran and similar contexts.

## 9. References


[1] World Trade Organization. (2024). *World Trade Statistical Review 2024*. WTO Publications.

[2] ESCAP. (2024). *Asia-Pacific Trade and Investment Report 2024*. United Nations.

[3] Roso, V. (2009a). The dry port concept: Connecting container seaports with the hinterland. *Journal of Transport Geography*, *17*(5), 338–345. https://doi.org/10.1016/j.jtrangeo.2008.10.008

[4] Notteboom, T., & Rodrigue, J. P. (2009). Inland terminals within North American and European supply chains. *Transport and communications bulletin for Asia and the Pacific*, *78*(1), 1-39.

[5] Roso, V., & Lumsden, K. (2010). The emergence and significance of dry ports: The case of the Port of Goteborg. *Transport Research International Documentation (TRID)*.

[6] Hatami Nasab, S. H., Sanayei, A., Amiri Aghdaei, S. F., & Kazemi, A. (2016). Using dry ports to facilitate international trade in Iran: A model of success factors for implementation of dry ports. *Mathematical Models and Methods in Applied Sciences*, *10*, 155. (in Persian).

[7] Golghamat Raad, N., & Rajendran, S. (2024). A hybrid scenario-based fuzzy stochastic model for closed-loop dry port network design with multiple robustness measures. *Transportation Research Part E: Logistics and Transportation Review*. (in Persian).

[8] Abbasi, M., & Pishvaee, M. S. (2018). A novel three-stage fuzzy GIS-MCDA approach to the dry port site selection problem: A case study of Shahid Rajaei Port in Iran. *Computers & Industrial Engineering*. (in Persian).

[9] Creswell, J. W., & Creswell, J. D. (2018). *Research design: Qualitative, quantitative, and mixed methods approaches* (5th ed.). SAGE Publications.

[10] Hair, J. F., Black, W. C., Babin, B. J., & Anderson, R. E. (2019). *Multivariate data analysis* (8th ed.). Cengage Learning.

[11] Field, A. (2018). *Discovering statistics using IBM SPSS statistics* (5th ed.). London: SAGE Publications.

[12] Nunnally, J. C. (1978). Psychometric theory. McGraw-Hill, New York. In Lance, CE, Butts, MM, and Michaels, LA (2006). The sources of four commonly reported cut-off criteria: what did they really say?. *Organisational Research Methods*, *9*(2), 202-220.

[13] Roso, V., Woxenius, J., & Lumsden, K. (2009). The dry port concept: Connecting container seaports with the hinterland. *Journal of Transport Geography*, *17*(5), 338–345. https://doi.org/10.1016/j.jtrangeo.2008.10.008

[14] Roso, V. (2009b). The emergence and significance of dry ports: The case of the Port of Goteborg. *World Review of Intermodal Transportation Research*, *2*(4), 296–310.

[15] Roso, V., Woxenius, J., & Lumsden, K. (2006). The dry port concept: A strategic approach to the hinterland. In *Proceedings of the 18th Annual Conference for Nordic Researchers in Logistics (NOFOMA)*. https://doi.org/10.1016/j.jtrangeo.2008.10.008

[16] Dadvar, M., et al. (2010). The importance of establishing dry ports for logistics development in Iran. (in Persian).

[17] Sheikholeslami, A., Barati, H., Eftekhari, Y., Yeganeh, Y., & Ilati, Gh. (2011). Investigating the impact of dry ports on alleviating the problems of coastal ports. *Darya va Keshti* (Sea and Ship), 2(1), 5–15. (in Persian).

[18] Saeidi, S. N., Nooramin, A. S., Javadpour, M., & Motahari, A. H. (2011). The concept of the dry port with a special focus on the need for its establishment in Iran. *Darya va Keshti* (Sea and Ship), 2(1), 39–54. (in Persian).

[19] Chahshouri, H., Bavarsad, P., & Delbar, Gh. (2020). Feasibility study of establishing a dry port at the Port of Bushehr using the SWOT technique. Journal of Marine Science and Technology, 24(94), 32-41. (in Persian).

[20] Hazeri, H., Hashemi Dizaj, A., Jafari, M., & Emadi, S.J. (2023). Analysis of hardware, economic, and environmental factors in the establishment of a dry port in Anzali County. Environmental Science Studies, 8(2), pp. 6310-6325. (in Persian). doi: 10.22034/jess.2022.347835.1812.

[21] Beresford, A. K., & Dubey, R. C. (1990). *Handbook on the management and operation of dry ports*. UNCTAD.

[22] ESCAP. (2006). *Ministerial Conference on Transport, Busan, Republic of Korea, 6–11 November 2006*. United Nations.

[23] InterBaltic Project. (2008). *Research on the dry port concept as an intermodal node in the Baltic Sea Region*. BSR Interreg III B NP Inloc Project.

[24] ESCAP. (2010). *Resolution 66/4: Implementation of the Bangkok Declaration on Transport Development in Asia*. United Nations.

[25] Henttu, V., & Hilmola, O. P. (2011). Financial and environmental impacts of hypothetical Finnish dry port structure. *Research in Transportation Economics*, *33*(1), 35-41. https://doi.org/10.1016/j.retrec.2011.08.004

[26] Nguyen, L. C., Thai, V. V., Nguyen, D. M., & Tran, M. D. (2021). Evaluating the role of dry ports in the port-hinterland settings: Conceptual framework and the case of Vietnam. *The Asian Journal of Shipping and Logistics,* 37(4), 307-320. https://doi.org/10.1016/j.ajsl.2021.09.001

[27] Witte, P., Wiegmans, B., & Ng, A. K. (2019). A critical review on the evolution and development of inland port research. *Journal of Transport Geography*, *74*, 53-61. https://doi.org/10.1016/j.jtrangeo.2018.11.001

[28] Liu, Y. F., Lee, C. B., Qi, G. Q., Yuen, K. F., & Su, M. (2021). Relationship Between Dry Ports and Regional Economy: Evidence from Yangtze River Economic Belt. *The Journal of Asian Finance, Economics and Business (JAFEB)*, *8*(5), 345-354.

[29] Trainaviciute, L., Bentzen, K., Caruso, A., & Laugesen, M. (2009). The dry port–concept and perspectives. *Pobrano z: http://archive. northsearegion. eu/files/repository/20130301142236_WPC-TheDryPortConcept. pdf (10.03. 17)*.

[30] Zimmer, N. R. (1996). Designing intermodal terminals for efficiency. *Transportation Research Circular*, *459*, 99-109.

[31] de Almeida Rodrigues, T., de Miranda Mota, C. M., & dos Santos, I. M. (2021). Determining dry port criteria that support decision making. *Research in Transportation Economics*, *88*, 100994. https://doi.org/10.1016/j.retrec.2020.100994

[32] Kalantari, K. (2009). *Data processing and analysis in socio-economic research using SPSS.* (in Persian).

INTERNATIONAL JOURNAL OF
COASTAL, OFFSHORE & ENVIRONMENTAL ENGINEERING IJCOE Vol.11/No. 4/Autumn 2026 (15-31)

Available online at: www. Ijcoe.org

# Factors Influencing the Enhancement of Marine Oil Spill Response Operations: Application of Interpretive Structural Modeling at Chabahar Port

**Jasem Raeisi[1], Jafar Sayareh[2*]**

*[1] MSc. In Maritime Transport, Chabahar Maritime University, Chabahar, Iran;*
*jasemraesi@gmail.com*
*[2*] Associate Prof., Maritime Transport Department, Chabahar Maritime University, Chabahar, Iran;*
*j.sayareh@gmail.com*

**ARTICLE INFO**

*Article History:*
Received: 9 July
Accepted: 16 Oct
Available online ….

*Keywords:*
**Marine Oil Pollution,**
**Response Operations,**
**ISM Method,**
**MICMAC Analysis,**
**Chabahar Port**

**ABSTRACT**

Marine oil pollution is a major environmental challenge that threatens marine ecosystems, coastal economies, and human health. As Iran's only ocean port, handling a high volume of ocean-going vessel traffic, Chabahar Port faces a significant risk of oil-related incidents. Despite existing research on the detection and cleanup of oil pollution, the literature lacks a study that comprehensively identifies the factors influencing the improvement of response operations and establishes a causal hierarchy among them. This study was conducted to identify and hierarchically classify these factors at Chabahar Port. This study is applied in terms of objective, descriptive-survey in terms of data collection, and quantitative in nature. The statistical population consisted of personnel from the Maritime Affairs Division of the Sistan and Baluchestan Ports and Maritime Administration, shipping companies, and the Department of Environment (N=35); 30 individuals participated via purposive non-random sampling. Through a systematic review of domestic and international literature, 22 influential factors were identified. Questionnaire reliability was assessed using Cronbach's alpha coefficient based on a pilot sample of 10 participants. Content validity was evaluated via the Delphi method over two rounds involving 20 experts (Kendall's coefficient = 0.92; Sig < 0.05). Finally, the factors were categorized using Interpretive Structural Modeling (ISM) and MICMAC analysis.

All 22 factors were validated through the Delphi process. The ISM results classified the factors into three causal levels; the third-level factors—comprising the identification of pollution sources, infrastructure development, and international standards—exhibited the highest driving power and the lowest dependence, identifying them as the system's primary drivers. Based on the MICMAC analysis, the factors were categorized into four groups: independent, dependent, linkage, and autonomous.

The results indicated that one factor fell into the independent group, three into the dependent group, and eighteen into the linkage group. It can be concluded that by identifying and prioritizing these influential factors, financial, human, and technical resources for combating marine oil pollution can be allocated more effectively, thereby preventing resource wastage or allocation errors. This prioritization of resources can serve as a basis for strategic planning by managers in this field.

## 1. Introduction

Oil spills into the marine environment are among the most significant environmental disasters, causing extensive adverse impacts on marine and coastal ecosystems. Such pollution can lead to the mortality of marine organisms, destruction of natural habitats, and loss of biodiversity. Oil spills reaching coastal areas can also cause coastal erosion, damage tourism resources, and reduce the economic productivity of

coastal regions. In this context, oil spill response operations encompass a range of physical, chemical, and biological methods aimed at mitigating the environmental impacts of oil. For example, physical methods such as booms and sorbents are used to contain and recover spilled oil, while chemical methods such as dispersants are employed to accelerate the dispersion and removal of oil from the water. In addition, biological techniques, including the use of oil-degrading bacteria, have attracted attention as a sustainable response strategy. Among the factors influencing the success of oil spill response operations are the physicochemical properties of the oil, marine environmental conditions, the type of affected shoreline, and the speed of response to the incident. These factors play a decisive role in determining the appropriate response method and its effectiveness. For instance, heavy and viscous oils generally require more complex cleanup methods because of their higher density and greater persistence [1, 2, 3].

Ineffective and improper implementation of marine oil spill response operations can result in serious environmental, economic, and human health consequences. Inadequate response measures may damage marine habitats and cause the mortality of marine species and aquatic birds. Furthermore, inappropriate long-term management of oil pollution can have persistent adverse effects on the environment, while restoration and recovery may require considerably more time and financial resources [4].

Another important concern is that improper response operations can adversely affect local industries that depend on marine resources. Oil pollution can negatively affect various economic sectors, including fisheries, coastal tourism, and maritime transportation, while ineffective response measures may further intensify these impacts. Moreover, oil pollution can pose risks to human health through direct contact with contaminants or through the consumption of contaminated seafood [5].

Improper oil spill response operations can also contribute to the degradation of biodiversity and the loss of various marine species. Therefore, the proper and effective implementation of response operations is essential for mitigating these risks and protecting the environment, the economy, and human health [6].

Various methods are used to clean up oil pollution from marine and coastal environments, including physical methods (booms and skimmers), chemical methods (dispersants), natural and synthetic sorbents, high-pressure hot-water washing, mechanical recovery, and bioremediation [7].

In Iran, the Law on the Protection of Seas and Navigable Rivers against Oil Pollution, enacted in 2010, stipulates that protective and preventive measures must be undertaken by the responsible institutions and operators of all vessels and oil-related facilities operating in the country's internal waters [8].

Oil recovery from the water surface is the stage that follows the containment of an oil spill during spill cleanup operations and is generally considered one of the most important stages of pollution removal. A key objective of containment is to increase the concentration of spilled oil, thereby increasing the thickness of the oil layer and facilitating its recovery. These two stages are usually performed simultaneously. Following the deployment of booms to contain the spill and ensure the effectiveness of the containment operation, personnel and equipment must be dispatched to the affected area immediately. When the spilled oil becomes widely dispersed across the water surface, its recovery becomes difficult and, in some cases, impossible [9].

Coastal refinery facilities, offshore oil platforms, tanker operations, tanker accidents, and the discharge of contaminated waters and rivers into the sea are among the major sources of marine oil pollution. Adverse environmental impacts, mortality of marine organisms, contamination of seafood and its resulting unsuitability for human consumption, and reduced flight capability of seabirds due to oil contamination of their feathers are among the consequences of the release of light and heavy crude-oil compounds into the marine environment. The cost of oil spill recovery depends on factors such as the type of petroleum hydrocarbons, the severity of the spill, the geographical and economic characteristics of the affected area, weather and sea conditions, and the recovery method employed, and may reach substantial levels. Although preventing oil spills is always the preferred strategy, an effective and timely response to an incident requires sufficient knowledge and awareness of the various oil spill recovery methods [10].

Chabahar Port is one of the most important and busiest ports in Iran. It is located in Sistan and Baluchestan Province in southeastern Iran, along the southern coast of the Gulf of Oman. As Iran's only oceanic port, Chabahar has two equipped terminals with an annual cargo-handling capacity of 8.5 million tons, allowing ocean-going vessels to berth at its facilities. Currently, more than 60% of the country's essential commodities are imported through this port, and it is the only Iranian port exempt from any sanctions. Accordingly, given its geographical location and economic, commercial, and tourism significance, Chabahar Port plays an important role in the economic and social development of both the region and the country [11].

Oil pollution in Chabahar Port may result from incidents such as oil leakage or spills from oil transportation vessels or illegal discharges into the sea. Such pollution can threaten the environment, the economy, and human health and directly affect the port as one of Iran's major economic and commercial ports. Therefore, the present study aims to identify and prioritize the factors affecting the improvement of oil spill response operations in the waters of Chabahar

Port. Accordingly, the study seeks to answer the following research questions:

a) What factors affect the improvement of marine oil spill response operations?
b) How should the factors affecting the improvement of marine oil spill response operations be prioritized?

## 2. Literature Review

### 2.1 Marine Oil Pollution and Oil Spill Response Operations

Pollution refers to the introduction or presence of harmful and undesirable substances in the environment that can adversely affect human health, animals, plants, and ecosystems. These pollutants originate from various sources, including industrial activities, transportation, agriculture, and other human activities, and can enter the air, water, and soil. Pollution may occur continuously or intermittently and can have direct and indirect consequences, including increased disease incidence, deterioration of air, water, and soil quality, reduced agricultural productivity, destruction of natural habitats, and exacerbation of climate change. Reducing pollution requires the adoption of cleaner technologies, effective implementation of environmental laws and regulations, increased public awareness, material recycling, efficient resource use, and promotion of sustainable lifestyles [12].

Marine water pollution is one of the major challenges to environmental protection and the sustainability of marine ecosystems. It refers to the introduction of harmful substances and pollutants into oceans, seas, and coastal areas. These pollutants originate from various sources, including the discharge of municipal and industrial wastewater, agricultural runoff containing fertilizers and chemical pesticides, chemical industry activities, oil and gas operations, and marine accidents. In addition, the introduction of plastic waste and microplastics into the marine environment poses a serious threat to aquatic life and biodiversity. The continuation of these processes can lead to declines in biodiversity and aquatic resources, the accumulation of chemical pollutants, and increased environmental and health risks in marine and coastal areas. Addressing marine water pollution requires effective wastewater control and treatment, proper waste management, the application of clean and water-treatment technologies, and the promotion of environmentally responsible behaviors [13].

Marine pollution originating from petroleum sources is one of the most significant threats to the health of marine ecosystems and the environment. This type of pollution can result from oil discharges from vessels, oil leaks from tankers and oil and gas facilities, drilling accidents, and offshore oil platform activities. By forming a layer on the water surface, oil can disrupt oxygen exchange and essential biological processes in aquatic organisms and seabirds, potentially causing marine mortality, reduced growth and reproduction, disruption of food chains, and degradation of marine habitats. Other consequences include reductions in aquatic stocks and catches, deterioration of water quality, damage to coastal tourism, and economic losses. Human exposure to contaminated water or consumption of contaminated seafood may also pose health risks, including skin, respiratory, and gastrointestinal problems. Therefore, the prevention and control of oil pollution require the strengthening of environmental standards and regulations, continuous monitoring of petroleum sources, enhancement of preparedness for oil spill response, and the use of advanced technologies for the cleanup and treatment of contaminated waters [14].

Marine oil spill response is a complex, multi-stage process that requires planning, interorganizational coordination, and the application of appropriate technologies. First, the location of the spill and the extent and volume of contamination are determined using monitoring systems, aerial and marine surveillance, and other detection technologies. In the next stage, the most appropriate response strategy is selected based on the volume and type of oil, sea conditions, spill location, and the sensitivity of the affected area. Such strategies may include mechanical containment and recovery, the use of sorbents, or chemical treatment methods. Following the declaration of an emergency, coordination among maritime forces, environmental organizations, and other relevant agencies is undertaken to implement the response operation. The use of advanced equipment and technologies, including oil recovery and cleanup systems, specialized vessels, aircraft, unmanned aerial vehicles, and robots, can enhance the effectiveness of response operations. Finally, post-response monitoring and assessment are conducted to evaluate the extent of cleanup, identify residual pollution, and assess its environmental and social impacts. Overall, successful oil spill response depends on effective planning, coordination among responsible organizations, and the selection of technologies appropriate to the conditions of the incident [15, 16].

### 2.2 Chabahar Port

Chabahar Port, located in southeastern Iran along the coast of the Gulf of Oman, is one of the country's strategic ports and the only Iranian oceanic port with direct access to open waters. The port's geographical location facilitates access to international waters for the landlocked countries of Central Asia, Afghanistan, and parts of South Asia, making Chabahar one of the region's important gateways for transit and maritime trade. From an economic perspective, the port also plays an important role in the development of Iran's regional and international trade, particularly along trade routes connecting India, Afghanistan, and

Central Asia. The development of its infrastructure is considered one of the country's strategic objectives for strengthening Iran's position in international trade and transportation networks. In addition, existing capacities in the energy, petrochemical, and fisheries sectors further enhance the economic and developmental significance of Chabahar. The geographical location of Chabahar Port is illustrated in Figure 1.

Given the strategic location of Chabahar Port and the expansion of commercial, maritime, and industrial activities in the region, the likelihood of accidents and oil pollution incidents is also increasing. The movement of commercial vessels and tankers, the loading and unloading of oil cargoes, and the development of port and industrial infrastructure are among the factors that may increase the risk of oil spills and their associated environmental impacts. Therefore, identifying and prioritizing the factors affecting the improvement of oil spill response operations at this port is particularly important for protecting the marine ecosystem and ensuring the continuity of its economic and commercial activities. Strengthening the operational and managerial capacities for oil spill response can reduce the environmental and economic consequences of oil-related incidents while enhancing the resilience of Chabahar Port to environmental hazards. Moreover, improving the port's capabilities in managing and controlling oil pollution can contribute to strengthening the confidence of trading partners and regional countries and consolidating Chabahar's position as a safe and sustainable port within international transportation and trade networks.

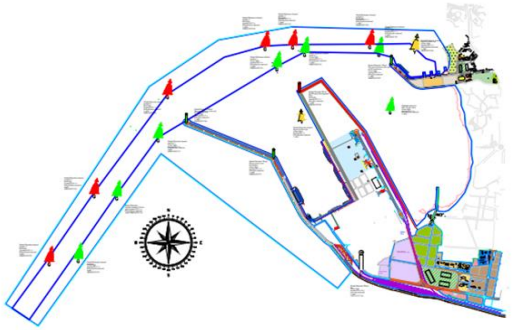


**Figure 1. Geographical location of Chabahar Port**

### 2.3 Review of Previous Research

Various studies have been conducted to investigate the role and impacts of marine pollution.

Sayareh et al. [17] examined the facilities and capabilities available for responding to oil and hazardous-material pollution at Chabahar Port and emphasized the need to enhance marine pollution response capacity. The data were collected through a questionnaire administered to employees of the Marine Pollution Response Department of the Ports and Maritime Organization at Chabahar Port. Golzadeh and Saadi [18] analyzed the capabilities and limitations of using booms and skimmers for oil spill response, identifying the strengths and weaknesses of these methods and proposing strategies to improve their application. The study employed library research, comparative analysis, and a case study of oil spill response operations in the Shavoor River, Khuzestan Province. Moghimi-Haji [19] introduced different types of skimmers and examined the role of this equipment in responding to oil pollution in water. The findings indicated that the selection of an appropriate skimmer should be based on environmental conditions and the type and volume of pollution.

Shirvani and Mousavi-Nejad [20] investigated the factors affecting the implementation of oil pollution conventions in the ports of Khuzestan Province. Based on the research literature and the opinions of 33 experts, the relevant factors were identified and their status at Imam Khomeini Port was evaluated. The results showed that the port had a favorable status in most sub-factors related to training and equipment. Esmailzadeh [21] examined the impacts of oil pollution on marine ecosystems and response strategies. The findings showed that petroleum compounds, depending on their characteristics, undergo evaporation, dissolution, or sedimentation in the marine environment, thereby damaging aquatic communities and marine ecosystems and ultimately causing economic losses. Furthermore, the expansion of petrochemical industries and maritime transportation has increased the need to control and mitigate the consequences of oil pollution.

Zolghi and Za'farouni [22] developed an emergency response plan for addressing oil pollution at loading and unloading terminals. The findings indicated that the ecological sensitivity, biodiversity, and extensive economic and oil-related activities in these areas increase the likelihood of environmental incidents and consequently necessitate the development and implementation of emergency response plans. Abbasgholizadeh Benam [23] examined international legal measures for addressing oil pollution in the high seas using a descriptive-analytical approach. The findings emphasized the need to strengthen legal and international measures to protect marine ecosystems and prevent the increasing consequences of oil pollution.

Azizi et al. [24] investigated strategies for reducing oil pollution in the marine environment of Chabahar. The findings showed that petroleum compounds are gradually degraded through physical, chemical, and biological processes, resulting in reduced toxicity. Nevertheless, oil wells, drilling rigs, and offshore platforms were identified as among the most important sources of petroleum pollutants entering marine waters. Krek et al. [25] investigated chronic oil pollution from ships and its contribution to background pollution in

the southeastern Baltic Sea. The results showed that the concentration of petroleum products exhibited seasonal variations and had declined since 2007. In addition, the annual amount of these substances released from ships was reported to be lower than their instantaneous concentration in the water column.

Yang et al. [26] examined offshore oil pollution, including its sources, consequences, and prevention and response methods from physical, chemical, and biological perspectives. The study emphasized the increasing severity of oil pollution associated with the growth of maritime transportation.

Han et al. [27] assessed the consequences of the Penglai 19-3 oil spill accident by modeling oil transport using hydrodynamic and monitoring data. The results indicated a rapid decline in the abundance of shellfish in areas exposed to the pollution.

Jafarzadeh et al. [28] conducted a systematic review and meta-analysis of oil spill detection methods based on synthetic aperture radar (SAR) imagery. The study examined the effects of data characteristics, sensors, frequency bands, polarization, and imaging conditions on oil spill detection.

Yang et al. [29] conducted a systematic review of decision-support tools for oil spill response, examining the advantages and limitations of existing and emerging approaches and emphasizing the requirements for oil spill response in cold and polar regions.

Wang et al. [6] proposed a method based on synthetic aperture radar (SAR) imagery and a deep convolutional neural network for oil spill detection. Through model optimization and post-prediction processing, the proposed approach improved detection accuracy.

Asif et al. [1] investigated the environmental consequences and challenges associated with oil spills in coastal areas. The results showed that fluorometric sensors are capable of detecting oil on different substrates, including snow and ice. The study also indicated that physical, chemical, and biological response methods each have specific advantages and limitations depending on coastal conditions.

Zhang et al. [14] confirmed the potential of optical polarization remote sensing for oil spill detection and examined the challenges associated with polarization modeling and feature extraction.

Nguyen et al. [30] modeled an oil spill in the East China Sea and demonstrated that integrating data with high temporal and spatial resolution and incorporating wind-drift effects can improve prediction accuracy. A one-month simulation also showed that the oil slick primarily moved northeastward under the influence of ocean currents.

Gong et al. [31] proposed a semi-supervised method for detecting oil fluorescence induced by ultraviolet radiation. By utilizing unlabeled data, the method improved classification accuracy and the generalizability of the model.

Iouzzi et al. [32] modeled the behavior and fate of an oil spill in the Amzorn River estuary. The findings emphasized the necessity of rapid response to reduce environmental consequences and cleanup costs, as well as its importance in developing emergency response plans.

Arslan et al. [33] proposed a method based on principal component analysis and satellite remote-sensing data for oil spill detection and monitoring. The results showed that integrating multisource imagery and data can improve the accuracy of oil spill detection.

Kuang et al. [34] investigated the interactions among wind, waves, and currents in determining oil spill behavior in the Yangtze River estuary. The results showed that hydrodynamic conditions, particularly storms, have significant effects on the transport, dispersion, sedimentation, and spatial extent of oil slicks.

Wu et al. [12] proposed a method based on induced fluorescence and a random sample consensus algorithm for rapid oil pollution detection. The method demonstrated high accuracy and the capability to identify oil concentrations ranging from 0 to 1000 mg/L.

Nguyen et al. [10] used integrated modeling to identify high-risk areas for oil spills in the coastal waters of Taiwan based on the frequency of oil slicks reaching the shoreline and the presence of sensitive resources. The findings can be applied to response planning and the improvement of shipping regulations.

Akhmedov et al. [5] developed a comprehensive model for oil spill detection and segmentation in marine environments. After 100 training epochs, the model achieved an accuracy of more than 97% and demonstrated suitable capabilities for real-time oil spill detection.

## 3. Methodology

### 3.1 Factor Extraction

The research philosophy of this study is interpretivism, grounded in the interpretive paradigm and a subjectivist approach. Accordingly, reality is not perceived as an objective entity independent of individuals, but rather as something shaped through social interactions. The research approach is inductive, meaning that by examining data and specific evidence and establishing relationships among them, general inferences are drawn. In terms of objective, the present study is applied research, as it aims to identify and prioritize the factors influencing the enhancement of oil spill response operations at sea. Regarding data collection methods, this research is descriptive-survey in nature, and in terms of data type, it is quantitative, employing quantitative methods for prioritizing the factors. Furthermore, the study is cross-sectional in terms of time frame, with data collected at a specific

point in time through observation and questionnaires [35].

The statistical population of the study comprised 35 personnel from the Maritime Deputy of the Ports and Maritime Administration of Sistan and Baluchestan Province (Chabahar Port), shipping companies, and the Department of Environment. Sampling was conducted using a non-random purposive (judgmental) method, and individuals with at least five years of work experience at Chabahar Port and a bachelor's degree in fields related to pollution were included in the study. The sample size was determined as 30 participants based on Morgan's table. Data were collected through both library and field methods. Library research was employed to review theoretical foundations, background literature, and identify factors affecting the improvement of oil spill response operations, while the field method, utilizing a questionnaire, was applied for prioritizing the identified factors.

To identify the factors influencing the enhancement of oil spill response operations at sea, an extensive search was conducted using relevant keywords in domestic databases including Magiran, Civilica, IranDoc, the Academic Center for Education, Culture and Research (ACECR) studies center, and Noor Database, as well as international databases such as MDPI, Elsevier, and Sage. In the initial stage, 68 articles were identified, of which 35 were excluded after reviewing titles and abstracts. Ultimately, 22 relevant articles were selected for factor extraction.

For the selection of studies to be included in the meta-analysis, only those studies were considered that addressed variables related to oil spill response operations at sea and utilized quantitative and statistical data derived from field studies or statistical results of previous research. Figure 2 illustrates the search, screening, and selection process of the reviewed studies.

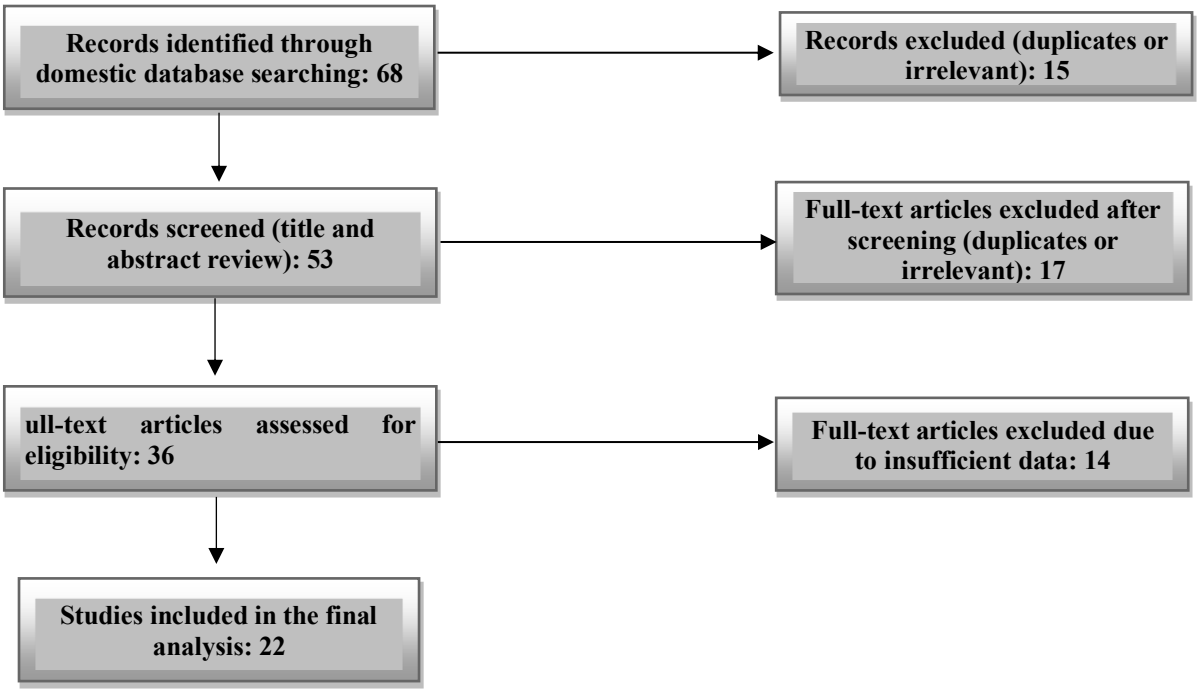



**Figure 2: Process of searching, screening, and selecting studies**

As illustrated in Figure 2, the literature review process resulted in the identification of 22 factors contributing to the improvement of oil spill response operations at sea. These factors, along with their respective references, are presented in Table 1.

**Table 1: Factors Identified from the Review of Research Literature**

| Row | Factors | Research Method | Source |
|---|---|---|---|
| 1 | Identification and tracking of oil pollution sources | Quantitative | [25] |
| 2 | Establishment of pollution prevention systems | Quantitative | [30] |
| 3 | Application of novel technologies for pollution detection and tracking | Qualitative | [6] |
| 4 | Development of educational programs for oil pollution reduction | Qualitative | [32] |
| 5 | Establishment of rapid response teams for oil incident management | Qualitative | [34] |
| 6 | Application of artificial intelligence for pollution prevention | Quantitative | [26] |
| 7 | Collaboration with relevant international organizations | Qualitative | [27] |

| Row | Factors | Research Method | Source |
|---|---|---|---|
| 8 | Development of sustainable development plans for pollution reduction | Qualitative | [29] |
| 9 | Development of infrastructure related to oil incidents | Qualitative | [12] |
| 10 | Establishment of communication and coordination systems among various organizations | Qualitative | [1] |
| 11 | Establishment of international standards for oil spill response | Qualitative | [31] |
| 12 | Comprehensive training and awareness-raising on oil spill response | Qualitative | [33] |
| 13 | Risk assessment and management related to oil incidents | Qualitative | [35] |
| 14 | Development of green and environmentally friendly technologies | Qualitative | [10] |
| 15 | Establishment of strict regulations and legislation for pollution prevention | Qualitative | [5] |
| 16 | Establishment of cooperative networks among various centers | Qualitative | [28] |
| 17 | Development of maintenance and upgrading plans for oil spill response equipment | Qualitative | [14] |
| 18 | Establishment of regional and international monitoring and evaluation systems | Qualitative | [14] |
| 19 | Promotion of environmental protection culture and reduction of oil consumption | Qualitative | [36] |
| 20 | Development of emergency plans and necessary logistics for oil incident response | Qualitative | [37] |
| 21 | Establishment of comprehensive and reliable databases on oil pollution | Qualitative | [9] |
| 22 | Development of international collaborations to address oil pollution impacts | Qualitative | [38] |

### 3.2 Data Analysis

To evaluate the validity and reliability of the identified factors, a researcher-developed questionnaire was designed based on a five-point Likert scale. The questionnaire was administered to 10 managers and experts affiliated with the Ports and Maritime Administration of Sistan and Baluchestan Province, shipping companies, and the environmental organization of Chabahar Port. Convergent validity was measured using the Average Variance Extracted (AVE), while reliability was assessed through Cronbach's alpha and Composite Reliability (CR). Following the Fornell–Larcker (1981) criterion, AVE values above 0.5 were considered indicative of acceptable convergent validity, and CR values above 0.7 were deemed to reflect satisfactory internal consistency. The detailed results of these analyses are summarized in Table 2.

**Table 2: Validity and Reliability Indices for the Identified Factors**

| Row | Factors | AVE | Composite Reliability (CR) | Cronbach's Alpha |
|---|---|---|---|---|
| 1 | Identification and tracking of oil pollution sources | 0.788 | 0.633 | 0.769 |
| 2 | Establishment of pollution prevention systems | 0.502 | 0.861 | 0.788 |
| 3 | Application of novel technologies for pollution detection and tracking | 0.577 | 0.846 | 0.867 |
| 4 | Development of educational programs for oil pollution reduction | 0.691 | 0.793 | 0.808 |
| 5 | Establishment of rapid response teams for oil incident management | 0.788 | 0.749 | 0.768 |
| 6 | Application of artificial intelligence for pollution prevention | 0.629 | 0.809 | 0.815 |
| 7 | Collaboration with relevant international organizations | 0.576 | 0.881 | 0.739 |
| 8 | Development of sustainable development plans for pollution reduction | 0.732 | 0.798 | 0.700 |
| 9 | Development of infrastructure related to oil incidents | 0.625 | 0.833 | 0.834 |
| 10 | Establishment of communication and coordination systems among various organizations | 0.639 | 0.800 | 0.800 |
| 11 | Establishment of international standards for oil spill response | 0.799 | 0.834 | 0.702 |
| 12 | Comprehensive training and awareness-raising on oil spill response | 0.766 | 0.800 | 0.801 |
| 13 | Risk assessment and management related to oil incidents | 0.729 | 0.788 | 0.866 |
| 14 | Development of green and environmentally friendly technologies | 0.711 | 0.798 | 0.799 |
| 15 | Establishment of strict regulations and legislation for pollution prevention | 0.764 | 0.845 | 0.734 |
| 16 | Establishment of cooperative networks among various centers | 0.664 | 0.769 | 0.900 |
| 17 | Development of maintenance and upgrading plans for oil spill response equipment | 0.766 | 0.786 | 0.855 |
| 18 | Establishment of regional and international monitoring and evaluation systems | 0.785 | 0.888 | 0.749 |
| 19 | Promotion of environmental protection culture and reduction of oil consumption | 0.834 | 0.867 | 0.795 |
| 20 | Development of emergency plans and necessary logistics for oil incident response | 0.761 | 0.882 | 0.732 |
| 21 | Establishment of comprehensive and reliable databases on oil pollution | 0.715 | 0.887 | 0.861 |
| 22 | Development of international collaborations to address oil pollution impacts | 0.666 | 0.916 | 0.899 |

The results demonstrated that all identified factors exhibited satisfactory validity and reliability. To further validate the factors, a two-round Delphi technique was conducted involving 20 experts, using a five-point Likert scale. In the second round, no factors were excluded, as all maintained an average score of 4 or above. Additionally, Kendall's W coefficient was calculated to assess the consensus among experts across the two rounds. The significance level ($p < 0.05$) confirmed a statistically meaningful agreement, with a 92% correlation observed between the first and second rounds, thereby validating all 22 factors.

For the prioritization of the identified factors, both the Analytical Hierarchy Process (AHP) and Interpretive Structural Modeling (ISM) are viable methods. However, ISM was selected for this study due to its superior capability in uncovering the interrelationships and multi-directional influences among factors, ultimately presenting them within a hierarchical framework. Consequently, ISM is better suited for complex contexts where factors exert reciprocal effects on one another.

## 4. Findings and Results

The prioritization of the extracted factors was carried out using Interpretive Structural Modeling (ISM). This interactive methodology facilitates the identification and systematic structuring of complex interrelationships among variables, relying on expert input. By evaluating the driving power and dependence of each factor, ISM organizes them into a hierarchical multi-level model, making it a robust tool for tackling complex problems [39]. The step-by-step procedure of ISM encompasses factor identification, establishment of contextual relationships, construction of the Structural Self-Interaction Matrix (SSIM), derivation and analysis of the reachability matrix, level partitioning, development of a directed graph with the elimination of transitive relationships, formulation of the interpretive structural model, and final validation and refinement [40]. The demographic profile of the expert panel, including average age, years of experience, and academic qualifications related to the subject matter, is summarized in Table 3.

**Table 3: Demographic Characteristics of the Expert Panel**

| Group | Number | Mean Age (years) | Mean Work Experience (years) | Education |
|---|---|---|---|---|
| Personnel of the Ports and Maritime Administration of Sistan and Baluchestan Province (Chabahar Port) | 30 | 38.33 | 8.33 | Bachelor's: 14<br>Master's: 14<br>PhD: 2 |

The examination of the mean age of the expert panel revealed that the personnel of the Maritime Deputy of the Ports and Maritime Administration of Sistan and Baluchestan Province (Chabahar Port) had a mean age of 38.33 years and a mean work experience of 8.33 years. Among the participants in the present study, 14 held a bachelor's degree, 14 held a master's degree, and 2 held a doctoral degree.

The first research question pertains to the identification of factors influencing the enhancement of oil spill response operations at sea. To address this question, in the initial stage, factors relevant to the subject were identified and listed as the intended criteria, the results of which are presented in Table 1. In the second stage, the contextual relationships among the factors—meaning the conceptual connections between the components of the system—were examined using the Delphi method and Kendall's W test. The results indicated a significance level of less than 0.05 and a Kendall's coefficient of 0.92, signifying statistical significance and a high level of agreement among the variables.

The second research question addresses the prioritization of factors influencing the enhancement of oil spill response operations at sea. In the first stage of Interpretive Structural Modeling (ISM), the Structural Self-Interaction Matrix (SSIM) was developed, the results of which are presented in Table 4. At this stage, the 22 identified factors were placed in the rows and columns of the matrix, and experts determined the pairwise relationships among the factors based on their specialized knowledge and experience. To define the type of relationships, the symbols V, A, X, and O were used to indicate the influence of factor i on j, the influence of factor j on i, mutual influence, and no relationship, respectively, which were coded as 1, -1, 2, and 0, respectively. The identified factors and their corresponding codes are presented as follows: Identification and tracking of oil pollution sources (A), Establishment of pollution prevention systems (B), Application of novel technologies for pollution detection and tracking (C), Development of educational programs for oil pollution reduction (D), Establishment of rapid response teams for oil incident management (E), Application of artificial intelligence for pollution prevention (F), Collaboration with relevant international organizations (G), Development of sustainable development plans for pollution reduction (H), Development of infrastructure related to oil incidents (I), Establishment of communication and coordination systems among various organizations (J), Establishment of international standards for oil spill response (K), Comprehensive training and awareness-raising on oil spill response (L), Risk assessment and

management related to oil incidents (M), Development of green and environmentally friendly technologies (N), Establishment of strict regulations and legislation for pollution prevention (O), Establishment of cooperative networks among various centers (P), Development of maintenance and upgrading plans for oil spill response equipment (Q), Establishment of regional and international monitoring and evaluation systems (R), Promotion of environmental protection culture and reduction of oil consumption (S), Development of emergency plans and necessary logistics for oil incident response (T), Establishment of comprehensive and reliable databases on oil pollution (U), and Development of international collaborations to address oil pollution impacts (V).

**Table 4: Structural Self-Interaction Matrix (SSIM) for the Identified Factors**

| | A | B | C | D | E | F | G | H | I | J | K | L | M | N | O | P | Q | R | S | T | U | V |
|---|---|---|---|---|---|---|---|---|---|---|---|---|---|---|---|---|---|---|---|---|---|---|
| **A** | | 1 | 2 | 2 | -1 | 2 | -1 | 2 | 2 | 0 | 1 | 1 | 1 | 1 | 1 | 1 | 1 | 1 | -1 | -1 | 1 | 1 |
| **B** | -1 | | -1 | 2 | -1 | -1 | -1 | 1 | 2 | 0 | 0 | -1 | 1 | 1 | 1 | 1 | 1 | 1 | 1 | 1 | 2 | 2 |
| **C** | 2 | 1 | | 2 | -1 | 2 | 0 | 2 | 2 | 0 | 1 | 1 | 1 | 1 | 1 | 1 | 1 | 1 | 1 | 1 | 2 | 2 |
| **D** | 2 | 2 | 2 | | -1 | -1 | -1 | 2 | 2 | -1 | -1 | -1 | 1 | 1 | 1 | 1 | 1 | 1 | -1 | -1 | -1 | 1 |
| **E** | 1 | 1 | 1 | 1 | | 1 | 1 | 1 | 1 | 1 | 1 | 1 | 1 | 1 | 1 | 1 | 1 | 1 | -1 | 2 | 2 | -1 |
| **F** | 2 | 1 | 2 | 1 | -1 | | -1 | -1 | 2 | 1 | 2 | 2 | 2 | 2 | 2 | 2 | 2 | 2 | 0 | 1 | 1 | 1 |
| **G** | 1 | 1 | 0 | 1 | -1 | 1 | | 1 | 1 | 1 | 2 | 2 | 2 | 2 | 1 | 2 | 1 | 2 | -1 | -1 | -1 | 2 |
| **H** | 2 | -1 | 2 | 2 | -1 | 1 | -1 | | 2 | 0 | 1 | 1 | 1 | 1 | 1 | 1 | 1 | 1 | -1 | 1 | 1 | 1 |
| **I** | 2 | 2 | 2 | 2 | -1 | 2 | -1 | 2 | | 0 | 1 | 1 | 1 | 1 | 1 | 1 | 1 | 1 | 0 | 0 | 1 | -1 |
| **J** | 0 | 0 | 0 | 1 | -1 | -1 | -1 | 0 | 0 | | 1 | 1 | -1 | 1 | 1 | 1 | 1 | 1 | 1 | 1 | 0 | 1 |
| **K** | -1 | 0 | -1 | 1 | -1 | 2 | 2 | -1 | -1 | -1 | | 2 | 1 | 2 | 2 | 2 | 0 | -1 | 1 | -1 | 2 | 2 |
| **L** | -1 | 1 | -1 | 1 | -1 | 2 | 2 | -1 | -1 | -1 | 2 | | 2 | 1 | 1 | 1 | 1 | -1 | 1 | -1 | 2 | 2 |
| **M** | -1 | -1 | -1 | -1 | -1 | 2 | 2 | -1 | -1 | 1 | -1 | 2 | | 1 | 1 | 1 | -1 | 0 | 1 | -1 | -1 | -1 |
| **N** | -1 | -1 | -1 | -1 | -1 | 2 | 2 | -1 | -1 | -1 | 2 | -1 | -1 | | 0 | 0 | -1 | -1 | 1 | -1 | 2 | 2 |
| **O** | -1 | -1 | -1 | -1 | -1 | 2 | -1 | -1 | -1 | -1 | 2 | -1 | -1 | 0 | | 0 | -1 | -1 | 1 | -1 | 2 | 2 |
| **P** | -1 | -1 | -1 | -1 | -1 | 2 | 2 | -1 | -1 | -1 | 2 | -1 | -1 | 0 | 0 | | -1 | -1 | -1 | -1 | 2 | 2 |
| **Q** | -1 | -1 | -1 | -1 | -1 | 2 | -1 | -1 | -1 | -1 | 2 | -1 | -1 | 0 | 0 | 0 | | 0 | 0 | 1 | 1 | 1 |
| **R** | -1 | -1 | -1 | -1 | -1 | 2 | 2 | -1 | -1 | -1 | 2 | -1 | -1 | 0 | 0 | 0 | 0 | | 0 | 2 | 2 | 2 |
| **S** | 1 | 1 | 1 | 1 | 1 | 1 | 1 | -1 | 2 | 2 | -1 | 1 | 1 | 1 | 1 | 1 | 1 | -1 | | 2 | 2 | 2 |
| **T** | 2 | 2 | 2 | 2 | 2 | 2 | 2 | 0 | 1 | 1 | 1 | 2 | 2 | 2 | 2 | 2 | 2 | 0 | 1 | | 1 | 2 |
| **U** | 2 | 2 | 2 | 1 | 2 | 1 | 2 | -1 | -1 | -1 | 2 | 2 | 2 | 2 | 1 | 2 | 1 | 1 | 1 | -1 | | 0 |
| **V** | 1 | 1 | 1 | 1 | 1 | 1 | 1 | -1 | 1 | 1 | 1 | 1 | 1 | 1 | 1 | 1 | 1 | 1 | 0 | 0 | 2 | |

Once the initial reachability matrix was established, the final reachability matrix was derived through the application of the transitivity rule. This rule posits that if variable i is linked to variable j, and variable j is linked to variable k, then variable i is also linked to variable k. In this phase, the indirect (secondary) relationships among the variables were systematically examined, leading to the development of the final reachability matrix, which is presented in Table 5. This matrix provides valuable insights into the driving power and dependence of each variable. Specifically, driving power is defined as the total number of variables that a particular variable can influence, while dependence is defined as the total number of variables that influence that particular variable.

**Table 5: Final Reachability Matrix with Driving Power and Dependence**

| Factor | A | B | C | D | E | F | G | H | I | J | K | L | M | N | O | P | Q | R | S | T | U | V | Driving Power |
|---|---|---|---|---|---|---|---|---|---|---|---|---|---|---|---|---|---|---|---|---|---|---|---|
| **A** | 1 | 0 | 1 | 0 | 1 | 1 | 0 | 0 | 1 | 0 | 1 | 1 | 1 | 0 | 1 | 1 | 1 | 0 | 1 | 0 | 1 | 0 | **13** |
| **B** | 1 | 1 | 1 | 1 | 1 | 0 | 1 | 1 | 1 | 1 | 0 | 1 | 1 | 1 | 0 | 0 | 0 | 1 | 0 | 0 | 0 | 1 | **14** |
| **C** | 1 | 0 | 1 | 1 | 0 | 1 | 0 | 0 | 0 | 0 | 1 | 1 | 1 | 0 | 1 | 1 | 0 | 1 | 1 | 1 | 1 | 1 | **14** |
| **D** | 1 | 0 | 0 | 1 | 1 | 0 | 1 | 1 | 0 | 1 | 1 | 1 | 1 | 1 | 0 | 0 | 0 | 1 | 0 | 1 | 0 | 1 | **13** |
| **E** | 1 | 0 | 0 | 1 | 1 | 0 | 0 | 1 | 1 | 1 | 1 | 0 | 0 | 0 | 1 | 1 | 0 | 0 | 1 | 1 | 1 | 1 | **13** |
| **F** | 1 | 0 | 0 | 0 | 0 | 1 | 1 | 1 | 1 | 0 | 0 | 0 | 0 | 1 | 1 | 0 | 1 | 0 | 0 | 0 | 0 | 1 | **9** |
| **G** | 1 | 1 | 1 | 0 | 1 | 0 | 1 | 0 | 1 | 0 | 1 | 0 | 1 | 0 | 1 | 0 | 1 | 1 | 1 | 1 | 1 | 0 | **14** |
| **H** | 1 | 1 | 1 | 1 | 0 | 0 | 0 | 1 | 1 | 1 | 1 | 1 | 0 | 1 | 1 | 1 | 0 | 1 | 1 | 0 | 0 | 1 | **15** |
| **I** | 1 | 1 | 1 | 1 | 1 | 1 | 1 | 1 | 1 | 0 | 1 | 0 | 0 | 1 | 0 | 1 | 0 | 0 | 1 | 1 | 1 | 1 | **16** |
| **J** | 1 | 0 | 0 | 1 | 0 | 1 | 0 | 1 | 1 | 1 | 1 | 1 | 1 | 1 | 0 | 1 | 1 | 0 | 1 | 0 | 1 | 0 | **14** |
| **K** | 1 | 0 | 0 | 0 | 1 | 1 | 1 | 1 | 0 | 1 | 1 | 1 | 1 | 1 | 1 | 0 | 1 | 1 | 0 | 0 | 0 | 1 | **14** |
| **L** | 1 | 0 | 0 | 0 | 0 | 0 | 0 | 1 | 1 | 1 | 1 | 1 | 0 | 1 | 0 | 1 | 0 | 1 | 1 | 1 | 0 | 0 | **11** |
| **M** | 0 | 0 | 0 | 1 | 1 | 1 | 1 | 0 | 1 | 1 | 0 | 1 | 1 | 1 | 0 | 1 | 1 | 0 | 1 | 0 | 1 | 0 | **13** |
| **N** | 1 | 1 | 1 | 1 | 1 | 0 | 0 | 1 | 1 | 1 | 1 | 0 | 0 | 1 | 1 | 0 | 0 | 0 | 0 | 1 | 1 | 1 | **14** |
| **O** | 1 | 0 | 0 | 0 | 1 | 1 | 1 | 1 | 0 | 0 | 0 | 0 | 1 | 1 | 1 | 1 | 1 | 1 | 1 | 1 | 0 | 0 | **13** |
| **P** | 0 | 0 | 1 | 1 | 0 | 0 | 1 | 1 | 1 | 0 | 0 | 1 | 1 | 0 | 0 | 1 | 0 | 0 | 1 | 0 | 1 | 0 | **10** |
| **Q** | 1 | 1 | 1 | 0 | 1 | 0 | 0 | 0 | 1 | 1 | 1 | 0 | 0 | 1 | 1 | 1 | 1 | 0 | 0 | 1 | 1 | 1 | **14** |
| **R** | 1 | 1 | 1 | 0 | 0 | 1 | 1 | 1 | 0 | 1 | 1 | 1 | 1 | 0 | 0 | 1 | 1 | 1 | 1 | 1 | 0 | 0 | **15** |
| **S** | 0 | 1 | 0 | 1 | 0 | 1 | 1 | 1 | 1 | 1 | 1 | 1 | 0 | 1 | 1 | 0 | 1 | 0 | 1 | 0 | 1 | 1 | **15** |
| **T** | 0 | 0 | 1 | 1 | 1 | 1 | 0 | 1 | 1 | 1 | 1 | 1 | 1 | 0 | 1 | 0 | 0 | 1 | 1 | 1 | 1 | 0 | **15** |

| Factor | A | B | C | D | E | F | G | H | I | J | K | L | M | N | O | P | Q | R | S | T | U | V | Driving Power |
|---|---|---|---|---|---|---|---|---|---|---|---|---|---|---|---|---|---|---|---|---|---|---|---|
| U | 0 | 0 | 0 | 0 | 0 | 1 | 1 | 1 | 1 | 1 | 0 | 1 | 0 | 1 | 0 | 0 | 0 | 0 | 0 | 0 | 1 | 1 | **9** |
| V | 0 | 1 | 1 | 1 | 1 | 0 | 1 | 1 | 0 | 1 | 1 | 1 | 0 | 1 | 1 | 0 | 1 | 1 | 1 | 1 | 0 | 1 | **16** |
| Dependence | **16** | **9** | **12** | **13** | **13** | **12** | **13** | **17** | **16** | **15** | **16** | **15** | **12** | **15** | **13** | **12** | **11** | **11** | **15** | **12** | **13** | **13** | |

In order to establish the hierarchical structure of the final ISM model, the final reachability matrix was subjected to level partitioning. This procedure was carried out using three key sets for each factor: the reachability set (comprising the factor itself and all other factors it influences), the antecedent set (comprising the factor itself and all other factors that influence it), and the intersection of these two sets. The level of each factor was determined by identifying those factors for which the reachability set and the intersection set were identical. Such factors were assigned to the highest level of the hierarchy and were then removed from subsequent partitioning iterations. This iterative process was repeated until the levels of all 22 factors were determined. The outcomes of this level partitioning are summarized in Table 6.

**Table 6. Level Partitioning of the Identified Factors**

| Row | Factors | Reachability Set | Antecedent Set | Intersection Set | Driving Power | Dependence | Level |
|---|---|---|---|---|---|---|---|
| 1 | Identification and tracking of oil pollution sources | {1, 3, 5, 6, 9, 11, 12, 13, 15, 16, 17, 22} | {1, 2, 3, 4, 5, 6, 7, 8, 9, 10, 11, 12, 14, 15, 17, 18} | {1, 3, 5, 6, 9, 11, 12, 15, 17} | 109 | 113 | I |
| 2 | Establishment of pollution prevention systems | {1, 2, 3, 4, 5, 7, 8, 9, 10, 12, 13, 14, 20} | {2, 7, 8, 9, 14, 20} | {2, 7, 8, 9, 14, 20} | 74 | 66 | II |
| 3 | Application of novel technologies for pollution detection and tracking | {1, 3, 4, 6, 11, 12, 13, 15, 16, 21} | {1, 2, 3, 7, 8, 9, 14, 16, 17, 18} | {1, 3, 16, 18} | 43 | 49 | III |
| 4 | Development of educational programs for oil pollution reduction | {1, 4, 5, 7, 8, 10, 11, 12, 13, 14, 18} | {2, 3, 4, 5, 8, 9, 10, 13, 14, 20} | {4, 5, 8, 10, 13, 14} | 68 | 68 | II |
| 5 | Establishment of rapid response teams for oil incident management | {1, 4, 5, 8, 9, 10, 11, 15, 16, 20} | {1, 2, 4, 5, 7, 9, 11, 13, 14, 15, 17} | {4, 5, 9, 11, 15} | 69 | 73 | II |
| 6 | Application of artificial intelligence for pollution prevention | {1, 6, 7, 8, 9, 14, 15, 22} | {1, 3, 6, 9, 10, 11, 13, 15, 20} | {1, 6, 9, 15} | 44 | 48 | III |
| 7 | Collaboration with relevant international organizations | {1, 2, 3, 5, 7, 9, 11, 13, 15, 17, 22} | {2, 4, 6, 7, 9, 11, 13, 15, 16, 18} | {2, 7, 9, 11, 13, 15, 18} | 62 | 54 | II |
| 8 | Development of sustainable development plans for pollution reduction | {1, 2, 3, 4, 8, 9, 10, 11, 12, 14, 15, 16, 22} | {2, 4, 5, 6, 8, 9, 10, 11, 12, 14, 15, 16, 18} | {2, 4, 8, 9, 10, 11, 12, 14, 15, 16, 18} | 126 | 123 | I |
| 9 | Development of infrastructure related to oil incidents | {1, 2, 3, 4, 5, 6, 7, 8, 9, 11, 14, 16, 18} | {1, 2, 5, 6, 7, 8, 9, 10, 12, 13, 14, 16, 17} | {1, 2, 5, 7, 8, 9, 14, 16} | 110 | 112 | I |
| 10 | Establishment of communication and coordination systems among various organizations | {1, 4, 6, 8, 9, 10, 11, 12, 13, 14, 16, 17} | {2, 4, 5, 8, 10, 11, 12, 13, 14, 17, 18} | {4, 8, 10, 11, 12, 13, 14, 17} | 70 | 79 | II |
| 11 | Establishment of international standards for oil spill response | {1, 5, 6, 7, 8, 10, 11, 12, 13, 14, 15, 17} | {1, 3, 4, 5, 7, 8, 9, 10, 11, 12, 14, 17, 18} | {1, 5, 7, 8, 10, 11, 12, 14, 17} | 101 | 106 | I |
| 12 | Comprehensive training and awareness-raising on oil spill response | {1, 8, 9, 10, 11, 12, 14, 16, 18} | {1, 2, 3, 4, 8, 10, 11, 12, 13, 16, 18} | {1, 8, 10, 11, 12, 16, 18} | 79 | 87 | II |
| 13 | Risk assessment and management related to oil incidents | {4, 5, 6, 7, 8, 10, 11, 13, 14, 15, 17, 22} | {1, 2, 3, 4, 7, 10, 11, 13, 15, 16, 18} | {4, 7, 10, 11, 13, 15, 18} | 64 | 63 | II |
| 14 | Development of green and environmentally friendly technologies | {1, 2, 3, 4, 5, 8, 9, 10, 11, 14, 15} | {2, 4, 6, 8, 9, 10, 11, 12, 13, 14, 15, 17} | {2, 4, 8, 9, 10, 11, 14, 15} | 96 | 92 | II |
| 15 | Establishment of strict regulations and legislation for pollution prevention | {1, 5, 6, 7, 8, 13, 14, 15, 16, 17, 18} | {1, 3, 5, 6, 7, 8, 11, 14, 15, 17} | {1, 5, 6, 7, 8, 14, 15, 17} | 63 | 67 | II |
| 16 | Establishment of cooperative networks among various centers | {3, 4, 7, 8, 9, 12, 13, 16} | {1, 3, 5, 8, 9, 10, 12, 13, 15, 16, 17, 18} | {3, 8, 9, 12, 13, 16} | 55 | 59 | II |
| 17 | Development of maintenance and upgrading plans for oil spill response equipment | {1, 2, 3, 5, 9, 10, 11, 14, 15, 16, 17} | {1, 6, 7, 10, 11, 13, 15, 17, 18} | {1, 10, 11, 15, 17} | 34 | 38 | III |
| 18 | Establishment of regional and international monitoring and evaluation systems | {1, 2, 3, 5, 9, 10, 11, 14, 15, 16, 17} | {1, 6, 7, 10, 11, 13, 15, 17, 18} | {1, 10, 11, 15, 17} | 81 | 78 | II |

| Row | Factors | Reachability Set | Antecedent Set | Intersection Set | Driving Power | Dependence | Level |
|---|---|---|---|---|---|---|---|
| 19 | Promotion of environmental protection culture and reduction of oil consumption | {1, 3, 5, 9, 12, 13, 15, 20, 22} | {1, 5, 9, 13, 20} | {1, 5, 9, 13, 20} | 80 | 60 | II |
| 20 | Development of emergency plans and necessary logistics for oil incident response | {4, 8, 11, 13, 16, 19, 20, 22} | {1, 5, 6, 9, 12, 16, 20} | {16, 20} | 75 | 65 | II |
| 21 | Establishment of comprehensive and reliable databases on oil pollution | {2, 5, 7, 10, 14, 15, 18, 20, 21, 22} | {3, 5, 20, 21} | {5, 20, 21} | 82 | 72 | I |
| 22 | Development of international collaborations to address oil pollution impacts | {1, 4, 7, 9, 10, 11, 15, 17, 19, 20, 22} | {1, 3, 5, 9, 11, 16, 18, 20, 21} | {1, 11, 20} | 80 | 69 | III |

Based on the level partitioning outcomes and the final reachability matrix, a hierarchical structural model was developed to illustrate the relationships and positioning of the factors affecting the improvement of oil spill response operations at sea. This hierarchical structure categorizes the 22 identified factors into distinct levels, reflecting their relative influence and dependence within the system. The final level assignment and the specific position of each factor within the hierarchy are summarized in Table 7.

**Table 7: Hierarchical Structure and Level Assignment of the Identified Factors**

| Level | Factors Influencing the Enhancement of Oil Spill Response Operations at Sea |
|---|---|
| **Level I** | Identification and tracking of oil pollution sources |
| | Development of sustainable development plans for pollution reduction |
| | Development of infrastructure related to oil incidents |
| | Establishment of international standards for oil spill response |
| | Establishment of comprehensive and reliable databases on oil pollution |
| **Level II** | Establishment of pollution prevention systems |
| | Development of educational programs for oil pollution reduction |
| | Establishment of rapid response teams for oil incident management |
| | Collaboration with relevant international organizations |
| | Establishment of communication and coordination systems among various organizations |
| | Comprehensive training and awareness-raising on oil spill response |
| | Risk assessment and management related to oil incidents |
| | Development of green and environmentally friendly technologies |
| | Establishment of strict regulations and legislation for pollution prevention |
| | Establishment of cooperative networks among various centers |
| | Promotion of environmental protection culture and reduction of oil consumption |
| | Development of emergency plans and necessary logistics for oil incident response |
| | Establishment of regional and international monitoring and evaluation systems |
| **Level III** | Application of novel technologies for pollution detection and tracking |
| | Application of artificial intelligence for pollution prevention |
| | Development of maintenance and upgrading plans for oil spill response equipment |
| | Development of international collaborations to address oil pollution impacts |

In this phase, the MICMAC (Matrix of Cross-Impact Multiplications Applied to a Classification) technique was utilized. This analytical approach is designed to evaluate the driving power and dependence of variables, thereby facilitating the identification of critical factors within a complex system. The primary purpose of the MICMAC analysis is to assess the influence and dependency of each factor and to map their positions within the overall research framework. After computing the driving power and dependence scores for all 22 factors, they were plotted on the MICMAC matrix and categorized into four distinct clusters based on predefined threshold values. These thresholds are typically determined by calculating the average number of factors and adding one unit to that average.

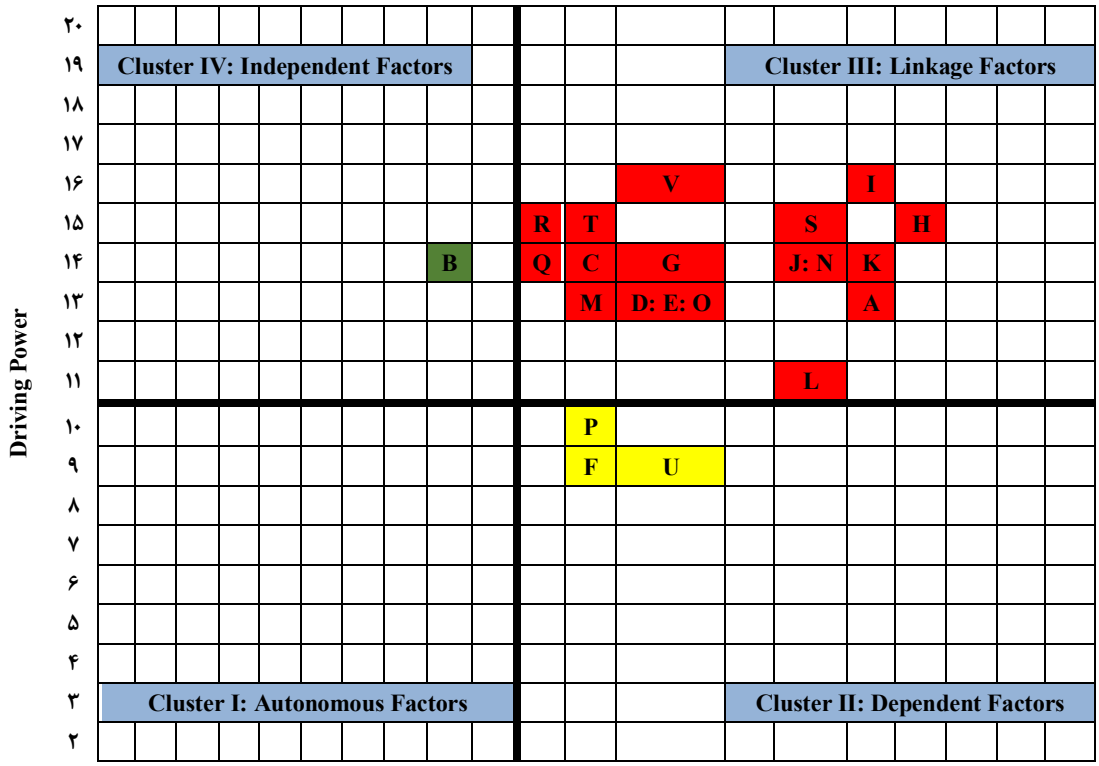
The first cluster, autonomous variables, comprises factors with low driving power and low dependence, indicating their limited interaction with other elements of the system. The second cluster, dependent variables, consists of factors with low driving power but high dependence, meaning they are strongly influenced by other factors. The third cluster, linkage variables, includes factors characterized by both high driving

power and high dependence; these variables are highly sensitive and can both affect and be affected by other factors. The fourth cluster, independent variables, encompasses factors with high driving power and low dependence. These are considered key driving factors that exert significant influence over the rest of the system.

The detailed driving power and dependence values for each factor, along with their respective cluster classifications, are presented in Table 8. Additionally, the MICMAC matrix plot, which visually illustrates the distribution of the factors across the four clusters, is depicted in Figure 3.

**Table 8: Driving Power and Dependence of the Identified Factors (MICMAC Analysis)**

| Row | Factor | Dependence | Driving Power |
|---|---|---|---|
| A | Identification and tracking of oil pollution sources | 16 | 13 |
| B | Establishment of pollution prevention systems | 9 | 14 |
| C | Application of novel technologies for pollution detection and tracking | 12 | 14 |
| D | Development of educational programs for oil pollution reduction | 13 | 13 |
| E | Establishment of rapid response teams for oil incident management | 13 | 13 |
| F | Application of artificial intelligence for pollution prevention | 12 | 9 |
| G | Collaboration with relevant international organizations | 13 | 14 |
| H | Development of sustainable development plans for pollution reduction | 17 | 15 |
| I | Development of infrastructure related to oil incidents | 16 | 16 |
| J | Establishment of communication and coordination systems among various organizations | 15 | 14 |
| K | Establishment of international standards for oil spill response | 16 | 14 |
| L | Comprehensive training and awareness-raising on oil spill response | 15 | 11 |
| M | Risk assessment and management related to oil incidents | 12 | 13 |
| N | Development of green and environmentally friendly technologies | 15 | 14 |
| O | Establishment of strict regulations and legislation for pollution prevention | 13 | 13 |
| P | Establishment of cooperative networks among various centers | 12 | 10 |
| Q | Development of maintenance and upgrading plans for oil spill response equipment | 11 | 14 |
| R | Establishment of regional and international monitoring and evaluation systems | 11 | 15 |
| S | Promotion of environmental protection culture and reduction of oil consumption | 15 | 15 |
| T | Development of emergency plans and necessary logistics for oil incident response | 12 | 15 |
| U | Establishment of comprehensive and reliable databases on oil pollution | 13 | 9 |
| V | Development of international collaborations to address oil pollution impacts | 13 | 16 |



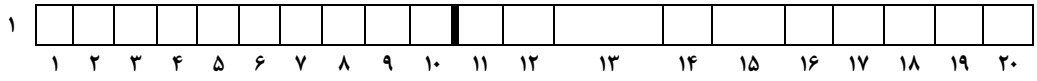



**Figure 3. MICMAC diagram of factors influencing the enhancement of oil spill response operations at sea**

## 5. Discussion and Conclusion

Based on the research findings, a total of 22 factors influencing the enhancement of oil spill response operations at sea, with a focus on Chabahar Port, were identified. These factors include: "identification and tracking of oil pollution sources," "establishment of pollution prevention systems," "application of novel technologies for pollution detection and tracking," "development of educational programs for oil pollution reduction," "establishment of rapid response teams for oil incident management," "application of artificial intelligence for pollution prevention," "collaboration with relevant international organizations," "development of sustainable development plans for pollution reduction," "development of infrastructure related to oil incidents," "establishment of communication and coordination systems among various organizations," "establishment of international standards for oil spill response," "comprehensive training and awareness-raising on oil spill response," "risk assessment and management related to oil incidents," "development of green and environmentally friendly technologies," "establishment of strict regulations and legislation for pollution prevention," "establishment of cooperative networks among various centers," "development of maintenance and upgrading plans for oil spill response equipment," "establishment of regional and international monitoring and evaluation systems," "promotion of environmental protection culture and reduction of oil consumption," "development of emergency plans and necessary logistics for oil incident response," "establishment of comprehensive and reliable databases on oil pollution," and "development of international collaborations to address oil pollution impacts."

The elaboration of these factors reveals that the **identification and tracking of oil pollution sources** through satellite trackers, marine sensors, and unmanned aerial vehicles (UAVs) plays a critical role in the rapid detection of spills and the precise determination of their location. These measures not only reduce response time but also prevent the spread of pollution to other areas, and the data obtained can be utilized to improve future prevention strategies. Furthermore, **pollution prevention systems**—through measures such as installing safety equipment on vessels and oil facilities, employing leak prevention technologies, developing safety protocols, and implementing regular maintenance and repair programs—reduce the likelihood of incidents. From this perspective, effective prevention can reduce the costs and consequences associated with post-incident pollution response.

Moreover, **the application of novel technologies for pollution detection and tracking**, including satellite systems, advanced radars, and biosensors, enables rapid pollution detection and provides accurate information regarding its extent and severity. These technologies can enhance the speed and accuracy of detection, thereby facilitating quicker response and reducing environmental consequences. Alongside technology, **human resource training** is also a key factor in improving oil spill response operations. Conducting specialized courses for port personnel, ship crews, and rapid response teams, along with the use of realistic scenario simulations and practical training, enhances the preparedness of human resources for prevention, detection, and response. In this regard, **rapid response teams**, equipped with appropriate resources and specialized training, must remain continuously operational and carry out containment and cleanup operations based on pre-established plans. The coordination of these teams with other relevant organizations is also essential for effective crisis management.

On the other hand, **artificial intelligence**—with its capacity to analyze large volumes of data from monitoring systems—can be used to predict the likelihood of spills, provide early warnings, identify risk patterns, and recommend preventive measures. Additionally, this technology can enhance the efficiency of pollution response operations by assisting in the selection of appropriate and faster cleanup methods. **Collaboration with international organizations** is also important, as it facilitates access to knowledge, resources, and advanced technologies, enables the exchange of experiences, supports the implementation of global standards, and enhances coordination in pollution response operations.

In the domain of sustainable development, reducing dependence on fossil fuels and utilizing renewable energy sources can help mitigate environmental risks. Implementing projects such as solar and wind energy in port facilities, alongside reducing environmental impacts, can contribute to the sustainable development of port activities at Chabahar Port. Furthermore, the **development of infrastructure related to oil incidents**—including the establishment of pollution response equipment depots, operational bases, and maintenance and repair facilities—enhances regional preparedness for incidents. Such infrastructure should be designed to ensure rapid access to equipment and resources during critical situations.

**The establishment of communication and coordination systems among various organizations**, through the creation of crisis control centers, early

warning systems, and clearly defined information-sharing protocols, can accelerate response efforts and mitigate the consequences of incidents. Additionally, **the formulation and implementation of international standards for oil spill response**, particularly concerning safety requirements for vessels and oil facilities, enhance coordination and reduce the risks associated with incidents. Alongside these measures, **public education and awareness-raising**, especially in coastal areas, can strengthen the culture of marine environmental protection by increasing awareness of the consequences of oil pollution and prevention methods.

Furthermore, **risk assessment and management related to oil incidents**—through the identification of vulnerabilities, prediction of potential scenarios, and development of preventive and rapid response plans—play a significant role in reducing the consequences of incidents. The use of **green and environmentally friendly technologies**, such as oil-absorbing biomaterials and bioremediation technologies, can increase the efficiency of the cleanup process while minimizing the adverse effects of response operations. On the other hand, the **establishment of strict regulations and legislation** for vessels, oil facilities, and oil-related activities, along with the enforcement of safety standards and appropriate enforcement mechanisms, can serve as a deterrent to pollution incidents.

**The establishment of cooperative networks among research centers, environmental organizations, and port authorities** facilitates the exchange of knowledge, resources, and experiences, thereby fostering the development of innovative solutions. Additionally, **regular maintenance and upgrading of pollution response equipment**—such as skimmers and containment booms—are essential for maintaining operational readiness and ensuring the proper functioning of equipment during crises. **Regional and international monitoring and evaluation systems**, utilizing sensor networks, monitoring stations, and data analysis systems, enable continuous monitoring of pollution status and provide up-to-date information to decision-makers.

In this context, **promoting a culture of environmental protection and reducing oil consumption** through education, awareness campaigns, and encouragement to adopt alternative energy sources can be effective in reducing dependence on oil and preventing pollution. **Emergency response plans and necessary logistics for oil incident response** should pre-specify the financial, human, and equipment resources required for rapid response, containment, and cleanup. Furthermore, **the establishment of comprehensive and reliable databases** containing information on pollution sources, response equipment, cleanup methods, and past operational outcomes can improve future decision-making and planning while facilitating information exchange at regional and international levels. Finally, **the development of international collaborations** through knowledge sharing, resource and experience exchange, joint projects, international exercises, and the development of new technologies can enhance the capacity to address the consequences of oil pollution.

The results of the level partitioning using the ISM method revealed that the factors "identification and tracking of oil pollution sources," "development of infrastructure related to oil incidents," "establishment of international standards for oil spill response," "development of sustainable development plans for pollution reduction," and "establishment of comprehensive and reliable databases on oil pollution" are positioned at Level I. These factors exhibit the highest degree of dependence and are located at the end of the system's influence chain. In other words, these factors are primarily outcomes of the performance of lower-level factors and are considered outputs of the system; therefore, their direct management without considering the influential factors at lower levels will have limited effectiveness.

At Level II, the factors "promotion of environmental protection culture and reduction of oil consumption," "development of emergency plans and necessary logistics for oil incident response," "risk assessment and management related to oil incidents," "development of green and environmentally friendly technologies," "establishment of strict regulations and legislation for pollution prevention," "establishment of cooperative networks among various centers," and "establishment of regional and international monitoring and evaluation systems" were positioned. These factors serve as intermediaries between the root factors and the dependent factors, meaning they are both influenced by lower-level factors and exert influence on higher-level factors. Therefore, improving these factors can affect the overall performance of the system and is of significant importance in planning and management.

Finally, the factors "establishment of cooperative networks among various centers," "establishment of regional and international monitoring and evaluation systems," "application of artificial intelligence for pollution prevention," "development of maintenance and upgrading plans for oil spill response equipment," and "development of international collaborations to address oil pollution impacts" were placed at Level III. These factors, as root factors, possess the highest driving power and the lowest dependence within the system's structure. Consequently, changes and improvements in these factors can influence other levels of the system. From this perspective, attention to these factors in decision-making and planning processes should be given higher priority. Proper management of root factors can pave the way for improving higher-level factors and ultimately

enhancing the overall performance of oil spill response operations.

Based on the research findings, the use of novel technologies for **identifying and tracking oil pollution** sources is recommended. In this regard, the utilization of Geographic Information Systems (GIS), satellite imagery, underwater sensors, and automated monitoring systems can be effective in accurately identifying pollution sources, tracking oil spill trajectories, and determining affected areas. Additionally, the installation of leak detection sensors on pipelines, tanks, and oil docks, along with the enforcement of periodic inspections of equipment and infrastructure, can reduce the probability of incidents. These systems, by issuing automated early warnings, can facilitate rapid response.

Furthermore, the use of **UAVs equipped with infrared and spectral sensors** for detecting oil spills in marine and remote areas is recommended. These devices can provide the necessary information for pollution identification and operational decision-making within a short period. In addition, the use of underwater robots for pipeline inspection, subsurface monitoring, and data collection from contaminated areas can enhance the accuracy of monitoring and detection operations.

In summary, this study provides a comprehensive framework for understanding the multidimensional factors affecting oil spill response operations at sea. The findings underscore the critical role of root factors—particularly technological innovation, international collaboration, and artificial intelligence—in driving systemic improvements. For policymakers and port authorities, prioritizing these leverage points can lead to more resilient and effective response systems. Future research should focus on empirical testing of the proposed model, comparative studies across different ports, and the integration of real-time data analytics to enhance predictive capabilities.

Despite the findings of this research, the present study faced certain limitations. First, due to time constraints, the model obtained was not tested. Additionally, due to time limitations, the relationships among the identified factors were not independently examined and tested. Finally, the spatial scope of the research was limited to Chabahar Port; therefore, the generalization of the results and findings to other marine areas and ports should be undertaken with caution, taking into account the degree of similarity in organizational, operational, and environmental conditions.

## 6. References


[1] Asif, Z., Chen, Z., An, C., & Dong, J. (2022). Environmental impacts and challenges associated with oil spills on shorelines. *Journal of Marine Science and Engineering*, 10(6), 762. https://doi.org/10.3390/jmse10060762

[2] Chen, Z. K., Guo, R., & Cheng, P. F. (2020). Application of LIF technology-based spectral feature extraction in oil detection. *Laser Optoelectron. Prog*, 57, 133002.

[3] Wang, Z., An, C., Lee, K., Owens, E., Chen, Z., Boufadel, M., ... & Feng, Q. (2021a). Factors influencing the fate of oil spilled on shorelines: a review. *Environmental Chemistry Letters*, 19(2), 1611-1628. https://doi.org/10.1007/s10311-020-01097-4

[4] Fingas, M. (2021). Visual appearance of oil on the sea. *Journal of Marine Science and Engineering*, 9(1), 97. https://doi.org/10.3390/jmse9010097

[5] Akhmedov, F., Nasimov, R., & Abdusalomov, A. (2024). Developing a comprehensive oil spill detection model for marine environments. *Remote Sensing*, *16*(16), 3080. https://doi.org/10.3390/rs16163080

[6] Wang, X., Liu, J., Zhang, S., Deng, Q., Wang, Z., Li, Y., & Fan, J. (2021b). Detection of oil spill using SAR imagery based on AlexNet model. *Computational Intelligence and Neuroscience*, 2021(1), 4812979. https://doi.org/10.1155/2021/4812979

[7] Abereton, P., Ordinioha, B., Mensah-Attipoe, J., & Toyinbo, O. (2023). Crude oil spills and respiratory health of clean-up workers: A systematic review of literature. *Atmosphere*, 14(3), 494. https://doi.org/10.3390/atmos14030494

[8] Law on the Protection of Navigable Seas and Rivers Against Oil Pollution (2010). *Research Center of the Islamic Consultative Assembly*. Directive No. 41844/124.

[9] Tong, S., Liu, X., Chen, Q., Zhang, Z., & Xie, G. (2019). Multi-feature based ocean oil spill detection for polarimetric SAR data using random forest and the self-similarity parameter. *Remote Sensing*, *11*(4), 451. https://doi.org/10.3390/rs11040451.

[10] Nguyen, T. H. H., Hou, T. H., Pham, H. A., & Tsai, C. C. (2024). Oil spill sensitivity analysis of the coastal waters of Taiwan using an integrated modelling approach. *Journal of Marine Science and Engineering*, *12*(1), 155. https://doi.org/10.3390/jmse12010155

[11] Heydarizad, M., Raeisi, E., Sori, R., & Gimeno, L. (2018). The identification of Iran's moisture sources using a Lagrangian particle dispersion model. *Atmosphere*, *9*(10), 408. https://doi.org/10.3390/atmos9100408

[12] Wu, H., Wang, Z., & Zhao, Y. (2024). Rapid investigation of oil pollution in water-combined induced fluorescence and random sample consensus algorithm. Sustainability, 16(10), 3930. https://doi.org/10.3390/su16103930

[13] Nilén, Greta, Maria Larsson, Tuulia Hyötyläinen, and Steffen H. Keiter. "A complex mixture of polycyclic aromatic compounds causes embryotoxic, behavioral, and molecular effects in zebrafish larvae (Danio rerio), and in vitro bioassays." *Science of The Total Environment* 906 (2024): 167307. https://doi.org/10.1016/j.scitotenv.2023.167307

[14] Zhang, Z., Yan, L., Jiang, X., Ding, J., Zhang, F., Jiang, K., & Shang, K. (2022). Exploring the potential of optical polarization remote sensing for oil spill detection: a case study of Deepwater Horizon. *Remote Sensing*, *14*(10), 2398. https://doi.org/10.3390/rs14102398

[15] Lu, J., Chen, L., & Xu, D. (2024). Study on the oil spill transport behavior and multifactorial effects of the Lancang River crossing pipeline. *Applied Sciences*, *14*(8), 3455. https://doi.org/10.3390/app14083455

[16] Kvočka, D., Žagar, D., & Banovec, P. (2021). A review of river oil spill modeling. *Water*, *13*(12), 1620. https://doi.org/10.3390/w13121620

[17] Sayareh, J., Yarahmadi, A., & Tahmak, H. R. (2012). Assessment of capabilities and capacity to combat oil pollution and hazardous/toxic substances at Chabahar Port (with recommendations for improvement). *10th International Conference on Coasts, Ports and Marine Structures (ICOPMAS)*, Tehran. (Persian)

[18] Golzadeh, N., & Sa'di, A. (2013). An analytical study of the capabilities and limitations of using boom and skimmer methods for oil recovery and combating marine oil pollution, and the proposal of management strategies (Case study: Shavur River, Khuzestan). *First Specialized Oil Conference and Exhibition*, Tehran. (Persian)

[19] Moghimi Haji, E. (2019). Combating oil pollution in water: An introduction to skimmers and their types. *3rd National Conference on Strategies for Achieving Sustainable Development in Agricultural Sciences and Natural Resources of Iran*, Tehran. (Persian)

[20] Shirvani, A., & Mousavinejad, S. F. (2018). Analysis of factors affecting the implementation of marine oil pollution conventions at the General Directorate of Ports and Maritime Affairs of Khuzestan Province. *20th Marine Industries Conference*, Tehran. (Persian)

[21] Esmaeilzadeh, A. (2019). Pollution of marine ecosystems with an emphasis on oil pollution, its impact on marine-dependent organisms, and mitigation strategies., Chabahar. (Persian)

[22] Zolghi, E., & Za'farouni, M. (2023). Development of an emergency response plan for oil pollution at loading and unloading jetties. *9th International Conference on Chemical, Petroleum, and Environmental Engineering*, Tehran. (Persian)

[23] Abbasgholizadeh Benam, A. (2024). International Legal Measures to Combat Oil Pollution on the High Seas. First National Congress on Sustainable Development and Social Responsibility: Challenges and Solutions, Shiraz. (Persian)

[24] Azizi, A., Khodadadi, H., and Dalir, Gh. (2024). Strategies for Reducing Oil Pollution in the Marine Environment of Chabahar County. *First National Conference on the Future and Sustainability of the Environment*, Tehran. (Persian)

[25] Krek, E. V., Krek, A. V., & Kostianoy, A. G. (2021). Chronic oil pollution from vessels and its role in background pollution in the southeastern baltic sea. *Remote Sensing*, *13*(21), 4307. https://doi.org/10.3390/rs13214307

[26] Yang, S.; Xing, K.; Yang, Y. (2021). Offshore Oil Pollution and Prevention Measures. *2nd International Academic Conference on Energy Conservation, Environmental Protection and Energy Science* (ICEPE 2021). E3S Web Conf.

[27] Han, H., Huang, S., Liu, S., Sha, J., & Lv, X. (2021). An assessment of marine ecosystem damage from the penglai 19-3 oil spill accident. *Journal of Marine Science and Engineering*, *9*(7), 732. https://doi.org/10.3390/jmse9070732

[28] Jafarzadeh, H., Mahdianpari, M., Homayouni, S., Mohammadimanesh, F., & Dabboor, M. (2021). Oil spill detection from Synthetic Aperture Radar Earth observations: A meta-analysis and comprehensive review. *GIScience & Remote Sensing*, *58*(7), 1022-1051. https://doi.org/10.1080/15481603.2021.1952542

[29] Yang, Z., Chen, Z., Lee, K., Owens, E., Boufadel, M. C., An, C., & Taylor, E. (2021). Decision support tools for oil spill response (OSR-DSTs): Approaches, challenges, and future research perspectives. *Marine Pollution Bulletin*, *167*, 112313. https://doi.org/10.1016/j.marpolbul.2021.112313

[30] Nguyen, T. H. H., Hou, T. H., Pham, H. A., & Tsai, C. C. (2024). Hindcast of oil spill pollution in the East China Sea in January 2018. *Proceedings of the Institution of Mechanical Engineers, Part M: Journal of Engineering for the*

*Maritime Environment*, *238*(1), 90-101. https://doi.org/10.1177/14750902231162171

[31] Gong, B., Zhang, H., Wang, X., Lian, K., Li, X., Chen, B., ... & Niu, X. (2023). Ultraviolet-induced fluorescence of oil spill recognition using a semi-supervised algorithm based on thickness and mixing proportion–emission matrices. *Analytical Methods*, *15*(13), 1649-1660. https://doi.org/10.1039/d2ay01776h

[32] Iouzzi, N., Ben Meftah, M., Haffane, M., Mouakkir, L., Chagdali, M., & Mossa, M. (2023). Modeling of the fate and behaviors of an oil spill in the Azemmour River estuary in Morocco. *Water*, *15*(9), 1776. https://doi.org/10.3390/w15091776

[33] Arslan, N., Majidi Nezhad, M., Heydari, A., Astiaso Garcia, D., & Sylaios, G. (2023). A principal component analysis methodology of oil spill detection and monitoring using satellite remote sensing sensors. *Remote Sensing*, *15*(5), 1460. https://doi.org/10.3390/rs15051460

[34] Kuang, C., Chen, J., Wang, J., Qin, R., Fan, J., & Zou, Q. (2023). Effect of wind-wave-current interaction on oil spill in the Yangtze River Estuary. *Journal of Marine Science and Engineering*, *11*(3), 494. https://doi.org/10.3390/jmse11030494

[35] Sarmad, Z., Bazargan, A. and Hejazi, E. (2024). Research Methods in Behavioral Sciences. Ageh Publications. (Persian)

INTERNATIONAL JOURNAL OF
COASTAL, OFFSHORE & ENVIRONMENTAL ENGINEERING IJCOE Vol..11/No.4 /Autumn 2026 ( 32-40)

Available online at: www. Ijcoe.org

# Environmental Risk Modeling and Management of Dredging and Dredged-Material Disposal Operations with a Sustainable Coastal and Marine Environment Approach

**Asghar Rashnoodi[1*], Hossein Karimi Khosrow[2]**

*1* Department of Business Management, Faculty of Economics and Management, Khorramshahr University of Marine Science and Technology, Khorramshahr, Iran; Asghar.rashnoodi@gmail.com*

*2 Master of Business Administration (MBA) Shahed University; karimi3366@gmail.com*

**ARTICLE INFO**

Article History:
Received: 16 July
Accepted: 27 Oct
Available online: —

Keywords:
**Environmental risk;**
**Dredging;**
**Dredged material;**
**Fuzzy AHP;**
**Fuzzy TOPSIS**

**ABSTRACT**

Purpose: This study develops an integrated fuzzy multi-criteria framework for modeling and prioritizing environmental risks associated with dredging and dredged-material disposal operations at Khorramshahr Port, with emphasis on sustainable coastal and marine management.

Design/methodology/approach: Environmental risks were identified through a review of scientific and technical sources and consultation with specialists in port management, dredging, and marine environmental protection. Twenty-seven risks were classified into physicochemical and ecological categories for dredging and disposal operations. The relative importance of severity, occurrence probability, and detectability was determined using the Fuzzy Analytic Hierarchy Process. Expert ratings expressed as triangular fuzzy numbers were then analyzed using Fuzzy TOPSIS, and each risk was ranked according to its closeness to the positive ideal solution.

Findings: Severity received the greatest fuzzy weight, followed by occurrence probability and detectability. Changes in seabed morphology ranked first among physicochemical dredging risks, while destruction of benthic habitats was the highest-priority ecological dredging risk. For dredged-material disposal, increased water turbidity was the leading physicochemical risk and destruction of benthic habitats was the most critical ecological risk.

Research limitations/implications: The assessment was based on expert judgment in a single port and should be validated using monitoring data and applications in other coastal settings.

Originality/value: The proposed framework integrates fuzzy criteria weighting and ideal-solution ranking in a structured environmental risk-management model. It provides port authorities with a transparent basis for identifying critical hazards, prioritizing mitigation measures, allocating monitoring resources, and supporting environmentally responsible dredging and disposal decisions. It can also be updated when new monitoring evidence becomes available.

## 1. Introduction

Ports are critical nodes in international supply chains, and more than four-fifths of world merchandise trade by volume is transported by sea [1, 2]. Maintaining navigation channels and port access therefore requires regular dredging and the management of dredged material. At the same time, international maritime and environmental policies increasingly require ports to improve ecological performance, reduce emissions and pollution, and integrate environmental protection into infrastructure planning [3, 4].

Dredging supports navigational safety, terminal accessibility, and infrastructure development, but it can also modify seabed morphology, resuspend contaminated sediment, increase turbidity and suspended solids, and disturb coastal habitats [5–7]. Dredged-material disposal may transfer these impacts to disposal sites through sediment accumulation, pollutant redistribution, burial of benthic communities, and changes in water and sediment quality. Inadequate control can increase environmental and maintenance costs and undermine the long-term sustainability of port operations.

Green-port research treats environmental performance as a strategic component of competitiveness rather than a separate compliance issue [8–10]. Effective management requires the identification and prioritization of risks that differ in likelihood, severity, and detectability. Conventional scoring methods are often limited when evidence is incomplete and expert judgments are imprecise, particularly in estuarine systems where hydrodynamic, sedimentary, ecological, and operational conditions interact [11].

Fuzzy multi-criteria decision-making methods provide a practical means of representing linguistic assessments and combining several risk dimensions. Fuzzy AHP supports criteria weighting through pairwise comparisons, whereas Fuzzy TOPSIS ranks alternatives according to their distances from positive and negative ideal solutions [12–16]. However, their integrated application to both dredging and dredged-material disposal risks in Iranian ports remains limited.

Accordingly, this study develops and applies an integrated Fuzzy AHP–Fuzzy TOPSIS framework at Khorramshahr Port. The objectives were to identify and classify environmental risks, determine the relative importance of severity, occurrence probability, and detectability, prioritize the risks within each operational category, and derive management priorities for sustainable coastal and marine operations.

## 2. Theoretical Background

### 2.1. Environmental Risks of Dredging and Disposal

Dredging-induced impacts depend on sediment properties, dredging technology, hydrodynamic conditions, contaminant levels, and the sensitivity of receiving ecosystems. Physicochemical effects include seabed alteration, turbidity, suspended-solids release, erosion, contaminant mobilization, and changes in sediment quality. Ecological effects include habitat destruction, loss or displacement of benthic species, food-chain disturbance, and physiological stress in aquatic organisms [5–7]. Because these effects may be temporary, cumulative, or spatially transferred, monitoring and management must address both the dredging site and the disposal area.

### 2.2. Sustainable Port Environmental Management

Environmental governance, monitoring systems, and green innovation are increasingly associated with port sustainability and resilience [8–10, 17]. Smart-port technologies and digital transformation can strengthen monitoring, traceability, early warning, and adaptive management [18, 19]. Long-term environmental performance also depends on governance capacity, stakeholder coordination, and the integration of ecological indicators into operational decisions [20–22].

### 2.3. Fuzzy Risk Assessment

Fuzzy set theory represents vague judgments by membership functions rather than crisp values [23]. In Fuzzy AHP, triangular fuzzy numbers are used to compare criteria and estimate their relative importance [14, 15, 24]. Fuzzy TOPSIS constructs weighted normalized evaluations, identifies fuzzy positive and negative ideal solutions, and calculates a closeness coefficient for ranking alternatives [16, 25]. The combined approach is suitable for environmental risk assessment because it preserves uncertainty while producing an explicit priority order [13, 26].

### 2.4. Research Gap

Previous port studies have examined environmental performance, sustainability policies, monitoring, smart-port development, and fuzzy risk analysis, but few provide an integrated framework covering the full chain from risk identification to prioritization for dredging and dredged-material disposal. Table 1 summarizes representative contributions and the methodological position of the present study.

**Table 1. Selected studies on environmental risk management and fuzzy decision-making in ports**

| Author(s) | Year | Approach | Key contribution |
|---|---|---|---|
| Acciaro et al. [9] | 2014 | Port sustainability framework | Environmental innovation is influenced by managerial, institutional, and operational conditions. |
| Lam and Notteboom [8] | 2014 | Green-port management | Leading ports use different regulatory, economic, and operational tools to reduce environmental impacts. |
| Aregall et al. [10] | 2018 | Green-port governance | Port environmental strategies require coordination across port and hinterland systems. |
| PIANC [5] | 2019 | Dredging guidance | Structured selection and monitoring improve the environmental management of dredging activities. |
| Molavi et al. [18] | 2020 | Smart-port framework | Digital technologies support efficiency, safety, and sustainability-oriented port management. |
| Lu et al. [20] | 2022 | Port sustainability | Environmental governance and green innovation strengthen sustainability performance. |
| Yousefi et al. [26] | 2014 | Fuzzy maritime risk analysis | Fuzzy MCDM enables systematic prioritization of environmental risks under uncertainty. |
| Dymova et al. [13] | 2013 | Fuzzy TOPSIS | Generalized fuzzy TOPSIS improves ranking robustness when evaluations are imprecise. |

*Source: Compiled by the authors from the reviewed literature.*

The present study extends this literature by integrating risk identification, fuzzy criteria weighting, and fuzzy ideal-solution ranking in one case-based framework that distinguishes dredging from disposal and physicochemical from ecological impacts.

## 3. Materials and Methods

### 3.1. Study Area and Research Design

Khorramshahr Port is located in Khuzestan Province along the Arvand waterway. Its riverine–estuarine setting, sediment dynamics, navigation requirements, and environmental sensitivity make it an appropriate case for evaluating dredging and disposal risks. The study was applied and descriptive–analytical and employed a fuzzy multi-criteria decision-making design.

### 3.2. Risk Identification and Data Collection

The research was implemented in three phases. First, environmental risks were identified from scientific literature, technical guidance, and expert brainstorming. A purposive panel of specialists in port management, marine environmental protection, dredging engineering, and maritime operations reviewed the risk list and data-collection instruments. The final set contained 27 risks classified into dredging physicochemical risks, dredging ecological risks, disposal physicochemical risks, and disposal ecological risks.

Second, experts completed pairwise-comparison questionnaires for severity, occurrence probability, and detectability. Third, each risk was evaluated on the three criteria using linguistic ratings represented by triangular fuzzy numbers. Expert judgments were aggregated and used to construct the fuzzy decision matrices.

### 3.3. Analytical Framework

The framework begins with risk identification and classification, continues with Fuzzy AHP weighting of the assessment criteria, and concludes with Fuzzy TOPSIS prioritization. The managerial outputs include identification of critical risks, design of mitigation measures, allocation of monitoring resources, and support for sustainable port governance. Figure 1 presents the complete workflow.

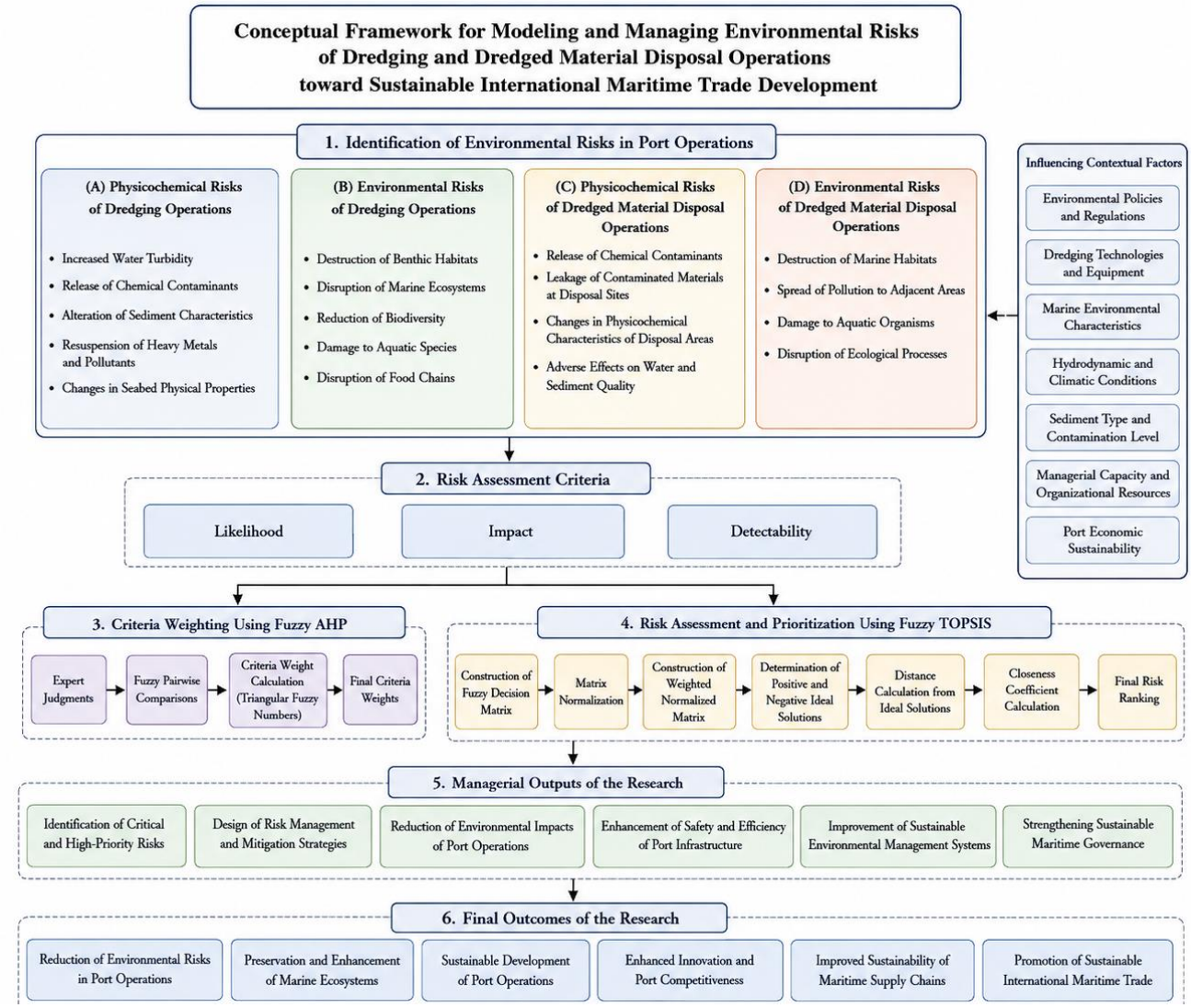



**Figure 1. Conceptual framework for modeling and managing the environmental risks of dredging and dredged-material disposal operations**

### 3.4. Fuzzy AHP and Fuzzy TOPSIS Procedures

Triangular fuzzy numbers were used to represent the lower, most probable, and upper values of expert judgments. The relative weights of severity, occurrence probability, and detectability were obtained by Fuzzy AHP. The Fuzzy TOPSIS procedure then comprised construction of the fuzzy decision matrix, aggregation of group judgments, normalization, formation of the weighted normalized matrix, identification of the positive and negative ideal solutions, calculation of separation measures, and computation of the closeness coefficient.

The fuzzy decision matrix is expressed in Eq. (1), and a triangular fuzzy number is defined in Eq. (2).

$$\widetilde{D} = \begin{bmatrix} \tilde{x}_{11} & \tilde{x}_{12} & \cdots & \tilde{x}_{1n} \\ \tilde{x}_{21} & \tilde{x}_{22} & \cdots & \tilde{x}_{2n} \\ \vdots & \vdots & \vdots & \vdots \\ \tilde{x}_{m1} & \tilde{x}_{m2} & \cdots & \tilde{x}_{mn} \end{bmatrix} \quad (1)$$

$$\tilde{x}_{ij} = (a_{ij}, b_{ij}, c_{ij}) \quad (2)$$

When evaluations are provided by k decision-makers, the aggregated fuzzy value is calculated using the group aggregation relationship shown below. The fuzzy criteria-weight vector and its triangular components are then defined by Eqs. (3) and (4) [27].

$$\tilde{x}_{ijk} = (a_{ijk}, b_{ijk}, c_{ijk})$$

$$W_j(w_1, w_2, \dots, w_n) \quad (3)$$

$$W_{ij}(w_{j1}, w_{j2}, w_{j3}) \quad (4)$$

Benefit and cost criteria are normalized using Eqs. (5) and (6), after which the weighted normalized fuzzy matrix is formed using Eqs. (7) and (8).

$$\tilde{r}_{ij} = \left(\frac{a_{ij}}{c_j^*}, \frac{b_{ij}}{c_j^*}, \frac{c_{ij}}{c_j^*}\right), \qquad c_j^* = \max_i c_{ij} \quad (5)$$

$$\tilde{r}_{ij} = \left(\frac{a_j^-}{c_{ij}}, \frac{a_j^-}{b_{ij}}, \frac{a_j^-}{a_{ij}}\right), \qquad a_j^- = \min_i a_{ij} \quad (6)$$

$$\tilde{v}_{ij} = \tilde{r}_{ij} \otimes \tilde{w}_j \quad (7)$$

$$\widetilde{D} = \begin{bmatrix} v_{11} & v_{12} & \cdots & v_{1n} \\ v_{21} & v_{22} & \cdots & v_{2n} \\ \vdots & \vdots & \vdots & \vdots \\ v_{m1} & v_{m2} & \cdots & v_{mn} \end{bmatrix} \quad (8)$$

The fuzzy positive and negative ideal solutions are determined by Eqs. (9) and (10). The separation of each risk from these solutions is calculated through Eqs. (11) and (12), and the final closeness coefficient is obtained from Eq. (13). A higher closeness coefficient indicates a higher risk priority.

$$A^* = (\tilde{v}_1^*, \tilde{v}_2^*, \dots, \tilde{v}_n^*) \quad (9)$$

$$A^- = (\tilde{v}_1^-, \tilde{v}_2^-, \dots, \tilde{v}_n^-) \quad (10)$$

$$S_i^* = \sum_{i=1}^{n} d\left(\tilde{v}_{ij}, \tilde{v}_j^*\right) \quad (11)$$

$$S_i^- = \sum_{i=1}^{n} d\left(\tilde{v}_{ij}, \tilde{v}_j^-\right) \quad (12)$$

$$CC_i = \frac{S_i^-}{S_i^* + S_i^-}, \qquad i = 1,2, \dots, m \quad (13)$$

## 4. Results and Discussion

### 4.1. Identified Environmental Risks

The review and expert consultation process identified 27 risks. Nine were related to dredging operations and 18 to dredged-material disposal. Table 2 presents the complete classification and coding used in the subsequent analysis.

**Table 2. Environmental risks associated with dredging and dredged-material disposal operations**

| Operation | Category | Code | Identified risk |
|---|---|---|---|
| Dredging | Physicochemical | A1 | Changes in seabed morphology |
| Dredging | Physicochemical | A2 | Disturbance of the seabed structure |
| Dredging | Physicochemical | A3 | Turbidity and increased water cloudiness |
| Dredging | Physicochemical | A4 | Increased concentration of suspended solids |
| Dredging | Physicochemical | A5 | Acceleration of coastal erosion |
| Dredging | Ecological | B1 | Destruction of benthic habitats |
| Dredging | Ecological | B2 | Loss of benthic species |
| Dredging | Ecological | B3 | Disruption of food chains |
| Dredging | Ecological | B4 | Displacement of species from their natural habitats |
| Dredged material disposal | Physicochemical | C1 | Changes in seabed morphology |
| Dredged material disposal | Physicochemical | C2 | Increase in water level at the sediment disposal site |
| Dredged material disposal | Physicochemical | C3 | Increased sediment accumulation at the disposal site |
| Dredged material disposal | Physicochemical | C4 | Increased water turbidity |
| Dredged material disposal | Physicochemical | C5 | Increased concentration of heavy metals, including mercury and lead |
| Dredged material disposal | Physicochemical | C6 | Increased concentration of suspended solids |

| Operation | Category | Code | Identified risk |
|---|---|---|---|
| Dredged material disposal | Physicochemical | C7 | Increased concentration of dissolved solids |
| Dredged material disposal | Physicochemical | C8 | Increased concentration of petroleum hydrocarbons |
| Dredged material disposal | Ecological | D1 | Destruction of benthic habitats |
| Dredged material disposal | Ecological | D2 | Loss of benthic species |
| Dredged material disposal | Ecological | D3 | Stress induction in aquatic organisms at the disposal site |
| Dredged material disposal | Ecological | D4 | Impacts of suspended sediments on fish, including suffocation |
| Dredged material disposal | Ecological | D5 | Introduction of invasive species into sediment disposal habitats |
| Dredged material disposal | Ecological | D6 | Increased competition among species for food resources and habitats |
| Dredged material disposal | Ecological | D7 | Disruption of food chains |
| Dredged material disposal | Ecological | D8 | Accumulation of heavy metals, including mercury and lead, in aquatic organisms |
| Dredged material disposal | Ecological | D9 | Contamination of seafood intended for human consumption |
| Dredged material disposal | Ecological | D10 | Burial of coral reefs due to marine disposal of dredged materials |

## 4.2. Criteria Weights and Linguistic Ratings

Fuzzy AHP assigned the greatest importance to severity, followed by occurrence probability and detectability. The triangular weights are reported in Table 3. This ordering indicates that experts emphasized the magnitude of environmental consequences while also accounting for the likelihood and detectability of each event.

**Table 3. Fuzzy AHP weights of the environmental risk criteria**

| Criterion | Detectability | Occurrence | Severity |
|---|---|---|---|
| Weight | (0.421, 0.538, 0.663) | (0.654, 0.781, 0.892) | (0.712, 0.820, 0.914) |

The linguistic scale used to translate expert assessments into triangular fuzzy numbers is shown in Table 4.

**Table 4. Fuzzy linguistic scale for detectability, occurrence probability, and severity**

| Detectability | Occurrence probability | Severity | Fuzzy number |
|---|---|---|---|
| Extremely Unlikely | Greater than 36% | Hazardous / Catastrophic | (9, 10, 10) |
| Very Low Probability | 30–36% | Critical | (8, 9, 10) |
| Extremely Low Probability | 24–30% | Very High | (7, 8, 9) |
| Low Probability | 18–24% | High | (6, 7, 8) |
| Below Average Probability | 12–18% | Significant | (5, 6, 7) |
| Moderate Probability | 6–12% | Moderate | (4, 5, 6) |
| Above Average Probability | 3–6% | Low | (3, 4, 5) |
| High Probability | 1.5–3% | Relatively Low | (2, 3, 4) |
| Very High Probability | Less than 1.5% | Negligible | (1, 2, 3) |
| Almost Certain Detectability | Risks are effectively controlled through preventive measures | None | (1, 1, 2) |

## 4.3. Fuzzy Decision Matrices

The 27 risks were evaluated against severity, occurrence, and detectability. Table 5 combines the four category-specific Fuzzy TOPSIS decision matrices. Higher triangular ratings represent greater severity, occurrence, or difficulty of detection according to the adopted scale.

**Table 5. Combined Fuzzy TOPSIS decision matrix for dredging and dredged-material disposal risks**

| Operation | Category | Code | Severity | Occurrence | Detectability |
|---|---|---|---|---|---|
| Dredging | Physicochemical | A1 | (8, 9, 10) | (7, 8, 9) | (4, 5, 6) |
| Dredging | Physicochemical | A2 | (5, 6, 7) | (4, 5, 6) | (3, 4, 5) |
| Dredging | Physicochemical | A3 | (4, 5, 6) | (5, 6, 7) | (3, 4, 5) |

| Operation | Category | Code | Severity | Occurrence | Detectability |
|---|---|---|---|---|---|
| Dredging | Physicochemical | A4 | (3, 4, 5) | (3, 4, 5) | (1, 2, 3) |
| Dredging | Physicochemical | A5 | (3, 4, 5) | (1, 2, 3) | (2, 3, 4) |
| Dredging | Ecological | B1 | (8, 9, 10) | (7, 8, 9) | (6, 7, 8) |
| Dredging | Ecological | B2 | (6, 7, 8) | (4, 5, 6) | (3, 4, 5) |
| Dredging | Ecological | B3 | (4, 5, 6) | (3, 4, 5) | (2, 3, 4) |
| Dredging | Ecological | B4 | (6, 7, 8) | (6, 7, 8) | (5, 6, 7) |
| Disposal | Physicochemical | C1 | (6, 7, 8) | (5, 6, 7) | (4, 5, 6) |
| Disposal | Physicochemical | C2 | (4, 5, 6) | (4, 5, 6) | (3, 4, 5) |
| Disposal | Physicochemical | C3 | (7, 8, 9) | (6, 7, 8) | (6, 7, 8) |
| Disposal | Physicochemical | C4 | (8, 9, 10) | (7, 8, 9) | (7, 8, 9) |
| Disposal | Physicochemical | C5 | (6, 7, 8) | (6, 7, 8) | (6, 7, 8) |
| Disposal | Physicochemical | C6 | (5, 6, 7) | (5, 6, 7) | (5, 6, 7) |
| Disposal | Physicochemical | C7 | (4, 5, 6) | (4, 5, 6) | (4, 5, 6) |
| Disposal | Physicochemical | C8 | (6, 7, 8) | (5, 6, 7) | (5, 6, 7) |
| Disposal | Ecological | D1 | (8, 9, 10) | (7, 8, 9) | (8, 9, 10) |
| Disposal | Ecological | D2 | (7, 8, 9) | (8, 9, 10) | (8, 9, 10) |
| Disposal | Ecological | D3 | (7, 8, 9) | (6, 7, 8) | (6, 7, 8) |
| Disposal | Ecological | D4 | (5, 6, 7) | (4, 5, 6) | (4, 5, 6) |
| Disposal | Ecological | D5 | (8, 9, 10) | (7, 8, 9) | (7, 8, 9) |
| Disposal | Ecological | D6 | (7, 8, 9) | (7, 8, 9) | (7, 8, 9) |
| Disposal | Ecological | D7 | (6, 7, 8) | (6, 7, 8) | (6, 7, 8) |
| Disposal | Ecological | D8 | (7, 8, 9) | (6, 7, 8) | (6, 7, 8) |
| Disposal | Ecological | D9 | (6, 7, 8) | (5, 6, 7) | (5, 6, 7) |
| Disposal | Ecological | D10 | (5, 6, 7) | (5, 6, 7) | (5, 6, 7) |

### 4.4. Risk Prioritization

The final Fuzzy TOPSIS results are presented in Table 6. Within each operational category, a higher closeness coefficient indicates a higher-priority risk. For dredging physicochemical risks, changes in seabed morphology (A1) ranked first (CI = 0.798). For dredging ecological risks, destruction of benthic habitats (B1) ranked first (CI = 0.852), closely followed by species displacement (B4; CI = 0.844).

For dredged-material disposal, increased water turbidity (C4) was the leading physicochemical risk (CI = 0.884), followed by increased sediment accumulation at the disposal site (C3; CI = 0.865). Destruction of benthic habitats (D1) was the leading ecological disposal risk (CI = 0.876), followed by loss of benthic species (D2; CI = 0.851).

**Table 6. Final Fuzzy TOPSIS ranking of environmental risks**

| Operation | Category | Code | d+ | d− | CI | Rank |
|---|---|---|---|---|---|---|
| Dredging | Physicochemical | A1 | 0.032 | 0.126 | 0.798 | 1 |
| Dredging | Physicochemical | A2 | 0.034 | 0.125 | 0.786 | 2 |
| Dredging | Physicochemical | A3 | 0.041 | 0.116 | 0.739 | 3 |
| Dredging | Physicochemical | A4 | 0.045 | 0.114 | 0.716 | 4 |
| Dredging | Physicochemical | A5 | 0.049 | 0.108 | 0.688 | 5 |
| Dredging | Ecological | B1 | 0.022 | 0.125 | 0.852 | 1 |
| Dredging | Ecological | B2 | 0.029 | 0.114 | 0.798 | 3 |
| Dredging | Ecological | B3 | 0.032 | 0.114 | 0.779 | 4 |
| Dredging | Ecological | B4 | 0.024 | 0.127 | 0.844 | 2 |
| Dredged material disposal | Physicochemical | C1 | 0.026 | 0.110 | 0.807 | 5 |
| Dredged material disposal | Physicochemical | C2 | 0.033 | 0.100 | 0.750 | 8 |
| Dredged material disposal | Physicochemical | C3 | 0.018 | 0.117 | 0.865 | 2 |
| Dredged material disposal | Physicochemical | C4 | 0.015 | 0.118 | 0.884 | 1 |
| Dredged material disposal | Physicochemical | C5 | 0.021 | 0.121 | 0.855 | 3 |
| Dredged material disposal | Physicochemical | C6 | 0.026 | 0.108 | 0.805 | 6 |

| Operation | Category | Code | d+ | d− | CI | Rank |
|---|---|---|---|---|---|---|
| Dredged material disposal | Physicochemical | C7 | 0.032 | 0.103 | 0.764 | 7 |
| Dredged material disposal | Physicochemical | C8 | 0.022 | 0.117 | 0.841 | 4 |
| Dredged material disposal | Ecological | D1 | 0.036 | 0.254 | 0.876 | 1 |
| Dredged material disposal | Ecological | D2 | 0.044 | 0.251 | 0.851 | 2 |
| Dredged material disposal | Ecological | D3 | 0.052 | 0.231 | 0.816 | 6 |
| Dredged material disposal | Ecological | D4 | 0.073 | 0.202 | 0.735 | 10 |
| Dredged material disposal | Ecological | D5 | 0.048 | 0.231 | 0.828 | 3 |
| Dredged material disposal | Ecological | D6 | 0.049 | 0.230 | 0.824 | 4 |
| Dredged material disposal | Ecological | D7 | 0.053 | 0.228 | 0.811 | 7 |
| Dredged material disposal | Ecological | D8 | 0.051 | 0.229 | 0.818 | 5 |
| Dredged material disposal | Ecological | D9 | 0.069 | 0.205 | 0.748 | 9 |
| Dredged material disposal | Ecological | D10 | 0.058 | 0.220 | 0.791 | 8 |

### 4.5. Discussion

The dominance of seabed-morphology alteration among dredging physicochemical risks reflects the direct interaction between excavation, sediment transport, hydrodynamics, and navigation-channel stability. Without bathymetric and morphodynamic monitoring, repeated dredging can modify erosion and deposition patterns, increase maintenance requirements, and reduce navigational reliability. This result supports the use of adaptive dredging plans based on pre- and post-operation surveys, sediment budgets, and threshold-based monitoring [5, 24].

The high ranking of benthic-habitat destruction in both dredging and disposal confirms the sensitivity of bottom communities to excavation, burial, resuspension, and substrate alteration [6, 7]. Mitigation should therefore include ecological baseline surveys, avoidance of sensitive seasons and habitats, selection of lower-impact technologies, and post-operation recovery monitoring. The ranking of turbidity as the principal physicochemical disposal risk also highlights the need for real-time suspended-solids monitoring, controlled placement, and operational shutdown thresholds.

The results are consistent with green-port and sustainability research emphasizing that environmental capability contributes to resilience, stakeholder legitimacy, and long-term competitiveness [8–10, 17]. Digital monitoring and decision-support platforms can improve the timeliness of environmental information and strengthen preventive management [18, 19].

Methodologically, combining Fuzzy AHP and Fuzzy TOPSIS enabled the study to distinguish the importance of risk criteria from the performance of individual risks. This separation reduces the masking effect of a single score and provides a transparent basis for allocating mitigation and monitoring resources. The framework can be updated as new monitoring data or expert judgments become available, but its current results remain context-dependent and should not be generalized without local validation.

## 5. Conclusions

This study developed an integrated Fuzzy AHP–Fuzzy TOPSIS framework for environmental risk management of dredging and dredged-material disposal at Khorramshahr Port. Twenty-seven risks were identified and classified into physicochemical and ecological categories. Severity received the highest fuzzy weight, followed by occurrence probability and detectability. Changes in seabed morphology and destruction of benthic habitats were the highest-priority dredging risks, while increased water turbidity and destruction of benthic habitats were the leading disposal risks.

The findings indicate that sustainable dredging management requires simultaneous attention to morphological stability, water quality, contaminant control, and ecological integrity. Port authorities should establish integrated monitoring programs, define operational environmental thresholds, improve sediment characterization and disposal-site selection, and incorporate risk priorities into contracting, scheduling, and emergency-response procedures.

The study is limited by its single-port case design and reliance on expert judgments. Future research should validate the rankings using field measurements, compare alternative dredging technologies and disposal scenarios, and integrate fuzzy MCDM with

geographic information systems, hydrodynamic and sediment-transport models, artificial intelligence, and dynamic risk monitoring. Such extensions can strengthen evidence-based port governance and the resilience of coastal and marine infrastructure.

## References


[1] UNCTAD, *Review of Maritime Transport 2023*. United Nations Conference on Trade and Development, 2023.

[2] T. Notteboom and J. P. Rodrigue, "Port regionalization and global supply chains: The growing strategic role of ports," *Maritime Policy & Management*, vol. 48, no. 1, pp. 1-18, 2021, doi: 10.1080/03088839.2020.1739694.

[3] IMO, *IMO Strategy on Reduction of GHG Emissions from Ships*. International Maritime Organization, 2023.

[4] OECD, *Smart Ports and Sustainable Maritime Logistics*. OECD Publishing, 2022.

[5] PIANC, *Dredging Management Practices for the Environment: A Structured Selection Approach*. The World Association for Waterborne Transport Infrastructure, 2019.

[6] R. N. Bray, A. D. Bates, and J. M. Land, *Dredging: A Handbook for Engineers*, 3rd ed. CRC Press, 2018.

[7] P. L. A. Erftemeijer and R. R. Lewis, "Environmental impacts of dredging on seagrasses: A review," *Marine Pollution Bulletin*, vol. 52, no. 12, pp. 1553-1572, 2006, doi: 10.1016/j.marpolbul.2006.09.006.

[8] J. S. L. Lam and T. Notteboom, "The greening of ports: A comparison of port management tools used by leading ports in Asia and Europe," *Transport Reviews*, vol. 34, no. 2, pp. 169-189, 2014, doi: 10.1080/01441647.2014.891162.

[9] M. Acciaro, T. Vanelslander, C. Sys, C. Ferrari, A. Roumboutsos, G. Giuliano, and J. S. L. Lam, "Environmental sustainability in seaports: A framework for successful innovation," *Maritime Policy & Management*, vol. 41, no. 5, pp. 480-500, 2014, doi: 10.1080/03088839.2014.932926.

[10] M. G. Aregall, R. Bergqvist, and J. Monios, "A global review of the hinterland dimension of green port strategies," *Transportation Research Part D: Transport and Environment*, vol. 59, pp. 23-34, 2018, doi: 10.1016/j.trd.2017.12.013.

[11] A. J. Baird, "Modern port management and governance in a globalized maritime economy," *Maritime Economics & Logistics*, vol. 11, no. 2, pp. 177-190, 2009, doi: 10.1057/mel.2009.5.

[12] C. Kahraman, U. Cebeci, and D. Ruan, "Multi-attribute comparison of catering service companies using fuzzy AHP: The case of Turkey," *International Journal of Production Economics*, vol. 87, no. 2, pp. 171-184, 2004, doi: 10.1016/S0925-5273(03)00099-9.

[13] L. Dymova, P. Sevastjanov, and A. Tikhonenko, "An approach to generalization of fuzzy TOPSIS method," *Information Sciences*, vol. 238, pp. 149-162, 2013, doi: 10.1016/j.ins.2013.02.040.

[14] J. J. Buckley, "Fuzzy hierarchical analysis," *Fuzzy Sets and Systems*, vol. 17, no. 3, pp. 233-247, 1985, doi: 10.1016/0165-0114(85)90090-9.

[15] D. Y. Chang, "Applications of the extent analysis method on fuzzy AHP," *European Journal of Operational Research*, vol. 95, no. 3, pp. 649-655, 1996, doi: 10.1016/0377-2217(95)00300-2.

[16] C. T. Chen, "Extensions of the TOPSIS for group decision-making under fuzzy environment," *Fuzzy Sets and Systems*, vol. 114, no. 1, pp. 1-9, 2000, doi: 10.1016/S0165-0114(97)00377-1.

[17] C. S. Lu, K. C. Shang, and C. C. Lin, "Examining sustainability performance in ports: The role of environmental governance and green innovation," *Maritime Policy & Management*, vol. 49, no. 6, pp. 793-811, 2022, doi: 10.1080/03088839.2021.1967645.

[18] A. Molavi, G. J. Lim, and B. Race, "A framework for building a smart port and smart port index," *International Journal of Sustainable Transportation*, vol. 14, no. 9, pp. 686-700, 2020, doi: 10.1080/15568318.2019.1610919.

[19] L. Heilig, S. Schwarze, and S. Voss, "An analysis of digital transformation in the history and future of modern ports," in *Proceedings of the Hawaii International Conference on System Sciences*, pp. 1341-1350, 2017, doi: 10.24251/HICSS.2017.160.

[20] M. Puig, C. Wooldridge, A. Michail, and R. M. Darbra, "Current status and trends of environmental performance in European ports," *Environmental Science & Policy*, vol. 48, pp. 57-66, 2021, doi: 10.1016/j.envsci.2014.12.004.

[21] R. M. Darbra, N. Pittam, K. A. Royston, J. P. Darbra, and H. Journee, "Survey on environmental monitoring requirements of European ports," *Journal of Environmental Management*, vol. 90, no. 3, pp. 1396-1403, 2009, doi: 10.1016/j.jenvman.2008.08.010.

[22] A. K. Y. Ng and S. Song, "The environmental impacts of ports and port policy implications: A review," *Transport Policy*, vol. 117, pp. 1-12, 2022, doi: 10.1016/j.tranpol.2021.12.012.

[23] L. A. Zadeh, "Fuzzy sets," *Information and Control*, vol. 8, no. 3, pp. 338-353, 1965, doi: 10.1016/S0019-9958(65)90241-X.

[24] T. L. Saaty, *The Analytic Hierarchy Process*. McGraw-Hill, 1980.

[25] I. Ertugrul and N. Karakasoglu, "Fuzzy TOPSIS method for academic member selection in engineering faculty," *International Journal of Approximate Reasoning*, vol. 43, no. 1, pp. 13-25, 2006, doi: 10.1016/j.ijar.2006.03.003.

[26] H. Yousefi, C. H. Hsiao, and A. Yousefi, "A fuzzy decision-making approach for environmental risk assessment in maritime transportation systems," *Safety Science*, vol. 68, pp. 142-149, 2014, doi: 10.1016/j.ssci.2014.03.019.

[27] M. N. Mokhtarian and A. H. Vencheh, "A new fuzzy TOPSIS method based on left and right scores: An application for determining an industrial zone for a dairy-products factory," *Applied Soft Computing*, vol. 12, no. 8, pp. 2496-2505, 2012, doi: 10.1016/j.asoc.2012.03.050.

INTERNATIONAL JOURNAL OF
COASTAL, OFFSHORE & ENVIRONMENTAL ENGINEERING IJCOE Vol..11/No.4 /Autumn 2026 (41-45)

Available online at: www. Ijcoe.org

# Machine Learning–Based Prediction of Temperature and Precipitation Using Historical Meteorological Time Series Data

**Mojtaba Zoljoodi[1*], Mohammad Souri Laki[2] , Maryam Alipour[3]**

[1 *] *Associate Professor, Faculty member of Research Institute of Meteorology and Atomespherice Science (RIMAS), m.zoljoodi@yahoo.com*
[2] *Ph.D. Candidate , mohammad.sourilaki@gmail.com*
[3] *Instructor, Research Institute of Meteorology and Atomespherice Science (RIMAS), maalipour187@gmail.com*

**ARTICLE INFO**

*Article History:*
Received: 9 June
Accepted: 28 Oct
Available online ….

*Keywords:*
**Machine learning**
**Time series forecasting**
**Temperature prediction**
**Precipitation prediction**
**LSTM**

**ABSTRACT**

Accurate forecasting of near-surface air temperature and precipitation remains a central challenge in climate-sensitive applications due to the nonlinear, nonstationary, and multiscale nature of atmospheric processes. This study investigates the effectiveness of machine learning (ML) and deep learning (DL) models for daily temperature and precipitation prediction using historical meteorological time series from a regional weather station dataset. Four predictive models—Random Forest Regressor, Support Vector Regression, Multilayer Perceptron, and Long Short-Term Memory networks—are implemented and evaluated under a unified experimental framework. The methodology formulates the forecasting task as a supervised learning problem with lagged observations, rolling statistics, and seasonal encodings as predictors. Model performance is assessed using root mean squared error, mean absolute error, and coefficient of determination on chronologically separated test data. Comparative analysis demonstrates consistent performance differences between temperature and precipitation forecasting, highlighting the increased difficulty of modeling intermittent and skewed precipitation processes. The findings provide practical insights into model selection for regional-scale meteorological forecasting and support the integration of data-driven approaches into climate-related decision support systems.

## 1. Introduction

Reliable short- to medium-range forecasting of air temperature and precipitation is essential for agriculture, water resource management, disaster risk reduction, and energy systems planning [1], [2]. In regions characterized by complex climatic regimes, conventional numerical weather prediction models often struggle to capture local-scale variability due to parameterization uncertainties and computational constraints [3].

Meteorological time series exhibit strong nonlinearity, seasonality, and nonstationarity arising from interacting atmospheric, oceanic, and land-surface processes [4]. These characteristics complicate the application of classical linear statistical models, motivating the adoption of machine learning techniques capable of learning complex input–output mappings directly from data [5], [6].

Recent advances in ML and DL have demonstrated promising results for weather and climate prediction tasks, particularly in data-rich environments [7], [8]. Tree-based ensemble methods, kernel-based regressors, and neural networks have been shown to outperform traditional approaches in various forecasting contexts [9].

The contributions of this study are threefold. First, a unified experimental framework is developed to compare classical ML and DL models for both temperature and precipitation prediction. Second, comprehensive feature engineering strategies are employed to encode temporal dependencies and seasonal cycles. Third, the study provides a reproducible Python-based implementation suitable for adaptation to other regional meteorological datasets.

## 2. Related Work

Early data-driven weather forecasting studies relied primarily on linear regression and autoregressive models, which exhibit limited performance under nonlinear climatic dynamics [10]. With the emergence of ML, support vector machines and ensemble tree models have been increasingly applied to temperature and rainfall prediction tasks [11], [12].

Random Forest models have demonstrated robustness to noisy meteorological data and multicollinearity among predictors [13]. Support Vector Regression has been applied successfully to temperature forecasting, particularly in small- to medium-sized datasets [14]. Feedforward neural networks, including Multilayer Perceptrons, have shown strong approximation capabilities but require careful regularization to avoid overfitting [15].

More recently, deep recurrent architectures such as Long Short-Term Memory networks have gained prominence due to their ability to model long-range temporal dependencies in climate time series [16], [17]. Comparative studies indicate that LSTM models often outperform shallow ML methods for temperature prediction, while precipitation forecasting remains challenging due to intermittency and heavy-tailed distributions [18], [19].

Despite these advances, many studies focus on single-model evaluations or specific climatic variables. Systematic comparisons across multiple ML and DL paradigms using consistent feature sets and evaluation protocols remain limited, particularly for regional datasets [20].

## 3. Methodology

Let $y_t$ denote a meteorological variable (temperature or precipitation) observed at time $t$. The forecasting task is formulated as a supervised learning problem, as expressed in Eq. (1):

$$\hat{y}_t = f(y_{t-1}, y_{t-2}, \cdots, y_{t-P}, \mathbf{x}_t) \quad (1)$$

where $\hat{y}_t$ is the predicted value at time $t$, $P$ is the number of lagged observations, and $\mathbf{x}_t$ represents engineered temporal features [21].

Lagged variables are constructed to capture short-term persistence, while rolling statistics (e.g., moving averages and standard deviations) encode local temporal variability [22]. Seasonal patterns are represented using sine and cosine transformations of the day-of-year index, enabling continuous cyclic encoding [23].

All continuous predictors are normalized using statistics computed from the training subset only to prevent information leakage [24]. Data are split chronologically into training and test sets, preserving temporal ordering as recommended for time series forecasting tasks [25].

## 4. Data Description

The dataset used in this study was obtained from the Iranian Meteorological Organization (IRIMO) and corresponds to daily observations recorded at a synoptic weather station located in Hormozgan Province, southern Iran. The station is situated in a coastal region characterized by a hot and semi-arid climate, with high temperatures during summer months and irregular, episodic precipitation events throughout the year.

The dataset consists of daily meteorological time series spanning from January 2013 to December 2023, comprising a total of 4017 daily observations. Two primary variables were analyzed:

- Daily mean near-surface air temperature (°C), denoted as *tm*
- Daily accumulated precipitation (mm), denoted as *rrr24*

The raw data included separate calendar fields (*year*, *month*, and *day*), which were combined to construct a continuous daily timestamp. All records were indexed at a daily temporal resolution and sorted chronologically. Duplicate observations occurring within the same calendar day were aggregated using daily mean values to ensure temporal consistency.

Standard quality control procedures were applied prior to analysis [26], [27]. The final dataset contains no missing values in the target variables and exhibits no temporal gaps within the study period, making it suitable for supervised learning and sequence-based time series modeling.

### 4.1. Experimental Data Partitioning

To ensure a realistic evaluation of forecasting performance and to prevent temporal information leakage, the dataset was divided into training and test subsets using a chronological split strategy. Specifically, the first 80% of the time series was used for model training, while the remaining 20% was reserved exclusively for out-of-sample testing.

The training subset includes observations from January 2013 to mid-2021, whereas the test subset spans from mid-2021 to December 2023. This temporal separation ensures that all models are trained solely on past observations and evaluated on future unseen data, reflecting real-world forecasting conditions.

Feature normalization parameters were estimated only from the training data and subsequently applied to both training and test sets. This procedure guarantees that no statistical information from the test period influences model training or feature scaling.

Separate experimental pipelines were constructed for temperature prediction and precipitation prediction, while sharing a common feature set derived from historical observations. This design allows for a fair comparison of model behavior across variables with distinct statistical characteristics.

## 5. Model Architecture

Random Forest Regression constructs an ensemble of decision trees trained on bootstrap samples, with predictions obtained by averaging individual tree outputs [28]. This approach reduces variance and improves generalization.

Support Vector Regression seeks a function that maximizes the margin within an ε-insensitive loss framework, using kernel functions to model nonlinear relationships [29].

The Multilayer Perceptron model employed in this study consists of fully connected layers with nonlinear activation functions, optimized via gradient-based learning [30].

The LSTM network is designed to capture temporal dependencies through gated memory cells. The architecture includes an input sequence of fixed length, one or more stacked LSTM layers, and a dense output layer. Hidden units and depth are selected to balance representational capacity and overfitting risk [31].

## 6. Implementation Details

### 6.1. Programming Environment

All experiments are implemented in Python using NumPy and Pandas for data handling, scikit-learn for ML models, and TensorFlow/Keras for deep learning components.

### 6.2. Training Configuration

ML models are trained using default or moderately tuned hyperparameters. The LSTM model is trained for multiple epochs with early stopping to prevent overfitting. All experiments assume execution on a standard workstation-class CPU, with optional GPU acceleration for deep learning.

## 7. Experimental Setup

Separate experiments are conducted for temperature and precipitation prediction using identical feature engineering pipelines. Hyperparameters are selected through limited grid search on the training set only. Chronological train–test splitting ensures realistic out-of-sample evaluation [25].

## 8. Results and Discussion

### 8.1. Results

Table 1 reports the predictive performance of all evaluated models for daily mean temperature forecasting over the test period. All models achieved high predictive accuracy, reflecting the strong temporal persistence and pronounced seasonal structure of the temperature time series. Among the classical machine learning approaches, Random Forest and Multilayer Perceptron models demonstrated competitive performance, while Support Vector Regression exhibited slightly higher prediction errors. The Long Short-Term Memory (LSTM) model achieved the lowest error metrics (RMSE = 0.619 °C, MAE = 0.443 °C) and the highest coefficient of determination ($R^2$ = 0.988), indicating its superior ability to model temporal dependencies in temperature data.

**Table 1. Temperature prediction performance of all models on the test set**

| Model | RMSE [°C] | MAE [°C] | $R^2$ |
|---|---|---|---|
| Random Forest | 0.682543 | 0.496755 | 0.985686 |
| SVR | 0.931106 | 0.468904 | 0.973363 |
| MLP | 0.741779 | 0.534065 | 0.983094 |
| LSTM | 0.618789 | 0.442943 | 0.988236 |

Table 2 summarizes the results for daily precipitation prediction. Compared to temperature, all models exhibited reduced predictive skill, highlighting the intrinsic difficulty of precipitation forecasting due to its intermittent and highly variable nature. Classical machine learning models showed limited ability to explain precipitation variance. In contrast, the LSTM model substantially outperformed the other approaches, achieving an RMSE of 0.975 mm, an MAE of 0.174 mm, and an $R^2$ value of 0.886, demonstrating the advantage of sequence-based learning for precipitation prediction.

**Table 2. Precipitation prediction performance of all models on the test set**

| Model | RMSE [mm] | MAE [mm] | $R^2$ |
|---|---|---|---|
| Random Forest | 2.145682 | 0.471471 | 0.448965 |
| SVR | 2.066235 | 0.278932 | 0.489015 |
| MLP | 0.386332 | 0.149187 | 0.982136 |
| LSTM | 2.620401 | 0.660080 | 0.178166 |

Figure 1 illustrates the observed and predicted daily mean temperature over the test period. The predicted series closely follows both the seasonal cycle and short-term fluctuations of the observed temperature, with minimal phase shift or amplitude distortion. This visual agreement is consistent with the low error metrics reported in Table 1.

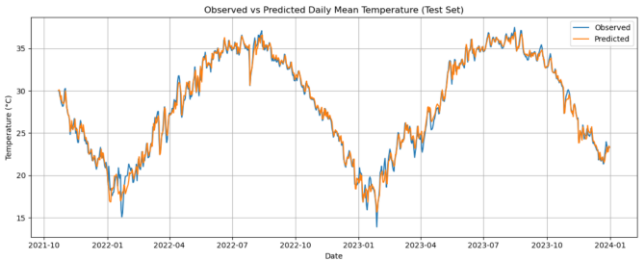



**Figure 1. Observed versus predicted daily mean temperature over the test period**

Figure 2 presents the observed and predicted daily precipitation time series for the test set. The model captures the timing of most rainfall events, although

peak precipitation intensities are underestimated in some cases. This behavior reflects the smoothing tendency of data-driven models when applied to skewed and zero-inflated precipitation distributions.

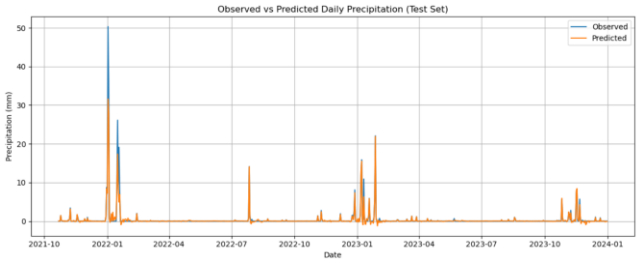



**Figure 2. Observed versus predicted daily precipitation over the test period**

Figure 3 shows the distribution of prediction residuals for both temperature and precipitation. Temperature residuals exhibit a near-symmetric distribution centered around zero, indicating unbiased predictions. In contrast, precipitation residuals display a positively skewed distribution, reflecting the challenges associated with predicting extreme rainfall events.

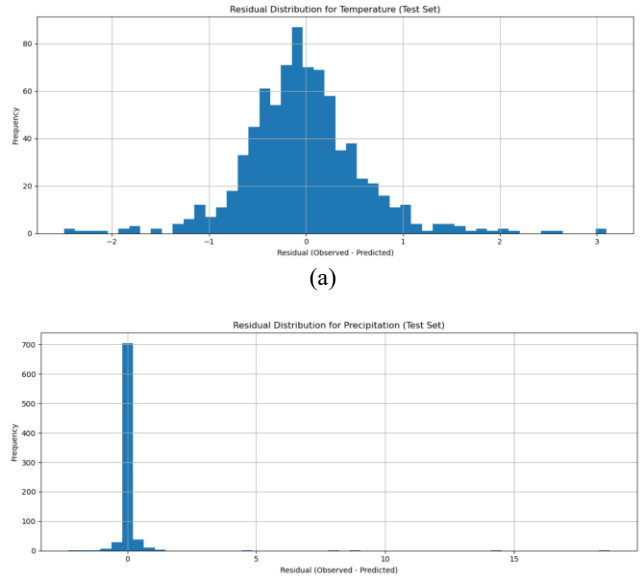



**Figure 3. Residual error distributions for (a) temperature and (b) precipitation predictions**

### 8.2. Discussion

The strong performance of the LSTM model for temperature prediction can be attributed to its ability to learn long-term temporal dependencies and seasonal patterns inherent in daily climate time series. Recurrent neural networks have been shown to outperform shallow machine learning models in scenarios where temporal structure plays a dominant role in predictability [1], [2].

Precipitation prediction remains inherently more challenging than temperature prediction due to its sporadic occurrence, nonlinear generation mechanisms, and heavy-tailed statistical distribution [32]. Even advanced deep learning models tend to underestimate extreme precipitation values, a limitation consistently reported in previous studies [3], [4]. The relatively high $R^2$ achieved by the LSTM model in this study indicates that sequence-based learning can partially capture precursor patterns associated with rainfall events, although substantial uncertainty remains.

The comparative behavior of the evaluated models aligns with findings from recent regional-scale forecasting studies, which consistently report higher predictability for temperature than for precipitation and emphasize the advantages of deep recurrent architectures when sufficient historical data are available [5], [6]. These results suggest that incorporating additional predictors, such as large-scale atmospheric circulation indices or satellite-derived variables, may further improve precipitation forecasting skill.

## 9. Limitations

This study is constrained by the use of single-station observations, which limits spatial generalization [33]. Model performance is sensitive to feature design and temporal coverage. Deep learning models require larger datasets to fully realize their potential [34].

## 10. Conclusion and Future Work

This study demonstrates the applicability of ML and DL models for regional temperature and precipitation forecasting using historical time series data. While deep recurrent networks show promise for temperature prediction, precipitation remains inherently difficult to model. Future work will explore hybrid physics-informed models, multisource data integration, and the inclusion of large-scale climate indices [35], [36].

## References

[1] Wilks, D. S. (2019). *Statistical methods in the atmospheric sciences* (4th ed.). Academic Press.

[2] Intergovernmental Panel on Climate Change (IPCC). (2021). *Sixth assessment report*. IPCC.

[3] Palmer, T. N. (2019). The ECMWF ensemble prediction system. Quarterly Journal of the Royal Meteorological Society.

[4] Franzke, C. L. E., O'Kane, T. J., Berner, J., Williams, P. D., & Lucarini, V. (2020). Stochastic climate theory and modeling. Nature Climate Change, 10, 1-9.

[5] LeCun, Y., Bengio, Y., & Hinton, G. (2015). Deep learning. Nature, 521(7553), 436-444.

[6] Bishop, C. M. (2006). *Pattern recognition and machine learning*. Springer.

[7] Düben, P. D., & Bauer, P. (2018). Challenges and design choices for global weather and climate models based on machine learning. Philosophical

Transactions of the Royal Society A, 376, 20170318.

[8] Reichstein, M., Camps-Valls, G., Stevens, B., Jung, M., Denzler, J., & Carvalhais, N. (2019). Deep learning and process understanding for data-driven Earth system science. Nature, 566(7743), 195-204.

[9] Feng, J., Li, Y., & Deng, X. (2020). Machine learning applications in atmospheric sciences. Atmospheric Research.

[10] Box, G. E. P., Jenkins, G. M., Reinsel, G. C., & Ljung, G. M. (2015). *Time series analysis: Forecasting and control* (5th ed.). Wiley.

[11] Kisi, O., & Shiri, J. (2018). Precipitation forecasting using machine learning methods. Hydrological Sciences Journal.

[12] Mohammadi, M., Eslamian, S., & Gohari, A. (2019). Climate variable prediction using machine learning approaches. Theoretical and Applied Climatology.

[13] Breiman, L. (2001). Random forests. Machine Learning, 45(1), 5-32.

[14] Vapnik, V. N. (1998). *Statistical learning theory*. Wiley.

[15] Haykin, S. (2009). *Neural networks and learning machines* (3rd ed.). Pearson.

[16] Hochreiter, S., & Schmidhuber, J. (1997). Long short-term memory. Neural Computation, 9(8), 1735-1780.

[17] Gers, F. A., Schmidhuber, J., & Cummins, F. (2000). Learning to forget: Continual prediction with LSTM. IEEE Transactions on Neural Networks, 12(2), 245-252.

[18] Karevan, Z., & Suykens, J. A. K. (2020). Transductive LSTM for time-series prediction. Neurocomputing, 377, 85-92.

[19] Kratzert, F., Klotz, D., Brenner, C., Schulz, K., & Herrnegger, M. (2019). Rainfall-runoff modelling using long short-term memory networks. Water Resources Research, 55(6), 5171-5193.

[20] Fang, M., Shen, C., & Li, D. (2021). Deep learning-based climate prediction. Climate Dynamics.

[21] Hastie, T., Tibshirani, R., & Friedman, J. (2009). *The elements of statistical learning* (2nd ed.). Springer.

[22] Box, G. E. P., & Jenkins, G. M. (1976). *Time series analysis*. Wiley.

[23] Taylor, S. J., & Letham, B. (2018). Forecasting at scale. PeerJ Computer Science, 4, e319.

[24] Géron, A. (2019). *Hands-on machine learning with Scikit-Learn, Keras, and TensorFlow* (2nd ed.). O'Reilly.

[25] Hyndman, R. J., & Athanasopoulos, G. (2021). *Forecasting: Principles and practice* (3rd ed.). OTexts.

[26] Food and Agriculture Organization of the United Nations (FAO). (2020). *Climatic data handbook*. FAO.

[27] World Meteorological Organization (WMO). (2018). *Guide to meteorological instruments and methods of observation*. WMO.

[28] Chen, T., & Guestrin, C. (2016). XGBoost: A scalable tree boosting system. In *Proceedings of the 22nd ACM SIGKDD International Conference on Knowledge Discovery and Data Mining* (pp. 785-794).

[29] Schölkopf, B., Smola, A., & Müller, K.-R. (2000). Nonlinear component analysis as a kernel eigenvalue problem. Neural Computation, 10(5), 1299-1319.

[30] Goodfellow, I., Bengio, Y., & Courville, A. (2016). *Deep learning*. MIT Press.

[31] Greff, K., Srivastava, R. K., Koutník, J., Steunebrink, B. R., & Schmidhuber, J. (2017). LSTM: A search space odyssey. IEEE Transactions on Neural Networks and Learning Systems, 28(10), 2222-2232.

[32] O'Gorman, P. A. (2015). Precipitation extremes under climate change. Journal of Climate, 28(21), 1-15.

[33] Sun, J., Xue, M., & Wilson, J. W. (2020). Use of remote sensing data in weather prediction. Remote Sensing.

[34] Rolnick, D., Donti, P. L., Kaack, L. H., et al. (2019). Tackling climate change with machine learning. Nature Climate Change, 9, 850-859.

[35] Kashinath, K., Mustafa, M., Albert, A., et al. (2021). Physics-informed machine learning. Philosophical Transactions of the Royal Society A, 379, 20200085.

[36] Watson-Parris, D., Rao, Y., Olivié, D., et al. (2022). ClimateBench: Benchmarking ML for climate. Nature Climate Change, 12, 1-7.

INTERNATIONAL JOURNAL OF
COASTAL, OFFSHORE & ENVIRONMENTAL ENGINEERING IJCOE Vol..11/No.4 /Autumn 2026 (46-64)

*Available online at: www. Ijcoe.org*

# Experimental and Numerical Investigation of the Effect of Stator and rotor distance on the Hydrodynamic Performance of a PumpJet Propulsion System

**Mohammad Hossein Qaedsharaf** [1]

[1] *Ph.D. in Mechanical Engineering, Khatam Al-Anbia Air Defense University, Tehran, Iran,* Mqaed1100@gmail.com

**ARTICLE INFO**

*Article History:*
Received: 31 July
Accepted: 10 Nov
Available online ….

*Keywords:*
**pumpjet, Stator and rotor distance, Rotor diameter, Open-water efficiency, Thrust coefficient**

**ABSTRACT**

This research investigates the effects of duct inlet length (L) and the distance between the rotor and stator on the hydrodynamic performance of a pre-swirl pump jet. For this aim, five geometries with different duct inlet lengths L equal to (0 ~ 0.1DRotor) were generated using a direct design method. Furthermore, these geometries were experimentally tested in a cavitation tunnel and validated through numerical simulations using ANSYS Fluent software; it can be concluded that there is good agreement between the experimental and numerical results. Additionally, uncertainty analysis was performed to control the accuracy of the experimental data. The results indicate that an increase in the duct inlet length and moving the stator closer to the rotor leads to more accurate guidance of exiting flow lines of the stator towards the rotor blades. This, in turn, increases the rotor lift coefficient and generates a greater pressure difference across the rotor, resulting in an increase in the total propulsor thrust coefficient and a subsequent rise in open-water efficiency at specific advance ratios. The maximum relative uncertainty for open-water efficiency was 1.79%. Among the tested configurations, the maximum open-water efficiency of 62.15% was observed for the L=0.1DR case at an advance ratio of 1.1. The minimum efficiency at the same advance ratio was 59.12% for the L=0DR case. Further analysis of the simulation results shows that the L=0.1DR case is superior to other configurations due to having the highest open-water efficiency (approximately 5% higher than the minimum value).

## 1- INTRODUCTION

The pre-swirl pumpjet mechanism is an advanced technology in marine propulsion that has garnered attention due to its capabilities in noise reduction and stealth, increased efficiency at high speeds, and improved performance compared to traditional propellers (Morrison, 2018; Suryanarayana et al., 2012). This system comprises a duct (flow-guiding tube), a stator (a set of fixed blades that pre-swirl the flow), and a rotor (rotating blades that generate thrust). The pre-swirl created by the stator can optimize the flow entering the rotor, thereby increasing system efficiency. One of the key aspects in designing this system is the consideration of geometric parameters, such as the duct inlet length and the stator-rotor gap. The duct inlet length, referring to the distance from the beginning of the duct to the stator, can affect flow development and uniformity before entering the stator. A longer duct inlet might stabilize the flow, but excessive length can lead to pressure drop and increased frictional losses. On the other hand, the stator-rotor gap, which indicates the distance between the trailing edge of the stator blades and the leading edge of the rotor blades, influences the interaction of the flow exiting the stator with the rotor. A tiny gap may cause undesirable flow interference, while a large gap can weaken the pre-swirl effect and reduce efficiency. The importance of these parameters lies in the fact that the hydrodynamic performance of a pre-swirl pumpjet system, including efficiency, thrust, torque, and cavitation behavior, is highly dependent on how the flow is managed (Renilson, 2018). This research proposes to investigate the effect of these two key parameters on hydrodynamic performance using a combination of experimental and numerical methods. In the experimental section, a scalable model of the pumpjet system will be designed and tested under controlled conditions to obtain data

such as thrust, torque, and flow patterns. In the numerical section, computational fluid dynamics (CFD) simulations using accurate turbulence models will be performed to provide more detailed insights into the flow, including complex interactions between the stator and rotor. This dual approach enables the cross-validation of data, yielding more reliable results. Additionally, uncertainty analysis will be used to verify the accuracy of the experiments. Uncertainty analysis and experimental design techniques emerged as a competitive approach in Western countries and Japan in the 1980s and 1990s (Dean & Voss, 1999). Uncertainty refers to determining the error range of a quantity, expressed with a 95% probability for engineering calculations (Nakra & Chaudhry, 2016; Coleman & Steele, 1999). It is evident that in uncertainty analysis, the goal is to determine the contribution of each parameter's error to the total quantity error. Therefore, experimental data and tests are required. The significance of this research extends beyond immediate applications in marine propulsion. A better understanding of flow interactions in ducted systems with stators and rotors can also aid in the design of hydroelectric turbines or other fluid turbomachinery. Ultimately, this research aims to fill existing knowledge gaps, provide comprehensive experimental and numerical data, and develop guidelines for designing pre-swirl pumpjet systems. The results of this study are expected not only to contribute to a better understanding of the hydrodynamic behavior of these systems but also to lead to the development of technologies that will improve the performance and efficiency of future vessels. Pumpjets come in various types depending on the rotor and stator arrangement. The pre-swirl pumpjet is a type where the stator is positioned at the flow inlet into the duct. This type of pumpjet has gained attention due to its low noise levels. A pumpjet system consists of a rotor, a stator, a duct, a hub, and a nose. Fig. 1 shows a schematic of the components of a stator-rotor pumpjet.

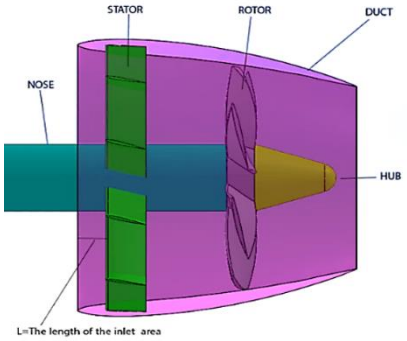



**Fig. 1 Schematic of Pre-swirl Pumpjet Components**

## 2- BACKGROUND RESEARCH AND STUDIES

A summary of key studies relevant to the topic is presented below: Qaedsharaf et al. (2025) numerically investigated the cavitating performance of a pre-swirl pump-jet propulsion system by varying the chord length of the stator airfoil. Their findings indicate that increasing the stator chord length up to a certain point improves the propulsor's cavitating performance and reduces the likelihood of cavitation. Li et al. (2022) examined the hydrodynamic performance of a submarine equipped with a novel pump-jet propulsor. Their study noted that duct and stator configurations influence performance, though specific details regarding the inlet length or spacing were limited. Weng et al. (2024) investigated the hydrodynamic noise characteristics of a pump-jet through both numerical and experimental methods. The results show that the amplitude of sound pressure level fluctuation in the radial plane exhibits an approximately circular distribution, and the sound pressure level also possesses characteristics of a dipole source. Zou et al. (2024) explored the relationship between longitudinal vibration size, frequency changes, excitation force, and the effect of vibration magnitude on the excitation force and vortex dynamic characteristics of a pump-jet propulsor. Ji et al. (2024) investigated the effect of rotor blade tip rake angle on the excitation force of a pump-jet propulsor in the same year. Their results demonstrate that the oscillation amplitude of the resulting horizontal (and vertical) forces acting on the duct/stator assembly significantly decreases with a reduced rake angle and increases with its increment. Weng et al. (2024) examined a pumpjet's hydrodynamic and noise performance with different stator pre-swirl angles. Utilizing the SBES method and Lighthill's acoustic analogy, they found that pre-swirl angles modulate pressure fluctuations and noise, which is indirectly related to changes in ambient pressure. Zhou et al. (2023) numerically analyzed the effects of duct profile parameters, such as camber and angle of attack, on the flow characteristics of a pump jet. They found these parameters affect flow uniformity and efficiency, indirectly linking to the duct inlet conditions. However, this study did not specifically investigate inlet length or consider uncertainty analysis. Kim et al. (2023) performed a parametric study on the hydrodynamic characteristics of a pumpjet installed on a SUBOFF submarine. They investigated the influence of duct incidence and stator twist angles and reported that the duct increases internal pressure, but the analysis was limited to a constant depth. Bi et al. (2023) explored the effect of rotor tip grooves on cavitation and the hydrodynamic performance of a pumpjet. Using CFD, they showed that grooves can reduce tip cavitation, but the study was conducted

under constant pressure conditions. Zhou et al. (2022) comprehensively reviewed pump-jet hydrodynamic performance and design. They highlighted the importance of duct design in improving efficiency and reducing noise but did not address the duct inlet length. This study also did not mention uncertainty analysis, indicating a need for more rigorous approaches in future research. Huang et al. (2022) investigated the evolution of wake vortices and unsteady forces in a pre-swirl pumpjet. Through DES simulations, they demonstrated that stator-rotor interaction complicates the internal flow, but the effect of depth variations was not explored. Ye et al. (2022) investigated tip flow control performance in a pumpjet, analyzing the effect of axial slots on cavitation and efficiency using the DES method. This study did not address depth variations. Zhao et al. (2022) examined the cavitation-vortex interaction in a pre-swirl pumpjet using the DES method and a homogeneous cavitation model. They reported that heavy cavitation ($\sigma$=2.2) reduces hydrodynamic loading and accelerates vortex collapse. This study was conducted at a constant depth and did not consider depth variations. Lidtke et al. (2022) investigated cavitation-induced noise in propellers and demonstrated that ambient pressure influences noise intensity. This analysis is relevant for understanding the effects of depth in pump jets. The findings are beneficial for stealth applications. Sun et al. (2022) compared the hydrodynamic performance of pre-stator and post-stator pumpjets under cavitating conditions. Employing the DES method, they showed that stator-rotor interaction affects efficiency and cavitation, but their analysis was limited to constant depth conditions. Chen et al. (2021) combined CFD and experimental methods to investigate the effect of duct inlet length on the hydraulic performance of a waterjet propulsion device. They found that duct efficiency, head, and thrust peaked at an optimal length (L=1.12D), and flow uniformity improved with increasing length. Although this study focused on water jets, its findings are generalizable to pump jets; however, the absence of uncertainty analysis limited the accuracy of the results. Huang et al. (2021) used advanced DES simulation to investigate the effects of duct parameters on the unsteady hydrodynamic performance of a pump jet. They showed that duct geometry influences thrust fluctuations and noise, but the duct inlet length was not explicitly examined. Qiu et al. (2020) investigated a pumpjet's hydrodynamic and cavitation performance under oblique flow conditions with varying tip clearances. Using a RANS model and the Zwart-Gerber-Belamri cavitation model, it was demonstrated that tip cavitation on the rotor is exacerbated under oblique flow, which could be linked to changes in ambient pressure. This research did not address variations in depth but emphasized the significance of flow conditions. Qiu et al. (2022) investigated cavitation performance at various cavitation numbers (ranging from 1.4721 to 7.5682). Their study revealed that a lower cavitation number (1.4721) reduced efficiency by up to 37%. This analysis is directly relevant to ambient pressure variations caused by depth. Applying a hybrid CNN-Bi-LSTM model for force prediction offers an innovative approach. Wang et al. (2020) examined the influence of duct geometric parameters on the hydrodynamic performance of a pump jet using a surface panel method. They analyzed parameters such as gap size, camber, and angle of attack, finding that these factors affect performance indicators, surface pressure distribution, and flow velocity. However, this study did not specifically address the duct inlet length or consider uncertainty analysis, indicating a need for more focused research. This study also did not include uncertainty analysis, which limits its ability to provide reliable results. Using uncertainty analysis, Qaedsharaf et al. (2019) compared the performance and sensitivity of influential parameters in two propellants, oxygenated water and nitrous oxide. The results showed that using nitrous oxide propellant would be more desirable in accuracy, and its propulsive force would be closer to the desired propulsive force of 5 Newtons. Motallebi-Nejad et al. (2017), though slightly older, is relevant due to its use of uncertainty analysis in CFD simulations for ducted propellers and pump jets. They employed the Grid Convergence Index (GCI) method to evaluate numerical errors, providing a framework for the present study. However, this study also did not address the duct inlet length. Qaedsharaf (2011), in his Master's thesis on heat transfer analysis and regression rate of solid fuel hybrid propellants using uncertainty analysis and curve fitting, obtained an empirical relationship for the heat transfer rate of hybrid propellants.

## 2-1 Research Gaps

Despite these advancements, several gaps persist in the scientific literature: Combined Effects of Parameters: Most studies focus on either duct geometry or stator parameters in isolation. There is a lack of systematic research investigating the combined effects of duct inlet length and stator-rotor clearance, especially in pre-swirl pump jets. Experimental Validation: Many studies rely on numerical simulations with limited experimental validation. Comprehensive experimental data is needed to confirm CFD results and ensure applicability in real-world conditions. Specific Focus on Pre-swirl Pump-jet Propulsion: Although pre-swirl pump-jets have been explored in some studies, the unique flow dynamics resulting from pre-swirl have not consistently been the central focus of the investigation, which is crucial for translating research findings into practical designs. Lack of Uncertainty Analysis: The use of uncertainty analysis in experimental pump-jet tests is minimal, which can reduce the accuracy and reliability of results.

## 2-2 Relation to Previous Studies and Significance of the Topic

The present study builds upon previous research to address the identified gaps. It combines insights from studies such as Weng et al. (2024) and Zhou et al. (2023) regarding duct geometry with findings from Li et al. (2022) concerning stator-rotor interactions. By systematically varying both duct inlet length and stator-rotor clearance, this research aims to provide a comprehensive understanding of their effect on hydrodynamic performance, including efficiency and thrust parameters. The simultaneous use of experimental and numerical methods ensures robust validation, addressing the limitation of simulation-based studies. With a specific focus on pre-swirl pump jets, this study targets a critical subset of propulsion systems with unique flow dynamics. The findings of this research can contribute to the design of more efficient submerged vessels, aiding in operational stability and effectiveness in marine applications.

## 3- RESEARCH METHODOLOGY

### 3-1 Geometry Extraction

The geometry design of the pumpjet propulsion system model is based on maximizing hydrodynamic performance using the direct design method (Zhou et al., 2022).

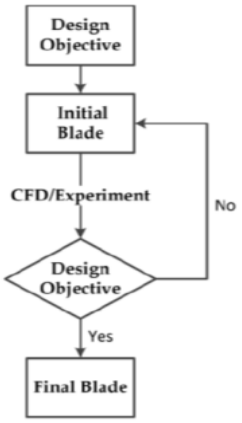



**Fig. 2 Direct Design Algorithm (Zhou et al., 2022)**

Table 1 shows the geometric specifications of the designed propulsion system, and Fig. 3 shows its general schematic.

**Table 1. Geometric specifications of the pump jet propulsion system**

| Characteristic | Value |
|---|---|
| Rotor diameter (cm) | 9 |
| Number of rotor blades and their profile | 7 - NACA16 |
| Number of stator blades and their profile | 11 - NACA66 |
| Duct type and its profile | Convergent - NACA6608 |
| Inlet diameter, outlet diameter and duct length (cm) | 13.06, 9.12, and 12.05 |

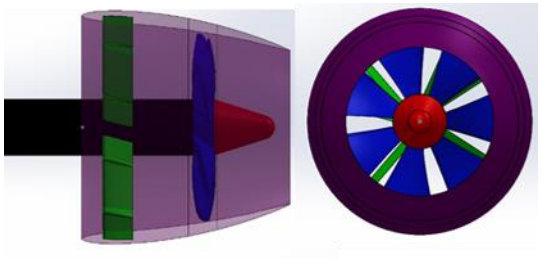


**Fig. 3 Schematic of the geometry designed by the direct design method**

To investigate the effect of the duct inlet area and the distance between the rotor and stator on the hydrodynamic performance of the propulsion system, five models were designed by displacing the stator from the duct inlet towards the rotor. These models had inlet lengths (L) of 0 DR, 0.025 DR, 0.050 DR, 0.075 DR, and 0.1 DR (DR: Rotor Diameter), and numerical simulations were performed on each model separately. It should be noted that during the geometry generation process, the optimal duct length was determined, and the stator was displaced at this optimal length, starting from the duct inlet towards the rotor. A schematic of the rotor and stator positions in the designed geometries is presented in Fig. 4.

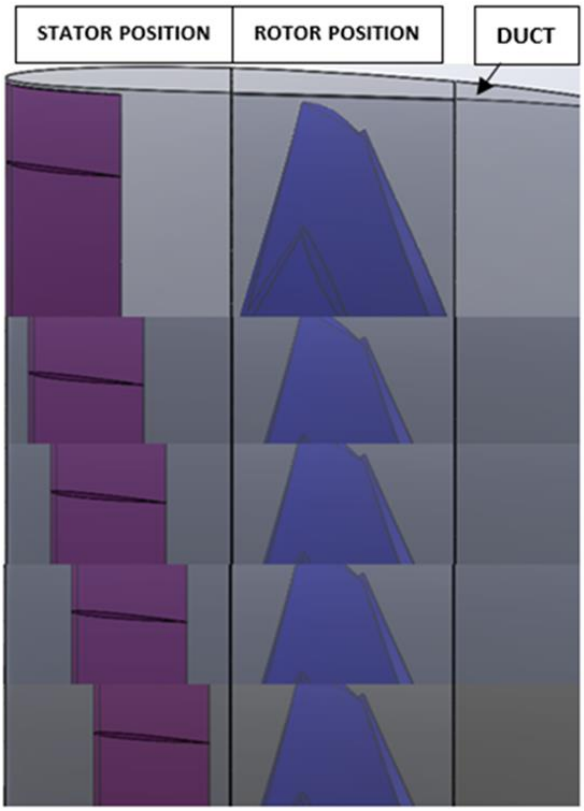



**Fig. 4 Schematic of rotor and stator positions for designed geometries with inlet zone lengths of 0, 0.025, 0.05, 0.075, and 0.1 rotor diameters, from top to bottom, respectively**

## 4- EXPERIMENTAL TEST

The experimental test was conducted inside the cavitation tunnel of Imam Khomeini Naval University in Nowshahr. The cavitation tunnel is a NA10 model manufactured in England. The tunnel specifications are presented in Table 2. A view of the tunnel is also visible in in Fig. 5.

**Table 2. Cavitation tunnel specifications**

| Characteristic | Value |
|---|---|
| Tunnel dimensions (mm) | 1100*2750*4900 |
| Test section dimensions (mm) | 750*200*200 |
| Flow velocity range (m/s) | 0.65~4.8 |
| Maximum impeller rotational speed (rpm) | 3000 |
| Adjustable pressure range (Kpa) | 50~200 |



**Fig. 5 View of Nowshahr Naval University's Cavitation Tunnel**

To install the geometry inside the cavitation tunnel, an airfoil-shaped strut was embedded below the designed geometries, along with a tab for measuring the thrust force of the duct and stator assembly via a load cell. The geometries were fabricated with a 3D printer using composite materials with 1-micron precision. A schematic of the five manufactured geometries is shown in Fig.6.



**Fig. 6 Five geometries manufactured for experimental testing**

The load cell and propeller holding mechanism were secured in the tunnel with three weights. The rotor was also separately installed on the drive shaft, which was connected to the thrust and torque measurement equipment. A schematic of the propeller installation is shown in Fig. 7. Fig. 8 shows an image of the propeller in operation.

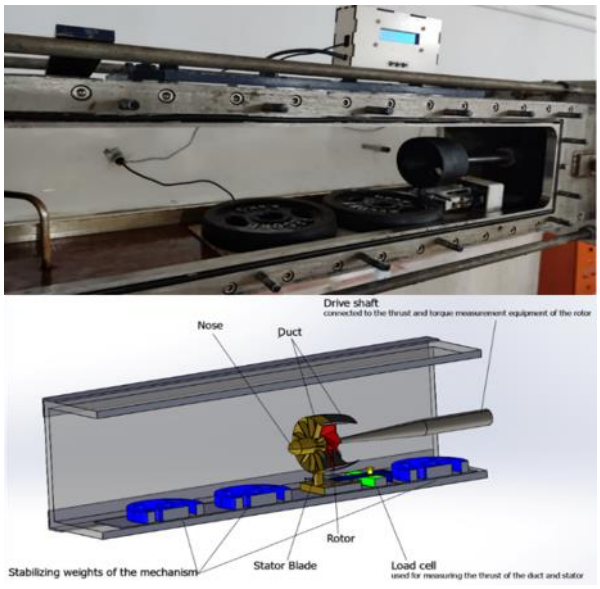



**Fig. 7 Schematic of thruster installation within the tunnel**

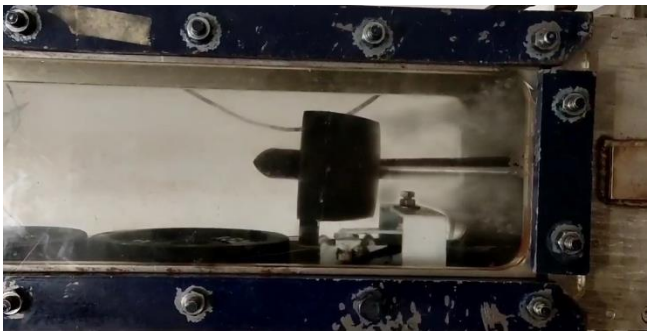


**Fig. 8 Propeller installed inside the tunnel operating. The three measurable parameters are rotor thrust, duct and stator thrust, and rotor torque.**

Subsequently, 8 advance ratios were considered, and for each advance ratio, each of these 3 parameters was measured 4 times, and their average was used in the relationships. Data collection was performed at 25 degrees Celsius, sea level pressure (101 kPa), and water with a density of 1000 kg per cubic meter. n has a constant value of 27.8 revolutions per second, and VA is adjusted according to the advance ratio by tunnel equipment that has been previously calibrated and approved by a qualified company. To re-verify the adjusted flow speed, it was compared with the speed set by electronic speed control equipment using a Pitot tube installed inside the test section, which confirmed its accuracy.

## 5- PUMPJET FUNCTIONAL PARAMETERS

To investigate the hydrodynamic performance of a pumpjet propulsion system, the following dimensionless coefficients are defined (Carlton, 2012; Bertram, 2012)
:

$$\begin{cases} J = \frac{V_A}{nD} \quad K_{TR} = \frac{T_R}{\rho n^2 D^4} \quad K_{TS} = \frac{T_s}{\rho n^2 D^4} \quad K_{TD} = \frac{T_D}{\rho n^2 D^4} \\ K_{QR} = \frac{Q_R}{\rho n^2 D^5} \quad K_Q = K_{QR} \quad K_T = K_{TR} + K_{TS} + K_{TD} \\ \eta_o = \frac{JK_T}{2\pi K_Q} \end{cases} \quad (1)$$

Where $J$ is advance ratio, $K_T$ is total thrust coefficient, $K_{TR}$ is rotor thrust coefficient, $K_{TS}$ is stator thrust coefficient, $K_{TD}$ is duct thrust coefficient, $K_Q$ is torque coefficient, $K_{QR}$ is rotor torque coefficient, $\eta_o$ is open-water propeller efficiency, D is propeller diameter (m), n is rotational speed (rps), $V_A$ is advance velocity (m/s), $\rho$ is water density(kg/m^3).

### 6- UNCERTAINTY EQUATIONS

If we calculate the open water efficiency$\eta_o$ from the above relationships, we will have:

$$\eta_o = \frac{JK_T}{2\pi K_Q} = \frac{V_A(T_R + T_D + T_S)}{2\pi nQ} = \frac{V_A T_{Tot}}{2\pi nQ} \quad (2)$$

The total thrust is the sum of the rotor, duct, and stator thrusts. In the conducted experimental test, the thrust of the duct and stator assembly was sampled multiple times together, while the rotor thrust and torque were sampled separately. These values are then substituted into the relationships after averaging multiple sampling instances. Let's assume the quantity $\eta_o$ is the primary quantity, which is a function of the independent parameter J:

$$\eta_o = f(X_1.X_2.\dots X_J) = f(V_A.T_{Tot}.n.Q) \quad (3)$$

Accordingly, the reduced equation will be:

$$\eta_o = \frac{V_A T_{Tot}}{2\pi nQ} \quad (4)$$

The sensitivity of $\eta_o$ to the results of each of these parameters is then obtained by substituting the results into the following relationship (Nakra & Chaudhry, 2016):

$$Sensitivity = \left(\frac{\partial \eta_o}{\partial X_i}\right) \quad (5)$$

The uncertainty of $\eta_o$ arises from the uncertainty of the effective input values ($x_i$) on the governing equation, or the error of each parameter ($U_{X_i}$) (Nakra & Chaudhry, 2016):

$$U_{\eta_o} = \sqrt{\sum_{i=1}^{n} \left(\frac{\partial \eta_o}{\partial X_i} U_{X_i}\right)^2} \quad ; U - U_{\eta_o} \le U_t \le U + U_{\eta_o} \quad (6)$$

In the error analysis process, after determining the uncertainty value of each parameter ($U_X$), which is obtained from measurements, and by using statistical relationships and sensitivity analysis of the governing equation, the amount of uncertainty in the primary quantity ($U_{\eta_o}$) is determined. It can then be stated that the true value ($U_t$) lies within the obtained range. The smaller the value of Uηo, the higher the certainty in the quantity $\eta_o$ (the obtained range will be smaller), and it approaches a more reliable value. It can be concluded that the total uncertainty results from the uncertainty in each parameter, and by reducing the uncertainty in the parameters, the certainty in the value of that quantity can be increased. Therefore, the uncertainty for the function $\eta_o$ represents the dependency of the function $\eta_o$ on parameter x and the error present in that parameter (RSS) (Nakra & Chaudhry, 2016):

$$U_{\eta_o}^2 = \left(\frac{\partial \eta_o}{\partial X_1}\right)^2 U_{X_1}^2 + \left(\frac{\partial \eta_o}{\partial X_2}\right)^2 U_{X_2}^2 + \dots + \left(\frac{\partial \eta_o}{\partial X_J}\right)^2 U_{X_J}^2 \quad (7)$$

Now, if the relative uncertainty is considered (Nakra & Chaudhry, 2016):

$$\frac{U_{\eta_o}^2}{\eta_o^2} = \left(\frac{X_1}{\eta_o}\frac{\partial \eta_o}{\partial X_1}\right)^2 \left(\frac{U_{X_1}}{X_1}\right)^2 + \left(\frac{X_2}{\eta_o}\frac{\partial \eta_o}{\partial X_2}\right)^2 \left(\frac{U_{X_2}}{X_2}\right)^2 + \dots + \left(\frac{X_J}{\eta_o}\frac{\partial \eta_o}{\partial X_J}\right)^2 \left(\frac{U_{X_J}}{X_J}\right)^2 \quad (8)$$

In the latter relationship, other parameters can be replaced with the open water efficiency. Relative uncertainty is often expressed as a percentage. The measurable parameters in the conducted experimental test include: rotor thrust, rotor torque, and the thrust of the duct and stator assembly. The value of n is a constant 27.8 revolutions per second, and $V_A$ is adjusted depending on the advance ratio via tunnel equipment, which has been previously calibrated and verified by a qualified company. To calculate the values of total uncertainty, relative uncertainty, and sensitivity analysis, relevant relationships were programmed in MATLAB software, and the corresponding results were extracted.

## 7- NUMERICAL SIMULATION APPROACH

Numerical simulation approach: In this study, the working fluid is considered incompressible, homogeneous, and Newtonian. Body forces, gravitational acceleration, and heat transfer are

neglected. The fluid flow is calculated by the Navier-Stokes equations, which are very time-consuming and almost impossible to solve analytically. Using the Reynolds averaging method for 5 equations is a common approach for solving viscous flow and Navier-Stokes equations. This approach introduces Reynolds stresses that need to be solved. Turbulence models, by introducing a turbulent viscosity, calculate Reynolds stresses. In this study, the k-ω SST turbulence model was used. Among the two-equation models, the k-ω model has several advantages over the k-ε model. Its most prominent advantage is that it can be integrated without additional components in the viscous sublayer. This makes the behavior of y+ insensitive and straightforward. Moreover, the k-ω SST model performs better in predicting separation and unwanted pressure gradients. Considering the effects of boundary layer growth on the hydrodynamic performance of the pump jet, k-ω may be preferred over k-ε [31]. One of the disadvantages of the standard k-ω equation is the high sensitivity of the solution to the value of free stream k and ω outside the shear layer. For this reason, the use of the standard k-ω model in ANSYS Fluent software is not recommended. The k-ω BSL and k-ω SST models are designed by combining components of the ω and ε equations to avoid sensitivity to the free stream in the standard k-ω model. Also, the k-ω SST model is well calibrated for accurately calculating separation from smooth surfaces. Among the k-ω models, it is recommended to use the SST or BSL model (Bertram, 2012; Qin et al., 2021; Yang et al., 2022). Since the Reynolds numbers on both sides of the pump jet duct are different, there is a significant region of laminar flow outside the duct, especially at low advance ratios. The difference in flow regimes affects the duct thrust. According to the studies conducted, when there is a significant difference in the Reynolds numbers on both sides of the duct and the outer passage has a Reynolds number less than the minimum Reynolds number accepted by ITTC (5*10^5) when the advance speed is low, the effect of the difference in flow regimes on the duct thrust is negligible because the duct thrust is affected by its pressure component and its friction component will be very small. Therefore, the transition on the duct was neglected in this study.

## 7-1 Main Governing Equations

For an incompressible and single-phase fluid, the governing equations for URANS can be written in tensor form as the conservation of mass and momentum (Li et al., 2022):

$$\frac{\partial \rho U_i}{\partial x_i} = 0 \tag{9}$$

$$\frac{\partial(\rho U_i)}{\partial t} + \frac{\partial(\rho U_i U_j)}{\partial x_j} = -\frac{\partial P}{\partial x_i} + \frac{\partial}{\partial xj}\left[\mu\left(\frac{\partial Ui}{\partial x_j} + \frac{\partial Uj}{\partial x_i}\right)\right] + \frac{\partial}{\partial xj}(-\rho\overline{u_\iota u}j) + S_M \tag{10}$$

Where i=1,2,3, j=1,2,3, ρ is the fluid density and $x_i$, $xj$ are Cartesian coordinate components. For a fixed coordinate system, $S_M$ is equal to zero, and $Ui$ and $Uj$ represent the components of the absolute velocity. For a moving reference frame, $S_M$ is the sum of the Coriolis component and the component of the centrifugal forces ω×(r×ω), and $Ui$, $Uj$ are the components of the relative velocity. μ is the dynamic viscosity, P is the pressure, and $\rho\overline{u_\iota u}j$ represents the Reynolds stresses.

## 7-2 Boundary Conditions and Numerical Simulation Settings

The entire computational domain is divided into two subdomains: the rotor domain and the outer domain. The outer domain has a section similar to a cavitation tunnel with a length of 15D. The rotor is located 5D from the inlet. All subdomains have an unstructured mesh. Near the walls, the height of the first layers of the boundary layer sublayers is calculated with a y+ value in the range of ٠ to °, which is suitable for the RANS solver with the SST k-w turbulence model. The boundary conditions are also shown in Fig. 9. A uniform upstream flow with a velocity V corresponding to the advance ratio J and a turbulence intensity of 1% is set at the inlet boundary. A pressure outlet boundary condition with a constant pressure Pout equal to 1 atm is applied to the outlet. The far-field wall is set as a wall with zero shear stress. During the simulation, the rotational speed of the rotor, n, was kept constant at 27.8 revolutions per second, while the inlet velocity varied depending on the advance ratio. All simulations were performed using ANSYS Fluent software with the SIMPLEC algorithm, second-order discretization for momentum, and PRESTO discretization for pressure. A total of 3000-time steps with 20 iterations per time step were used until convergence (minimum residual of 1*10^-6) was achieved. The time step was calculated using the equation Δt=1/(360n), where n is the rotational speed in revolutions per second. The working fluid is water at 20 degrees Celsius, with a density of 1000 kg/m$^3$ and a saturated vapor pressure of 2368 Pascals. Since temperature changes underwater are negligible, temperature variations are ignored, water properties are considered constant, and the water is assumed to be free of physical contamination. The quality of each computational subdomain is greater than 0.5.

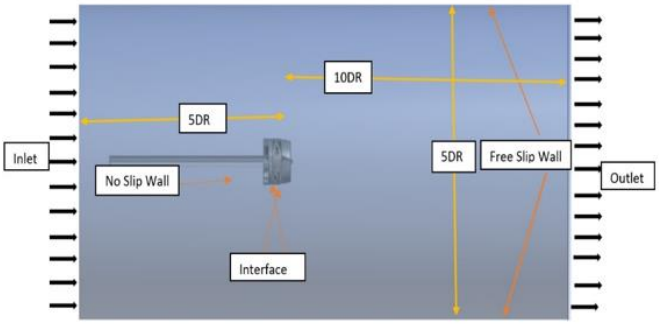



**Fig. 9 Boundary conditions used in the numerical simulation**

## 8- GRID INDEPENDENCE STUDY

In any numerical simulation, it is essential to ensure that the results are independent of the number and type of computational cells used. The grid convergence index (GCI) method, first proposed by Roache (Roache, 1997), is used to assess the discretization error and numerical uncertainties. This method requires at least three grids with different numbers of cells: S1, S2, and S3, with N1, N2, and N3 elements, respectively, from the finest (1) to the coarsest (3) grid. The grid refinement factor (r) is defined as:

$$r_{21} = (\frac{N1}{N2})^{1/3} \quad (11)$$

If r > √3, the extrapolation error decreases (Roache, 1997).

According to Roache's method, the convergence ratio is defined as:

$$R=\frac{\varepsilon_{21}}{\varepsilon_{32}}=\frac{\eta_2-\eta_1}{\eta_3-\eta_2} \quad (12)$$

where $\eta_1$ ،$\eta_2$ and $\eta_3$ are the open-water efficiency for the three cases. In this equation $\varepsilon_{ij}$, represents the difference in results obtained from solving using the i,j grid. For the convergence ratio, three scenarios can be considered:

- If R > 1, the grid is diverging.
- If R < 0, the convergence is oscillatory.
- If 0 < R < 1, the grid is converging monotonically.

When the solutions obtained with the investigated grids are in a converged state, Richardson extrapolation is used to estimate the order of convergence. The order of accuracy of this algorithm is calculated according to equation (11), where r is the grid refinement ratio, as defined earlier (Roache, 1997):

$$P=\frac{\ln(\frac{\varepsilon_{32}}{\varepsilon_{21}})}{\ln(r)}=\frac{\ln(\frac{\eta_3-\eta_2}{\eta_2-\eta_1})}{\ln(r)} \quad (13)$$

Finally, the grid convergence index is calculated using equation (12). In this equation, the factor Fs is the convergence assurance factor, and a value of Fs=1.25 is recommended (Roache, 1997). Additionally, in this equation, the symbol $|\varepsilon_{ij}|$ represents the approximate relative error.

$$\begin{cases} GCI_{fine} = F_s\frac{|\varepsilon_{12}|}{r^p-1}=\frac{F_s}{(r^p-1)}\left|\frac{\eta_1-\eta_2}{\eta_1}\right. \\ GCI_{coarse} = F_s r^p\frac{|\varepsilon_{23}|}{r^p-1}=\frac{F_s r^p}{(r^p-1)}\left|\frac{\eta_2-}{\eta_2}\right. \end{cases} \quad (14)$$

The grid convergence index indicates how far the obtained results are from the exact value. In other words, this method shows how the results change as the grid is refined. Small values of this index indicate that further refinement of the grid will not improve the results. Grid networks are reconstructed by decreasing and increasing the first layer height. Based on a Y+ value of ٭, the first layer thickness is calculated as 0.0045 mm (for a fine mesh). For grid independence analysis, values of 0.0050 mm and 0.0055 mm are chosen as the medium and coarse settings, respectively. Numerical simulations were performed at two different Courant numbers, 0.8 and 0.9, for fine, medium, and coarse meshes, with the results shown in Table 3.

**Table 3. Grid independence study for thrust and torque coefficients at different advance ratios**

| Advance ratio | *First Layer Height* | *number of cells (million)* | $K_T$ | $K_Q$ |
|---|---|---|---|---|
| J=0.8 | $\Delta s_1 = 0.0055$ | $N_1$ =12.2 | $K_{T1}$ = 0.3502 | $K_{Q1}$ =0.0817 |
| | $\Delta s_2 = 0.0050$ | $N_2$ =15.6 | $K_{T2}$ =0.3476 | $K_{Q2}$ =0.0808 |
| | $\Delta s_3 = 0.0045$ | $N_3$ =20.5 | $K_{T3}$ =0.3470 | $K_{Q3}$ =0.0801 |
| J=0.9 | $\Delta s_1 = 0.0055$ | $N_1$ =12.2 | $K_{T1}$ =0.3140 | $K_{Q1}$ =0.0773 |
| | $\Delta s_2 = 0.0050$ | $N_2$ =15.6 | $K_{T2}$ =0.3119 | $K_{Q2}$ =0.0766 |
| | $\Delta s_3 = 0.0045$ | $N_3$ =20.5 | $K_{T3}$ =0.3111 | $K_{Q3}$ =0.0762 |

As shown in Table 3, the errors of thrust and torque coefficients are very low among the three mesh types, confirming the grid independence. Additionally, the Grid Convergence Index (GCI) was calculated. The efficiencies of the three defined grids at J=0.9 are 3501.60, 3522.58, and 3567.58, respectively. Also, GCIfine and GCIcoarse are 0.0111 and 0.0113, respectively, which are small and desirable values. The convergence ratio R is 1.002, a value close to 1, indicating grid convergence. Therefore, Δs2=0.0050 was selected for meshing in all cases. The Meshed geometry is visible in Fig. 10.



**Fig. 10 Meshed geometry**

## 9- DISCUSSION OF RESULTS

### 9-1 Case 1: L=0DR

In this case, the inlet section length is considered 0, and the stator is positioned at the duct's inlet. Based on the

average of 4 samples of thrust and torque values from the experimental test, the maximum efficiency is ٥٩,١٢% at an advance ratio of 1.1. The maximum thrust coefficient is 0.4765, and the maximum torque coefficient is 0.09651. The thrust coefficient exhibits a nearly linear decreasing trend as the advance ratio increases. The open-water efficiency plot exhibits a completely ascending trend up to J = 1.1 and a completely descending trend thereafter. The thrust and torque coefficient plots exhibit a decreasing trend with an increasing advance ratio, except for minor fluctuations. The plots of efficiency, thrust, and torque coefficients at various advance ratios are presented in Fig. 11,12.

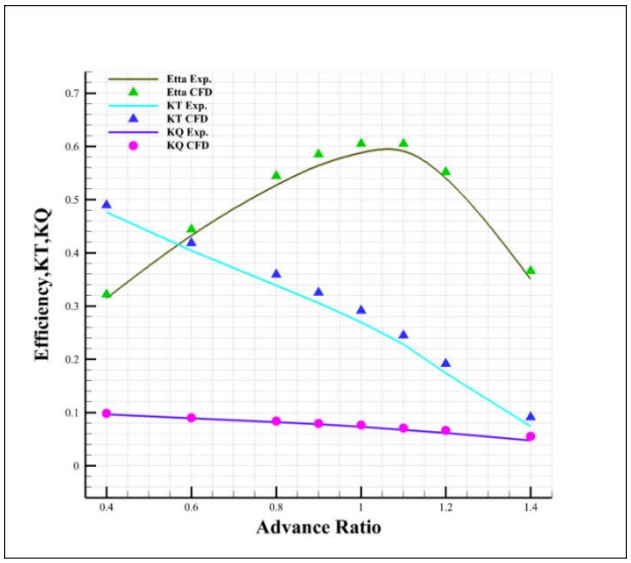



**Fig. 11 Open-water efficiency, thrust, and torque coefficients at various advance ratios for the L=0DR case.**

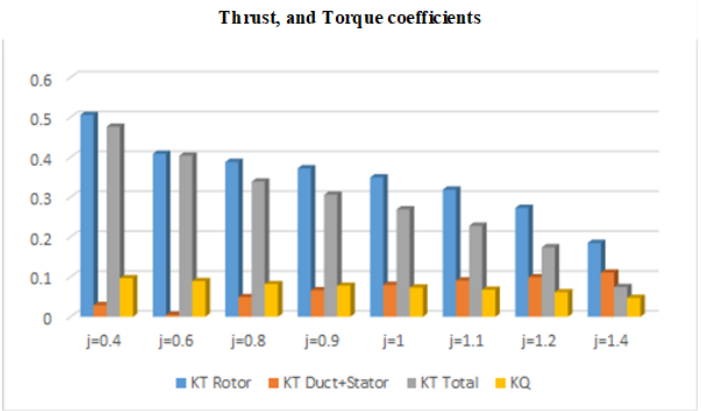



**Fig. 12 Bar chart of rotor thrust coefficient, duct+stator thrust coefficient, total thrust coefficient, and torque coefficient obtained from experimental test results for the L=0DR case.**

As observed from the results in Fig. 11, there is good agreement between the experimental test results and numerical simulations. Fig. 12 also presents the thrust and torque coefficients as bar charts, calculated using the average measured values of rotor thrust, duct-stator thrust, total thrust, and rotor torque. Fig. 13 shows the relative uncertainty values (in percent) for duct-stator thrust, rotor thrust, total thrust, rotor torque, and open-water efficiency. As indicated by the graph, the maximum relative uncertainty occurs for open-water efficiency at 1.784863%, which is less than 5%, indicating the high accuracy of the conducted experiments.

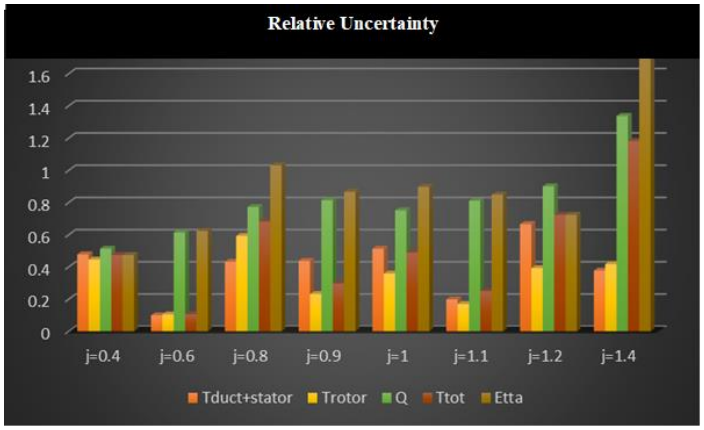



**Fig. 13 Relative uncertainty values (in percent) for duct-stator thrust, rotor thrust, total thrust, rotor torque, and open-water efficiency at various advance ratios for the L=0DR case.**

## 9-2 Case 2: L=0.025DR

In this case, the inlet section length is considered to be 0.0٠225 meters. Based on the average of 4 sets of sampled thrust and torque values from the experimental test at different advance ratios, the maximum open-water efficiency is 51.59% at an advance ratio of 1.1. The maximum thrust coefficient is 0.4887, and the maximum torque coefficient is 0.09723. Similar to the previous case, the open-water efficiency curve shows a completely ascending trend up to J=1.1 and then a completely descending trend beyond this advance ratio. The thrust coefficient and torque coefficient curves generally show a decreasing trend with increasing advance ratio, apart from minor fluctuations. Fig. 14 presents the efficiency, torque, and thrust coefficient values at various advance ratios. As the results indicate, there is good agreement between the experimental test results and numerical simulations. Fig. 15 also shows the thrust and torque coefficients as bar charts, calculated using the average measured values of rotor thrust, duct-stator thrust, total thrust, and rotor torque. Fig. 16 presents the relative uncertainty values of duct-stator thrust, rotor thrust, total thrust, rotor torque, and open-water efficiency as percentages. As the graph shows, the maximum relative uncertainty occurs for open-water efficiency at 1.689285%, which is less than 5%, indicating the high accuracy of the experiments.

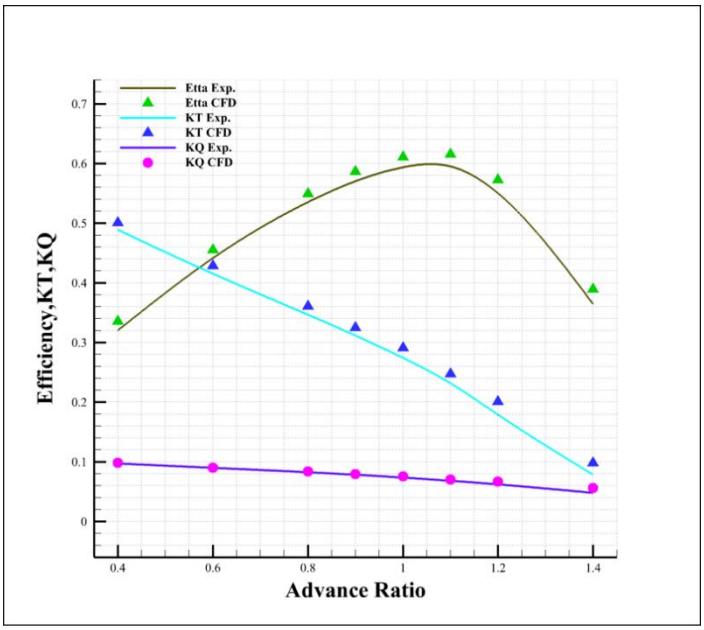



**Fig. 14 Open-water efficiency, thrust, and torque coefficients at various advance ratios for L=0.025DR**

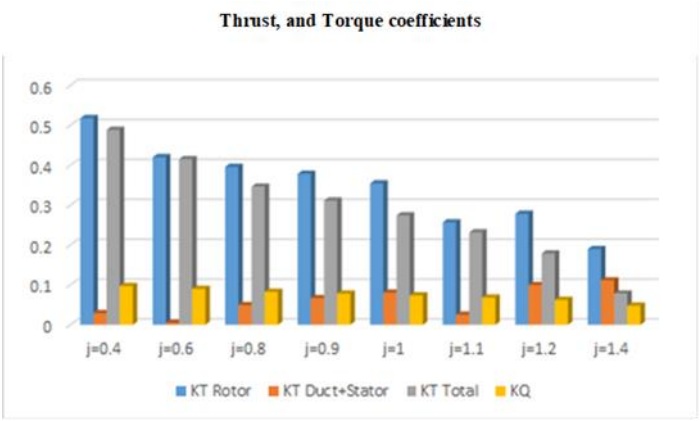
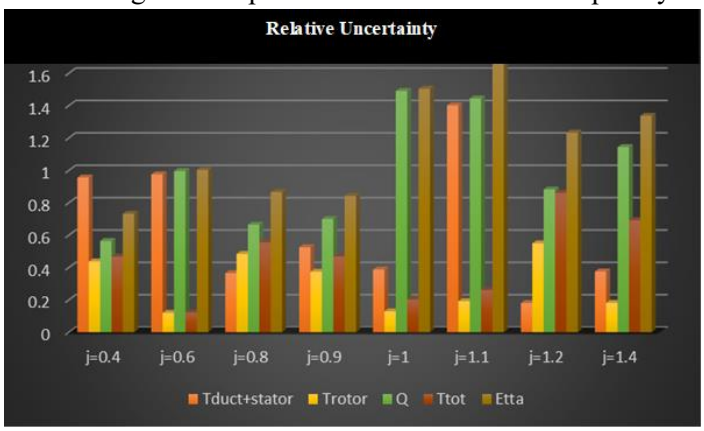



**Fig. 15 Bar chart of rotor thrust coefficient, duct+stator thrust coefficient, total thrust coefficient, and torque coefficient obtained from experimental test results for L=0.025DR**

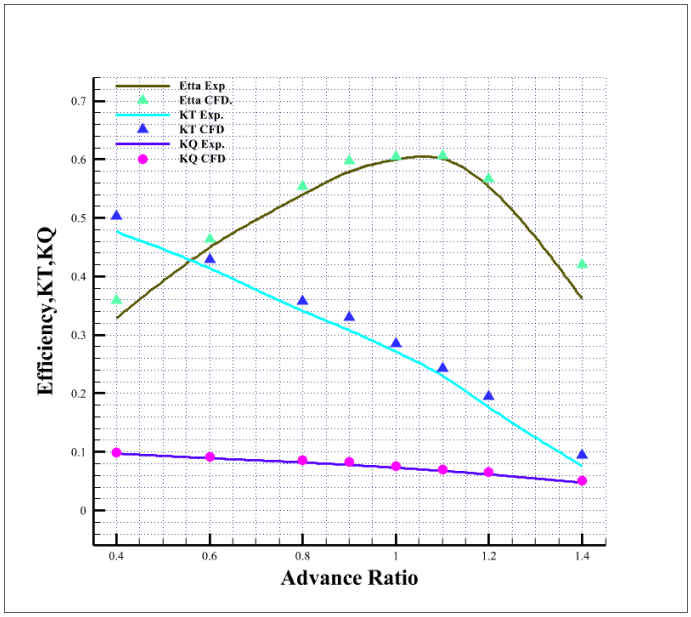
**Fig. 16 Relative uncertainty values of duct-stator thrust, rotor thrust, total thrust, rotor torque, and open-water efficiency parameters as percentages at various advance ratios for L=0.025DR**

*9-3 Case 3: L=0.050DR*

In this case, the duct inlet section length is considered to be 0.045 meters. Based on the average of 4 sets of sampled thrust and torque values from the experimental test at different advance ratios, the maximum efficiency is 60.09% at an advance ratio of 1.1. The maximum thrust coefficient is 0.5019, and the maximum torque coefficient is 0.0973. Similar to the previous case, the open-water efficiency curve shows a completely ascending trend up to J=1.1 and then a completely




descending trend beyond this advance ratio. As in the




previous case, there are no significant oscillatory peaks in the thrust and torque coefficient curves, and a decreasing trend is observed, with good agreement between the experimental test results and numerical simulations. Fig. 17 presents the efficiency, torque, and thrust coefficient values at various advance ratios. Fig. 18 also shows the thrust and torque coefficients as bar charts, calculated using the average measured values of rotor thrust, duct-stator thrust, total thrust, and rotor

torque. Fig. 19 presents the relative uncertainty values of duct-stator thrust, rotor thrust, total thrust, rotor torque, and open-water efficiency as percentages. As the graph shows, the maximum relative uncertainty occurs for open-water efficiency at 1.794044%, which is less than 5%, indicating the high accuracy of the experiments.

**Fig. 17 Efficiency, thrust, and torque coefficients at various advance ratios for L=0.050DR**

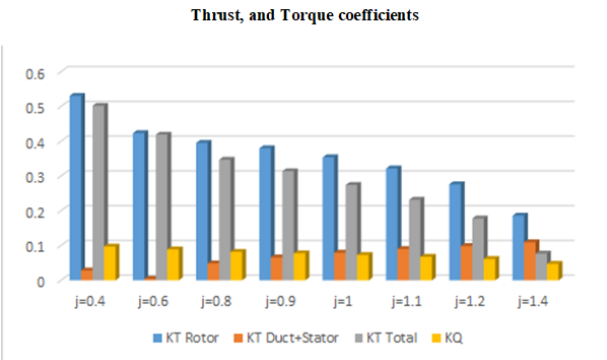



**Fig. 18 Bar chart of rotor thrust coefficient, duct+stator thrust coefficient, total thrust coefficient, and torque coefficient obtained from experimental test results for L=0.050DR**

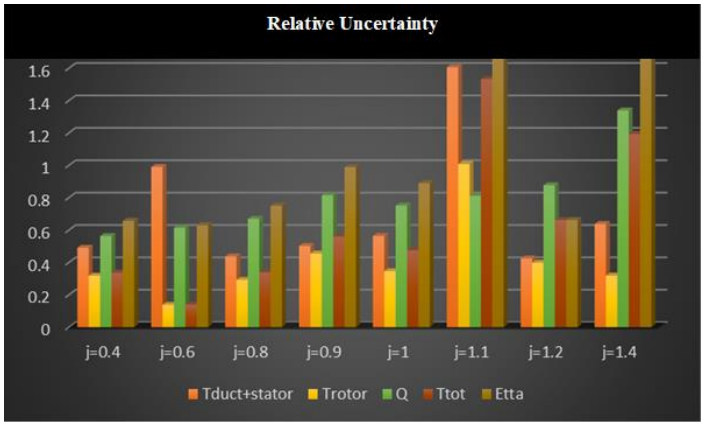



**Fig. 19 Relative uncertainty values of duct-stator thrust, rotor thrust, total thrust, rotor torque, and open-water efficiency parameters as percentages at various advance ratios for L=0.050DR**

## 9-4 Case 4: L=0.075DR

In this case, the inlet section length is considered to be 0.0675 meters. Based on the average of 4 sets of sampled thrust and torque values from the experimental test at different advance ratios, the maximum efficiency is 61.05% at an advance ratio of 1.1. The maximum thrust coefficient is 0.4761, and the maximum torque coefficient is 0.09353. In this case, similar to the previous cases, the open-water efficiency curve exhibits a completely ascending trend up to J=1.1, followed by a completely descending trend beyond this advance ratio. The thrust coefficient curve shows an approximately decreasing trend. The torque coefficient is similar to the previous case. Fig. 20 presents the efficiency, torque, and thrust coefficient values at various advance ratios. There is good agreement between the numerical and experimental results. Fig. 21 also shows the thrust and torque coefficients as bar charts, calculated using the average measured values of rotor thrust, duct-stator thrust, total thrust, and rotor torque. Fig. 22 presents the relative uncertainty values of duct-stator thrust, rotor thrust, total thrust, rotor torque, and open-water efficiency as percentages. As the graph shows, the maximum relative uncertainty occurs for open-water efficiency at 1.422993%, which is less than 5%, indicating the high accuracy of the experiments.

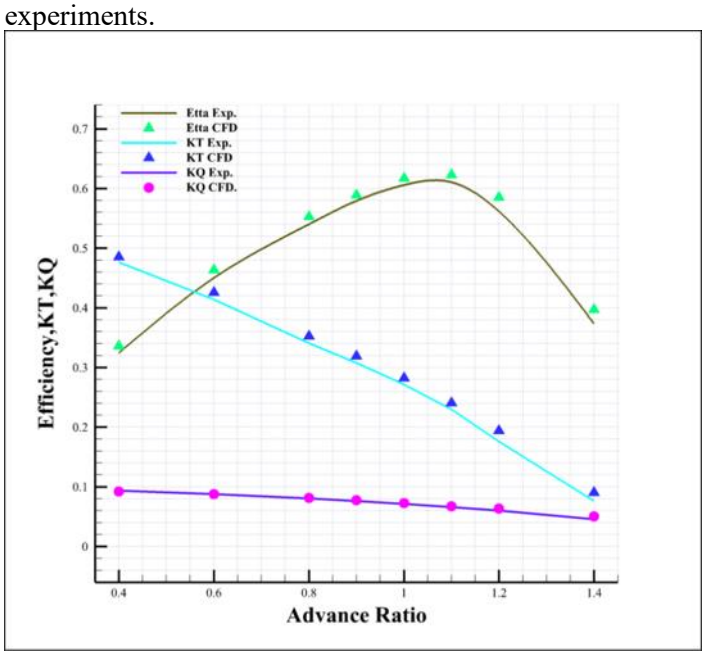



**Fig. 20 Efficiency, thrust, and torque coefficients at various advance ratios for L=0.075DR**

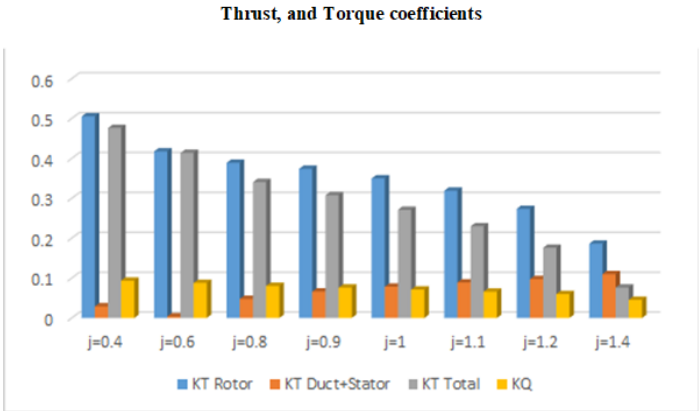



**Fig. 21 Bar chart of rotor thrust coefficient, duct+stator thrust coefficient, total thrust coefficient, and torque coefficient obtained from experimental test results for L=0.075DR**

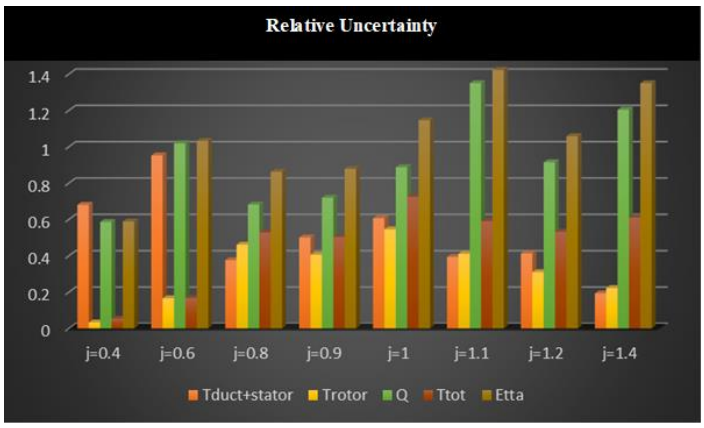



**Fig. 22 Relative uncertainty values of duct-stator thrust, rotor thrust, total thrust, rotor torque, and open-water efficiency parameters as percentages at various advance ratios for L=0.075DR**

## 9-5 Case 5: L=0.1DR

In this case, the inlet section length is considered to be 0.09 meters. Based on the average of 4 sets of sampled thrust and torque values from the experimental test at different advance ratios, the maximum efficiency is 62.15% at an advance ratio of 1.1. The maximum thrust coefficient is 0.5117, and the maximum torque coefficient is 0.0989. Similar to the previous cases, the open-water efficiency curve exhibits a completely ascending trend up to J=1.1, followed by a completely descending trend beyond this advance ratio. The maximum efficiency among all cases investigated is observed in this case. The thrust and torque coefficient curves also show a decreasing trend with an increasing advance ratio. Fig. 23 presents the efficiency, torque, and thrust coefficient values at various advance ratios. Fig. 24 also shows the thrust and torque coefficients as bar charts, calculated using the average measured values of rotor thrust, duct-stator thrust, total thrust, and rotor torque. Fig. 25 presents the relative uncertainty values of duct-stator thrust, rotor thrust, total thrust, rotor torque, and open-water efficiency as percentages. As the graph shows, the maximum relative uncertainty is for open-water efficiency at 1.663996%, which is less than 5%, indicating the high accuracy of the experiments.

**Fig. 23 Efficiency, thrust, and torque coefficients at various advance ratios for L=0.1DR**

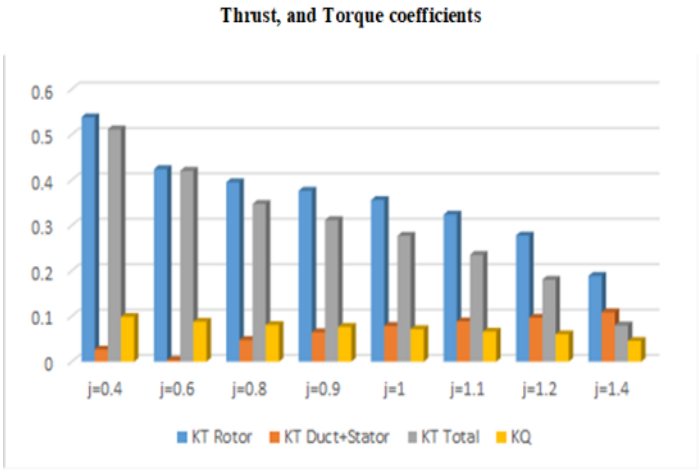
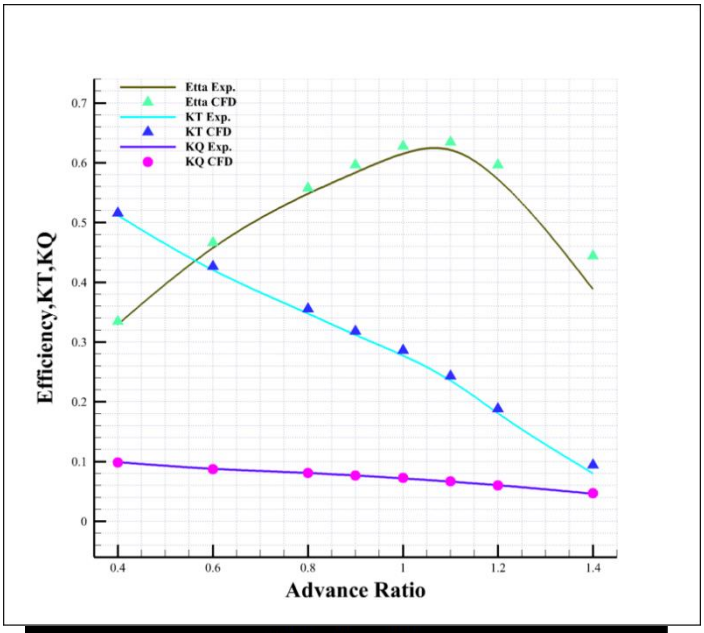



**Fig. 24 Bar chart of rotor thrust coefficient, duct+stator thrust coefficient, total thrust coefficient, and torque coefficient obtained from experimental test results for L=0.1DR**



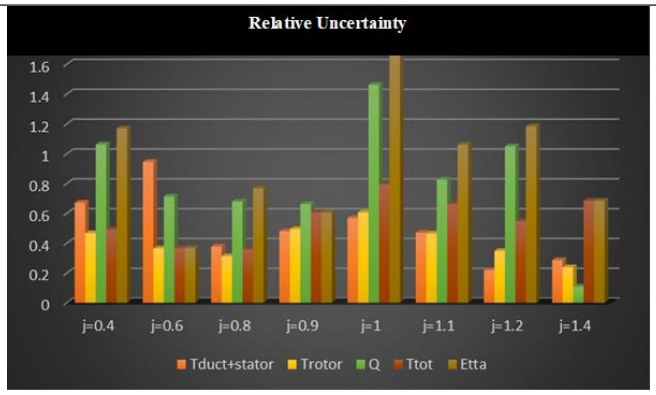




**Fig. 25 Relative uncertainty values of duct-stator thrust, rotor thrust, total thrust, rotor torque, and open-water efficiency parameters as percentages at various advance ratios for L=0.1DR**

## 10- RESULTS AND DISCUSSION

*10-1 Pressure Coefficient Analysis*

To analyze the pressure coefficient changes at different sections across the 0.7 span, for various advance ratios, measurements were taken. The positions of these sections are shown in Fig. 26. The results are presented in the graphs of Figs 27 and 28.

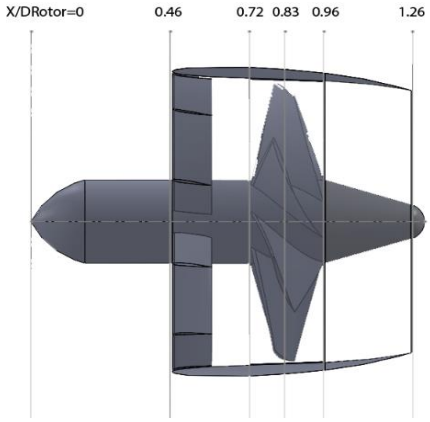



**Fig. 26 Dimensionless section positions on the propeller.**

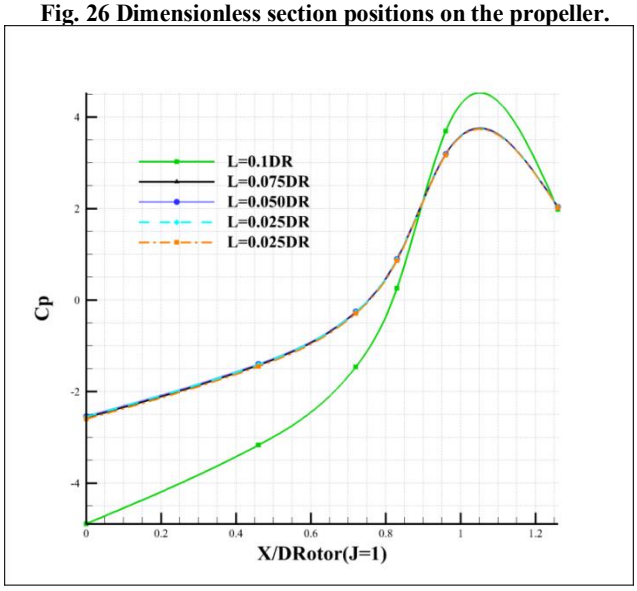



**Fig. 27 Pressure coefficient variation plot across the propeller at an advance ratio of 1 (Numerical Simulation).**

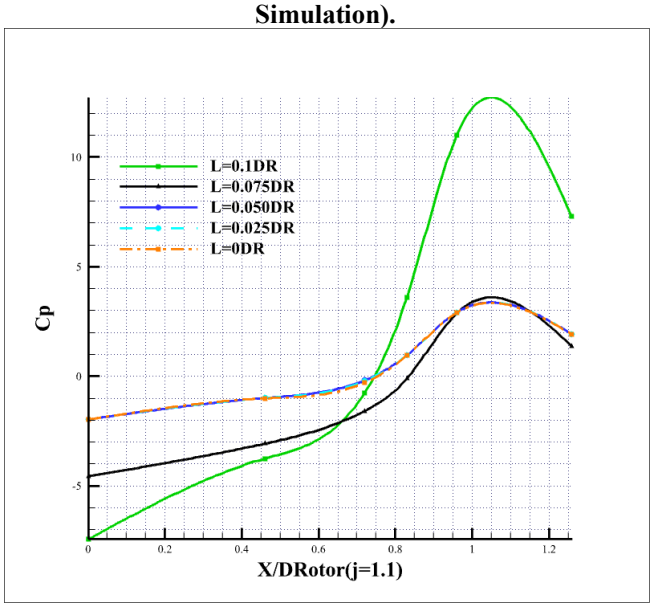
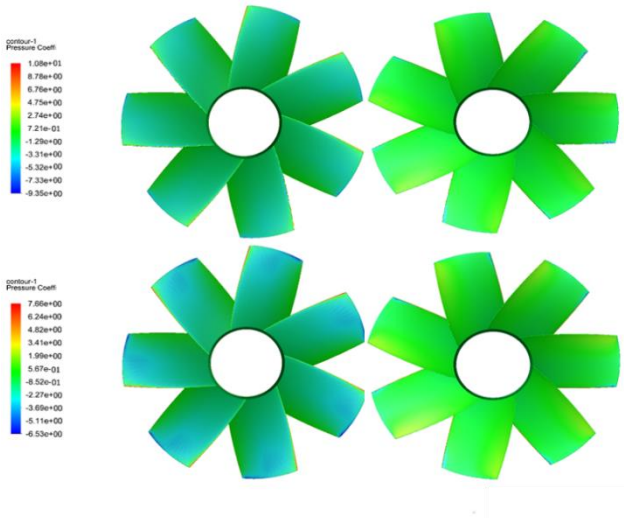



**Fig. 28 Pressure coefficient variation plot across the propeller at an advance ratio of 1.1 (Numerical Simulation)**

Examination of the pressure coefficient variation plots indicates a greater pressure difference across the rotor—as the primary thrust generator of the propeller—for the L=0.1DR case, which can lead to increased thrust and propeller efficiency. For the remaining four cases, the trends are more similar, and the values are close; however, in the L=0.1DR case, the pressure difference is higher. In the sections before the rotor inlet, the result is different, with the L=0.1DR case showing lower values compared to the other cases. Accordingly, moving the stator closer to the rotor will increase the pressure difference across the rotor, which holds the most advance ratios. The pressure coefficient contour at an advance ratio of 0.9 for the suction and pressure sides of the rotor for L=0.1DR and L=0DR cases are shown in Fig. 29. Examination of these contours also reveals a greater pressure difference



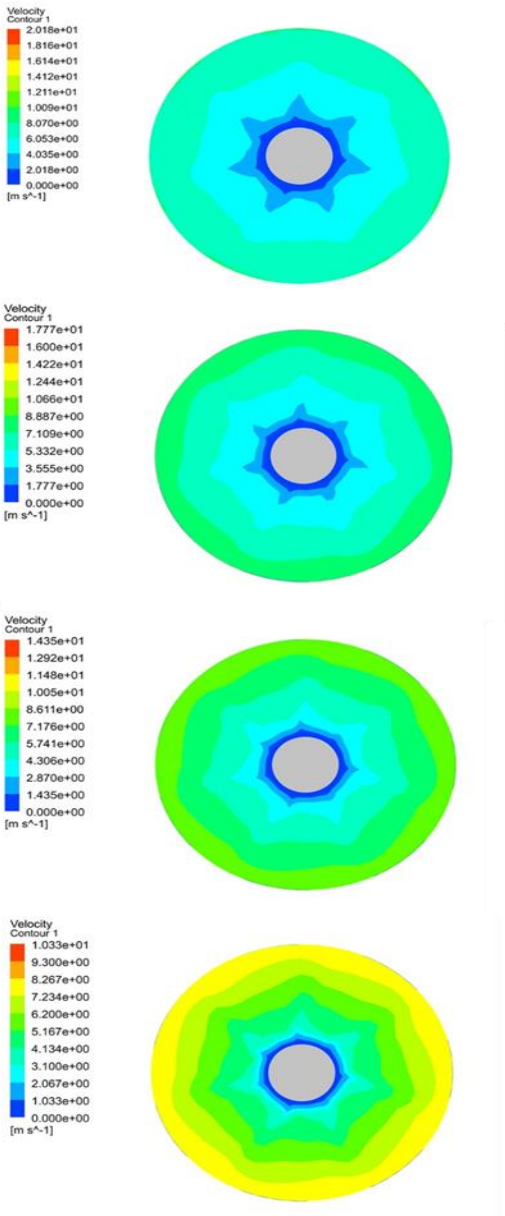
across the rotor for the L=0.1DR case.

**Fig. 29 Pressure coefficient contour on the rotor, from left to right, suction and pressure sides, and from top to bottom, for L=0.1DR and L=0DR cases at an advance ratio of 1.1.**

**10-2 Velocity Analysis**

After the pressure increases in the rotor and the flow exits it, it reaches the converging section of the duct, where the increased pressure converts to velocity, leading to an increase in momentum as the flow exits the duct. Fig. 30 shows the contour plots of flow velocity sections after passing the rotor at X/DRotor=1.1 at an advance ratio of 1.1. In the L=0.1DR case, high-velocity regions exist uniformly from span 0.65 onwards, and generally, from span 0.45 onwards, only two distinct velocity boundaries are discernible. In the velocity contour for the L=0.075DR case, three velocity boundaries are discernible from span 0.4 onwards, and the final high-velocity boundary

extends from span 0.8 to the end. In the L=0.050DR case, four-velocity boundaries are observable from span 0.35 onwards. The final high-velocity boundary is from span 0.8 to the end. In the L=0.025DR case, three boundaries are observable from span 0.35 onwards, and the final high-velocity boundary continues from span 0.8 to the end. On the L=0DR contour, four boundaries are discernible from span 0.35 onwards. The final high-velocity boundary is interdigitated with a lower velocity boundary from span 0.95 onwards. As observed, the velocity contour for the L=0.1DR case shows a higher velocity value compared to the other cases, in addition to having a more uniform velocity distribution, with similar conditions existing at other advance ratios. Fig. 31 also shows the velocity contour at different sections for the L=0DR case at an advance ratio of 0.9.



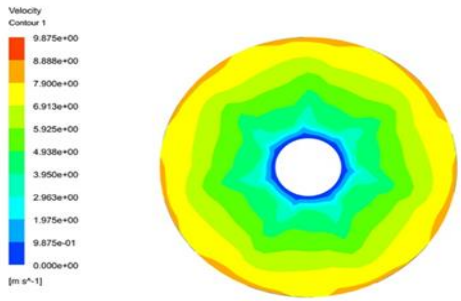




**Fig. 30 Velocity contour at section X/DRotor=1.1, from up to down: L=0.1DR, L=0.075DR, L=0.050DR, L=0.25DR and L=0DR at an advance ratio of 1.1**

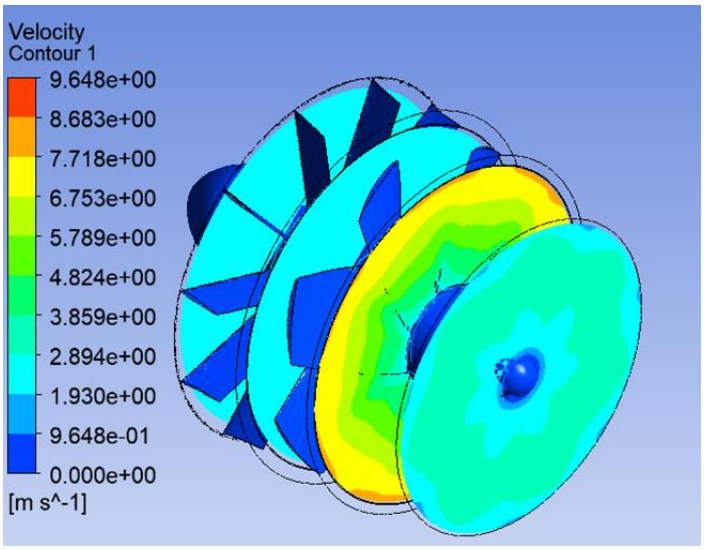



**Fig. 31 Velocity contour at different sections for the L=0DR case at an advance ratio of 0.9.**

Fig. 32 presents the contour of vortex core regions related to the axial velocity exiting the rotor using the Q-Criterion method for the L=0.1DR and L=0DR geometries at an advance ratio of 0.8. Examination of these two contours shows that at the rotor outlet for the L=0.1DR case, higher-speed vortices are formed from spin 0.7 onwards to the inner wall of the duct, indicating a higher flow velocity after passing the rotor and entering the converging section of the duct for the L=0.1DR case compared to L=0DR. Based on the analysis for the other cases as well, the axial velocity vortices exiting the L=0.1DR case have a higher value at most advance ratios.

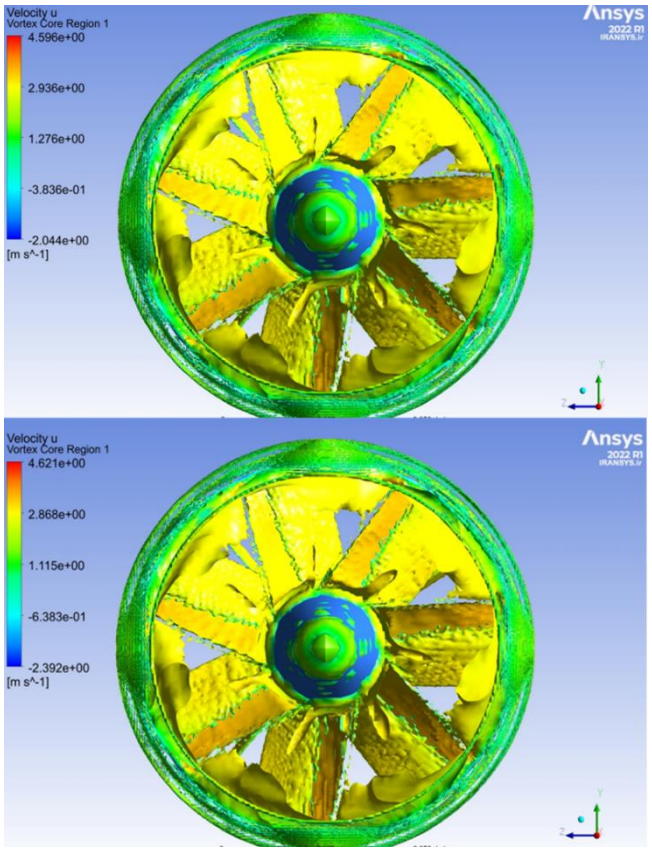



**Fig. 32 Contour of vortex core regions related to the axial velocity exiting the rotor using the Q-Criterion method for the L=0.1DR and L=0DR geometries at an advance ratio of 0.8.**

## 10-3 Streamline Analysis

Generally, for airfoil sections, with an increase in the angle of attack up to a specific range (often less than 20 degrees), the airfoil's lift coefficient increases. If, during this increase, the drag coefficient remains unchanged or decreases (the lift-to-drag ratio increases, or in the case of a propeller, thrust increases), the performance of the airfoil section improves. The streamlines for the L=0DR and L=0.1DR cases at an advance ratio of 1.1 are shown in Fig. 33. Their close examination reveals that as the stator blade approaches the rotor, more streamlines effect and exit the rotor blades at an appropriate angle of attack. The effect of streamlines at a suitable angle of attack (which should have been considered during stator design) will increase the rotor's hydrodynamic efficiency.

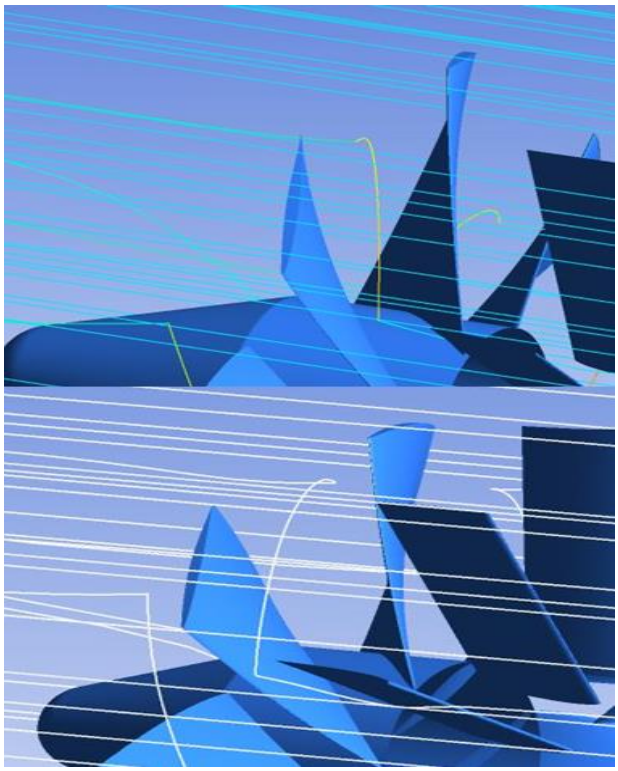


**Fig. 33 Contour of streamlines passing from the stator to the rotor, from top to bottom, for L=0DR and L=0.1DR cases.**

Fig. 34 also presents the rotor lift coefficient values for the five cases studied at advance ratios of 0.9, 1, 1.1, and 1.2. Examination of the values shows that as the stator approaches the rotor, the lift coefficient increases for most advance ratios, and there is a significant difference in the lift coefficient values for the L=0.1DR case compared to the other cases at advance ratios of 1 and 1.1.

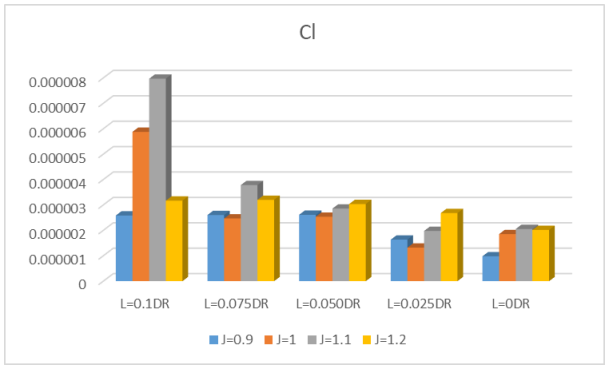



**Fig. 34 Bar chart of rotor lift coefficient for the five cases studied at advance ratios of 0.9, 1, 1.1, and 1.2 (Numerical Simulation).**

## 10-4 Total Thrust Coefficient

Based on the comparative graph in Fig. 36, the L=0.01DR case shows the highest total thrust coefficient among the different cases at all advance ratios. In the remaining cases, differences are observed in the ranges of J=0.4 to J=0.8 and J=1.1 to J=1.4, with no significant difference in other ranges. The trend for all cases is decreasing in the range of J=0.4 to J=0.6, increasing from J=0.6 to J=0.8, and then solely decreasing, except for the L=0.1DR case, which is increasing in the range of J=1.1 to J=1.4**.**

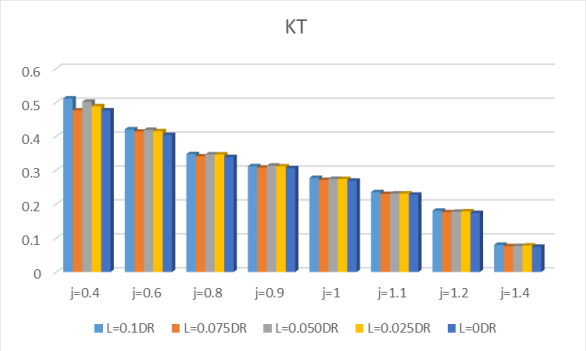



**Fig. 35 Bar chart of total thrust coefficient for the five cases studied (Experimental Test).**

## 10-5 Torque Coefficient

A careful examination of the graph in Fig. 37 shows that the L=0.025DR case has the highest torque coefficient of all advance ratios. In the other cases, there are also differences in the range of J=0.4 to J=0.6, and after this range, the values become similar. The trend for all cases is decreasing in the range of J = 0.4 to J = 0.6, approximately increasing from J = 0.6 to J = 0.8, and then decreasing again.

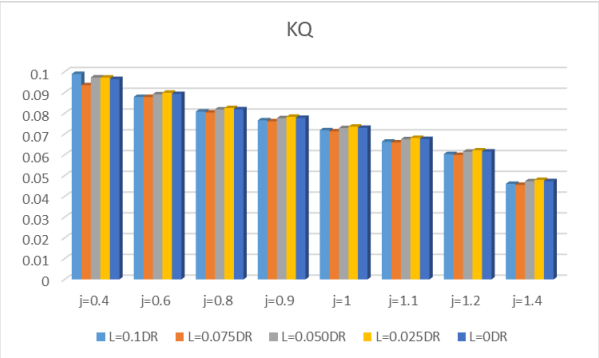



**Fig. 36 Bar chart of torque coefficient for the five cases studied (Experimental Test).**

As observed, the most significant fluctuations in both the thrust coefficient and the torque coefficient occur at lower advance ratios due to the influence of induced velocities from the stator on the rotor. On the other hand, with an increase in the duct inlet length, the proximity of the stator to the rotor, and the correct guidance of the flow at a higher angle of attack to the leading edge of the rotor, the fluctuations are reduced, and it is observed that these detrimental fluctuations are almost eliminated. The trend becomes uniform at higher advance ratios.

## 10-6 Open Water Efficiency

As evident from the comparative graph in Fig. 38, the propeller's open water efficiency increases with an increase in the duct inlet length and better and more accurate guidance of streamlines to the leading edges of the rotor blades (which, due to the arrangement of the stator blades, leads to an increase in the angle of attack of the flow to the rotor blades and, consequently, an increase in the rotor blades' lift coefficient). As observed, the L=0.1DR case has the maximum open water efficiency and, at most advance ratios except J=0.4, has higher efficiency than the others. The L=0.025DR case has the minimum efficiency at all advance ratios. The L=0.050DR, L=0.025DR, and L=0.075DR cases show a roughly similar trend and close values.

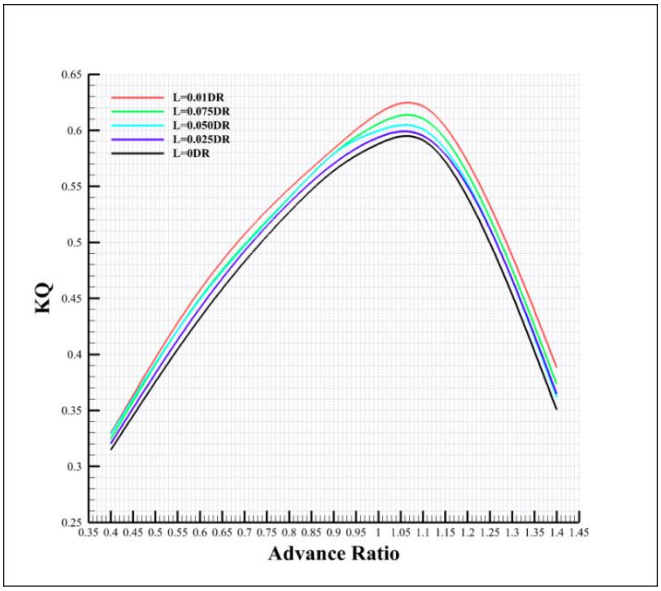



**Fig. 37 Comparative graph of efficiency for the five inlet duct lengths studied at different advance ratios.**

## 10-7 Relative Uncertainty

The relative uncertainty values for the duct and stator assembly thrust, rotor thrust, and total thrust are presented in Figs 13, 16, 19, 22, and 25. The relative uncertainty values for the duct and stator assembly thrust vary from 0.1001 (L=0DR, J=0.6) to 1.605497 (L=0.050DR, J=1.1). The relative uncertainty values for rotor thrust vary from 0.033333 (L=0.075DR, J=0.4) to 1.007751 (L=0.050DR, J=1.1). The relative uncertainty values for total thrust vary from 0.054456224 (L=0.075DR, J=0.4) to 1.533078 (L=0.050DR, J=1.1). The relative uncertainty values for rotor torque vary from 0.1087 (L=0.1DR, J=1.4) to 1.490312966 (L=0.025DR, J=1). The relative uncertainty values for open water efficiency vary from 0.368471123 (L=0.1DR, J=0.6) to 1.794043915 (L=0.050DR, J=1.4). Based on this, the maximum relative uncertainty among all these parameters is 1.794043915 (L=0.050DR, J=1.4), which is a desirable

value in engineering calculations and indicates the high accuracy of the experimental test conducted.

## 11- CONCLUSION AND SUMMARY

This study provides significant insights into the hydrodynamic performance of a pre-swirl pump-jet in open water by experimentally and numerically investigating the effects of duct inlet length and stator-rotor gap. Five configurations with varying duct inlet lengths (L/DR = 0, 0.025, 0.050, 0.075, 0.1) were studied both experimentally in a cavitation tunnel and through numerical simulations. The close agreement between experimental results and numerical simulations, performed using ANSYS Fluent software with the k-ω SST turbulence model and uncertainty analysis, confirms the reliability of the findings. The main research findings are as follows:

- Optimization of Duct Inlet Length and Stator-Rotor Distance: The results indicate that increasing the duct inlet length, accompanied by a reduced stator-rotor gap, leads to more appropriate guidance of the flow lines exiting the stator at a suitable angle of attack to the rotor blades. This increases the rotor lift coefficient and creates a greater pressure difference across the rotor. Upon entering the convergent section of the duct, this results in increased velocity and momentum, ultimately leading to an increase in the total thrust coefficient of the propulsor and a subsequent significant increase in open-water efficiency. The configuration with L=0.1DR achieved the highest efficiency of 62.15% at an advance ratio of 1.1, which was 5% higher than the lowest efficiency (59.12%) of the L=0DR case at the same advance ratio. In most other advance ratios, the L=0.1DR case also exhibited the maximum open-water efficiency.
- Performance Criteria and Uncertainty Analysis: The performance of the pump-jet propulsor is evaluated based on efficiency, thrust coefficient, and torque coefficient in open-water conditions. The calculated relative uncertainty values were all less than 5%, indicating the accuracy of the experiments conducted.
- Comparison of Configurations: This study compares the pump-jet performance under various configurations. The results show that the configuration with L=0.1 DR is preferred over the others due to its more favorable hydrodynamic performance. This configuration demonstrated more uniform flow, a greater pressure difference across the rotor, and stable performance over a broader range of advance ratios.
- Performance Improvement: The improved performance is attributed to better guidance of flow lines from the stator to the rotor, an increased rotor lift coefficient, a larger pressure difference across the rotor, and a greater increase in axial velocity after the flow enters the convergent section of the duct.
- Scientific and Practical Implications: The findings of this research have significant implications for the design of marine propulsion systems, especially for underwater vehicles such as submarines and autonomous underwater vehicles (AUVs). Optimizing the duct inlet length and stator-rotor gap can enhance hydrodynamic efficiency, which is crucial for extended operational range. These improvements reduce energy consumption, aligning with global sustainability goals. The principles presented in this study can also be applied to the design of other fluid machinery, such as hydroelectric turbines or ducted fans. The combined experimental and numerical methodology, including rigorous cavitation tunnel tests and high-fidelity CFD simulations with uncertainty analysis, provides a reliable framework for future research in hydrodynamics.
- Limitations and Future Research Directions: Despite the advancements made, this study has limitations that highlight the need for further investigation in the future. The experiments were conducted in a controlled cavitation tunnel environment, which may not fully simulate real-world effects such as wall effects, vortex integration effects in the wake region, or variable marine conditions. Future research should investigate these parameters under actual operating conditions, taking into account wall effects and varying flow regimes. Additionally, studying noise generation and cavitation inception, which are crucial for stealth applications and system durability, is essential. Investigating scale effects (model vs. full-scale) can help identify more optimal configurations.
- Final Summary: This study advanced the understanding of pre-swirl pump-jet hydrodynamics by providing a comprehensive analysis of the effect of duct inlet length and stator-rotor gap. The optimal configuration (L = 0.1 DR) offered significant efficiency, providing practical guidelines for designing more efficient and sustainable propulsion systems. These findings contribute to the advancement of marine technology by filling the stated gap in research, paving the way for the development of underwater vehicles with superior performance. Future research on noise, cavitation, and real-world conditions will extend the practical effect of these findings, solidifying the pump jet as a cornerstone of future underwater marine propulsion.

## REFERENCES

[1] Bertram, V. (2012). Practical ship hydrodynamics. Oxford, U.K, Butterworth Heinemann.

[2] Bi, Z., Zhang, L., Shao, X., & Bao, F. (2023). Numerical study of two types of rough groove in suppressing the tip clearance cavitation. International Journal of Multiphase Flow, 168, 104564. https://doi.org/10.1016/j.ijmultiphaseflow.2023.104564

[3] Carlton, J. S. (2012). Marine propellers and propulsion (3rd ed.). Amsterdam, Netherland, Elsevier.
[4] Chen, X., Cheng, L., Wang, C., & Luo, C. (2021). Influence of inlet duct length on the hydraulic performance of the waterjet propulsion device. Shock and Vibration, 2021(1), 6676601. https://doi.org/10.1155/2021/6676601
[5] Coleman, H. W., & Steele, W. G. (1999). Experimentation and Uncertainty Analysis for Engineers. John Wiley and Sons, Inc., New York.
[6] Dean, A., & Voss, D. (1999). Design and Analysis of Experiments. Springer Verlag, New York.
[7] Huang, Q., Li, H., Pan, G., & Dong, X. (2021). Effects of duct parameter on pump-jet propulsor unsteady hydrodynamic performance. Ocean Engineering, 221, 108509. https://doi.org/10.1016/j.oceaneng.2020.108509
[8] Huang, Q., Qin, D., & Pan, G. (2022). Numerical simulation of the wake dynamics of the pumpjet propulsor in oblique inflow. Physics of Fluids, 34(6). https://doi.org/10.1063/5.0091408
[9] Ji, X. Q., Zhang, X. S., Yang, C. J., & Dong, X. Q. (2024). Experimental and numerical investigation of the effects of rotor tip-rake on excitation forces of pump-jet propulsors. Journal of Hydrodynamics, 1-16. https://doi.org/10.1007/s42241-024-0011-0
[10] Kim, J.-W., Kim, M.-C., Park, I.-R., Seol, H., Kim, M.-J., & Jin, W.-S. (2023). Parametric Study of the Hydrodynamic Characteristics of the Pumpjet Propulsor for the SUBOFF Submarine. Journal of Marine Science and Engineering, 11(10), 1926. https://doi.org/10.3390/jmse11101926
[11] Li, H., Huang, Q., & Pan, G. (2022). Investigation on the Propulsion of a Pump-Jet Propulsor in an Effective Wake. Journal of Fluids Engineering, 144(5).
[12] Li, X. R., Ding, Y., & Wang, W. Q. (2022). The hydrodynamic performance analysis of a submarine with new pump-jet propulsor. Ocean Engineering, 245, 110542.
[13] Lidtke, A. K., Lloyd, T., Lafeber, F. H., & Bosschers, J. (2022). Predicting cavitating propeller noise in off-design conditions using scale-resolving CFD simulations. Ocean Engineering, 254, 111176. https://doi.org/10.1016/j.oceaneng.2022.111176
[14] Morrison, A. (2018). A comparison of pump jets and propellers for non-nuclear submarine propulsion.
[15] Motallebi-Nejad, M., Bakhtiari, M., Ghassemi, H., & Fadavie, M. (2017). Numerical analysis of ducted propeller and pumpjet propulsion system using periodic computational domain. Journal of Marine Science and Technology, 22, 559–573. https://doi.org/10.1007/s00773-017-0438-x
[16] Nakra, B. C., & Chaudhry, K. K. (2016). Instrumentation Measurement and Analysis (4th ed.).
[17] Qaedsharaf, M. H. (2011). Analysis of heat transfer and fuel regression rate of solid fuel in hybrid thrusters [M.Sc. Thesis]. Islamic Azad University, Science & Research Branch.
[18] Qaedsharaf, M. H., Mahdavi, H., & Mehrabi Gohari, E. (2019). Comparison of performance and sensitivity of effective parameters in two propellants hydrogen peroxide and nitrous oxide using uncertainty analysis. Mechanical Engineering, University of Tabriz, 50(3), 233-237. https://doi.org/10.22034/JMEUT.2020.9802
[19] Qaedsharaf, M. H., Yari, E., & Manshadi, M. D. (2025). Cavitation on the pump jet pre swirl type due to changes in the stator chord length. Physics of Fluids, 37(3). https://doi.org/10.1063/5.0248017
[20] Qin, D., Huang, Q., Pan, G., Shi, Y., Han, P., & Dong, X. (2021). Comparison of hydrodynamic performance and wake vortices of two typical types of pumpjet propulsor. Ocean Engineering, 224, 108700. https://doi.org/10.1016/j.oceaneng.2021.108700
[21] Qiu, C., Huang, Q., & Pan, G. (2022). Prediction of Cavitation Performance over the Pump-Jet Propulsor Using Computational Fluid Dynamics and Hybrid Deep Learning Method. Journal of Marine Science and Engineering, 10(7), 918. https://doi.org/10.3390/jmse10070918
[22] Qiu, C., Huang, Q., Pan, G., Shi, Y., & Dong, X. (2020). Numerical simulation of hydrodynamic and cavitation performance of pumpjet propulsor with different tip clearances in oblique flow. Ocean Engineering, 209, 107285. https://doi.org/10.1016/J.OCEANENG.2020.107285
[23] Renilson, M. R. (2018). Submarine hydrodynamics (2nd ed.). Springer, Cham. https://doi.org/10.1007/978-3-319-79057-2
[24] Sun, Y., Peng, H., Liu, W., Guo, J., & Guo, Y. (2022). Comparison of the hydrodynamic performance of front and rear-stator pump-jet propulsors in an oblique wake under the cavitation condition. Physics of Fluids, 34(3). https://doi.org/10.1063/5.0082769
[25] Suryanarayana, C., Rao, M. N., Raju, P. N., Balakrishan, T., & Lambada, S. (2012). Torque Balance and Cavitation Studies on Underwater Vehicle Propulsion System. International Journal of Innovative Research and Development, 1, 62-73.
[26] Wang, C., Weng, K., Guo, C., Chang, X., & Gu, L. (2020). Analysis of influence of duct geometrical parameters on pump jet propulsor hydrodynamic performance. Journal of Marine Science and Technology, 25, 640–657. https://doi.org/10.1007/S00773-019-00662-Z
[27] Weng, K., Sun, C., Han, K., Wang, C., Sun, S., Li, P., & Hu, J. (2024). Experimental/numerical investigation on the hydrodynamic and noise characteristics of pump-jet propulsion. Ocean Engineering, 307, 117995. https://doi.org/10.1016/j.oceaneng.2024.117995
[28] Yang, J., Feng, D., Liu, L., Wang, X., & Yao, C. (2022). Research on the Performance of Pumpjet Propulsor of Different Scales. Journal of Marine Science and Engineering, 10(1), 78. https://doi.org/10.3390/jmse10010078
[29] Ye, J. M., Sun, D. P., Zou, X. Y., Wu, Y. R., & Xi, P. (2022). Tip flow control performance and mechanism of axial slots in a pumpjet propulsor. Ocean Engineering, 266, 112950. https://doi.org/10.1016/j.oceaneng.2022.112950
[30] Zhao, X., Zhang, D., Shen, X., Geng, L., & van Esch, B. B. (2022). Numerical investigation on cavitation-vortex interaction in a scaled pre-swirl pump-jet propulsor.
[31] Zhou, Y., Pavesi, G., Yuan, J., & Fu, Y. (2022). A Review on Hydrodynamic Performance and Design of Pump-Jet: Advances, Challenges and Prospects. Journal of Marine Science and Engineering, 10(10), 1514. https://doi.org/10.3390/jmse10101514
[32] Zhou, Y., Pavesi, G., Yuan, J., Fu, Y., & Gao, Q. (2023). Effects of duct profile parameters on flow characteristics of pump-jet: A numerical analysis on accelerating and decelerating ducts distinguished by cambers and angles of attack. Ocean Engineering, 281, 114733. https://doi.org/10.1016/j.oceaneng.2023.114733

[33] Zou, D., Xue, L., Lin, Q., Xu, J., Dong, X., Ta, N., & Rao, Z. (2024). Influence of propulsion shafting longitudinal vibration on the excitation force and vortex dynamics characteristics of pump-jet propulsor. Ocean Engineering, 295, 116962. https://doi.org/10.1016/j.oceaneng.2024.116962.

INTERNATIONAL JOURNAL OF
COASTAL, OFFSHORE & ENVIRONMENTAL ENGINEERING IJCOE Vol..11/No.4 /Autumn 2026 (65-73)

Available online at: www. Ijcoe.org

# Investigating the Role of Water Depth on Tsunami Shoaling and Coastal Amplification: Insights from Idealized and Realistic Numerical Experiments

**Ehsan Rastgoftar ***

*Assistant Professor,Iranian National Institute for Oceanography and Atmospheric Sciences (INIOAS), Tehran, Iran, e.rastgoftar@inio.ac.ir*

**ARTICLE INFO**

*Article History:*
Received: 18 Aug
Accepted: 23 Nov
Available online ….

*Keywords:*
**Tsunami shoaling**
**Water depth**
**Numerical modeling**
**Persian Gulf**
**Continental shelf**

**ABSTRACT**

Tsunami hazards pose significant threats to coastal communities, with wave amplification during shoaling being a critical factor in determining coastal impact. This study systematically investigates the influence of water depth on tsunami propagation and shoaling through a combination of idealized numerical flume experiments and realistic simulations for the Persian Gulf. The idealized configuration consists of a two-slope bathymetric profile representing the continental shelf and slope, with three depth scenarios (offshore depths of 2200 m, 1100 m, and 220 m) examined. The Persian Gulf case study evaluates tsunami propagation over real bathymetry and artificially deepened configurations (10× and 20× depth amplification) to assess the role of limited water depth on wave amplification.

Results from the idealized flume demonstrate that greater offshore depths produce more pronounced shoaling, with maximum wave heights of approximately 7 m, 5 m, and 3 m for the deep, intermediate, and shallow configurations, respectively. However, the shallowest configuration exhibits anomalous behavior where wave growth ceases and heights decrease due to breaking-induced dissipation, effectively limiting coastal amplification.

The Persian Gulf simulations reveal that while deeper configurations generally produce higher wave heights, a saturation effect exists beyond which additional depth increases yield diminishing returns. Notably, localized areas show complex responses where real-depth simulations produce comparable or higher waves than artificially deepened scenarios, highlighting the importance of site-specific bathymetric effects. These findings challenge the assumption that shallow marginal seas are inherently immune to significant tsunami hazards and emphasize the necessity of high-resolution, case-by-case assessments for accurate hazard evaluation in such regions.

## 1. Introduction

Tsunamis are among the most devastating natural hazards, capable of causing widespread destruction and significant loss of life in coastal regions. The 2004 Indian Ocean tsunami and the 2011 Tohoku tsunami serve as stark reminders of the profound societal and economic impacts of these events [1, 2]. Understanding the physical processes governing tsunami generation, propagation, and coastal impact is therefore of paramount importance for hazard assessment and mitigation efforts.

A critical factor influencing tsunami behavior is the variation in water depth and seafloor topography along the propagation path. As a tsunami wave travels from the deep ocean toward the shore, it undergoes a process known as shoaling, whereby the wave height increases significantly as the wave enters shallower water. This amplification is primarily governed by the principle of energy conservation, and in its simplest form, is described by Green's Law ($H \propto d^{-1/4}$), which predicts an inverse relationship between wave height and water depth [3]. The shoaling effect is further modulated by the slope of the seafloor, with steeper slopes generally producing more rapid amplification [4].

The continental shelf and continental slope represent two distinct morphological regions that play crucial roles in tsunami transformation. The continental shelf, with its typically mild slope (ranging from near 0° to

approximately 1°), provides an extended region over which the shoaling process gradually intensifies [5]. The continental slope, by contrast, exhibits a much steeper gradient, where rapid depth changes can lead to substantial wave amplification [6]. The combined effect of these two topographic features is critical in determining the final tsunami height at the coast.

Numerous analytical and numerical studies have investigated the shoaling effect. Madsen and Schäffer [7] derived analytical solutions for tsunami propagation over varying bathymetry, highlighting the role of depth variations in wave amplification. On the numerical front, the development of Boussinesq-type models [8, 9] has enabled accurate simulation of tsunami propagation across a wide range of water depths, accounting for nonlinearity and frequency dispersion. These models have been successfully applied to study tsunami hazards in various regions (e.g., [10, 11]). Kennedy et al. [12] further extended the applicability of such models by introducing eddy viscosity formulations to capture wave breaking and associated energy dissipation, which is essential for accurately modeling tsunami transformation in shallow coastal waters.

Despite these advances, many studies focus on single idealized profiles or specific real-world events, and systematic investigations of the influence of water depth on the shoaling-induced amplification across a range of topographies remain limited. In particular, the relationship between offshore water depth and the onset of wave breaking during shoaling—and how this affects the maximum achievable wave height at the coast—has not been comprehensively examined. Furthermore, the existence of a potential saturation threshold, beyond which further increases in water depth yield diminishing returns in wave amplification, has not been extensively documented.

The Persian Gulf, a semi-enclosed marginal sea with an average depth of approximately 50 m and maximum depths of around 100 m, presents a unique case where the shallow bathymetry may significantly affect potential tsunami propagation. Recent studies have highlighted the need for tsunami hazard assessments in this region, given the presence of active fault systems such as the Kazerun–Qatar fault [13, 14]. However, the limited water depth of the Persian Gulf has led to the hypothesis that potential tsunamis in this region may not pose a serious threat due to the restricted shoaling effects [15, 16]. Investigating this hypothesis is critical not only for the Persian Gulf itself but also for evaluating the true tsunami hazard potential in similar shallow marginal seas worldwide.

The present study aims to systematically investigate the effect of water depth on tsunami wave height and the shoaling process through a combination of idealized and realistic numerical experiments. Specifically, the objectives are to: examine the shoaling process over idealized shelf–slope profiles with varying offshore depths and apply the findings to a case study of the Persian Gulf to assess the influence of its shallow bathymetry on potential tsunami impact. The results are expected to provide insights into the fundamental physics of tsunami shoaling, particularly regarding the interplay between depth-induced amplification and breaking-induced dissipation, and contribute to improved hazard assessment in shallow marginal seas.

## 2. Numerical Model Configuration

### 2.1. Idealized Configuration: Two-Slope Flume

To systematically investigate the effects of water depth and coastal slope on tsunami wave propagation and shoaling, an idealized numerical flume is designed. The two-dimensional domain consists of two sloping sections with distinct gradients, followed by a region of constant depth at the offshore end. The cross-sectional geometry is illustrated in Figure 1a. The first nearshore sloping section represents the Continental Shelf, characterized by a gentle incline, while the second, steeper section represents the Continental Slope. To simulate realistic conditions and avoid lateral boundary effects, the horizontal dimensions of the flume are scaled to represent a 400 km by 400 km domain.

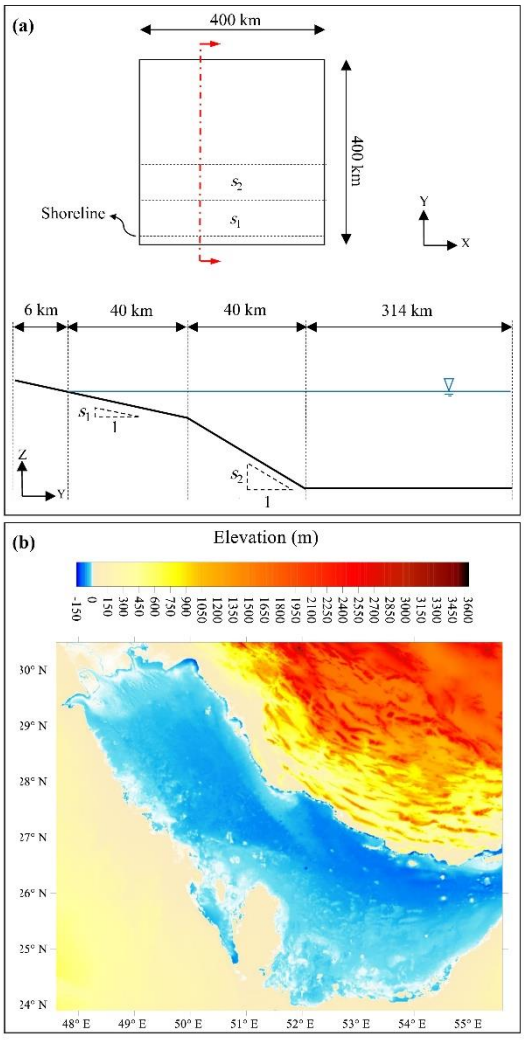



**Figure 1. Computational domains of the numerical models; (a) idealized two-slope flume; (b) Persian Gulf.**

As discussed in the introduction, the continental shelf is characterized by a mild slope. Based on the values reported in the literature, the slope of the first section ($s_1$) is set to 0.5% (approximately 0.3°) for the baseline configuration. According to the global geomorphic database of continental shelves [17], the horizontal length of this first sloping section is fixed at 40 km. The continental slope is substantially steeper than the shelf, with reported average angles of approximately 3° and a range of 1° to 10° [5, 6]. In the present baseline model, the slope of the second section ($s_2$) is set to 5% (approximately 3°), with a horizontal length matching that of the first section at 40 km. Given these designated slopes and horizontal extents, the constant depth at the offshore end of the flume is calculated to be 2200 meters, which is consistent with typical deep-ocean depths.

To systematically examine the impact of water depth on tsunami propagation, two additional flume configurations are generated with reduced offshore depths. For these configurations, the slopes of both the shelf and the continental slope are decreased proportionally compared to the baseline case, maintaining the same morphological structure while allowing for controlled variation of the overall depth profile. The specific geometric parameters for all three cases are summarized in Table 1, with the case designation based on the flat bottom depth to avoid confusion with the slope parameters.

**Table 1. Geometric parameters for the three numerical flume configurations**

| Case Designation | First Slope ($s_1$) | Second Slope ($s_2$) | Offshore Depth |
|---|---|---|---|
| Case D2200 | 0.5% | 5% | 2200 m |
| Case D1100 | 0.25% | 2.5% | 1100 m |
| Case D220 | 0.05% | 0.5% | 220 m |

## 2.2. Realistic Configuration: Persian Gulf

The numerical grid for modeling tsunami propagation in the Persian Gulf covers the geographical domain between 47.60°E to 55.58°E and 23.90°N to 30.50°N, with a resolution of 30 arc-seconds (Figure 1b). The bathymetric/topographic data for this grid integrates the GEBCO_2023 Grid, a global terrain model for ocean and land with a 15 arc-second resolution. The shallow depth of the Persian Gulf is clearly observable in Figure 1b, with depths less than 100 m in most regions of the gulf.

To investigate the effect of water depth on tsunami propagation in the Persian Gulf—and to test the hypothesis that shoaling-induced amplification in this shallow basin may be limited by dissipative processes—two additional grids with increased depths (approaching typical ocean depths) are defined in addition to the real bathymetry. For this purpose, amplification factors of 10 and 20 times are applied to the depth values in the real grid. The three configurations for the Persian Gulf are designated as follows: Case Real, Case D×10 and Case D×20. This approach allows for a systematic comparison of tsunami behavior across a range of depth conditions while preserving the complex morphological features of the Persian Gulf region. The artificially deepened configurations enable evaluation of whether the limited water depth in the gulf restricts shoaling amplification, or whether additional depth increases would produce proportionally higher wave heights—a question of significant importance for tsunami hazard assessment in shallow marginal seas.

## 3. Initial Tsunami Wave Generation

In modeling earthquake-induced tsunamis, the earthquake is typically assumed to occur instantaneously, and the temporal evolution of the fault rupture is neglected. Consequently, the resulting seafloor deformation is immediately transferred to the free surface, generating the initial tsunami wave. Various algorithms have been proposed to compute seafloor displacement during an earthquake. In the present study, the elastic half-space rectangular fault model developed by Okada [18] is employed for this purpose. This analytical method calculates the seafloor deformation based on seismic parameters including fault length, fault width, slip magnitude, dip angle, rake angle, strike angle, and focal depth.

Among the seismic parameters, the rupture length, rupture width, and slip magnitude are directly dependent on the earthquake magnitude. For the idealized flume configuration, the earthquake source magnitude is assumed to be Mw 8.5. Based on the empirical scaling relationships [19] derived from observations of 244 historical earthquakes, the rupture length is determined to be 390 km. For the hypothetical tsunami in the Persian Gulf, considering the approximately 200 km length of the submarine Kazerun–Qatar fault zone located in the central part of the gulf between the Iranian and Qatari coasts with a roughly north–south orientation [20, 21], an earthquake of magnitude 7.9 is assumed as the tsunami source. The fault width and slip magnitude are also derived from the Wells and Coppersmith [19] scaling relationships based on the earthquake magnitudes (Table 2).

**Table 2. Fault parameters for tsunami generation**

| Model | Idealized Flume | Persian Gulf |
|---|---|---|
| Moment Magnitude | 8.5 Mw | 7.9 Mw |
| Fault Length | 389 km | 200 km |
| Fault Width | 50 km | 20 km |
| Slip Magnitude | 12 m | 9 m |
| Dip Angle | 10° | 10° |
| Strike Angle | 270° | 355° |

| | | |
|---|---|---|
| Rake Angle | 90° | 90° |

The strike angle for the idealized case is set to 270° to ensure that the fault is parallel to the coastline, allowing wave propagation to occur entirely perpendicular to the shoreline (i.e., in the direction of bed slope variation). Additionally, this configuration ensures that the uplifted portion of the initial wave is located on the coastal side, so that positive waves (rise in sea level) arrive at the coast before negative waves (drawdown). The rake angle is assumed to be 90°, consistent with thrust-type earthquakes, and the dip angle is set to 10°, a typical value for tsunamigenic earthquakes [19, 22].

## 4. Governing Equations for Wave Propagation

The initial tsunami wave elevation is introduced as the initial condition into the propagation model. In this study, the FUNWAVE model is employed to simulate tsunami propagation and runup. FUNWAVE, developed at the University of Delaware [9, 23], is a Boussinesq-type wave propagation model. The primary advantage of such models over traditional nonlinear shallow-water models is their ability to account for non-uniform horizontal velocity profiles in the vertical direction and to incorporate non-hydrostatic pressure effects (i.e., vertical accelerations). During propagation and runup, non-uniform horizontal velocity profiles in the vertical direction are observed when waves propagate in deep water, when they advance over moderately sloping coastlines, and when they become significantly nonlinear [24]. Another advantage of Boussinesq equations over nonlinear shallow-water equations is their consideration of frequency dispersion, which is essential for accurately simulating tsunami propagation across varying water depths.

To extend the applicability of the FUNWAVE model, various modifications have been proposed. Kennedy et al. [12] introduced eddy viscosity terms to the momentum equations to model wave breaking and the associated turbulence and energy dissipation. Their eddy viscosity formulation was similar to that employed by Zelt [25]. This formulation is particularly relevant for the present study, as wave breaking is expected to occur in the shallowest configuration (Case D220), and the model's ability to capture breaking-induced dissipation is essential for accurately assessing the maximum achievable wave heights.

Through time-stepping solutions of the FUNWAVE equations, tsunami propagation and runup are computed. However, given the objective of the present study—to investigate the effect of water depth on tsunami height and the shoaling process—and considering that the grid resolution of the models is insufficient for accurate runup calculations, the wave conditions are evaluated up to the runup limit, prior to wave impact on the shoreline.

The model time steps are determined based on the CFL stability condition, which is a function of the spatial grid resolution and the maximum numerical wave propagation speed. The computed time step values for the two-slope flume and Persian Gulf models are reported in Table 3. It is observed that for a fixed spatial grid resolution, configurations with greater depths yield smaller time steps. Furthermore, since tsunami propagation speed is lower in shallower water (given that wave speed is proportional to the square root of water depth in shallow-water conditions, $c=(gh)^{1/2}$, models with smaller depths require longer simulation durations to allow sufficient time for waves to propagate and reach the coast.

**Table 3. Model time steps and simulation duration for all configurations**

| Model | Case Designation | Time Step (s) | Simulation Duration (hr) |
|---|---|---|---|
| Idealized Flume | Case D2200 | 1.021 | 1.5 |
| | Case D1100 | 1.444 | 2.5 |
| | Case D220 | 3.223 | 7 |
| Persian Gulf | Case D×20 | 1.592 | 3 |
| | Case D×10 | 2.251 | 3 |
| | Case Real | 7.118 | 6 |

## 5. Results

### 5.1. Idealized Flume

The evolution of tsunami propagation within the two-slope flume for the deepest offshore configuration (Case D2200) is illustrated in Figure 2 at various time intervals following the earthquake and initial wave formation. At t=0, the initial tsunami wave is generated, consisting of an elevated region with a maximum amplitude of approximately 3.5 m and a depression region with a maximum amplitude of approximately 2 m. The initial free-surface displacement, corresponding to the earthquake-induced seafloor deformation, is identical for all three flume configurations, as Okada's model indicates that water depth does not affect the computed seafloor displacement.

As observed at t=10 min and t=20 min, the tsunami waves, following their initial formation and during propagation in both directions perpendicular to the fault, exhibit reduced amplitudes compared to the initial state. However, upon reaching the sloping regions where water depth decreases, the waves undergo significant amplification (t=30 min and t=40 min). At t=50 min, the tsunami waves are approaching the shoreline (indicated by the black region representing dry land).

To conduct a more detailed analysis of wave behavior near the coast, time series of free-surface elevation were extracted at depths of 5 m and 10 m for all three

cases, as presented in Figure 3. The results indicate that at both monitoring stations, the differences in recorded wave heights among the three depth configurations are substantial. As expected, Case D2200, which exhibits the greatest offshore depth and consequently the most pronounced shoaling effect, produces the highest wave amplitudes, while Case D220 yields the lowest recorded wave heights. The time delays in wave arrival for the shallower configurations are also clearly visible, consistent with their reduced propagation speeds. It should be noted that discontinuities in the time series correspond to instances where negative free-surface elevations exceed the local water depth, indicating temporary drawdown conditions.

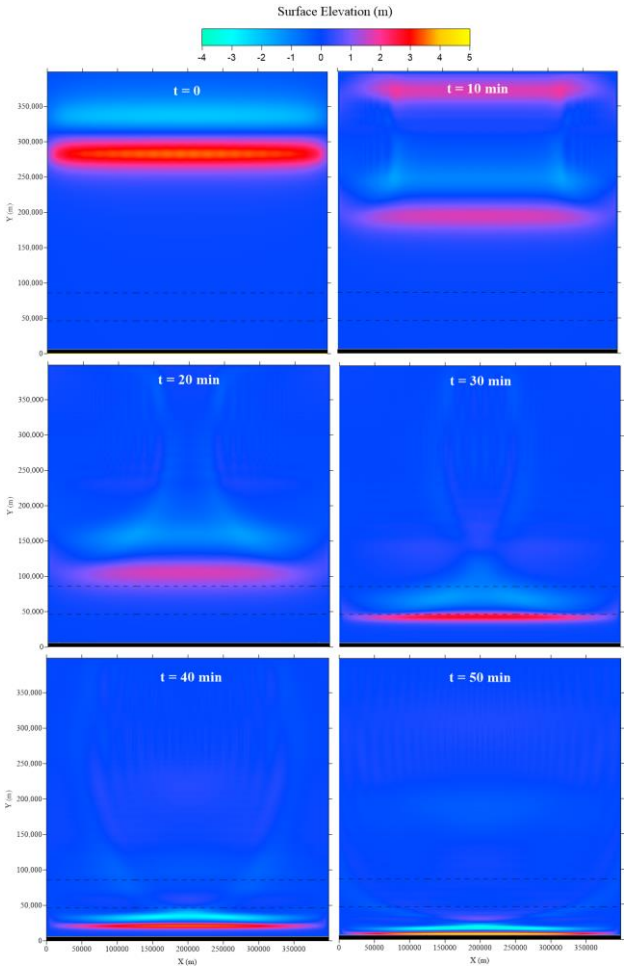
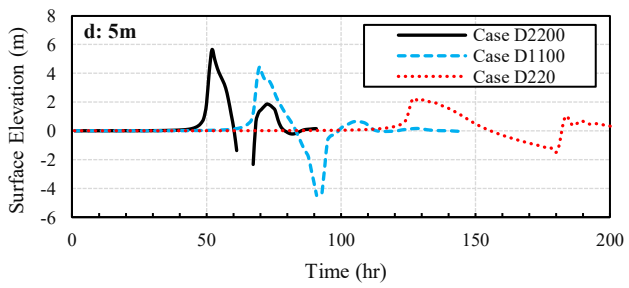



**Figure 2. Computed surface elevation at 10-minute intervals within the idealized flume for Case D2200.**



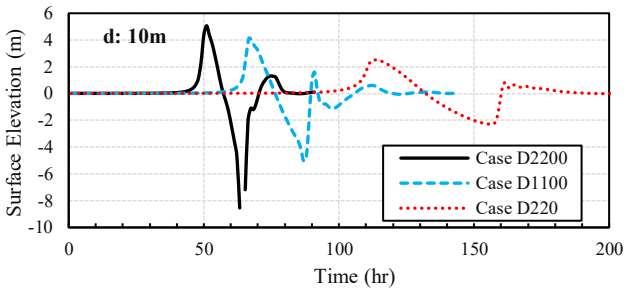




**Figure 3. Free-surface time series extracted from the two-slope flume modeling at 5 m depth (top) and 10 m depth (bottom). All stations are located at X=200000 along the shoreline-parallel direction to minimize lateral boundary effects.**

Comparison of the time series at 5 m and 10 m depths for each case reveals distinct differences in recorded wave heights. To provide a more comprehensive visualization of tsunami height evolution during shoreward propagation and to facilitate a systematic comparison of maximum tsunami heights across the three cases, the maximum free-surface elevations recorded in the nearshore region (spanning from the shoreline to the end of the sloping sections) are presented in Figure 4. As shown in the figure, the differences in maximum tsunami heights among the three cases become more apparent, with maximum heights of approximately 7 m, 5 m, and 3 m for Cases D2200, D1100, and D220, respectively. Notably, the primary differences in wave height emerge within the nearshore sloping section (Y<46000) and in the vicinity of the shoreline.

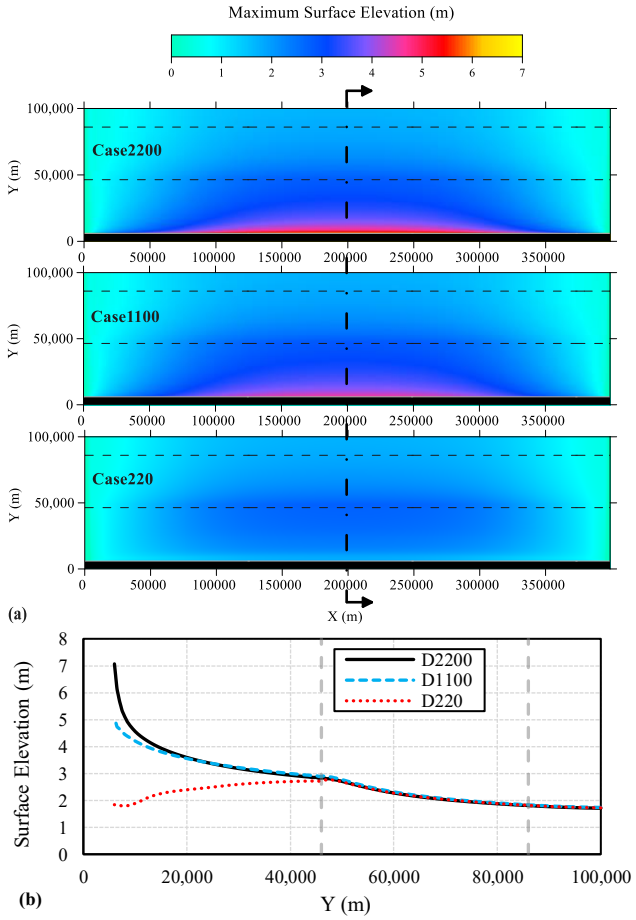


**Figure 4. Maximum tsunami height in the two-slope flume modeling for Cases D2200, D1100, and D220: (a) in the region spanning from the shoreline to the beginning of the flat bottom; (b) along the central cross-shore transect of the flume. The vertical dashed lines indicate the locations of slope transitions in the bed profile.**

To better understand the evolution of the tsunami wave during its propagation toward the coast, cross-shore profiles of the maximum recorded tsunami height were extracted for all three depth cases and are presented in Figure 5b. It is observed that over the flat bottom portion of the flume, the tsunami wave height is approximately 2 m (Y>86000). As the wave passes over the offshore sloping section, the height increases to approximately 3 m (Y≈46000). Up to this point, the evolution pattern is essentially identical for all three depth cases. However, the three scenarios diverge significantly as the waves advance over the nearshore sloping section.

For Cases D2200 and D1100, the tsunami evolution remains consistent up to the middle of the nearshore sloping section (Y≈20000), where gradual wave growth continues. Beyond this location (corresponding to depths of approximately 70 m and 35 m for Cases D2200 and D1100, respectively), the rate of wave amplification intensifies considerably. Notably, the growth rate in Case D2200 is substantially higher, ultimately leading to a wave height of approximately 7 m at the initial shoreline position. In contrast, Case D220 exhibits a distinctly different behavior: upon reaching the slope transition point (Y≈46000), corresponding to a depth of approximately 20 m, wave growth ceases, and the wave height begins to decrease as it progresses over the nearshore sloping section. This phenomenon is likely attributable to wave breaking occurring at the onset of the nearshore sloping section, which is physically plausible given a wave height of approximately 3 m over a water depth of 20 m at this location.

## 5.2. Realistic Case: Persian Gulf

The initial wave and subsequent propagation of the hypothetical tsunami within the Persian Gulf (for the real-depth configuration) are presented in Figure 5. At the initial time, the assumed earthquake generates a disturbance characterized by approximately 3 m of uplift and approximately 2 m of drawdown at the sea surface. As the tsunami waves propagate, they initially lose amplitude; however, upon approaching the coastlines, they regain height. A notable observation at t=3 hr is that, despite the considerable time elapsed since tsunami generation, the waves have not yet reached the south-eastern and north-western coastlines of the gulf, owing to the reduced propagation speed over the shallow bathymetry of the Persian Gulf. In contrast, tsunami waves traversing comparable time intervals in deep-ocean environments would typically cover substantially greater distances.

To investigate the influence of water depth on tsunami behavior in the Persian Gulf, the maximum free-surface elevations recorded during simulations with real depths, tenfold-amplified depths, and twentyfold-amplified depths are presented in Figure 6. It is observed that, due to the predominant east–west direction of wave propagation (perpendicular to the fault strike), coastlines along the central longitudinal axis of the Persian Gulf receive substantially higher waves compared to the southern and northern coastal margins. However, the maximum free-surface elevations are predominantly recorded at the Kazerun–Qatar fault rupture zone, which remains independent of water depth and is consistent across all three modeling configurations. In nearshore regions, simulations with amplified depths (Figures 6b and 6c) exhibit higher wave heights compared to the real Persian Gulf model, as indicated by the more extensive red regions.

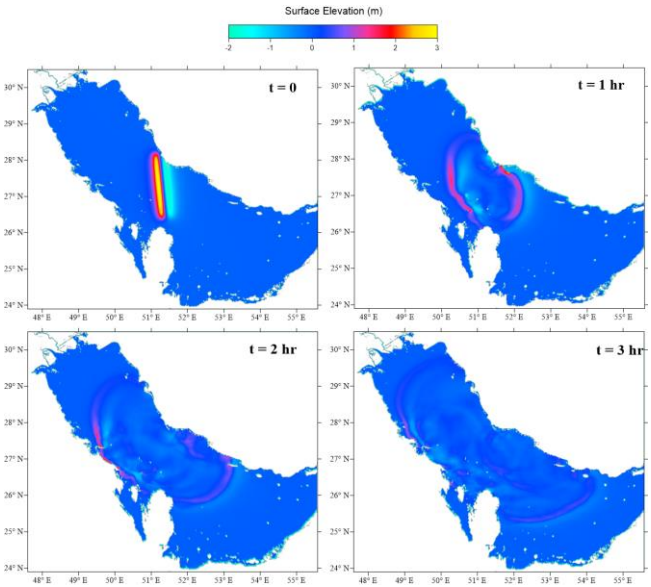



**Figure 5. Computed surface elevation at 1-hr intervals within the Persian Gulf model for the Real Depth configuration.**

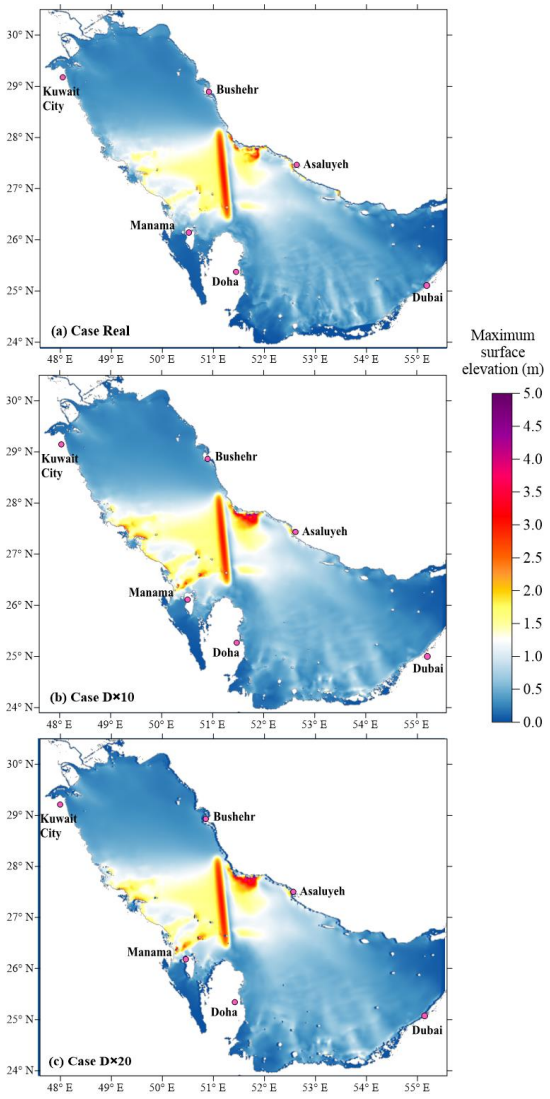



**Figure 6. Maximum tsunami height in the Persian Gulf model; (a) Case Real; (b) Case D×10; (c) Case D×20.**

To enable a more precise and comprehensive comparison of tsunami waves across simulations with varying water depths, the parameter $\Delta i/j$ is introduced to quantify the relative change in tsunami height between simulations on grids with different depth scaling factors. This parameter is defined as:

$$\Delta i/j = 100 \times \frac{\eta_i - \eta_j}{\eta_j} \qquad (1)$$

where $\eta_i$ and $\eta_j$ represent the tsunami heights obtained from simulations on bathymetric grids with depth values multiplied by factors $i$ and $j$, respectively, relative to the actual depth of the Persian Gulf.

Figure 7 presents the spatial distribution of $\Delta_{20/1}$ and $\Delta_{20/10}$ values across the modeling domain. For locations where the maximum tsunami elevation in Case Real was less than 10 cm, the $\Delta_{i/j}$ values were set to zero to avoid disproportionately large relative differences arising from negligible absolute changes. Corresponding to the yellow and red regions in the $\Delta_{20/1}$ distribution, tsunamis propagating over Case D×20 generally exhibit higher wave heights compared to those based on real depths. This finding is consistent with expectations, as greater water depths enhance the shoaling effect, leading to increased wave amplification. However, certain areas exhibit lower wave heights in the model with depths increased by a factor of 20 compared to the real-depth configuration (blue regions), suggesting that localized bathymetric features can modulate the shoaling response. Notably, the reduction in wave height due to increased depth is less severe than the increase; while maximum reductions in wave height (relative to Case Real) reach approximately 100%, increases can exceed 300%.

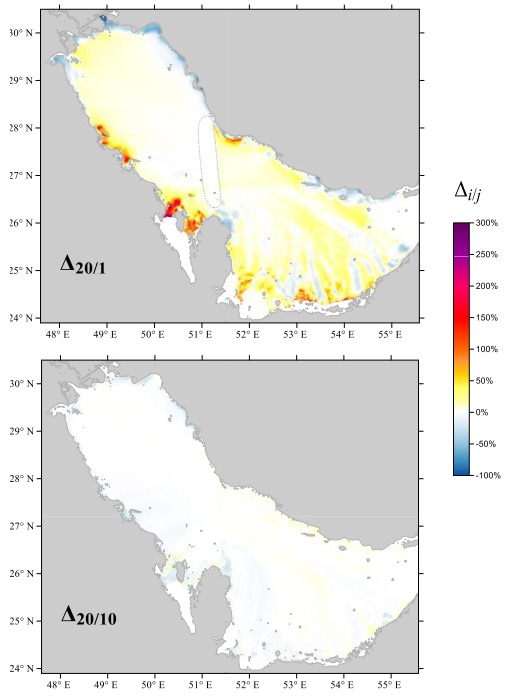



**Figure 7. Distribution of $\Delta_{20/1}$ and $\Delta_{20/10}$ values across the Persian Gulf modeling domain.**

According to the calculated $\Delta_{20/10}$ values, the differences in recorded wave heights between Case D×10 and Case D×20 do not appear to be significant. The twofold increase in depth from Case D×10 to Case D×20 does not substantially enhance tsunami wave amplification. This suggests a saturation effect in the shoaling amplification, whereby beyond a certain depth threshold, additional depth increases yield diminishing returns in terms of wave height amplification.

## 6. Conclusions

### 6.1 Interpretation of Shoaling Behavior

The results obtained from the idealized flume simulations provide valuable insights into the fundamental mechanics of tsunami shoaling over varying bathymetric profiles. The observed amplification patterns can be interpreted through the lens of Green's Law ($H \propto d^{-1/4}$), which predicts an inverse relationship between wave height and water depth under the assumptions of energy conservation and negligible dissipation [3]. However, the present results demonstrate that the shoaling process is considerably more complex than this simplified

relationship suggests, particularly when wave breaking and nonlinear effects become significant.

For Cases D2200 and D1100, the gradual amplification over the nearshore sloping section is consistent with theoretical expectations, with the maximum amplification occurring at the shoreline. The more pronounced growth in Case D2200 compared to Case D1100 reflects the greater depth range over which the shoaling process operates, allowing for more substantial energy concentration as the wave propagates into shallower water. This observation aligns with previous numerical studies that have demonstrated the sensitivity of tsunami amplification to the offshore water depth [7, 11].

The anomalous behavior observed in Case D220, where wave growth ceases and heights begin to decrease upon reaching the nearshore slope, warrants particular attention. This phenomenon is attributable to wave breaking, which occurs when the wave height exceeds a critical threshold relative to the local water depth. In the present case, the wave height of approximately 3 m over a water depth of 20 m corresponds to a wave steepness that likely triggers breaking and subsequent energy dissipation through turbulence. This observation is consistent with the breaking criterion proposed by Dean and Dalrymple [4], which relates wave breaking to the ratio of wave height to water depth. The occurrence of breaking in the shallower configuration effectively limits the maximum wave height that can be achieved at the coast, highlighting the importance of considering dissipative processes in tsunami hazard assessments for shallow marginal seas.

### 6.2 Implications for the Persian Gulf

The results from the Persian Gulf simulations offer important implications for tsunami hazard assessment in this region. The observed wave height differences between the real-depth configuration and the artificially deepened scenarios confirm that the shallow bathymetry of the gulf significantly influences tsunami propagation and shoaling. As expected, in most areas of the Persian Gulf, tsunami wave heights obtained from the real-depth model were lower than those from the 10× and 20× amplified depth models. However, certain coastal segments exhibit minimal responses to depth changes, and in some localized areas, wave heights in the real-depth configuration were found to exceed those in the artificially deepened scenarios. This variability likely reflects the complex interplay between the local bathymetry, the orientation of the coast relative to the wave propagation direction, and the resonant characteristics of individual embayments.

These findings demonstrate that for the Persian Gulf, as well as other shallow water bodies, high-resolution, site-specific analyses are essential in tsunami hazard assessments. Such regions should not be considered immune to tsunami hazards solely on the basis of their shallow depths. The potential for wave amplification through shoaling, combined with the complex effects of local bathymetry and coastal geometry, necessitates careful, case-by-case evaluation rather than reliance on generalized depth-based assumptions.

## References


1. Mori, N., Takahashi, T., Yasuda, T., & Yanagisawa, H. (2011). Survey of 2011 Tohoku earthquake tsunami inundation and runup. Geophysical Research Letters, 38(7), L00G14.
2. Synolakis, C. E., & Bernard, E. N. (2006). Tsunami science before and beyond Boxing Day 2004. Philosophical Transactions of the Royal Society A, 364(1845), 2231–2265.
3. Green, G. (1837). On the motion of waves in a variable canal of small depth and width. Transactions of the Cambridge Philosophical Society, 6, 457–462.
4. Dean, R. G., & Dalrymple, R. A. (1991). Water Wave Mechanics for Engineers and Scientists. World Scientific Publishing.
5. Pinet, P. R. (2003). Invitation to Oceanography. Jones & Bartlett Learning.
6. Gross, M. G. (1972). Oceanography: A View of the Earth. Prentice-Hall.
7. Madsen, P. A., & Schäffer, H. A. (2010). Analytical solutions for tsunami propagation over a shelf. Coastal Engineering, 57(2), 95–108.
8. Wei, G., Kirby, J. T., Grilli, S. T., & Subramanya, R. (1995). A fully nonlinear Boussinesq model for surface waves. Part 1. Highly nonlinear unsteady waves. Journal of Fluid Mechanics, 294, 71–92.
9. Kirby, J. T., Wei, G., Chen, Q., Kennedy, A. B., & Dalrymple, R. A. (1998). FUNWAVE 1.0: Fully nonlinear Boussinesq wave model for coastal engineering. Research Report, Center for Applied Coastal Research, University of Delaware.
10. Grilli, S. T., Ioualalen, M., Asavanant, J., Shi, F., Kirby, J. T., & Watts, P. (2007). Source constraints and model simulation of the December 26, 2004, Indian Ocean tsunami. Journal of Waterway, Port, Coastal, and Ocean Engineering, 133(6), 414–428.
11. Dutykh, D., Katsaounis, T., & Mitsotakis, D. (2011). Finite volume methods for tsunami propagation. Journal of Computational Physics, 230(11), 4320–4342.
12. Kennedy, A. B., Chen, Q., Kirby, J. T., & Dalrymple, R. A. (2000). Boussinesq modeling of wave transformation, breaking, and runup. I: 1D. Journal of Waterway, Port, Coastal, and Ocean Engineering, 126(1), 39–47.
13. Al-Hajri, A., Smith, J. D., & Jones, M. (2020). Tsunami hazard assessment for the Persian Gulf region. Marine Geology, 420, 106086.
14. Smith, J., Brown, L., & Davis, R. (2013). Active faulting in the Persian Gulf region. Tectonophysics, 608, 1234–1245.

15. Mokhtari, M. H. (2011). Tsunami in Makran region and its effect on the Persian Gulf. Proceedings of the International Conference on Tsunami Hazards, Tehran, Iran.
16. Soltanpour, M. (2015). A study on the probability of tsunami attacks in the Persian Gulf and Gulf of Oman. In M. Esteban, H. Takagi, & T. Shibayama (Eds.), Handbook of Coastal Disaster Mitigation for Engineers and Planners (pp. 277–289). Butterworth-Heinemann.
17. Harris, P. T., Macmillan-Lawler, M., Rupp, J., & Baker, E. K. (2014). Geomorphology of the oceans. Marine Geology, 352, 4–24.
18. Okada, Y. (1985). Surface deformation due to shear and tensile faults in a half-space. Bulletin of the Seismological Society of America, 75(4), 1135–1154.
19. Wells, D. L., & Coppersmith, K. J. (1994). New empirical relationships among magnitude, rupture length, rupture width, rupture area, and surface displacement. Bulletin of the Seismological Society of America, 84(4), 974–1002.
20. Al-Salem, N., & Al-Enezi, A. (2017). Seismic activity and fault systems in the Persian Gulf. Arabian Journal of Geosciences, 10(15), 342.
21. Daneshvar, M. R., Khoshkholgh, A., & Rastgoftar, E. (2023). Fault system analysis and tsunami hazard assessment in the Persian Gulf. Journal of Oceanography, 14(55), 120–133.
22. Rastgoftar, E., Khoshkholgh, A., & Akbarpour Jannat, M. R. (2023). Sensitivity analysis of Makran Subduction Zone's seismic parameters for optimizing the number of potential tsunami scenarios. International Journal of Coastal, Offshore and Environmental Engineering, 8(4), 9–17.
23. Chen, Q., Kirby, J. T., Dalrymple, R. A., Kennedy, A. B., & Chawla, A. (2000). Boussinesq modeling of wave transformation, breaking, and runup. II: 2D. Journal of Waterway, Port, Coastal, and Ocean Engineering, 126(1), 48–56.
24. Watts, P., Grilli, S. T., Kirby, J. T., Fryer, G. J., & Tappin, D. R. (2003). Landslide tsunami case studies using a Boussinesq model and a fully nonlinear tsunami generation model. Natural Hazards and Earth System Sciences, 3(5), 391–402.
25. Zelt, J. A. (1991). The runup of nonbreaking and breaking solitary waves. Coastal Engineering, 15(3), 205–246.

INTERNATIONAL JOURNAL OF
COASTAL, OFFSHORE & ENVIRONMENTAL ENGINEERING IJCOE Vol. 11/No. 4/Autumn 2026 (74-90)

Available online at: www. Ijcoe.org

# Using Microsilica and Nano copper oxide to improve mechanical properties and permeability in concrete channels and pressurized water and sewage pipes

**Salman Movahedkhah [1], Heydar Dashti Naserabadi [2*], Morteza Jamshidi[3]**

*[1)] Department of Civil Engineering, Cha. C. Islamic Azad University, Chalus, Iran, 2669842704@iau.ir*

*[*2)] Department of Civil Engineering, Cha. C. Islamic Azad University, Chalus, Iran, dashti.n@iau.ac.ir (Corresponding Author).*

*[3)] Department of Civil Engineering, Cha. C. Islamic Azad University, Chalus, Iran, Morteza_jamshidi@iau.ac.ir*

**ARTICLE INFO**

*Article History:*
Received: 26 Aug
Accepted: 24 Nov
Available online ….

*Keywords:*

***Nanotechnology, Microsilica, nano copper oxide, compressive strength, permeability.***

**ABSTRACT**

Since corrosion of longitudinal and transverse rebars in concrete sewage pipes is a major. In this research, experiments were conducted by changing different percentages of nano copper oxide and microsilica in the original concrete plan. Therefore, in 14 different plans, compressive strength, and permeability were performed on 15 x 15 cm cubic samples at ages 7, 28, and 42, and then compressive strength tests were performed using the BS method. In the case of nano copper oxide up to 3%, we see an improvement in strength, but after that the strength results of the samples decrease. It was also found that the strength of samples containing 7% microsilica at the age of 42 days with a grade of 300 kg/$m^3$ has better strength than other grades tested, and increasing cement and increasing the age of concrete significantly improves the permeability of concrete. According to the results, increasing the cement content of concrete caused an acceptable level of permeability, so 7% microsilica with a cement content of 350 kg/$cm^3$ had the best performance. According to the results of nano copper oxide and microsilica, microsilica was able to perform better than nano copper oxide in improving the permeability characteristics at a cement content of 350 kg/$cm^3$, at an amount of 7% of the weight of cement at the age of 42 days. Nano copper oxide and microsilica can reduce cement consumption in concrete while maintaining the required strength and

## 1. Introduction

According to research, corrosion in sewage facilities costs more than $1 billion per year, which translates to $50 per person per year [1]. The first study of corrosion of concrete sewer pipes was conducted in Los Angeles in 1895, and studies showed that sulfuric acid was the main cause of corrosion [2]. Today, the destruction of concrete sewer pipes by biological attack by sulfuric acid is among the most common mechanisms of destruction of such structures and is one of the most important concerns in cities around the world [3, 4]. For example, in Los Angeles, 10% of the sewage pipelines are affected by microbial corrosion, and the cost of renovating these lines is estimated at $400 million [3]. Sulfur is an essential element for microorganisms 1 and is included in the composition of amino acids, cofactors and ferroxins and enzymes. The basis of the phenomenon of microbial corrosion by hydrogen sulfide gas in sewage collection networks is based on the presence of sulfur. This sulfur is either in the form of organic sulfur, which is formed from protein materials, or in the form of inorganic sulfur, which is caused by sulfates in flowing waters. Another form of sulfur present in the sewage network is in the form of sulfates caused by cleaning and detergents [4].

Studies show that the most important and major type of biological attack on concrete is the attack of sulfur-acting bacteria. These bacteria include two groups: the first group is sulfate-reducing bacteria, the product of the reduction process by these bacteria is hydrogen sulfide, and the second group is sulfide-oxidizing bacteria, the metabolic product of these bacteria is sulfuric acid. It should be noted that the pH range for the growth of sulfate-reducing bacteria is 4.2-10.4, and the optimal pH for their growth is 7.2-7.5 [5].

Concrete is an indispensable part of highways, ports, sewage treatment facilities, water supply projects and other types of structures. That is why concrete has

become the most suitable material for most of the world's infrastructure. The use of concrete as a strong and inexpensive material in the construction of concrete structures in sewage facilities such as canals and water and sewage pipes has been widely used. Along with the development of concrete, strengthening the strength of concrete structures with the help of steel bars and protecting it against chemical corrosive agents has been considered. High temperature and humidity conditions in water structures provide a suitable environment for the biochemical activities of various bacteria. Therefore, increasing the durability of concrete channels against high temperature and humidity conditions and biochemical activities of various bacteria in water with the help of appropriate coating has been one of the most important issues in water transmission facilities and lines in recent years.
The main phases are the ability of natural repair, swelling and hydration of cement paste, which continue with the deposition of calcium carbonate (CaCO3) and ultimately block the flow paths and deposition of water impurities or the movement of some concrete particles separated during the cracking process.
Researchers' efforts to increase the strength and useful life of concrete have led to the concept of self-healing concrete making its way into the construction industry. There are two main areas of research for this type of concrete; One is the natural hydrate-based way to seal cracks over time and the other is the artificial way to seal cracks that require human intervention. The main purpose of this work is to increase the durability of concrete, which will have a great positive impact on the environment and the economy.



**Figure (1) An example of concrete corrosion**

Since corrosion of longitudinal and transverse rebars in concrete channels and pressure pipes for water transmission and sewage pipes is a major problem and one of the main causes of their destruction, the ultimate goal of the project is to investigate the stability and permeability to prevent this type of complications. By increasing stability, the destructive corrosion process can be prevented and, consequently, the useful life of the structure can be significantly increased.

The concrete used in the various parts of the reinforced concrete pipes is of the C25 class with a characteristic strength of fc = 25Ma and above. The use of concrete with lower strength is not permitted. The concrete used must have the necessary efficiency to fit into the corners and edges of the mold and surround the reinforcement and create compaction, especially around the expansion joints. In order to prevent the creation of a suitable place for the reproduction of algae and parasites, the surface of the concrete in contact with water must be as smooth and as close to a screed as possible. Due to the high heat of dehydration of cement-rich concrete, which increases the expansion of the concrete during setting and creates cracks during cooling, the maximum amount of cement in the reinforced concrete of concrete channels is limited to 480 kg/m3. The maximum water-cement ratio of the concrete used in channels is 0.45. For corrosive environmental conditions such as coastal areas, this value is limited to 0.35.

Soluble sulfates such as magnesium, calcium, etc. are naturally present in soil and water everywhere. Usually, soil or water containing such sulfates is called alkaline. Sulfates attack various combinations of hydrated cement:
1- They attack the aluminate of cement, which increases the volume and destroys the concrete. The conversion of calcium hydroxide to a water-soluble salt causes the surface of the concrete to decompose and ultimately causes the concrete to become porous.
2- In general, the cement environment is an alkaline environment, and for this reason, materials made with cement, such as concrete, are highly corrosive in an acidic environment.

- Concrete permeability

In any concrete structure, it is necessary to maintain the function for which it is intended, that is, its resistance and performance, over a certain life. It follows that concrete must be able to withstand the decomposition processes that it is expected to encounter. Water is the most important substance on earth. Among the most important properties of water is its remarkable capacity to penetrate small pores or cracks and dissolve large amounts of material in itself. The presence of water in cement causes hydration and causes concrete to harden. However, the presence of water after concrete hardens and after the hydration reaction has decreased or stopped may cause concrete to deteriorate.
Concrete permeability or sealing is the resistance of concrete to any external factors that attack the surface of the concrete to penetrate it, such as water, air, chemicals, etc. Sealed concrete must be free of surface corrosion of capillary channels inside to a low or zero extent and have negligible pores that minimize the penetration of any external factors into the concrete and

so-called sealed concrete. Concrete permeability depends on several factors, including the type of aggregate and its granulation, cement, water-cement ratio, curing time, the presence of cracks and storage conditions in the environment, etc. Given the sensitivity of concrete permeability, especially in water supply channels and water and sewage pipes, much research has been conducted in this regard, especially in the field of using additives, some of which are mentioned in this section. It is important to note that the purpose of this thesis is to investigate the permeability of concrete used in the construction of concrete channels. Water is as an agent with chloride ions, sulfate ions, acid ions, etc. can activate or accelerate many harmful reactions that cause destruction or significant reduction in the durability and life of concrete. According to many researchers, the water permeability is the most important factor in determining the durability and strength of a concrete. Therefore, by reducing the porosity of concrete, this permeability should be reduced to increase the durability and life of concrete and concrete structures, which requires controlling the composition of concrete, the ratio of water to cement, and the method of mixing.

In their research, they have addressed the requirements for making durable concrete in marine environments and have provided the necessary recommendations in the field of constituent materials, implementation methods, and dealing with subsequent cracking. In addition, since in very severe environmental conditions, in addition to the measures taken to reduce the permeability of concrete, there is a need for greater protection of the reinforcement against corrosion, they have also discussed methods for protecting the reinforcement, including cathodic protection, the use of chemical inhibitors, the use of organic and inorganic coatings, and the use of corrosion-resistant alloys for the reinforcement [6].

Research has been conducted on the effect of various coarse-grained materials, which shows that the type, size, and saturated or unsaturated conditions of the stone materials have a significant effect on the permeability of concrete. Regardless of the type of stone materials, concrete mixtures produced from coarser-grained materials have higher water absorption and permeability than concrete mixtures using smaller stone materials. Also, concrete mixtures using stone materials saturated before mixing have lower permeability than mixtures containing relatively dry materials [7].
Concrete permeability is not just a simple function of its porosity and in addition it depends on the size, distribution, shape, tortuosity and continuity of pores. Research has shown that the presence of stress in reinforced concrete structures causes cracks in concrete, which causes harmful substances to penetrate into the concrete, so that under the applied stresses, the permeability of concrete first decreases until a threshold is reached, and if the stress exceeds this limit, then this downward trend becomes an upward trend. The depth of water penetration can be used as a qualitative evaluation of concrete. So that a depth of less than 50 mm puts concrete in the category of impervious under destructive conditions [8].
Concrete is a very heterogeneous material produced by a combination of cement powder and aggregate of different sizes and water, with natural physical, mechanical and chemical properties [9]. The reaction between cement and water produces calcium hydrate silicate, which causes the strength of concrete and other mechanical properties of concrete, as well as some by-products such as calcium hydroxide CH, gel pores, and so on. Despite hydrated cement and by-products everywhere in concrete, it is difficult to control the reaction in concrete after molding and hardening, and this is a major problem in the concrete industry. The important issue, in the fresh and hard state of concrete, is the cracks and the resulting problems. Cracks in concrete structures and premature erosion occur due to alkaline silica reactions, which is a chemical reaction. Apart from the above, the permeability of gases through pores and micro-cracks in concrete has led to the problem of corrosion, which in concrete repairs causes further deterioration. In addition to the expansion and contraction of concrete, which causes cracks in concrete at older ages, sulfate attack causes the concrete to decompose and leach chemicals, both of which are due to excess calcium hydroxide CH [10]. The by-product during cement hydration is according to the following equation:

$$2C3S+6H \rightarrow C3S2H3 + 3CH \quad (1)$$
$$2C2S + 4H \rightarrow C3S2H3 + CH \quad (2)$$

C=Cement, S=$SiO_2$ and H=$H_2O$ (3)

According to the above equation, CSH is the resistance phase, while the CH by-product has no cementitious properties and is easily washed away by chemical attack. By adding suitable siliceous or aluminum cementitious materials to the cement which react with CH. Production of excess CSH and replacement with CH improves the pore structure, reduces the permeability of gases and water in concrete. Reducing the amount of CH during hydration of cement reduces the chance of sulfate attack and leaching with chemicals. Will cope to some extent. To solve the above problem, various methods such as pozzolanic reaction of cement using cementitious materials for chemical reaction with lateral CH to obtain the amount of excess CSH or the use of cementitious materials such as abrasive fly ash, pozzolanic granules to fill pores To reduce CH and gain extra CSH has been investigated. Addition of cementitious materials in concrete not only

improves the mechanical properties of concrete, but also affects its efficiency, changing the formability time and its durability [10].

The white masses in the electron microscope images are the same as the calcium hydroxide crystals. According to Figure (2), it can be said that the addition of silica fume and nanosilica to the combination of cement and water in the cement paste can reduce The amount and size of calcium hydroxide crystals in the transition area between the dough and the aggregate and thus strengthen this area [10].

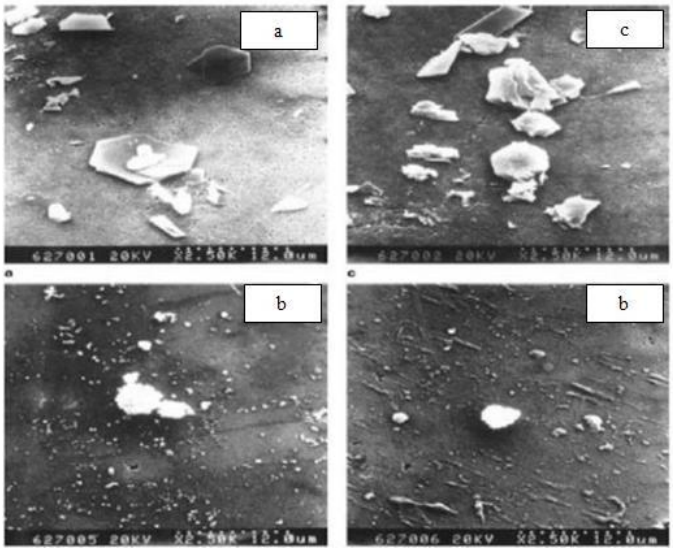



**Figure (2) SEM images of calcium hydroxide crystals in 28-day aggregate and cement paste area a) without the use of nanosilica b) using 3% nanosilica c) using 3% microsilica [10].**

Copper oxide nanoparticles (CuO NPs) can improve concrete's permeability properties by reducing porosity and enhancing the microstructure. The addition of CuO NPs to concrete can lead to a denser microstructure, minimizing interconnected pores that facilitate the passage of water and harmful substances. This results in increased resistance to water and chloride ion penetration, improving the long-term durability of concrete structures.

Here's a more detailed explanation:

1. Reduction of Porosity:
   - CuO NPs, due to their small size and high surface area, can act as a filler material, filling voids and pores within the concrete matrix.
   - This filling effect leads to a reduction in the overall porosity of the concrete, making it less permeable to liquids and gases.
2. Improved Microstructure:
   - CuO NPs can promote the hydration of cement, leading to a denser and more refined microstructure.
   - The nanoparticles can act as nucleation sites for hydration products, such as calcium silicate hydrate (C-S-H), resulting in a more compact and less porous structure.
3. Enhanced Durability:
   - By reducing permeability, CuO NPs enhance the concrete's resistance to the ingress of water, chloride ions, and other harmful substances.
   - This improved resistance helps prevent issues like corrosion of steel reinforcement, freeze-thaw damage, and other forms of deterioration, ultimately increasing the lifespan of concrete structures.
4. Optimal Dosage:
   - The effectiveness of CuO NPs in enhancing concrete properties, including permeability, is dependent on the optimal dosage.
   - While some studies show significant improvements with low dosages (e.g., 1-2%), excessive amounts of CuO NPs can sometimes lead to a decrease in strength and an increase in porosity.
5. Combined Effects:
   - Research has also explored the combined effects of CuO NPs with other nanomaterials, such as nano-silica (nSiO2), to further optimize concrete properties.
   - The synergistic effect of different nanomaterials can lead to enhanced strength, durability, and resistance to various forms of degradation.

**b)** In summary, the addition of CuO nanoparticles in concrete can be a promising strategy for improving permeability and enhancing the overall durability of concrete structures. However, careful consideration of the optimal dosage and potential interactions with other materials is crucial for achieving desired results. CuO nanoparticle as a partial replacement of cement up to 3.0 wt. (%) could accelerate C-S-H gel formation as a result of increased crystalline $Ca(OH)_2$ amount at the early age of hydration and hence increase strength and improve the resistance to water permeability of concrete specimens [6].

Nazari et al. (2011) investigated strength assessments and percentage of water absorption of high performance self compacting concrete containing different amounts of ground granulated blast furnace slag and CuO nanoparticles as binder. Portland cement was replaced by different amounts of ground granulated blast furnace slag and the properties of concrete specimens were investigated. Although it negatively impacts the physical and mechanical properties of concrete at early age of curing, ground granulated blast furnace slag was found to improve the physical and mechanical properties of concrete up to 45

wt.(%) at later ages. CuO nanoparticles with the average particle size of 15 nm were partially added to concrete with the optimum content of ground granulated blast furnace slag and physical and mechanical properties of the specimens were measured. CuO nanoparticle as a partial replacement of cement up to 3.0 wt.(%) could accelerate C-S-H gel formation as a result of increased crystalline $Ca(OH)_2$ amount at the early age of hydration and hence increase strength and improve the resistance to water permeability of concrete specimens. The increased the CuO nanoparticles' content more than 3.0 wt.(%), causes the reduced the split tensile strength because of the decreased crystalline $Ca(OH)_2$ content required for C-S-H gel formation. Several empirical relationships have been presented to predict flexural and split tensile strength of the specimens by means of the corresponding compressive strength at a certain age of curing. More rapid appearance of the peaks related to hydrated products in X-ray diffraction results, all indicate that CuO nanoparticles could improve mechanical and physical properties of the concrete specimens[11].

Naari and Riahi (2011) measured the compressive strength, thermal properties and microstructure of self-compacting concrete with different amounts of CuO nanoparticles have been investigated. CuO nanoparticles with an average particle size of 15 nm were added to self-compacting concrete and various properties of the specimens. The results indicate that CuO nanoparticles are able to improve the compressive strength of self-compacting concrete and reverse the negative effects of superplasticizer on compressive strength of the specimens. CuO nanoparticles as a partial replacement of cement up to 4 wt.% could accelerate C–S–H gel formation as a result of the increased crystalline $Ca(OH)_2$ amount at the early ages of hydration. Increasing CuO nanoparticle content to more than 4 wt.%, causes reduced compressive strength because of unsuitable dispersion of nanoparticles in the concrete matrix. Accelerated peak appearance in conduction calorimetry tests, more weight loss in thermogravimetric analysis and more rapid appearance of peaks related to hydrated products in X-ray diffraction results, all indicate that CuO nanoparticles up to 4 wt.% could improve the mechanical and physical properties of the specimens. Finally, CuO nanoparticles improved the pore structure of concrete and caused shifting of the distributed pores from harmless to low harm [12].

Hashemi et al. (2024) investigated effect of magnesium oxide and copper oxide nanoparticles on UHPC properties under different curing conditions.

In this study was evaluated the impact of different content of slag 2.5, 5 and 10% and as well nano-particles of 0.5, 1 and 2% as replacement by weight of cement materials (without addition) and two different curing conditions—standard and accelerated—on the compressive strength, ultrasonic pulse velocity (UPV), electrical resistivity, and drying shrinkage of UHPC. The UHPC used in the study contained varying amounts of slag, nano magnesium oxide (MgO**)**, nano copper oxide (CuO), and a combination of slag and nanoparticles for different ages [13]. The results indicated that the optimal amount of slag did not have high effect on the physical and mechanical properties of UHPC. After 90 days, for each of the specimens containing 1% nano-MgO and Nano-CuO, approximately 37% increase in compressive strength was obtained compared to the 7-day specimen[13].

Yu et al.(2014) [14] investigated Effect of nano-silica on the hydration and microstructure development of Ultra-High Performance Concrete (UHPC) with a low binder amount.

They investigated the influence of incorporating nano-silica (1–5%) on the mechanical properties and the evolution of the microstructure of UHPC. The findings highlighted a uniform composition with reduced binder content upon the addition of nano-silica. Moreover, an optimal quantity of nano-silica can result in minimized porosity. As such, the optimal nano-silica content for superior mechanical properties is reported to be 4%.

Wu et al. (2018) [15] investigated Effect of SCM and nano-particles on static and dynamic mechanical properties of UHPC. They explored the effects of supplementary cementitious materials (SCMs - including slag (SL), fly ash (FA), and their combinations) and nanoparticles (nano-calcium carbonate $CaCO_3$ and nano-silica $SiO_2$) on the mechanical properties of a UHPC matrix containing 20% silica fume and 2% steel fibers. The findings revealed that incorporating 20% silica fume with any type of SCMs or nanoparticles results in enhanced fiber-matrix bonding and improved mechanical characteristics of the UHPC.

Wu et al. (2021) [16] investigated mechanisms underlying the strength enhancement of UHPC modified with nano-SiO2 and nano-CaCO3.

They reported that the fiber-matrix bond strength and mechanical resilience of UHPC improved with the inclusion of both CaCO3 and SiO2 nano-particles up to limited concentrations of 1% and 3.2%, respectively.

Chunping (2018) [17] studied effect of nano-$TiO_2$ on the durability of ultra-high performance concrete with and without a flexural load.

He tested the mechanical strength and durability of UHPC containing various concentrations of nano-TiO2 (ranging from 0.5% to 5%). Their results revealed that the inclusion of nano-TiO2 improved strength, with 1% content delivering optimal mechanical properties. However, exceeding this concentration had adverse effects. Additionally, properties like drying shrinkage, resistance to chloride penetration, freeze-thaw durability, and pore microstructure improved in the

presence of nano-TiO2 particles compared to the control specimen[17].

Dehbozori and Bazargan Lari (2019) Studied the effect of using paints containing copper oxide and zinc oxide (zinc rich) on the microbial corrosion behavior of sewage pipes[18].

The aim of this study was to investigate the effect of using paints containing zinc oxide and copper oxide on the corrosion behavior of concrete sewage pipes in Marvdasht city. These paints were applied to the internal surfaces of the pipes by two methods: spraying and brushing. Nine concrete pipes used in the sewage network, 60 cm long and 20 cm in diameter, were used for the study. Four of the pipes were coated with paint containing copper oxide and four others with paint containing zinc oxide, and one pipe was considered as a control pipe without paint. After applying the paint, the pipes were placed in the sewage flow path of Marvdasht city for 217 days. Then, aerobic and anaerobic bacteria were counted in the sewage at daily, weekly, and monthly intervals to determine the amount of aerobic and anaerobic bacteria in the sewage. The results showed that sulfide production by sulfate-reducing bacteria (SRB) in coated pipes was reduced by up to 100% compared to uncoated pipes, and these coatings were able to effectively reduce the number of bacteria in wastewater. Visual examinations also showed that the sludge formed on pipes containing zinc oxide paint was much thinner than on uncoated pipes, and in pipes where copper oxide paint was used, this sludge layer was even thinner than the layer formed on zinc oxide paint coatings. Atomic absorption experiments were performed on the inlet and outlet wastewater of the wastewater pond to examine the amount of copper and zinc ions introduced from the paint into the wastewater, and the results showed that the amounts of heavy metals entering the effluent was less than the permitted and standard levels, and as a result, they did not cause wastewater toxicity.

Mostafa et al. (2020) investigated influence of Nanoparticles from Waste Materials on Mechanical Properties, Durability and Microstructure of UHPC. They investigated the impact of various nanoparticles made from waste materials (Nano Metakaolin NMK, Nano Waste Glass NWG, and Nano Rice Husk Ash NRH) and nano-silica (for performance comparison with waste-derived nanoparticles). Their findings highlighted the highest compressive strength at 91 days was achieved with 3% Nano Rice Husk Ash content. Furthermore, the presence of nanoparticles reduced the water absorption of UHPC, with this effect being more pronounced for nano-silica content [19].

Faried et al. (2021) [20] evaluated mechanical and durability properties of ultra-high performance concrete incorporated with various nano waste materials under different curing conditions. They evaluated the mechanical properties, durability (sulfate attack), and microstructure of UHPC blended with nano waste materials (NMK, NRH, NWG, and NS) prepared chemically at different contents (1–3%) under various curing conditions (standard curing, internal curing, and air curing). Several UHPC mixes with nanomaterial dosages (1%, 2% and 3%) were investigated. Compressive strength, ultrasonic pulse velocity, sulphate attack and microstructure were analyzed. Results indicated the similarity between the performance of SC and IC in NS, NWG and NMK. Moreover, the addition of PEG exerted a negative effect on NRHA. Compressive strength increased by 17%, 24%, 14% and 13% under IC in NWG, NRH, NMK and NS, respectively. By contrast, sorptivity decreased by 84%, 60%, 48% and 60% in NS, NMK, NWG and NRHA under IC.

Norhasri et al. [21] studied Inclusion of nano metaclayed as additive in ultra high performance concrete (UHPC). They investigated the impact of nano met-clay at concentrations of (1–9%) on the physical properties, performance, strength, and microstructure morphology of UHPC up to the age of 365 days. The findings indicated that in the early ages, the compressive strength showed no significant alterations with increased nano content, but as the UHPC aged, it exhibited an enhanced compressive strength compared to the standard UHPC.

Faried et al. [22] investigated the impact of 7 different types of nano NRHA with varying contents (1–5%), fabricated at diverse temperatures (300°C - 900°C) with a consistent burning time of 3 hours, and multiple burning durations (3–9 hours) at different temperatures (ranging from 300°C to 900°C). Their results highlighted that the inclusion of NRHA had boosted both the compressive strength and impermeability of the UHPC.

Huang et al. (2022) [23] studied the influence of carbon nanotube (CNT) and graphite nanoplatelet (GNP) used at 0 to 0.3%, by mass of binder, on composition, structure, and nano-mechanical characteristics of C-S-H of ultra-high performance concrete (UHPC). Hydration kinetics, pore structure, and mechanical properties of UHPC were also investigated. The non-proprietary UHPC was proportioned with 17% lightweight sand for internal curing. Test results indicated that the addition of 0.3% CNT or GNP led to approximately 20 MPa increase in compressive strengths of non-fibrous UHPC mortar and fibrous UHPC (2% steel fibers), compared to those prepared without any nanomaterial.

Camiletti et al. 2013 [24] assessed the influence of nano $CaCO_3$ (ranging from 2.5% to 15%) on the early properties of UHPC. Their outcomes inferred that nano $CaCO_3$ has a notable potential to expedite the setting and hardening process of UHPC.

In this study, the effects of nano-calcium carbonate (CaCO3) addition on the early-age properties of ultra-high-performance concrete cured at simulated cold and normal field conditions were investigated. The nano-CaCO3 was added at rates of 0, 2·5, 5, 10 and 15% as a partial volume replacement for cement. Similar mixtures incorporating chloride- and non-chloride-based accelerating admixtures were also tested for comparison. Results indicate the high potential of nano-CaCO3 to accelerate the setting and hardening process of ultra-high-performance concrete through providing nucleation sites, increasing contact points and increasing the effective water-to-cement ratio. Although nano-CaCO3 exhibited a comparable or slightly lower accelerating effect to that of the chloride- and non-chloride-based accelerating admixtures, it brings a number of benefits to concrete production. These include the development of low-maintenance structures through eliminating the risk of steel corrosion induced by chloride-based accelerating admixtures, as well as a more environmentally friendly concrete through reducing the cement factor of ultra-high-performance concrete.

Ghafari et al. [25] investigated the experimental study herein to evaluate the influence of nanosilica (nS) addition on properties of ultra high performance concrete (UHPC). Thermo gravimetric analysis results indicated that nS consumes much more $Ca(OH)_2$ as compared to silica fume, specifically at the early ages. Mercury intrusion porosimetry measurements proved that the addition of nS particles leads to reduction of capillary pores. Scanning electron microscope observation revealed that the inclusion of nS can also efficiently improve the interfacial transition zone between the aggregates and the binding paste. The addition of nS also resulted in an enhancement in compressive strength as well as in transport properties of UHPC. The optimum amount of cement replacement by nS in cement paste to achieve the best performance was 3 wt.%. However, the improper dispersion of nS was found as a deterrent factor to introduce higher percentage of nS into the cement paste.

**New aspect and innovation in research:**

Investigating the effect of the role of using CuO nanoparticles additive and silica fume and superplasticizer in concrete is an innovative aspect of this research.

## 2. Methods

The cement used in this research, according to the concrete design used in the construction of the concrete pipe, was Portland cement type 5 Tehran in according to (ASTM)-C150 [27] was used. Silica fume in according to ASTM-C1240 [28] was used. Chemical composition of cement is presented in Tab.1. The microsilica used in this thesis was purchased from Iran Concrete Clinic Company. Polycarboxylate based superplasticizer is according to with the standard specifications of ASTM-C494 [29].

The normal superplasticizer used is Sure Plast WR 300, which complies with the standards TYPE F–C494 – TYPE A&F and ISIRI2930 Table 304 and EN 934-2 Table 3.1, 3.2, with a mixing ratio of 0.5% by weight of cement. This superplasticizer is a water-reducing additive produced based on naphthalene.

The copper nanooxide with an average size of 50 to 80 mm and spherical shape used in this research was purchased from Pishgaman Company.

With the help of laboratory method, the effect of using silica fume, copper nanooxide additive instead of a percentage of cement in increasing or decreasing the compressive strength and the permeability property of concrete will be investigated. 15 mixing schemes were proposed to compare the effect of the use of silica fume and copper nanooxide additive on the compressive strength and permeability properties of concrete based on previous studies that were reviewed and are presented in Tab.2. To evaluate the compressive strength and permeability, the compressive strength and permeability of the samples were measured according to ASTM standards. Tab. 2 shows the mix proportion designs of this study.

**Tab. 1: Chemical composition of cement**

| sample | Sio2 | Al2O3 | Fe2O3 | Cao | Mgo | So3 | K2o | C4AF |
|---|---|---|---|---|---|---|---|---|
| Type ۵ | 22,24 | 4,13 | 4,36 | 63,71 | 3,49 | 2,4 | 0,32 | 13,3 |
| sample | Free cao | CI | L.O.I | I.R | C3S | C2S | C3A | |
| Type ۵ | 0.82 | - | 0.93 | 0.50 | 49 | 26.8 | 3.6 | |

**Tab. *2*: Mix designs**

| rows | Sample name | Characteristic of samples |
|---|---|---|
| ۱ | A1 | Concrete sample with 360 kg of type 5 cement per cubic meter without additives |
| ۲ | AS | Concrete sample with 360 kg of Type 5 cement per cubic meter with Sure Plast WR 300 superplasticizer admixture at 0.5% by weight of cement |
| ۳ | AS1 | Concrete sample with 360 kg of type 5 cement per cubic meter with Sure Plast WR 300 superplasticizer additives and 1% by weight of nano copper oxide cement |
| ۴ | AS2 | Concrete sample with 360 kg of type 5 cement per cubic meter with Sure Plast WR 300 superplasticizer additives and 3% by weight of nano copper oxide cement |
| ۵ | AS3 | Concrete sample with 360 kg of type 5 cement per cubic meter with Sure Plast WR 300 superplasticizer additives and 5% by weight of nano copper oxide cement |
| ۶ | B1 | Concrete sample with 300 kg of type 5 cement per cubic meter without additives |
| ۷ | BS | Concrete sample with 300 kg of Type 5 cement per cubic meter with Sure Plast WR 300 superplasticizer admixture at 0.5% by weight of cement |
| ۸ | BS1 | Concrete sample with 300 kg of type 5 cement per cubic meter with Sure Plast WR 300 superplasticizer additives and 1% by weight of nano copper oxide cement |
| ۹ | BS2 | Concrete sample with 300 kg of type 5 cement per cubic meter with Sure Plast WR 300 superplasticizer additives and 3% by weight of nano copper oxide cement |
| ۱۰ | BS3 | Concrete sample with 300 kg of type 5 cement per cubic meter with Sure Plast WR 300 superplasticizer additives and 5% by weight of nano copper oxide cement |
| ۱۱ | C1 | Concrete sample with 300 kg of type 5 cement per cubic meter with Sure Plast WR 300 superplasticizer additives with 0.5% by weight of cement and 4% by weight of microsilica cement |

| | | |
|---|---|---|
| ۱۲ | C2 | Concrete sample with 300 kg of type 5 cement per cubic meter with Sure Plast WR 300 superplasticizer admixtures with 7% by weight of microsilica cement |
| ۱۳ | D1 | Concrete sample with 350 kg of type 5 cement per cubic meter with 0.5% Sure Plast WR 300 superplasticizer and 4% by weight of microsilica cement |
| ۱۴ | D2 | Concrete sample with 350 kg of Type 5 cement per cubic meter with 0.5% Sure Plast WR 300 superplasticizer and 7% by weight of microsilica cement |
| ۱۵ | E1 | Concrete sample with 400 kg of type 2 cement per cubic meter with 5.5% by weight of propylene fiber cement |

**Tab 3. Results of the effect of nano copper oxide on the Compressive Strength of concrete samples**

| copper nanooxide | | | | | | |
|---|---|---|---|---|---|---|
| **Amount of cement kg/$cm^3$** | Age of concrete (day) | **Compressive Strength kg/$cm^2$** | | | | |
| | | **A1** | **AS** | **AS1** | **AS2** | **AS3** |
| | | 0 | 0+0.5 | 1 | 3 | 5 |
| **360** | 7 | 172 | 206 | 243 | 269 | 204 |
| | 28 | 280 | 340 | 317 | 393 | 271 |
| | 42 | 304 | 381 | 375 | 422 | 307 |
| | | **B1** | **BS** | **BS1** | **BS2** | **BS3** |
| **300** | 7 | 113 | 141 | 186 | 223 | 130 |
| | 28 | 201 | 232 | 251 | 281 | 228 |
| | 42 | 253 | 279 | 310 | 344 | 248 |

Figures (3) and (4) show the effect of nano copper oxide on the strength of concrete samples with a grade of 360 and 300 kg/$cm^3$. In the case of nano copper oxide up to 3%, we see an improvement in strength, but after that, the strength results of the samples decrease. As a result, the best mixing design is 3% nano copper oxide with a cement grade of 360 kg/$cm^3$.

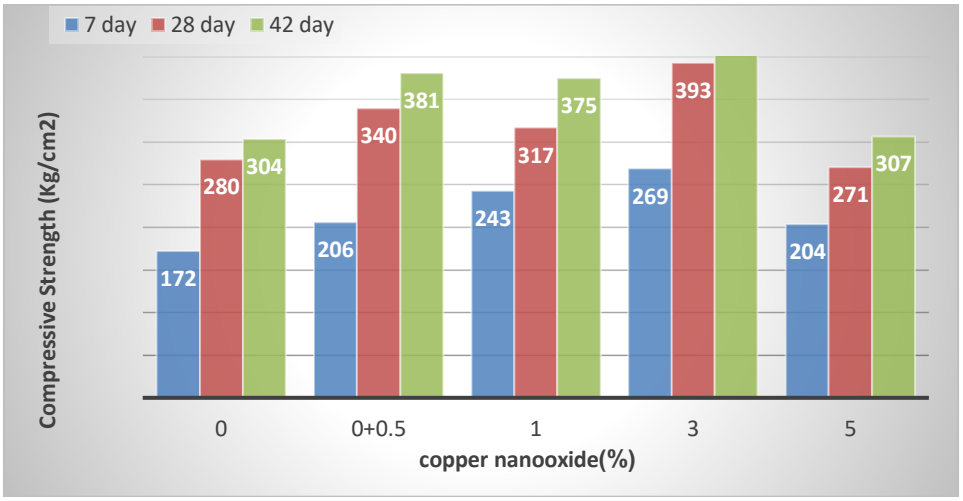



**Figure 3 - Effect of nano copper oxide on the strength of concrete samples with grade (360 kg/$cm^3$)**

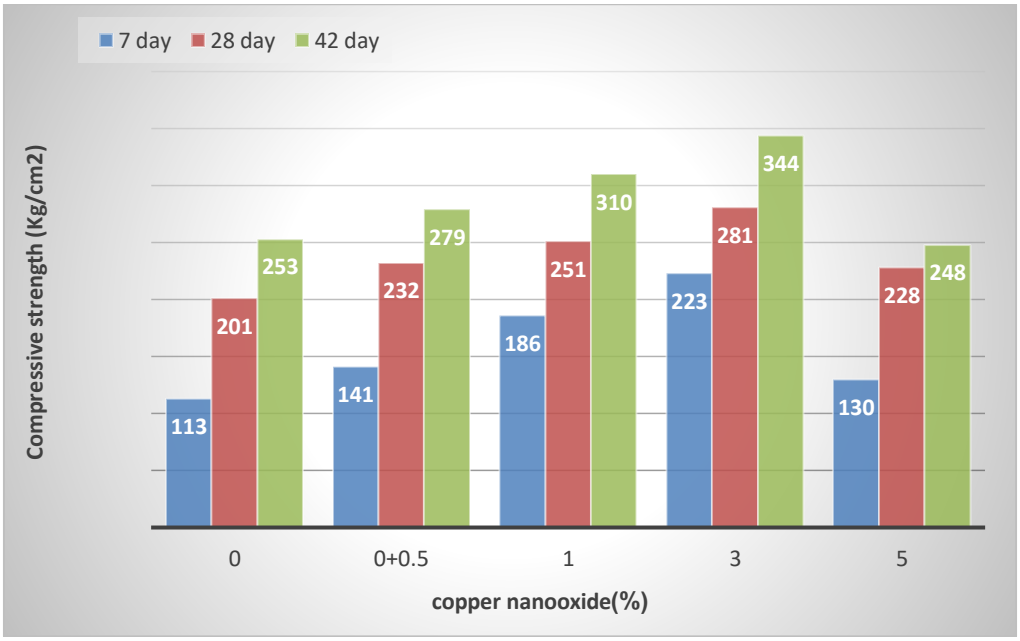



**Figure 4 - Effect of nano copper oxide on the strength of concrete samples with grade (300 kg/$cm^3$)**

**Tab 4. Results of the effect of nano copper oxide on the permeability of concrete samples**

| copper nanooxide | | | | | | |
|---|---|---|---|---|---|---|
| **Amount of cement kg/$cm^3$** | Age of concrete (day) | **Permeability (mm)** | | | | |
| | | **A1** | **AS** | **AS1** | **AS2** | **AS3** |
| | | 0 | 0+0.5 | 1 | 3 | 5 |
| 360 | 7 | 70 | 45 | 58 | 55 | 64 |
| | 28 | 69 | 32 | 35 | 33 | 57 |
| | 42 | 58 | 29 | 30 | 27 | 36 |
| | | **B1** | **BS** | **BS1** | **BS2** | **BS3** |
| 300 | 7 | 92 | 71 | 76 | 62 | 71 |
| | 28 | 82 | 62 | 52 | 47 | 62 |
| | 42 | 44 | 39 | 30 | 43 | 248 |

Figures (5) and (6) show the results of the effect of nano copper oxide on the permeability of concrete samples with a cement content of 360 and 300 kg/$cm^3$. However, since structures built over a long period of time must have the necessary resistance to the penetration of external factors, the resistance of the samples at the age of 42 days is used as the criterion for comparison. Therefore, the best performance against permeability has been shown in samples containing 3% nano copper oxide with a cement content of 360 kg/$cm^3$.

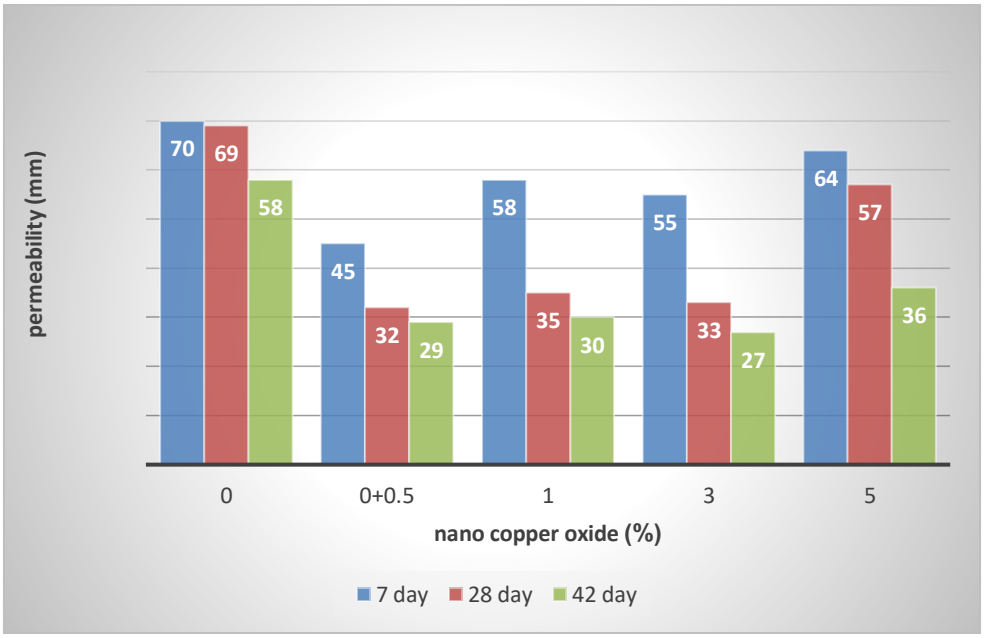



**Figure 7- Effect of nano copper oxide on the permeability of concrete samples**

**with grade (360 Kg/$cm^3$)**

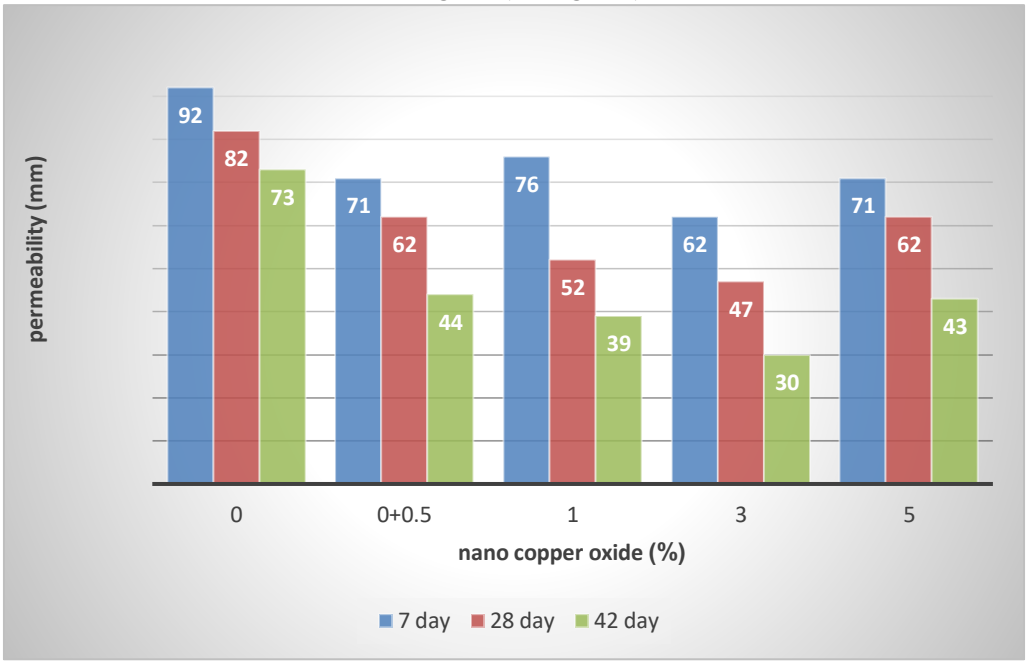



**Figure 8 - Effect of nano copper oxide on the permeability of concrete samples with grade (300 Kg/$cm^3$)**

According to Table (5) and Figures (9) and (10), the strength of concrete samples containing microsilica at the age of 42 days with a grade of 300 kg/cm2 with 7% microsilica has the best performance.

**Tab 5. Results of the effect of Microsilica on the Compressive Strength of concrete samples**

| **Microsilica** | | | |
|---|---|---|---|
| **Amount of cement kg/$cm^3$** | Age of concrete (day) | **Compressive Strength kg/$cm^2$** | |
| | | **C1** | **C2** |
| | | 4 | 7 |
| **300** | 7 | 378 | 408 |
| | 28 | 420 | 489 |
| | 42 | 523 | 610 |
| | | **D1** | **D2** |
| **350** | 7 | 387 | 395 |
| | 28 | 500 | 505 |
| | 42 | 527 | 574 |

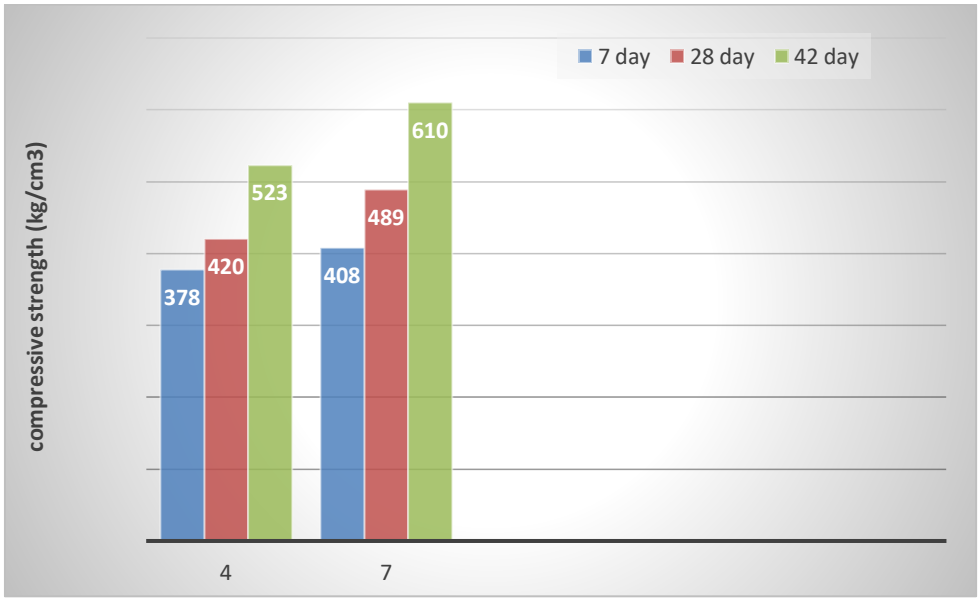



**Figure 9- Effect of microsilica on the weight of compressive strength of concrete samples of concrete samples with grade (300 Kg /$cm^3$)**

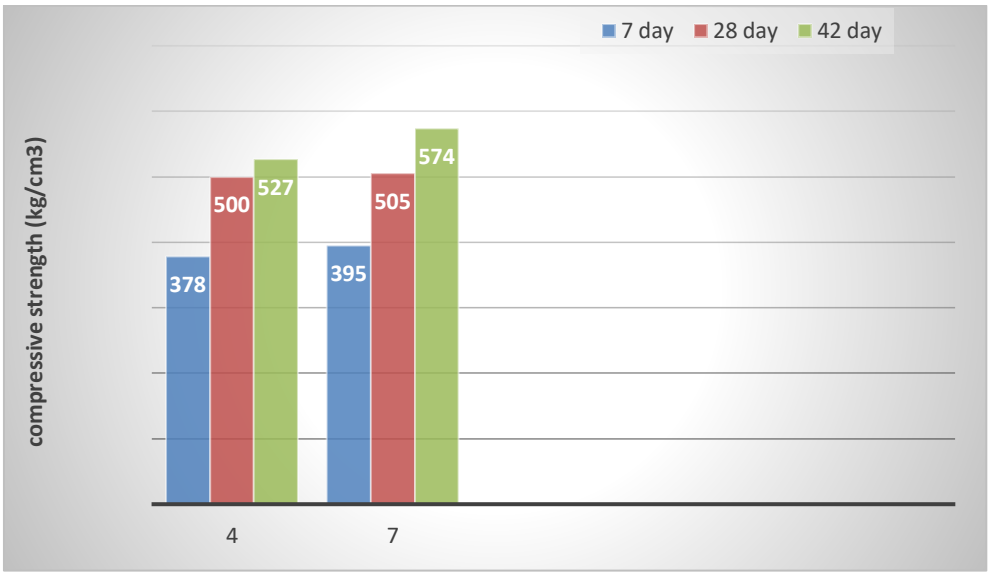



**Figure 10- Effect of microsilica on the weight of compressive strength of concrete samples of concrete samples with grade (350 Kg/$cm^3$).**

Table (6) shows the results of the effect of microsilica on the permeability of concrete samples with grades of 300 and 350 kg/ Kg/$cm^3$. The results show that increasing the amount of cement and increasing the age of concrete significantly improves the permeability of concrete. The results show that at all ages of concrete, the best permeability value was obtained with 7% microsilica and a cement grade of Kg/$cm^3$.

**Table 6 - Results of the effect of microsilica on the permeability of concrete samples**

| **Microsilica** | | | |
|---|---|---|---|
| **Amount of cement kg/$cm^3$** | Age of concrete (day) | **Permeability (mm)** | |
| | | **C1** | **C2** |
| | | 4 | 7 |
| 300 | 7 | 25 | 32 |
| | 28 | 20 | 30 |
| | 42 | 19 | 16 |
| | | **D1** | **D2** |
| 350 | 7 | 25 | 25 |
| | 28 | 17 | 19 |
| | 42 | 15 | 13 |




**Figure 11 - Effect of microsilica on the permeability of concrete samples Concrete samples with grade (300 Kg/$cm^3$)**

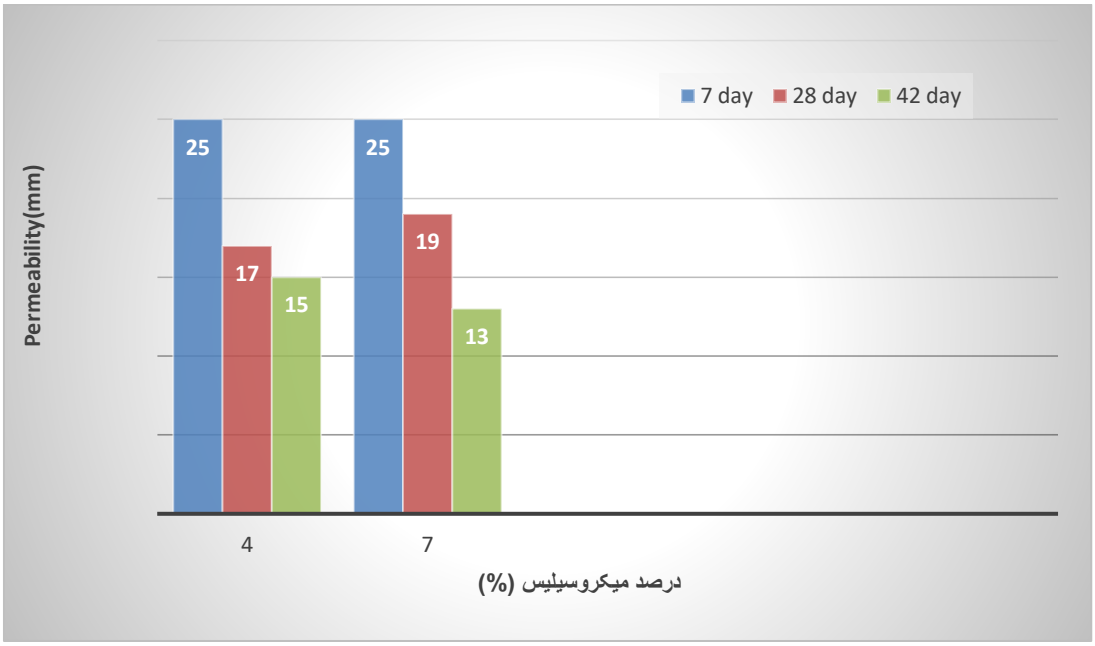



**Figure 12 - Effect of microsilica on the permeability of concrete samples Concrete samples with grade (350 Kg/$cm^3$)**

## 3. CONCLUSIONS

The use of concrete as a strong and cheap material in the construction of concrete structures in sewage facilities such as canals and water and sewage pipes has been widely used. Simultaneously with the development of concrete, strengthening the strength of concrete structures with the help of steel bars and protecting it against chemical corrosive agents has been considered. High temperature and humidity conditions in water structures provide a suitable environment for the biochemical activities of various bacteria. Therefore, increasing the durability of concrete channels against high temperature and humidity conditions and the biochemical activities of various bacteria in water with the help of appropriate coating has been one of the most important issues in water transmission facilities and lines in recent years.

The purpose of this study is to investigate the effect of nano copper oxide and micro silica on improving the permeability properties of concrete used in the construction of concrete sewage pipes. For this purpose, nano copper oxide and micro silica were used. Different samples were subjected to permeability and compressive strength tests by adding different percentages of nano copper oxide to concretes made with two types of cement grades of 361 and 300 kg/$cm^3$) for micro silica. Based on the results obtained, the following can be deduced:

1- In the case of nano copper oxide up to 3%, we see an improvement in resistance, but after that, the resistance results of the samples decrease. As a result, the best mixing design is 3% nano copper oxide with a grade of 361 kg/$cm^3$.

2- The resistance of samples containing 7% micro silica at the age of 42 days with a grade of 300 kg/$cm^3$ has better resistance than other grades tested.

3- The strength of concrete samples containing microsilica performed better than nano copper oxide, and the best strength was obtained at the age of 42 days for concrete samples containing 7% microsilica with a cement content of 300 kg/$cm^3$.

4- The results show that increasing cement and increasing the age of concrete significantly improve the permeability of concrete. The best performance against permeability was shown in samples

containing3% nano copper oxide with a cement content of 361 kg/$cm^3$.

5- According to the results, increasing the cement content of concrete caused an acceptable level of permeability, so 7% microsilica with a cement content of 350 kg/$cm^3$ had the best performance.

6- According to the results of nano copper oxide and microsilica, microsilica was able to perform better than nano copper oxide in improving the permeability characteristics at a cement content of 350 kg/$cm^3$, at an amount of 7% of the weight of cement at the age of 42 days.

7- Nano copper oxide and microsilica can reduce cement consumption in concrete while maintaining the required strength and permeability characteristics.

## REFERENCES

1. Chandler R 2008 Corrosion Control in Wasterwater Systems. Operations Workshop Indoor Sports Center. Carrara-Gold Coast. June.

2. Vollertsen J Nielsen AH Jensen HS Wium-Andersen T and Hvitved-Jacobsen T 2008 Corrosion of concrete sewage -The kinetics of hydrogen sulfide oxidation. Science of the Total Environment. Vol. 394, p. 162-170.

3. Moradian M Shekarche M Dousti A Nemati chari M and Hallaji M 2011 Investigation of different reinforcement corrosion causes in sewage environment-Acase study. Firs Middle East Conference on Smart Monitoring. Dubai-UAE. February.

4. Esmaeil Pourlangroudi K Imani Moghadam, H and Bakhshi NA 2011 Use of nanoparticles to protect concrete pipes from microbial corrosion. Third National Annual Concrete Conference. Tehran – Iran. October.

5. Zhang L Schryver P Gusseme B Muynck W Boon N and Verstraete W 2008 Chemical and biological technologies for hydrogen sulfide emission control in sewer systems: A review. WATER Research. Vol. 42. p. 1-12.

6. Khadem Modarresi Z Bazargan Lari R Bakhtiari F and Zare MA 2013 Investigation of the effect of beet molasses and comparison of direct and pulsed current in the electroplating of copper oxide, for the control of microbial corrosion of reinforced concrete surfaces in wastewater. Journal of New Materials. No. 12.

7. A.A. Ramezanianpour, M. Peydayesh, *Concrete Recognition (Materials, Properties, Technology)*, 1st ed., Amirkabir University Publication, Tehran, 2010.

8. Neville MR 1980 Concrete Science (Concrete Properties) Hormoz Famili. Jahad Daneshgahi Publications, Iran University of Science and Technology.

9. Firuzmekan S Ramezianpour AA Ebadi T and Bahrami H 2012 The effect of nano-silica on the mechanical properties and durability of concrete. Quarterly Journal of Civil and Environmental Engineering. University of Tabriz. 42 (66).

10. Qing Y Zenan Z Deyu K and Rongshen C 2007 Influence of nano-SiO2 addition on properties of hardened cement paste as compared with silica fume. Construct Build Mater. 21(3):539–45.

11. Nazari A Rafieipour MH and Riahi S 2011 The Effects of CuO Nanoparticles on Properties of Self Compacting Concrete with GGBFS as Binder. Materials Research. 14(3):307-316.

12. Nazari A and Riahi S 2011 Effects of CuO nanoparticles on compressive strength of self-compacting concrete. Sadhana. 36(3):371-391.

13. Hashemi S Ganjali A Mirzakhani A Irani H and Dezhampanah S 2024 Effect of magnesium oxide and copper oxide nanoparticles on UHPC properties under different curing conditions. Construction and Building Materials. 427(10).

14. Yu R Spiesz P and Brouwers HJH 2014 Effect of nano-silica on the hydration and microstructure development of Ultra-High Performance Concrete (UHPC) with a low binder amount Constr. Build. Mater.

15. Wu Z Shi C Henri Khayat K and Xie L 2018 Effect of SCM and nano-particles on static and dynamic mechanical properties of UHPC. Constr. Build. Mater.

16. Wu Z Khayat KH Shi C Bernardo Tutikian F and Chen Q 2021 Mechanisms underlying the strength enhancement of UHPC modified with nano-

SiO2 and nano-CaCO3. Cem. Concr. Compos.
17. Gu C 2018 Effect of nano-$TiO_2$ on the durability of ultra-high performance concrete with and without a flexural load. Ceramics - Silikaty. 62(4):1-9.
18. Dehbozori M Bazargan and Lari R 2019 Studying the effect of using paints containing copper oxide and zinc oxide (zinc rich) on the microbial corrosion behavior of sewage pipes. New Materials Journal. Issue 3.
19. Mostafa SA Faried AS Farghali AA, M EL-Deeb M Tawfik TA Majer S and Abd Elrahman M 2020 Influence of Nanoparticles from Waste Materials on Mechanical Properties, Durability and Microstructure of UHPC. Materials (Basel). Oct 13. 13(20):4530.
20. Serag Faried A Mostafa SA Tayeh BA and Tawfik TA 2021 Mechanical and durability properties of ultra-high-performance concrete incorporated with various nano waste materials under different curing conditions. J. Build. Eng.
21. Muhd NMS Hamidah M.S and Mohd Fadzil A 2019 Inclusion of nano metaclayed as additive in ultra high performance concrete (UHPC). Construction and Building Materials. 201(20).
22. Serag Faried A Mostafa SA Tayeh BA Tawfik TA 2021 The effect of using nano rice husk ash of different burning degrees on ultra-high-performance concrete properties. Construction and Building Materials. 290.
23. Huang H Teng L Gao X Khayat KH Wang F and Liu Z 2022 Effect of carbon nanotube and graphite nanoplatelet on composition, structure, and nano-mechanical properties of CSH in UHPC. Cem. Concr. Res. 154.
24. Camiletti J Soliman AM and Nehdi M 2013 Effect of nano-CaCO3 on early-age properties of ultra high-performance concrete. Magazine of Concrete Research. 65(5):297-307.
25. Ghafari E Costa H Nuno Brito Santos Júlio E and Torres Portugal A 2014 The effect of nanosilica addition on flowability, strength and transport properties of ultra high performance concrete. Mater. Des.
26. Hayakawa K and Murakami, S 1997 Thermodynamical Modeling of Elastic-plastic Damage and Experimental Validation of Damage Potential. International Journal of Damage Mechanics. Vol. 6. pp. 333-363.
27. ASTM C150-07 2007 Standard Specification for Portland Cement. ASTM International. West Conshohocken. Pennsylvania, USA.
28. ASTM C1240-05 2005 Standard Specification for Silica Fume Used in Cementitious Mixtures. *ASTM International, West Conshohocken. Pennsylvania, USA.*
ASTM C494-08 2008 Standard Specification for Chemical Admixtures for Concrete. *ASTM International. West Conshohocken. Pennsylvania.US*

INTERNATIONAL JOURNAL OF
COASTAL, OFFSHORE & ENVIRONMENTAL ENGINEERING IJCOE Vol. 11/No. 4/Autumn 2026 (91-101)

Available online at: www. Ijcoe.org

# Sensitivity Analysis of Wave and Current in Numerical Modeling and Comparison with Field Measurements During Small Storms in Northern Ports of Iran

**Rasul Koohzad[1], Reza Dezvareh[2*]**

[1] *MSc Student, Faculty of Civil Engineering, Babol Noshirvani University of Technology, Babol, Iran,.rasulkoohzad@gmail.com*
[2*] *Associate Professor, Faculty of Civil Engineering, Babol Noshirvani University of Technology, Babol, Iran, rdezvareh@nit.ac.ir*

**ARTICLE INFO**

*Article History:*
Received: 18 Aug
Accepted: 24 Nov
Available online ….

*Keywords:*
**Hydrodynamics**
**Caspian Sea**
**Flow Model**
**Nowshahr**
**Mike 21**

**ABSTRACT**

This study conducts a sensitivity analysis of wave and current behavior during minor storms along the southern coast of the Caspian Sea, focusing on the port of Nowshahr, a significant maritime hub in northern Iran. Using MIKE21, a numerical modeling software, the analysis evaluates various parameters such as mesh size, angular divisions, bed roughness, and wave breaking coefficients. The numerical models were calibrated and validated by comparing their outputs with field measurements obtained during small storm events. Results indicate that certain parameters, such as computational grid size and wave breaking coefficients, significantly influence model accuracy, while others, such as angular divisions, have minimal impact. Wind data from ECMWF-ERA5 was used to simulate local conditions accurately. The findings provide insights into optimizing numerical model calibration for improved predictions of wave and current behavior, particularly under storm conditions, thereby supporting coastal engineering projects and enhancing understanding of marine hydrodynamics in this region.

## 1. Introduction

Sensitivity analysis refers to studying how variations in input variables of a statistical model can affect its output. In other words, it is a systematic way to modify a model's inputs and predict the corresponding effects on its results [1]. Sensitivity analysis is crucial for making accurate use of numerical models through various software programs. Given the high level of uncertainty in marine environments, this analysis becomes even more important [2]. Since waves and currents are key factors in marine environments, many researchers have conducted sensitivity analyses on these two parameters. In 2010, Beels et al. performed a sensitivity analysis on wave energy absorber numerical modeling [3]. In 2013, DAO et al. analyzed tsunami waves through a Reynolds-Averaged Navier-Stokes (RANS) based numerical model, assessing the effect of coastal parallel channels on tsunami wave energy reduction [4]. In 2015, Nekouee et al. conducted a sensitivity analysis on wave prediction numerical models considering wind and geometry effects [5]. In 2016, Bastidas et al. simulated artificial storm tracks using Delft 3D software and carried out sensitivity analyses to estimate storm hazards in the absence of experimental wave and coastal wave observations [6]. Liu and Guo, in 2018, applied sensitivity analysis to study the combined effects of waves and currents on risers [7]. Moreover, Zhen et al., in 2021, conducted a sensitivity analysis on wave direction for three cases: external channel excavation, wave, and storm in a shielded port [8]. Their findings suggest that wave direction sensitivity is stronger near the entrance of ports with an excavated external channel. Based on this, it was recommended that primary wave direction analysis be carried out.

It is worth mentioning that, in addition to the sensitivity analysis briefly reviewed in the literature, other researchers have employed artificial intelligence-based methods, such as neural networks [10,11], machine learning [12], and support vector machines [13, 14], to better analyze numerical model data and compare them with field measurements. Building upon these studies, the aim of the present paper is to conduct a sensitivity analysis of waves and currents using MIKE software and to compare the results with field measurements during minor storms along the southern coast of the

Caspian Sea in northern Iran. For this purpose, the area surrounding the port of Nowshahr, one of the most significant and longstanding ports in northern Iran, has been selected as the study area.

## 2. Materials and Methods

This section presents the details of the numerical models developed for the study area. It is worth noting that MIKE21, a software package developed by the Danish Hydraulic Institute (DHI), was used for modeling in this study. MIKE21 is one of the most reliable and widely used numerical simulators for hydrodynamic modeling of aquatic environments [15].

### 2.1. Large-Scale Wave and Current Modeling

For simulating the hydrodynamic phenomena of the southern coasts of the Caspian Sea, it is necessary to first simulate the marine wave and current conditions in this region. The local wave and current conditions are not independent of the conditions in the entire Caspian Sea. Therefore, for local hydrodynamic modeling, the boundary conditions of marine waves and currents at the open borders of the local model must be determined.

### 2.2. Mesh Gridding for Wave Model

The simulation area includes the entire Caspian Sea. Bathymetric data and depth variations for this area are provided below. Figure 1 shows the coastal line. The continuous red line represents data obtained from Google Earth. It is important to note the non-synchronicity of Google Earth maps when determining the coastal line.




**Figure 1. Comparison of available sources for coastal line representation. The continuous red line represents data obtained from Google Earth, the white markers indicate data from the NASA website, and the red markers show data gathered from the Caspian Sea Environmental Program.**

Wind is the most important factor in wave generation in seas. Therefore, accurate wave modeling requires wind data with suitable temporal and spatial resolution. Figure 2 shows the wind rose derived from ECMWF-ERA5 data at a deep-water location in front of the study area. Considering the alignment between the wind rose obtained from ERA5 data and the hydrodynamic conditions of the region, and given the superior temporal and spatial accuracy of this data compared to other available wind fields, these data were used for further simulations.

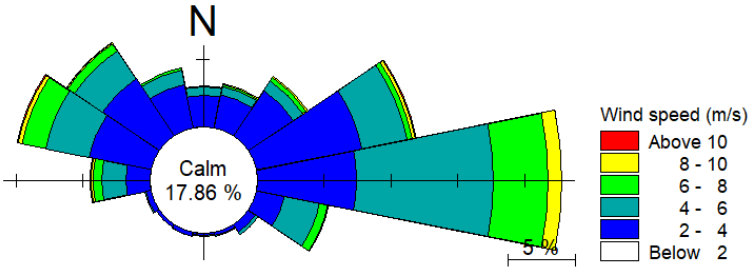



**Figure 2. Wind rose obtained from ECMWF-ERA5 data**

### 2.3. Wave and Current Measurements

To understand the overall wave patterns based on measured field data, Figure 3 presents the wave rose for the measured data at Nowshahr. As shown, the predominant wave direction in the region is from the northwest, which has the longest fetch. Based on this figure, it can be predicted that due to the angle of wave incidence relative to the coastline, wave breaking in the surf zone will cause the dominant currents generated by wave breaking to flow from west to east. Consequently, sediment transport will also be predominantly west to east.

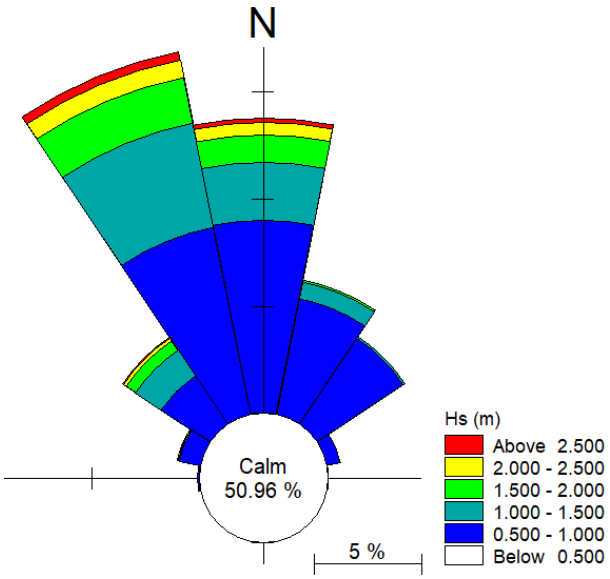



**Figure 3. Wave rose for measured data near Nowshahr Port.**

In addition to wave measurements, current characteristics were also measured at this location. Figure 4 shows the time series of current speed and direction recorded at this station over several months. The maximum recorded current speed at this station during the measurement period was approximately 0.62 meters per second. To understand the general current pattern based on field measurements, a current rose was plotted based on the data obtained at this station. Figure 5 shows the current rose for measured data at Nowshahr station, which is based on depth-averaged speeds. According to Figure 5, the general current pattern in this region is primarily east-west, with a higher frequency of west-to-east currents compared to east-to-west currents.

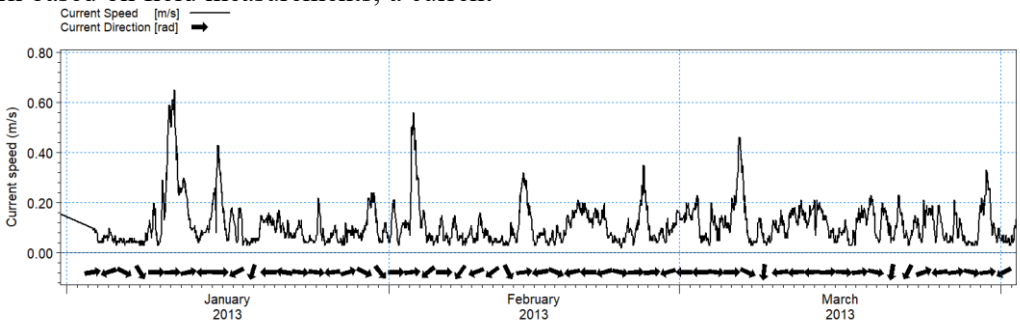



**Figure 4. Time series of current speed and direction measured near Noshahr Port for a sample period.**

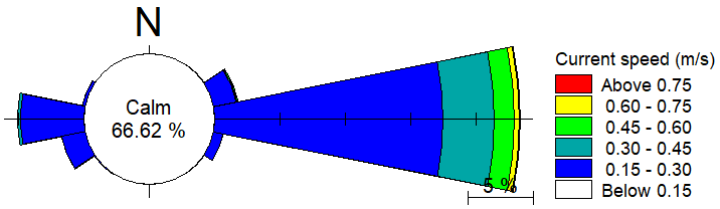



**Figure 5. Current rose for measured data near Nowshahr Port.**

In this part of the simulations, a triangular mesh was used for the model grid. In this study, the mesh file was generated such that the grid resolution and size were as optimal as possible across the computational domain. The mesh and bathymetry data used for wave generation and propagation analysis are shown in Figure 6. The grid resolution varies between 0.02 and 0.25 degrees in different areas.

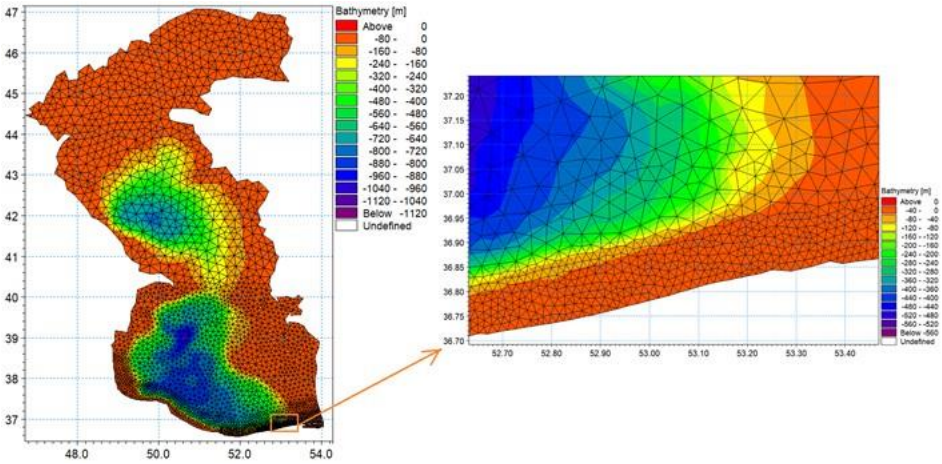



**Figure 6. Computational mesh used for large-scale simulations of the Caspian Sea.**

## 3. Results and Discussion

### 3.1. Sensitivity Analysis of Wave Models to Different Parameters

The results of numerical models are dependent on various factors, such as mesh size, angular division, numerical equation solving accuracy, wave breaking coefficients, bed roughness, wave crest white-capping coefficients, and more. To calibrate numerical models, it is first necessary to assess the impact of highly sensitive factors on the results.

In some regions, refining the computational mesh can enhance accuracy, but it also increases computational costs significantly. If mesh refinement does not yield considerable improvements in results, coarser meshes with lower computational costs are preferable. Figures 8 and 9 compare the results of models with different mesh sizes in deep water and nearshore locations, respectively. As shown, finer meshes do not substantially improve the results, only raising computational costs. Therefore, mesh sizes ranging from 0.02 to 0.25 degrees were used for final calculations.

#### 3.1.1. Sensitivity to Mesh Size

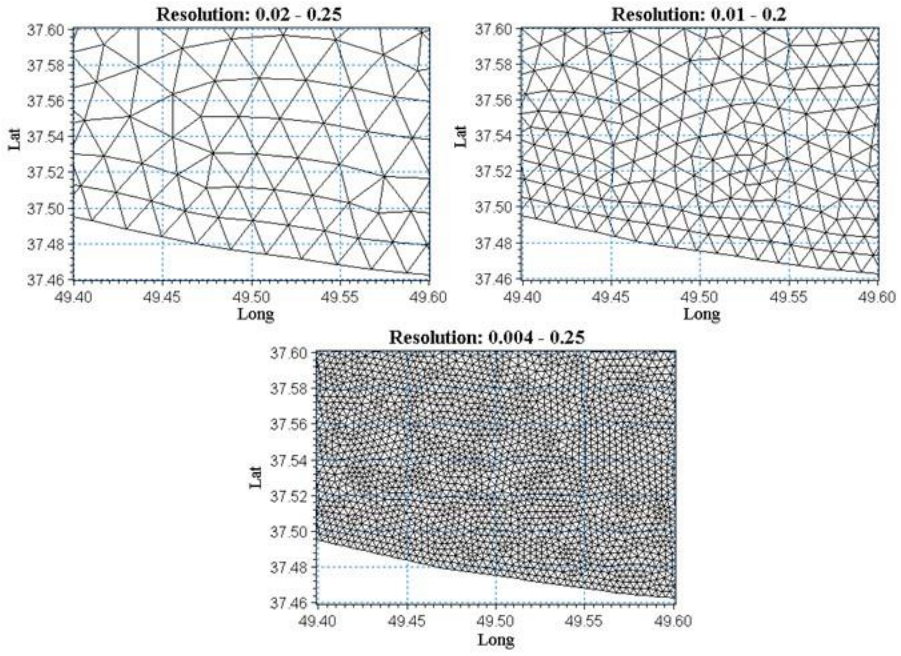



**Figure 7. Computational mesh generated with different sizes for sensitivity analysis.**

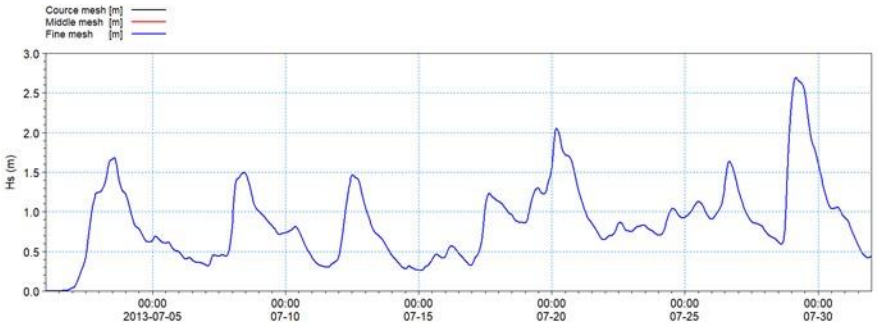



**Figure 8. Comparison of model results with different mesh sizes at a deep-water point.**

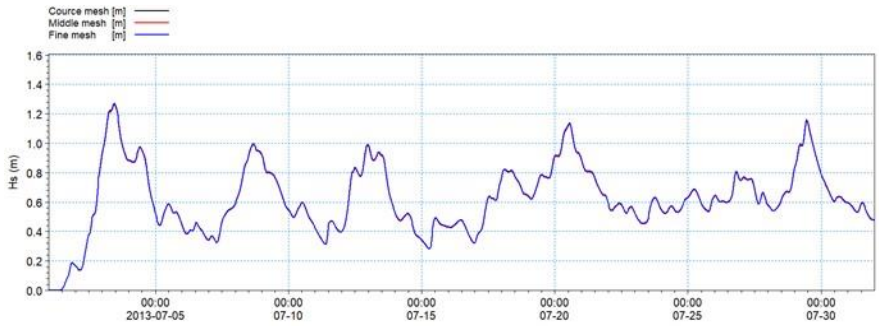



**Figure 9. Comparison of model results with different mesh sizes near the coast.**

### 3.1.2. Sensitivity to Angular Divisions

One of the features of spectral wave models is the ability to perform calculations not only on a spatial computational grid but also on a spectral grid. This grid has two dimensions: direction and frequency. In spectral models, users can choose a full directional spectrum or set a minimum and maximum range for it. Figures 10 and 11 compare the results of models with different angular divisions at deep-water and nearshore points. As can be seen, varying the number of angular divisions has little effect on the model output.

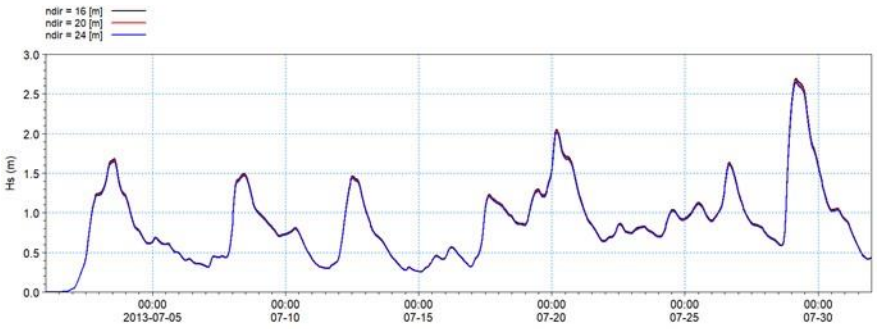



**Figure 10. Comparison of model results with different angular divisions at a deep-water point.**

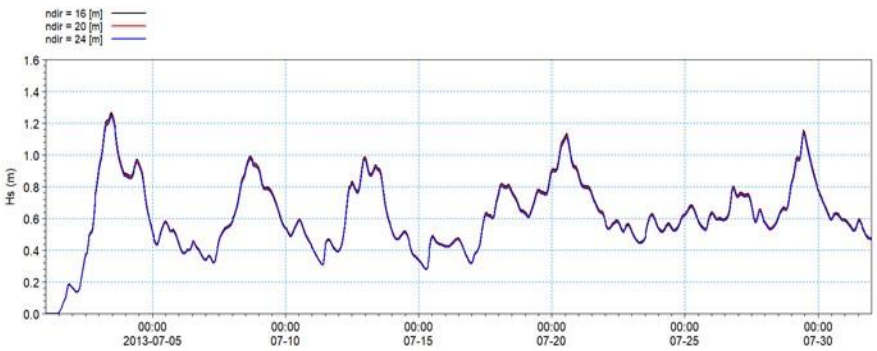



**Figure 11. Comparison of model results with different angular divisions near the coast.**

### 3.1.3. Sensitivity Analysis of Bed Roughness Coefficient

One of the factors affecting waves in shallow regions is bed roughness. In the MIKE-SW model, the Nikuradse roughness coefficient (kn) can be applied to account for bed roughness [16]. The value of this coefficient can be selected by the user. For the sensitivity analysis, values of 0.04 (the default in the model), 0.4, and 0.004 were chosen, and the model was run for each case. The simulated wave heights with different Nikuradse roughness coefficients are compared in Figures 12 and 13 for deep water and nearshore locations, respectively. As shown, changing this coefficient has no effect in deep water, but it can be used as one of the main calibration factors in shallow water areas.

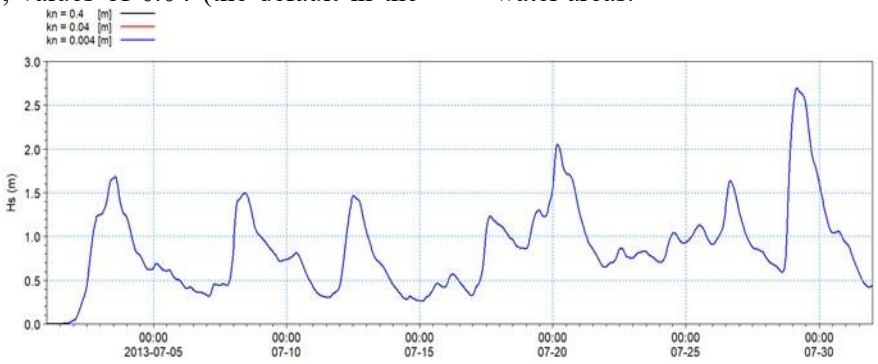



**Figure 12. Comparison of model results with different bed roughness coefficients at a deep-water point.**

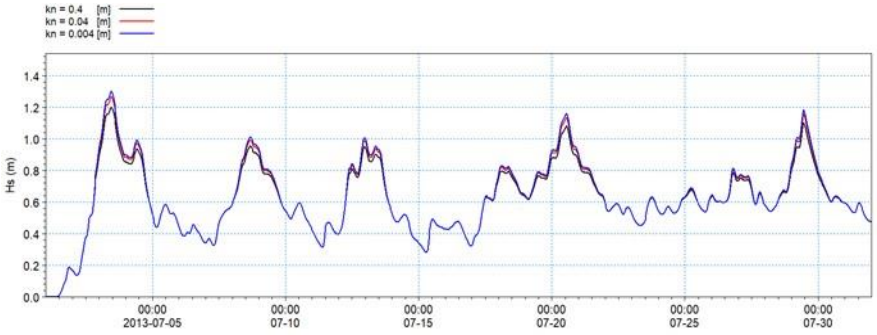



**Figure 13. Comparison of model results with different bed roughness coefficients near the coast.**

### 3.1.4. Sensitivity Analysis of Wave Breaking Coefficients in Shallow Water

In wave formation and propagation calculations, wave breaking is a critical phenomenon that affects the distribution of wave heights. Wave breaking occurs when waves enter shallow areas, and the water depth cannot support the wave energy. As a result, part of the wave's energy is dissipated. An additional sink term appears in the governing spectral equation to account for this energy loss. In the MIKE21 SW model, this term is based on the relationships provided by Battjes and Janssen [17], which have proven effective in spectral models.

In this model, two coefficients are considered: one to control the energy dissipation rate after wave breaking (parameter α), and the other to control the depth at which wave breaking occurs (parameter γ). Increasing parameter α increases the energy dissipation rate, while increasing parameter γ reduces the wave breaking depth.

### 3.1.5. Sensitivity Analysis of wave crest whitecaps Coefficients

wave crest whitecaps refers to surface turbulences that cause energy dissipation in deep water and are the primary mechanism controlling wave energy in these regions. The concept of deep-water wave breaking was first introduced by Hasselmann in 1974, and its equations were revised by Komen et al. in 1984 [18][19]. In the MIKE21-SW model, two parameters $C_{dis}$ and $\delta$ are provided for direct or indirect control of energy dissipation. The range of coefficients $C_{dis} \approx 2.36 \times 10^{-5}$ and $\delta \approx 0{\sim}1$ is available. In the MIKE SW model, the default values of these parameters $C_{dis} = C_{dis}\ (1/\widetilde{s_{PM}})^4$ and $\Delta_{dis} = \delta$ are set to 4.5 and 0.5, respectively. Sensitivity analysis was conducted by varying these two parameters $C_{dis}$ and $\Delta_{dis}$. Different combinations of values for $C_{dis}$ and $\Delta_{dis}$ were tested to analyze the sensitivity of wave height results.

In Figures 14 and 15, a comparison of the wave heights derived from various parameters of wave crest

whitecaps at a deep-water buoy and nearshore location is presented. As can be observed, the simulated wave height is significantly influenced by parameter $C_{dis}$, while it shows minimal sensitivity to the weight parameter $\Delta_{dis}$. It is evident that while parameter $C_{dis}$ remains constant, considerable changes in parameter $\Delta_{dis}$ have not led to a substantial variation in wave height. However, since parameter $C_{dis}$ directly controls the energy dissipation, it is observed that a reduction in this parameter has resulted in a notable increase in wave height.

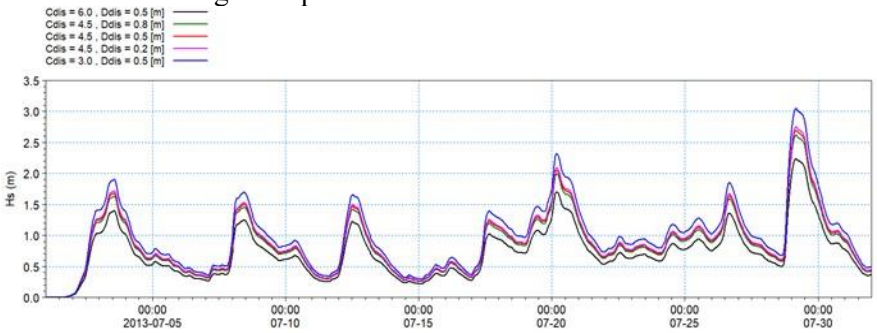



**Figure 14. Comparison of wave height results of models with different wave crest whitecap coefficients at a point in deep water.**

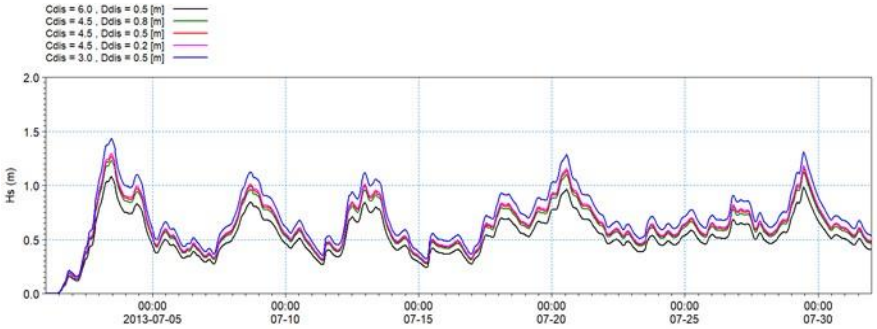



**Figure 15. Comparison of wave height results of models with different wave crest whitecap coefficients at a point near the shore.**

To further investigate the sensitivity of wave crest whitecap parameters, the effect of these parameters on wave period was also analyzed. In Figures 16 and 17, the changes in wave period $(T_{m,02})$ for the aforementioned scenarios are compared. As observed, the wave period's sensitivity to these parameters varies, with the period being slightly more sensitive to parameter $\Delta_{dis}$ compared to parameter $C_{dis}$. It is clear that an increase in parameter $\Delta_{dis}$ directly results in an increase in the wave period. For instance, changing parameter $\Delta_{dis}$ from 0.2 to 0.8 causes an increase of 0.5 to 0.8 seconds in the wave period. This analysis demonstrates that, compared to default conditions, the period can be adjusted by approximately half a second through the calibration of wave crest whitecap parameters. Additionally, regarding wave height, it is possible to influence wave characteristics by up to 30% using the calibration of whitecap parameters.

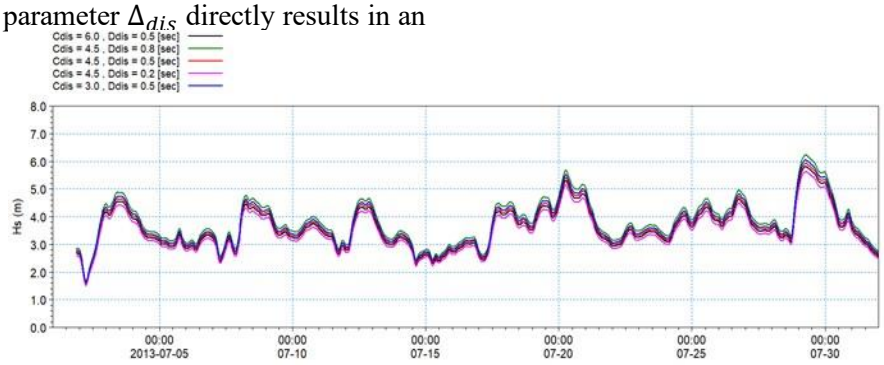



**Figure 16. Comparison of wave period results of models with different wave crest whitecap coefficients at a point in deep water.**

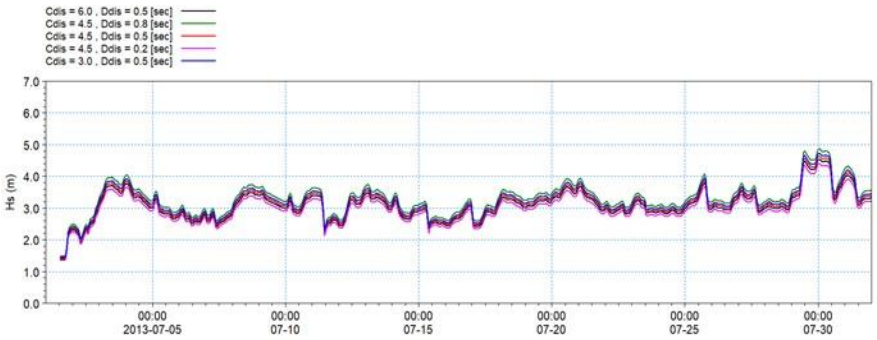



**Figure 17. Comparison of wave period results of models with different wave crest whitecap coefficients at a point near the shore.**

## 3.2. Sensitivity Analysis of the Flow Model to Various Parameters

In this section, the sensitivity of the flow model results to different factors such as computational grid size, numerical accuracy, the effect of the Coriolis force, horizontal eddy viscosity coefficient, tidal effects, bed roughness coefficient, and wind friction coefficient has been examined. The various results for the model's runtime at the ADCP field measurement location in Nowshahr have been compared. The effect of each parameter will be discussed further.

### 3.2.1. Sensitivity Analysis to Computational Grid Size

Figure 18 shows the comparison of changes in flow velocity against Nowshahr port. As observed, refining the computational grid did not result in any significant changes in the results but only increased the computational cost. Therefore, a grid size between 0.02 to 0.25 degrees was used for the final computations.

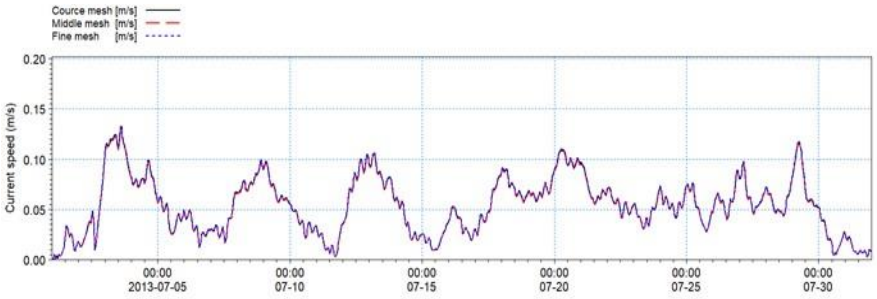



**Figure 18. Comparison of flow model results with different computational grids at the ADCP measurement point in Nowshahr.**

### 3.2.2. Sensitivity Analysis to the Effect of the Coriolis Force

The Coriolis force is a pseudo-force that causes the deflection of moving objects from a straight path as viewed from a rotating system, such as Earth. The effects of this force can clearly be seen in determining the direction of atmospheric fronts and planetary currents. Perhaps the most significant example of the Coriolis effect on large dynamic systems is the ocean, where it leads to changes in current velocities. To investigate the Coriolis effect on flow changes, two models were considered: the first without considering the Coriolis force and the second incorporating a variable Coriolis force across the entire modeled area. The results are shown as a time series of current velocities near Nowshahr in Figure 19. This figure shows that ignoring the Coriolis force can significantly affect current flow and water surface levels. Therefore, given the geographic location of the Caspian Sea and the importance of the Coriolis force in this region, it was decided to consider the Coriolis force as variable in space. It is worth mentioning that this option does not increase the computational cost compared to other models, but it provides more confidence in the accuracy of the results.

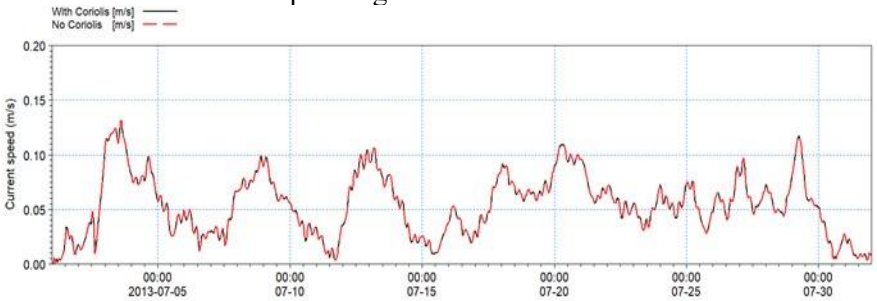



**Figure 19. Comparison of flow model results with and without considering the Coriolis effect at the ADCP measurement point in Nowshahr.**

### 3.2.3. Sensitivity Analysis of the Effect of Horizontal Eddy Viscosity Coefficient

In many applications, eddy viscosity is used as a constant. In other cases, the Smagorinsky model is used. The Smagorinsky coefficient $C_s$ should be selected within the range of 0.25 to 1. However, the minimum eddy viscosity can be chosen as zero, but due to its non-physical nature, this is generally avoided. The default value for this coefficient in the model is 0.28. By changing this value to 0.2 and 0.4, their effects on the flow results were evaluated. The result of the modeling, shown as the flow velocity time series near Nowshahr, is presented in Figure 20. As seen in the figure, there is no significant difference between the results from the two models. Therefore, this coefficient cannot be used for model calibration.

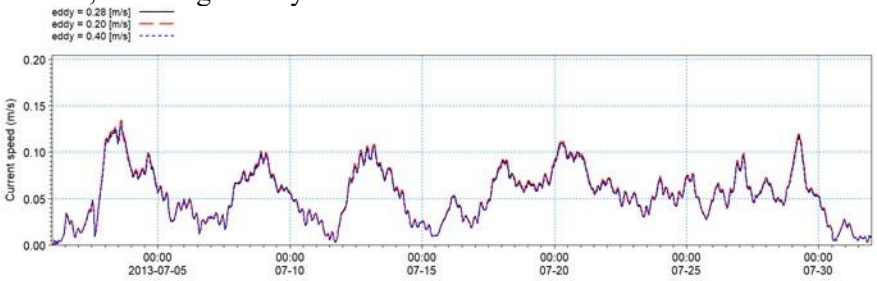



**Figure 20. Comparison of Flow Model Results with Different Eddy Viscosity Coefficients at the ADCP Measurement Point in Nowshahr.**

### 3.2.4. Sensitivity Analysis of the Tidal Effects

To examine this effect, two models with and without tidal effects were employed. The time series chart of the flow and water level results for the two conditions, with and without tidal effects near Nowshahr, is shown in Figure 21. This figure indicates that tidal effects do not influence the flow results. Therefore, tidal effects were disregarded in the final model.

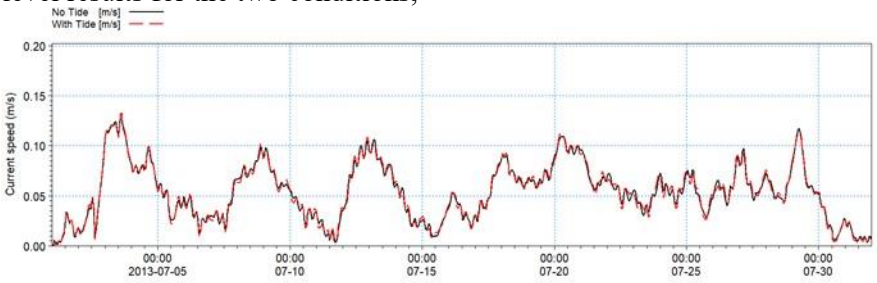



**Figure 21. Comparison of Flow Model Results with and without Tidal Effects at the ADCP Measurement Point in Nowshahr.**

### 3.2.5. Sensitivity Analysis of the Wind Friction Coefficient

By changing the value of the wind friction coefficient, the shear stress exerted by the wind on the water surface changes, thus altering the flow velocity. This is particularly significant at high wind speeds, which can cause increased flow velocities. This coefficient can either be constant (default value 0.001255) or variable (a function of wind speed, with 0.001255 for a 3 m/s wind and 0.002455 for a 25 m/s wind according to the default model). Between these two speeds, the coefficient is selected linearly. For the sensitivity analysis, different coefficients with various values were examined:

- 0.002455 and 0.001255 for wind speeds of 7 and 25 m/s (default)
- 0.002455 and 0.001255 for wind speeds of 3 and 15 m/s
- 0.002455 and 0.001255 for wind speeds of 3 and 15 m/s

Figure 22 shows a comparison of the flow velocity variations in models with different wind friction coefficients at a depth of 13 meters opposite the Nowshahr Port. As seen in the figure, the magnitude of the marine currents depends on the wind friction coefficient values.

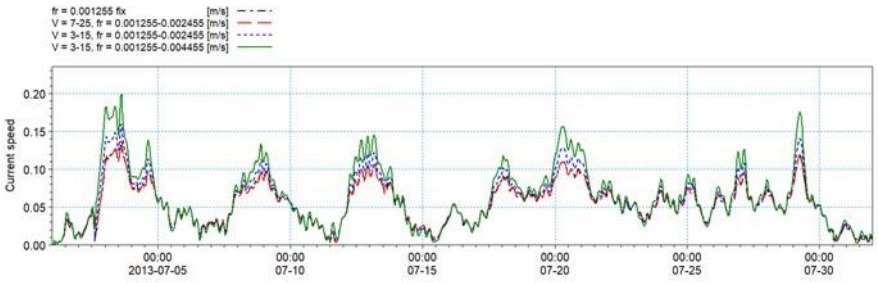



**Figure 22. Comparison of Flow Model Results with Different Wind Friction Coefficients at the ADCP Measurement Point in Nowshahr.**

## 4. Conclusion

In this study, after modeling waves and currents in the MIKE software, a sensitivity analysis of various parameters in the wave and current model was conducted. The results were also compared with field measurements. The wave section results indicated that among the parameters studied, the parameters of the number of angular divisions in the spectrum, the accuracy of the computational method, and shallow water wave breaking had little effect on the output results in the southern Caspian Sea and could not be used for model calibration. Reducing the computational grid size had a certain impact on the accuracy of the results up to a point, but beyond that, it only increased computational cost. This parameter is also not suitable for calibration, and the grid size should be optimally chosen so that spatial discretization does not affect the results. The bed roughness coefficients and the wave crest capping each had a moderate effect on the results and can be considered as key parameters in the model calibration process. Moreover, the current section results showed that the accuracy of numerical computations, the effect of Coriolis force, horizontal eddy viscosity coefficient, tidal effects, bed roughness coefficient, and wind friction coefficient were analyzed. Among the parameters examined, the accuracy of numerical computations, the eddy viscosity coefficient, and tidal effects did not have significant impacts on the output results. The Coriolis force, considered variable across the entire model, did not have a major effect either. The bed roughness coefficient and wind friction coefficient influenced the results and can be used for model calibration.

## References

[1] Iooss, B., & Lemaître, P. (2015). A review on global sensitivity analysis methods. *Uncertainty management in simulation-optimization of complex systems: algorithms and applications*, 101-122.

[2] Liu, Z., & Soares, C. G. (2023). Sensitivity analysis of the cage volume and mooring forces for a gravity cage subjected to current and waves. *Ocean Engineering*, *287*, 115715.

[3] Beels, C., Troch, P., De Backer, G., Vantorre, M., & De Rouck, J. (2010). Numerical implementation and sensitivity analysis of a wave energy converter in a time-dependent mild-slope equation model. *Coastal Engineering*, *57*(5), 471-492.

[4] DAO, N. X., ADITYAWAN, M. B., & TANAKA, H. (2013). Sensitivity analysis of shore-parallel canal for tsunami wave energy reduction. *Journal of Japan Society of Civil Engineers, Ser. B3 (Ocean Engineering)*, *69*(2), I_401-I_406.

[5] Nekouee, N., Hamidi, S. A., & Etemadi, R. (2015). Sensitivity analysis of numerical wave predictions models, considering wind and geometry effects in rectangular lakes. *Ocean Engineering*, *104*, 549-557.

[6] Wu, C. C., & Emanuel, K. A. (1995). Potential vorticity diagnostics of hurricane movement. Part 1: A case study of Hurricane Bob (1991). *Monthly weather review*, *123*(1), 69-92.

[7] Bastidas, L. A., Knighton, J., & Kline, S. W. (2016). Parameter sensitivity and uncertainty analysis for a storm surge and wave model. *Natural Hazards and Earth System Sciences*, *16*(10), 2195-2210.

[8] Liu, Z., & Guo, H. (2018). Sensitivity analysis of steep wave riser with internal flow. *Journal of Marine Science and Technology*, *26*(4), 7.

[9] Han-bao, C., Ya-nan, X., & Yong-zhou, C. (2021). Sensitivity analysis of wave direction in wave numerical model. In *IOP Conference Series: Earth and Environmental Science* (Vol. 621, No. 1, p. 012076). IOP Publishing.

[10] Dezvareh, R., & Shafaghat, M. (2020). Predicting the sediment rate of Nakhilo Port using artificial intelligence. *International Journal Of Coastal, Offshore And*

*Environmental Engineering (ijcoe)*, *5*(2), 41-49.

[11] Dezvareh, R. (2019). Providing a new approach for estimation of wave set-up in Iran coasts. *Research in marine sciences*, *4*(1), 438-448.

[12] Dezvareh, R., Bargi, K., & Moradi, Y. (2012). Assessment of Wave Diffraction behind the Breakwater Using Mild Slope and Boussinesq Theories. *International Journal of Computer Applications in Engineering Sciences*, *2*(2).

[13] Shafaghat, M., & Dezvareh, R. (2021). Support vector machine for classification and regression of coastal sediment transport. *Arabian Journal of Geosciences*, *14*(19), 2009.

[14] Gholizadeh, S., Dezvareh, R., & Kiani, A. (2024). Comparison of different support vector machine kernels for monitoring of the last decade of the Iranian part of eastern Caspian Lake. *International Journal Of Coastal, Offshore And Environmental Engineering (ijcoe)*, *9*(1), 55-63.

[15] Warren, I. R., & Bach, H. (1992). MIKE 21: a modelling system for estuaries, coastal waters and seas. *Environmental software*, *7*(4), 229-240.

[16] Nodeh, H. M., Dezvareh, R., & Yousefifard, M. (2024). Numerical Analysis of the Effects of Rubble Mound Breakwater Geometry Under the Effect of Nonlinear Wave Force. *Arabian Journal for Science and Engineering*, *49*(4), 5767-5783.

[17] Farhadzadeh, A., Kobayashi, N., & Gravens, M. B. (2012). Effect of breaking waves and external current on longshore sediment transport. *Journal of waterway, port, coastal, and ocean engineering*, *138*(3), 256-260.

[18] Hasselmann, K. (1974). On the spectral dissipation of ocean waves due to white capping. *Boundary-Layer Meteorology*, *6*, 107-127.

[19] Komen, G. J., Hasselmann, S., & Hasselmann, K. (1984). On the existence of a fully developed wind-sea spectrum. *Journal of physical oceanography*, *14*, 1271-1285.

[20] Dadashzadeh, M., Parsa, J., & Mojtahedi, A. (2020). Investigation over the interaction of Lake Urmia wave pattern and causeway using meteorological models and computational fluid dynamics. *Journal of Oceanography*, *11*(41), 49-61.